METAL TRANSPORT IN PLANTS

EDITED BY: Tomoko Nozoye, Stephan Clemens, Seçkin Eroğlu and Louis Grillet

PUBLISHED IN: Frontiers in Plant Science

frontiers Research Topics

frontiers

ISSN 1664-8714
ISBN 978-2-88966-952-3
DOI 10.3389/978-2-88966-952-3

About Frontiers

Frontiers is more than just an open-access publisher of scholarly articles: it is a pioneering approach to the world of academia, radically improving the way scholarly research is managed. The grand vision of Frontiers is a world where all people have an equal opportunity to seek, share and generate knowledge. Frontiers provides immediate and permanent online open access to all its publications, but this alone is not enough to realize our grand goals.

Frontiers Journal Series

The Frontiers Journal Series is a multi-tier and interdisciplinary set of open-access, online journals, promising a paradigm shift from the current review, selection and dissemination processes in academic publishing. All Frontiers journals are driven by researchers for researchers; therefore, they constitute a service to the scholarly community. At the same time, the Frontiers Journal Series operates on a revolutionary invention, the tiered publishing system, initially addressing specific communities of scholars, and gradually climbing up to broader public understanding, thus serving the interests of the lay society, too.

Dedication to Quality

Each Frontiers article is a landmark of the highest quality, thanks to genuinely collaborative interactions between authors and review editors, who include some of the world's best academicians. Research must be certified by peers before entering a stream of knowledge that may eventually reach the public - and shape society; therefore, Frontiers only applies the most rigorous and unbiased reviews.
Frontiers revolutionizes research publishing by freely delivering the most outstanding research, evaluated with no bias from both the academic and social point of view. By applying the most advanced information technologies, Frontiers is catapulting scholarly publishing into a new generation.

What are Frontiers Research Topics?

Frontiers Research Topics are very popular trademarks of the Frontiers Journals Series: they are collections of at least ten articles, all centered on a particular subject. With their unique mix of varied contributions from Original Research to Review Articles, Frontiers Research Topics unify the most influential researchers, the latest key findings and historical advances in a hot research area! Find out more on how to host your own Frontiers Research Topic or contribute to one as an author by contacting the Frontiers Editorial Office: frontiersin.org/about/contact

METAL TRANSPORT IN PLANTS

Topic Editors:
Tomoko Nozoye, Meiji Gakuin University, Japan
Stephan Clemens, University of Bayreuth, Germany
Seçkin Eroğlu, Middle East Technical University, Turkey
Louis Grillet, National Taiwan University, Taiwan

Citation: Nozoye, T., Clemens, S., Eroğlu, S., Grillet, L., eds. (2021). Metal Transport in Plants. Lausanne: Frontiers Media SA. doi: 10.3389/978-2-88966-952-3

Table of Contents

frontiers in Plant Science

EDITORIAL
published: 26 February 2021
doi: 10.3389/fpls.2021.644960

Editorial: Metal Transport in Plants

Stephan Clemens[1], *Seckin Eroglu*[2], *Louis Grillet*[3] *and Tomoko Nozoye*[4,5]*

[1] Department of Plant Physiology, University of Bayreuth, Bayreuth, Germany, [2] Department of Biological Sciences, Middle East Technical University, Ankara, Turkey, [3] Department of Agricultural Chemistry, National Taiwan University, Taipei, Taiwan, [4] Center for Liberal Arts, Meiji Gakuin University, Tokyo, Japan, [5] Graduate School of Agricultural and Life Sciences, The University of Tokyo, Tokyo, Japan

Keywords: metal, transport, translocation, plant, essential nutrient elements, toxic metal

Editorial on the Research Topic

Metal Transport in Plants

Plants have to acquire 17 different essential elements (nitrogen, phosphorus, potassium, oxygen, hydrogen, carbon, calcium, magnesium, sulfur, iron, manganese, boron, zinc, molybdenum, copper, chlorine, and nickel) mainly from the rhizosphere by their roots to complete their life cycle. Both shortage and excess of these lead to impaired growth, which is often reflected as yield loss in agriculture. Plants have developed sophisticated and tightly regulated mechanisms for uptake and translocation of the essential elements. On the other hand, plants also take up harmful elements such as cadmium and arsenic non-specifically which may interfere with essential nutrients' uptake. Recent studies have shown that molecular networks to maintain homeostasis of the essential elements are intertwined. How elements are interacting with each other during acquisition and translocation determines yield quality and quantity in agriculture, yet is poorly understood. In this Research Topic, we aim at covering essential nutrient homeostasis in plants; including, but not limited to their transport, translocation and interactions.

The Research Topic succeeded in collecting six original research papers, one review, one perspective and one mini review, which discuss not only the essential but also the toxic metals under various physiological conditions. Escudero et al. reported that iron transport to rhizobia is important for nitrogen fixation. Symbiotic nitrogen fixation by rhizobia in roots of legumes requires relatively large amounts of transition metals. Escudero et al. focused on the model legume *Medicago truncatula*, searched for metal-related symbiotic phenotypes of mutants with defects in symbiosis establishment, and found a mutant whose growth was impaired only under symbiotic condition, since a nicotianamine (NA) synthase gene (*MtNAS2*) was disrupted by insertion of a transposon. NA is known as a chelator involved in iron translocation in plant bodies. Escudero et al. suggested that proper distribution of ferric iron in the nodule is necessary for symbiotic nitrogen fixation.

Ceasar et al. reported on the function of the di-cysteine motifs in the Arabidopsis plasma membrane Heavy Metal ATPase 4 (HMA4) transporter which mediates xylem loading of cadmium for export to shoots, in addition to zinc. The authors revealed that the di-cysteine motifs present in the AtHMA4 C-terminal extension were not essential for cadmium transport from root to shoot, even though the di-cysteine motif had been shown to be essential for high-affinity zinc binding and transport in *planta*. In addition, Ceasar et al. showed that the affinity of the di-cysteine motif was lower for cadmium than for zinc, suggesting that it is possible to identify or engineer HMA4 variants able to discriminate zinc and cadmium transport.

Perea-García et al. investigated the link between copper and iron homeostasis in Arabidopsis. Both copper and iron are transition metals and their reduced forms facilitate the formation of reactive oxygen species (ROS), which can damage plant cells. In some cases, these transition metals can be substituted for one another, in different proteins to perform similar functions. The concentrations of copper and iron are therefore linked to each other. Perea-García et al. analyzed the physiological and transcriptional change in transgenic Arabidopsis overexpressing the high affinity copper transporters COPT1 and COPT3 ($COPT^{OE}$). They found that iron accumulated

Edited by:
Kendal Hirschi,
Baylor College of Medicine,
United States

Reviewed by:
Toshiro Shigaki,
The University of Tokyo, Japan
Wayne Versaw,
Texas A&M University, United States

***Correspondence:**
Tomoko Nozoye
atom1210@mail.ecc.u-tokyo.ac.jp

Specialty section:
This article was submitted to Plant Membrane Traffic and Transport, a section of the journal Frontiers in Plant Science

Received: *22 December 2020*
Accepted: *09 February 2021*
Published: *26 February 2021*

Citation:
Clemens S, Eroglu S, Grillet L and Nozoye T (2021) Editorial: Metal Transport in Plants. Front. Plant Sci. 12:644960. doi: 10.3389/fpls.2021.644960

in roots as copper increased in the media, while iron homeostasis genes were downregulated *in planta*, suggesting that adequate copper uptake is important for iron homeostasis.

A study by Uraguchi et al. showed how gelling agents' contaminants could dramatically influence the elemental accumulation and metal sensitivity in *planta*. Uraguchi et al. used three types of agar and analyzed phenotypes of three established mutants [*Cadmium sensitive (cad)1-3* and *cad1-6*, loss of function alleles of the main phytochelatin (PC) synthase in Arabidopsis, *AtPCS1*; *ATP-binding cassette C* (*abcc)1/2*, the double knockout mutant of *AtABCC1* and *AtABCC2*, Arabidopsis PC-metal (loid) complex transporters on tonoplast]. Uraguchi et al. found that the established phenotypes of these mutants depended on the agar, suggesting that the selection of agar reagents is important and can mask even reliable phenotypes.

Nishida et al. examined two species of nickel hyperaccumulator plants in the genus *Noccaea*: *N. caerulescens* and *N. japonica*. Nishida et al. found that *N. japonica* tolerated excess nickel better than *N. caerulescens*, and the translocation of nickel from root to shoot was lower in *N. japonica* compared to *N. caerulescens*. On the other hand, zinc concentrations in both roots and shoots were similar between *N. japonica* and *N. caerulescens* even under zinc excess conditions. In addition, the expression of the gene encoding the vacuolar nickel transporter *iron-regulated 2* (*IREG2*) was higher in *N. japonica* compared to *N. caerulescens*, suggesting that sequestration of nickel in the vacuole by IREG2 is one reason for the nickel tolerance in *N. japonica*.

Krishna et al. analyzed the sequences of 113 zinc-regulated, iron-regulated transporter-like proteins (ZIP) family from 14 plants species. ZIP family transporters are involved in cellular uptake of zinc, as well as in transport of other divalent metal cations such as cadmium, iron, and copper. Krishna et al. used bioinformatics to show that the plant ZIP transporters are mainly in one cluster together, however some residues involved in metal binding and transport are not conserved among members of the ZIP family, suggesting that distinct metal transport mechanism may exist. It was suggested that manipulation of critical amino acid residues of ZIP transporters may improve zinc homeostasis in planta.

In the review and perspective articles, Rai and Kawabata discuss the mechanisms of cesium uptake into rice plants which has been a serious problem following the accidents at the nuclear power plants of Chernobyl and Fukushima Daiichi. Roschzttardtz et al. summarized the transcriptional regulation of iron distribution in Arabidopsis seeds. Aung and Masuda reviewed recent findings about the molecular mechanisms defending rice plants against excess iron.

The present Research Topic shows that the mechanism of the essential and toxic metals overlap, but are not entirely identical. Results suggest that the manipulation of metal transport systems has the potential to generate high quality crops, with high yield and abundant essential nutrients, while largely excluding toxic metals.

AUTHOR CONTRIBUTIONS

TN wrote a draft manuscript. SC, SE, and LG revised the manuscript. All authors contributed to the article and approved the submitted version.

FUNDING

SE acknowledged support by the Scientific and Technological Research Council of Turkey (Project no: 118Z788). TN acknowledged support by JSPS KAKENHI (Grant Numbers: 15K18658 and 15KK0286), and by a grant from Uragami-zaidan.

Conflict of Interest: The authors declare that the research was conducted in the absence of any commercial or financial relationships that could be construed as a potential conflict of interest.

frontiers in Plant Science

ORIGINAL RESEARCH
published: 30 January 2020
doi: 10.3389/fpls.2019.01780

Nicotianamine Synthase 2 Is Required for Symbiotic Nitrogen Fixation in *Medicago truncatula* Nodules

*Viviana Escudero[1], Isidro Abreu[1], Eric del Sastre[1], Manuel Tejada-Jiménez[1], Camille Larue[2], Lorena Novoa-Aponte[3], Jorge Castillo-González[4], Jiangqi Wen[5], Kirankumar S. Mysore[5], Javier Abadía[4], José M. Argüello[3], Hiram Castillo-Michel[6], Ana Álvarez-Fernández[4], Juan Imperial[7] and Manuel González-Guerrero[1,8]**

[1] Centro de Biotecnología y Genómica de Plantas (UPM-INIA), Universidad Politécnica de Madrid, Madrid, Spain, [2] EcoLab, Université de Toulouse, CNRS, Toulouse, France, [3] Department of Chemistry and Biochemistry, Worcester Polytechnic Institute, Worcester, MA, United States, [4] Estación Experimental de Aula Dei, Consejo Superior de Investigaciones Científicas, Zaragoza, Spain, [5] Noble Research Institute, Ardmore, OK, United States, [6] ID21 Beamline, European Synchrotron Radiation Facility, Grenoble, France, [7] Instituto de Ciencias Agrarias, Consejo Superior de Investigaciones Científicas, Madrid, Spain, [8] Escuela Técnica Superior de Ingeniería Agronómica, Alimentaria y de Biosistemas, Universidad Politécnica de Madrid, Madrid, Spain

OPEN ACCESS

Edited by:
Seçkin Eroğlu,
Middle East Technical University,
Turkey

Reviewed by:
Pierre Frendo,
University of Nice Sophia Antipolis,
France
Emre Aksoy,
Niğde Ömer Halisdemir University,
Turkey
Alexandra Lešková,
Slovak Academy of Sciences (SAS),
Slovakia

***Correspondence:**
Manuel González-Guerrero
manuel.gonzalez@upm.es

Specialty section:
This article was submitted to Plant Traffic and Transport, a section of the journal Frontiers in Plant Science

Received: 08 August 2019
Accepted: 20 December 2019
Published: 30 January 2020

Citation:
Escudero V, Abreu I, del Sastre E, Tejada-Jiménez M, Larue C, Novoa-Aponte L, Castillo-González J, Wen J, Mysore KS, Abadía J, Argüello JM, Castillo-Michel H, Álvarez-Fernández A, Imperial J and González-Guerrero M (2020) Nicotianamine Synthase 2 Is Required for Symbiotic Nitrogen Fixation in Medicago truncatula Nodules. Front. Plant Sci. 10:1780. doi: 10.3389/fpls.2019.01780

Symbiotic nitrogen fixation carried out by the interaction between legumes and diazotrophic bacteria known as rhizobia requires relatively large levels of transition metals. These elements are cofactors of many key enzymes involved in this process. Metallic micronutrients are obtained from soil by the roots and directed to sink organs by the vasculature, in a process mediated by a number of metal transporters and small organic molecules that facilitate metal delivery in the plant fluids. Among the later, nicotianamine is one of the most important. Synthesized by nicotianamine synthases (NAS), this molecule forms metal complexes participating in intracellular metal homeostasis and long-distance metal trafficking. Here we characterized the *NAS2* gene from model legume *Medicago truncatula*. MtNAS2 is located in the root vasculature and in all nodule tissues in the infection and fixation zones. Symbiotic nitrogen fixation requires of *MtNAS2* function, as indicated by the loss of nitrogenase activity in the insertional mutant *nas2-1*, phenotype reverted by reintroduction of a wild-type copy of *MtNAS2*. This would result from the altered iron distribution in *nas2-1* nodules shown with X-ray fluorescence. Moreover, iron speciation is also affected in these nodules. These data suggest a role of nicotianamine in iron delivery for symbiotic nitrogen fixation.

Keywords: iron, metal homeostasis, nicotianamine synthases, nodulation, metal nutrition

INTRODUCTION

Nitrogen is one of the main limiting nutrients in the biosphere, in spite of N_2 abundance (Smil, 1999; Hoffman et al., 2014). Nitrogenase is the only enzyme that can convert, fix, N_2 into NH_3 under physiological conditions, in an energy consuming process (Burk, 1934; Burgess and Lowe, 1996). This enzyme is only expressed by the small group of diazotrophic archaea and bacteria, some of them

participating in symbiosis with other organisms (Boyd and Peters, 2013). Arguably, one of the best characterized symbiosis with diazotrophic bacteria is the one established between rhizobia and legumes (Brewin, 1991; Downie, 2014). This symbiosis is the basis for legume use in crop rotation strategies and their potential as an alternative to polluting and expensive synthetic nitrogen fertilizers (Johnson and Mohler, 2009; Mus et al., 2016).

Symbiotic nitrogen fixation by the legume-rhizobia system is carried out in root nodules (Downie, 2014). These are differentiated organs that develop after a complex exchange of chemical signals between the symbionts (Oldroyd, 2013). Detection of the nodulation factors released by the rhizobia, triggers cell proliferation in the pericycle-inner cortex of the root to originate nodule primordia (Xiao et al., 2014). As nodules grow, rhizobia from the root surface are directed by infection threads to the nodule cells (Gage, 2002). There, they are released in an endocytic-like process, originating pseudo-organelles known as symbiosomes (Roth and Stacey, 1989; Catalano et al., 2006). Within the symbiosomes, rhizobia differentiate into bacteroids and express the enzymatic machinery required for nitrogen fixation (Kondorosi et al., 2013). Nodule development follows either an indeterminate or a determinate growth pattern, based on whether they maintain an apical meristem to sustain growth (Vasse et al., 1990). As this meristem allows for sustained growth in indeterminate nodules, four developmental zones appear: the meristematic region or zone I; the infection-differentiation zone or zone II, where rhizobia are released in the cell and start differentiating; the fixation zone or zone III, where nitrogenase is active; and the senescent zone or zone IV, where symbiosomes are degraded and nutrients recycled (Burton et al., 1998). In addition, some authors define a transition interzone between zones II and III (Roux et al., 2014).

Nutrient exchange between the symbionts enables nitrogen fixation (Udvardi and Poole, 2013). Availability of fixed nitrogen forms in soils inhibits nodulation (Streeter, 1987). Similarly, low levels of photosynthates, phosphate, or sulphate transfer from the host plant decrease nodulation and nitrogen fixation rates (Singleton and van Kessel, 1987; Valentine et al., 2017; Schneider et al., 2019). Transition metals such as iron, copper, zinc, or molybdenum are also critical for nodulation and nitrogen fixation as cofactors in many of the involved enzymes (González-Guerrero et al., 2014; González-Guerrero et al., 2016). This includes not only nitrogenase (Rubio and Ludden, 2005), but also nicotinamide adenine dinucleotide phosphate (NADPH)-oxidases that participate in nodule signaling (Montiel et al., 2016), leghemoglobin that maintains nodule O_2 homeostasis (Appleby, 1984), high-affinity cytochrome oxidases providing energy to the bacteroids (Preisig et al., 1996), as well as many enzymes involved in free radical control (Dalton et al., 1998; Santos et al., 2000; Rubio et al., 2007). Consequently, deficiencies in the uptake of these nutrients or alterations in the metal delivery pathways lead to defects in nodulation and/or nitrogen fixation (Tang et al., 1991; O'Hara, 2001; Senovilla et al., 2018; Gil-Díez et al., 2019).

To reach the bacteroids, metals must first cross from soil into the roots using the general mechanisms common to all dicots (Kobayashi and Nishizawa, 2012; Curie and Mari, 2017). Metal uptake is facilitated by soil acidification, the release of phenolics/coumarins and flavins, and cation reduction when required (Jain et al., 2014). Metals are then introduced into the root epidermis and symplastically or apoplastically reach the root endodermis, to cross into the vasculature, and delivered to sink organs. In model legume *Medicago truncatula,* metals are released from the vessels into the apoplast of the infection-differentiation zone of nodules (Rodríguez-Haas et al., 2013). These nutrients will be introduced in rhizobia-infected cells and targeted to symbiosomes for nitrogen fixation. In recent years, many of the membrane transporters participating in metal transfer from the plant to the bacteroids have been identified. For instance, iron transfer to nitrogen-fixing cells is facilitated by plasma membrane iron uptake protein MtNramp1 (Tejada-Jiménez et al., 2015), and its transport across the symbiosome membrane by MtSEN1 and MtFPN2 (Hakoyama et al., 2012, Escudero et al., 2019b). However, little is known on how metals are sorted intracellularly and on the speciation of these elements.

Unlike alkali or alkali-earth elements, transition metals are not "free," hydrated, in physiological solutions. Instead, they are bound to a plethora of organic molecules that maintain them soluble under different pH, prevent metal-catalyzed production of free radicals in Fenton-style reactions, and avoid mis-metallation of enzymes (Finney and Halloran, 2003; Rellán-Álvarez et al., 2008; Flis et al., 2016). Systematic studies of the nature of these chemical species in the sap of model plants have revealed the importance of citrate and nicotianamine in this role (von Wiren et al., 1999; Durrett et al., 2007; Roschzttardtz et al., 2011; Schuler et al., 2012). Citrate is the main iron chelator in xylem and facilitates iron delivery across symplastically disconnected tissues (Durrett et al., 2007; Rellán-Álvarez et al., 2010; Roschzttardtz et al., 2011). It has also been associated with iron trafficking to nodules (LeVier et al., 1996). Citrate efflux proteins LjMATE1 and MtMATE67 are required for iron allocation to nodules and contribute to nitrogen fixation (Takanashi et al., 2013; Kryvoruchko et al., 2018). Citrate efflux is relevant for iron delivery to bacteroids, as indicated by the symbiosome localization of nodule-specific protein MtMATE67 (Kryvoruchko et al., 2018).

Nicotianamine is also an important player in plant metal homeostasis. This molecule is a non-proteinogenic amino acid synthesized by nicotianamine synthases (NAS) from S-adenosyl methionine (Higuchi et al., 1999). Nicotianamine-metal complexes mediate long-distance metal trafficking, particularly along the phloem, as well as participate in vacuolar metal storage (von Wiren et al., 1999; Haydon et al., 2012; Flis et al., 2016). A nodule-specific NAS gene was identified in senescent nodules of *L. japonicus*, likely participating in the metal redistribution to the developing flowers and embryos, as orthologues do with older leaves (Hakoyama et al., 2009; Schuler et al., 2012). No such nodule-specific NAS gene can be found in transcriptomic databases from indeterminate type nodules, but tentative evidence shows that a *M. truncatula* NAS protein, MtNAS1, might be responsible for iron allocation to these organs (Avenhaus et al., 2016). Here, we have characterized a second

NAS protein, MtNAS2, identified in a screening of *M. truncatula Tnt1*-insertion mutants. This gene, although primarily expressed in roots, is important for metal allocation for symbiotic nitrogen fixation.

MATERIALS AND METHODS

Biological Material and Growth Conditions

M. truncatula Gaertn R108 and *nas2-1* (NF15101) seeds were scarified in concentrated sulfuric acid (96%) for 7.5 min. After removing the acid, the seeds were washed eight times with cold water, and surface-sterilized with 50% (v/v) bleach for 90 s. Seeds were embedded overnight in the dark at room temperature in sterile water, and transferred to 0.8% water-agar plates for 48 h at 4°C (stratification). Germination was carried out at 22°C in the dark. Seedlings were planted on sterile perlite pots, and inoculated with *Sinorhizobium meliloti* 2011 or the same bacterial strain transformed with pHC60 (Cheng and Walker, 1998). Plants were grown in a greenhouse under 16 h light/8 h dark at 25/20°C conditions. In the case of perlite pots, plants were watered every 2 days with Jenner's solution or water alternatively (Brito et al., 1994). Nodules were obtained at 28 dpi. Plants growing in non-symbiotic conditions were watered every 2 weeks with Jenner's solution supplemented with 20 mM NH_4NO_3. For hairy-root transformation experiments, *M. truncatula* seedlings were transformed with *Agrobacterium rhizogenes* strain ARqua1, fused to the appropriate binary vector as described (Boisson-Dernier et al., 2001). Briefly, the root tips of *M. truncatula* seedlings were removed and the wound was placed in contact with a fresh solid culture of *A. rhizogenes* ARqua1 containing the binary vector of interest. These seedlings were placed in Fahraeus medium (Fahraeus, 1957) containing 50 μg/ml kanamycin to select for transformed roots, and transferred a germination chamber at 16 h light/8 h dark at 25/20°C conditions. After 3 weeks, plants that had developed roots were placed in perlite pots and inoculated as indicated above.

Ribonucleic Acid Extraction and Quantitative Real-Time Polymerase Chain Reaction

RNA was extracted from 28 dpi plants using TRI-reagent (Life Technologies), treated using DNase turbo (Life Technologies), and cleaned with RNeasy Mini-Kit (Qiagen). Complementary DNA (cDNA) was obtained from 500 ng RNA using PrimeScript RT reagent Kit (Takara). Expression studies were carried out by real-time reverse transcription polymerase chain reaction (RT-qPCR; StepOne plus, Applied Biosystems) using the Power SyBR Green Master Mix (Applied Biosystems). The primers used are indicated in **Supplementary Table 2**. cDNA levels were normalized by using the ubiquitin conjugating enzyme E2 (*Medtr7g116940*) gene as internal standard. Real time cycler conditions have been previously described (González-Guerrero et al., 2010). Expression levels were determined in three independent experiments with four pooled plants.

β-Glucuronidase Staining

MtNAS2 promoter region was obtained by amplifying the 1,940 bp upstream of the start codon using the primers indicated in **Supplementary Table 2**, and cloned by Gateway Cloning Technology (Invitrogen) in pDONR207 (Invitrogen) and transferred to destination vector pGWB3 (Nakagawa et al., 2007). Hairy-root transformations of *M. truncatula* seedlings were carried out with *A. rhizogenes* ARqua1 as described by Boisson-Dernier et al. (2001). After 3 weeks on Fahraeus media plates with kanamycin (50 μg/ml), plant transformants were transferred to sterilized perlite pots and inoculated with *S. meliloti* 2011. GUS activity was determined in 28 dpi plants as described (Vernoud et al., 1999). Whole nodule and root images were taken with a Leica MZ10F dissecting microscope using the Leica AF software. Some nodules and roots were embedded in 6% agarose and sectioned in 100 μm slides using a Vibratome 1000 Plus. These sections were observed in a Zeiss Axiophot microscope using the Leica AF software.

Immunolocalization and Imaging

The coding sequence region of *MtNAS2* and 1,940 bp upstream of its start codon were cloned in pGWB13 vector (Nakagawa et al., 2007) using Gateway Cloning Technology (Invitrogen). This fuses three HA epitopes to C-terminus of the protein. Hairy-root *M. truncatula* transformants were transferred to sterilized perlite pots and inoculated with *S. meliloti* 2011 containing the pHC60 plasmid that constitutively expresses GFP. Nodules and roots were collected from 28 dpi plants and fixed at 4°C overnight in 4% para-formaldehyde and 2.5% sucrose in phosphate-buffered saline (PBS). Fixative was removed by washing for 5 min in PBS and 5 min in water. Nodule and roots were included in 6% agarose for sectioning with a Vibratome 1000 Plus. Sections were dehydrated by serial incubation with methanol (30, 50, 70, and 100% in PBS) for 5 min and then rehydrated following the same methanol series in reverse order. Cell wall permeabilization was carried out by incubation with 2% (w/v) cellulase in PBS for 1 h and 0.1% (v/v) Tween 20 for 15 min. Sections were blocked with 5% (w/v) bovine serum albumin in PBS and then incubated with 1:50 anti-HA mouse monoclonal antibody (Sigma) in PBS at room temperature for 2 h. Primary antibody was washed three times with PBS for 15 min and subsequently incubated with 1:40 Alexa 594-conjugated anti-mouse rabbit monoclonal antibody (Sigma) in PBS at room temperature for 1 h. Secondary antibody was washed three times with PBS for 10 min. DNA was stained using 4′,6-diamidino-2-phenylindol (DAPI). Images were obtained with a confocal laser-scanning microscope (Leica SP8) using excitation light at 488 nm to GFP and 561 nm for Alexa 594, collecting the emission at 500–554 nm for GFP and at 597-654 for Alexa594.

Acetylene Reduction Assays

Nitrogenase activity assay was measured by acetylene reduction test (Hardy et al., 1968). Wild-type and *nas2-1* nodulated roots from 28 dpi were separately introduced in 30 ml vials. Each tube contained four or five independently transformed plants. Three milliliters of

air from each bottle was replaced by the same volume of acetylene, tubes were subsequently incubated for 30 min at room temperature. Gas samples were measured by analyzing 0.5 ml of ethylene from each bottle in a Shimadzu GC-8A gas chromatograph using a Porapak N column. The amount of the ethylene produced was determined by measuring the ethylene peaks relative to the standards. Acetylene reduction was measured in duplicate from three sets of three-four pooled plants.

Chlorophyll Content Assays

Total chlorophyll content was determined as previously described with some modifications (Inskeep and Bloom, 1985). Leaves were collected from 28 dpi plants and poled to obtain 50 mg of fresh material. Chlorophyll was extracted with 500 µl of dimethyl-formamide at 4°C overnight. Leaves were centrifuged for 5 min at 600 g at room temperature. After transferring the supernatant to another vial, the chlorophyll extraction was repeated with the same leave using strong vortexing. After spinning for 5 min at 600 g, the supernatant was pooled with the previous one. Chlorophyll was quantified at 647 and 664 nm in a Ultrospec 3300 Spectrophotometer (Amersham Bioscience). Data are the mean ± SE of three sets of five pooled plants.

Metal Content Determination

Shoots, roots, and nodules were collected from 28 dpi plants and mineralized with 15.6 M HNO_3 (trace metal grade) at 75°C for 3 h and 2 M H_2O_2 at 20°C overnight. Metal quantifications were performed in duplicate by Atomic Absorption Spectroscopy, using a Perkin Elmer PinAAcle 900Z GF-AAS equipment. Metal concentration was normalized against fresh tissue weight. Three sets of three-four pooled organs were analyzed.

Synchrotron Radiation X-Ray Fluorescence Spectroscopy and X-Ray Absorption Near-Edge Spectroscopy

X-ray fluorescence spectroscopy (XRF) hyperspectral images and µXANES spectra were acquired on the beamline ID21 of the European Synchrotron Radiation Facility (Cotte et al., 2017), at 110 K in the liquid nitrogen (LN2) cooled cryostat of the Scanning X-ray Micro-spectroscopy end-station. Seven sections from *M. truncatula* R108 nodules and five from *nas2-1* nodules were obtained from independent nodules embedded in optimal cutting temperature (OCT) medium and cryo-fixed by plunging in isopentane chilled with LN2. The 25 µm-thick sections of frozen samples were obtained using a Leica LN2 cryo-microtome and accommodated in a Cu sample holder cooled with LN2, sandwiched between Ultralene (SPEX SamplePrep) foils. The beam was focused to 0.4×0.9 μm^2 with a Kirkpatrick-Baez (KB) mirror system. The emitted fluorescence signal was detected with energy-dispersive, large area (80 mm^2) SDD detector equipped with Be window (SGX from RaySpec). Images were acquired at the fixed energy of 7.2 keV, by raster-scanning the sample in the X-ray focal plane, with a step of 3×3 μm^2 and 100 ms dwell time. Elemental mass fractions were calculated from fundamental parameters with the PyMCA software package, applying pixel-by-pixel spectral deconvolution to hyperspectral maps normalized by the incoming flux (Solé et al., 2007). The incoming flux was monitored using a drilled photodiode previously calibrated by varying the photon flux at 7.2 keV obtaining a response of 1,927.9 charges/photon with a linear response up to 200 kcps. In PyMCA the incoming flux and XRF detector parameters were set to $2x10^9$ photons/s, 0.7746 cm^2 active area, and 4.65 cm sample to XRF detector distance. Sample matrix was assumed to be amorphous ice (11% H, 89% O, density 0.92 g/cm^3), the sample thickness set at 25 µm obtained with the use of a cryo-microtome. Iron average mass fraction values from pixels in zone III and apical region from three wild type and three *nas2-1* nodule samples were obtained using a mask tool that removes pixels with mass fractions below a threshold of $2\ 10^{-6}$ µg iron.

Fe-K edge (7.050 to 7.165 keV energy range, 0.5 eV step) µXANES spectra were recorded in regions of interest of the fluorescence maps acquired on ID21 beamline. Individual spectra were processed using Orange software with the Spectroscopy add-on (Demsar et al., 2013). The pre-processing step consisted of vector normalization and a Savitzky-Golay filter for the smoothing. Then a principal component analysis was performed on the second derivative of the spectra to highlight potential differences among genotypes within a given region of the nodule. A reference library was used for linear combination fitting (LCF) procedure. This library consisted of: Fe-foil [Fe(0)], Fe(II)-nicotianamine, Fe(II)S2 (http://ixs.iit.edu/database/), Fe(III)-haem (50 mM, pH7, bought from Sigma, CAS number: 16009-13-5), Fe(III)-cellulose (5 mM $FeCl_3$ + 50 mM cellulose, pH 5.8, bought from Sigma, CAS number: 9004-34-6), Fe(III) glutamic acid (5 mM $FeCl_3$ + 50 mM glutamic acid, pH 7, bought from Sigma, CAS number: 56-86-0), and Fe(III) ferritin (bought from Sigma, CAS number: 9007-73-2, 50 mM, pH7).Reference compounds were classified as Fe(II)-S (FeS2), Fe (II)-O/N (Fe-NA) and Fe(III)-O (Fe-cellulose, Fe-glutamic acid, and ferritin). XANES data treatment was performed using Athena software (Ravel and Newville, 2005) as previously described (Larue et al., 2014).

Statistical Tests

GraphPad Prism was used for the statistical analyses. Data were analyzed by ANOVA to test the differences between wild type, mutant and complemented *M. truncatula* plants. Tukey's or Student's *t* tests were used to calculate statistical significance of observed differences. Test results with p-values < 0.05 were considered as statistically significant

For nodule structure analysis and nicotianamine concentration determination see **Supplementary Materials** and Methods.

RESULTS

Medicago truncatula Tnt1 Line NF15101 Phenotype Is Due to Transposon Insertion in *MtNAS2*

A search for metal-related symbiotic phenotypes of the mutants available at the Noble Research Institute LLC *M. truncatula*

Mutant Database (Sun et al., 2019; https://medicago-mutant.noble.org/mutant/index.php) showed NF15101 as one of the available mutants with a nitrogen fixation deficient phenotype. This line has 22 *Tnt1* insertions, 10 of which interrupted different *M. truncatula* genes (**Supplementary Table 1**), *Medtr2g070310* among them. This gene encodes a protein with 52% identity and 67% similarity to *Arabidopsis thaliana* NAS2 protein, and consequently was renamed *MtNAS2*. *MtNAS2* was expressed at similar levels in roots from plants inoculated or non-inoculated with *S. meliloti* (**Figure 1A**). Significantly, lower expression was observed in nodules, and no signal was detected in shoots from either inoculated or non-inoculated plants. *Tnt1* was inserted in position +760 of *MtNAS2* (**Figure 1B**), interrupting the reading frame of its only exon. Homozygous plants from a R2 seed population were identified by a PCR reverse screening (Cheng et al., 2014). These homozygous plants were considered as null mutants for *MtNAS2*, since *MtNAS2* expression levels were below our detection limit (**Figure 1C**). As expected, NF15101, *nas2-1* in this report, had reduced biomass production in nitrogen fixation conditions (**Figures 2A, B**). While nodule development and nodule number were not significantly altered in *nas2-1* compared to wild type (**Figures 2C, D**, **Supplementary Figure 1**), nitrogenase activity was reduced three-fold in *nas2-1* plants (**Figure 2E**). No significant differences in nicotianamine concentration were observed between wild-type and mutant plants (**Supplementary Figure 2**). The *nas2-1* phenotype was reverted when a wild-type copy of *MtNAS2* regulated by its own promoter was reintroduced in *nas2-1* (**Figure 2**). No significant changes in nitrogenase activity were observed either when iron and/or zinc were removed from the nutrient solution or when they were added at higher concentrations (**Supplementary Figure 3**) The data indicate that among all the *Tnt1* insertions, loss of *MtNAS2* function was determinant for the reduction of nitrogenase activity and overall growth alterations.

MtNAS2 Is Not Required for Plant Growth Under Non-Symbiotic Conditions

To determine whether the symbiotic phenotype of *nas2-1* was the result of additional physiological processes being affected, these plants and their controls were grown in the same conditions as above, but supplemented with ammonium nitrate in the nutrient solution to compensate for the lack of rhizobial inoculation. In these conditions, no significant differences were found in plant growth, biomass production, or chlorophyll content between wild-type and *nas2-1* plants (**Figure 3**). Considering the role of nicotianamine in plant iron homeostasis (von Wiren et al., 1999; Inoue et al., 2003) and the added pressure of symbiotic nitrogen fixation on iron nutrition (Terry et al., 1991), *nas2-1* phenotype was also studied under non-symbiotic, low-iron conditions (no iron added to the nutrient solution). Low-iron supply did not lead to different growth between control and *nas2-1* plants (**Supplementary Figure 4**).

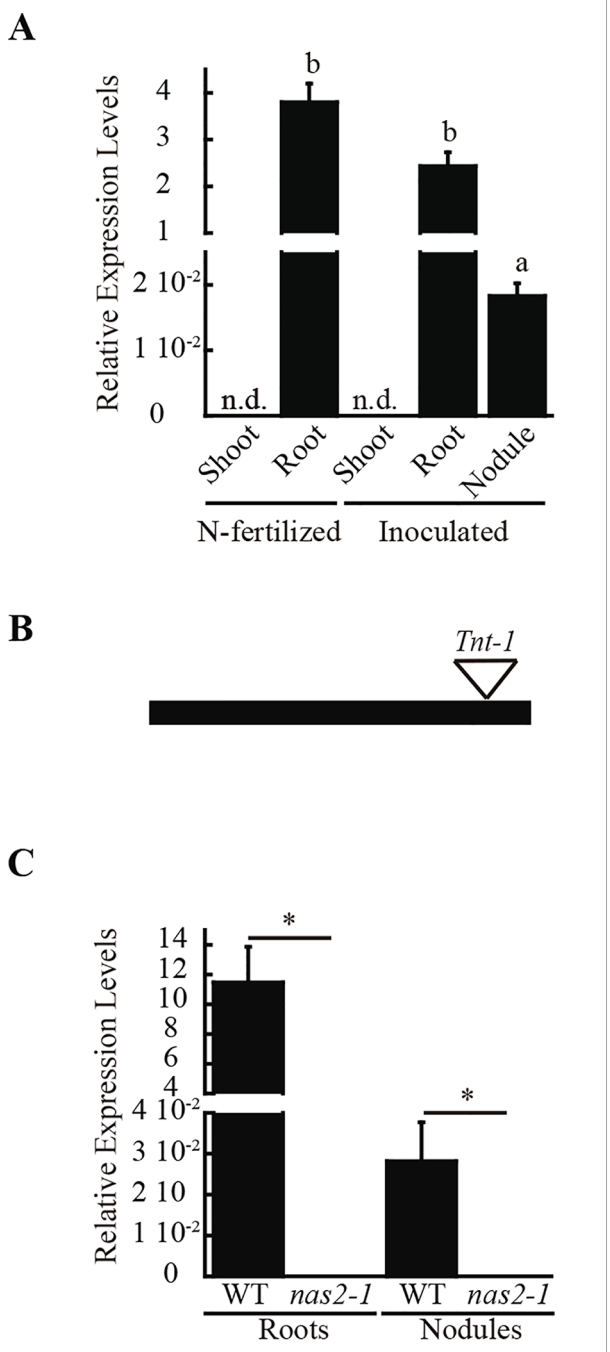

FIGURE 1 | *MtNAS2* is expressed in roots and nodules of *M. truncatula*. **(A)** Expression data was normalized to the expression of ubiquitin conjugating enzyme E2 gene (*Medtr7g116940*) as standard. Data are the mean ± SE of three independent experiments with 4 pooled plants. Different letters indicate statistical differences at P > 0.05 (Tukey t-test). **(B)** *Tnt1* insertion in the only exon of MtNAS2 causes loss of *MtNAS2* transcripts. **(C)** MtNAS2 expression was determined in 28 dpi roots and nodules of wild-type (WT) and nas2-1 plants. Data was relativized to the expression of ubiquitin conjugating enzyme E2 (*Medtr7g116940*) and expressed as mean ± SE of three independent experiments with 4 pooled plants. *indicates statistical differences at P > 0.05 (Student t-test).

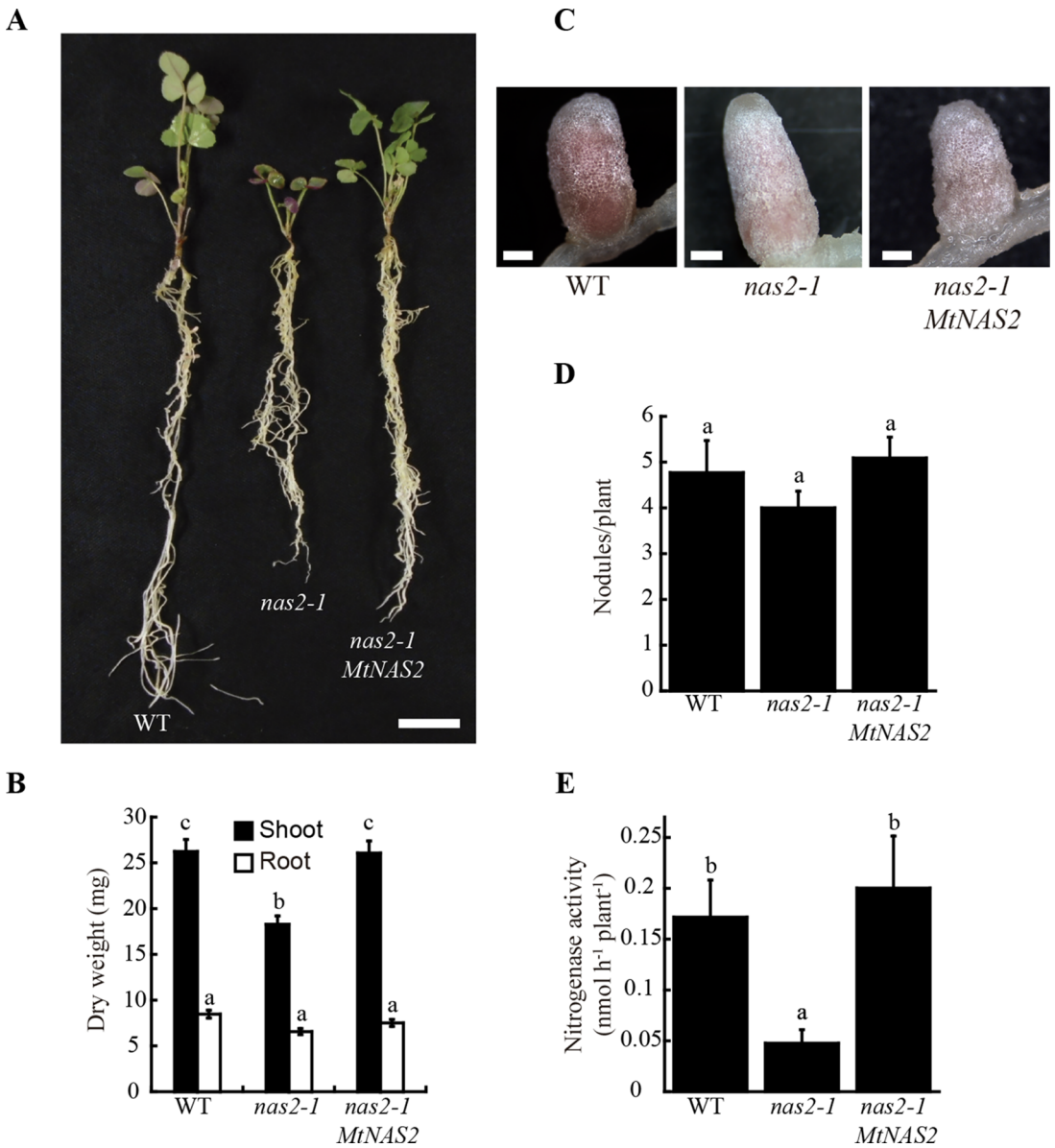

FIGURE 2 | *MtNAS2* is required for nitrogen fixation. **(A)** Growth of representative wild-type (WT), *nas2-1*, and *nas2-1* plants transformed with *MtNAS2* controlled by its own promoter (*nas2-1 MtNAS2*). Bar = 1.5 cm. **(B)** Dry weight of WT, *nas2-1*, and *nas2-1 MtNAS2* plants. Data are the mean ± SE of at least 9 transformed plants. **(C)** Detail of representative nodules of WT, *nas2-1*, and *nas2-1 MtNAS2* plants (n = 40–50 nodules). Bars = 500 μm. **(D)** Number of nodules in 28 dpi WT, *nas2-1*, and *nas2-1 MtNAS2* plants. Data are the mean ± SE of at least nine transformed plants. Different letters indicate statistical differences at $P < 0.05$ (Tukey t-test). **(E)** Nitrogenase activity in 28 dpi nodules from WT, *nas2-1*, and *nas2-1 MtNAS2* plants. Acetylene reduction was measured in duplicate from three sets of three-four pooled plants. Data are the mean ± SE. Different letters indicate statistical differences at $P < 0.05$ (Tukey t-test).

MtNAS2 Is Expressed in the Xylem Parenchyma in Roots and in the Nodule Differentiation and Fixation Zones

The physiological role of *MtNAS2* is determined by its differential tissue and cellular expression. To establish the gene tissue expression, *M. truncatula* plants were transformed with a binary vector containing the *MtNAS2* promoter region driving the *β-glucuronidase* (*gus*) gene transcription and GUS activity visualized using X-Gluc. *MtNAS2* was expressed in roots and nodules (**Figure 4A**), in agreement with the transcript data (**Figure 1**). Longitudinal section of the nodules showed GUS activity in cells from the late zone II to the fixation zone of the nodule (**Figure 4B**). Nodule cross-sections showed expression in all nodule tissues (**Figure 4C**). In roots, *MtNAS2* promoter was active in vasculature cells (**Figure 4D**).

Supporting the gene expression results, immunolocalization of HA-tagged MtNAS2 under control of its own promoter showed that the protein was located in cells neighboring the

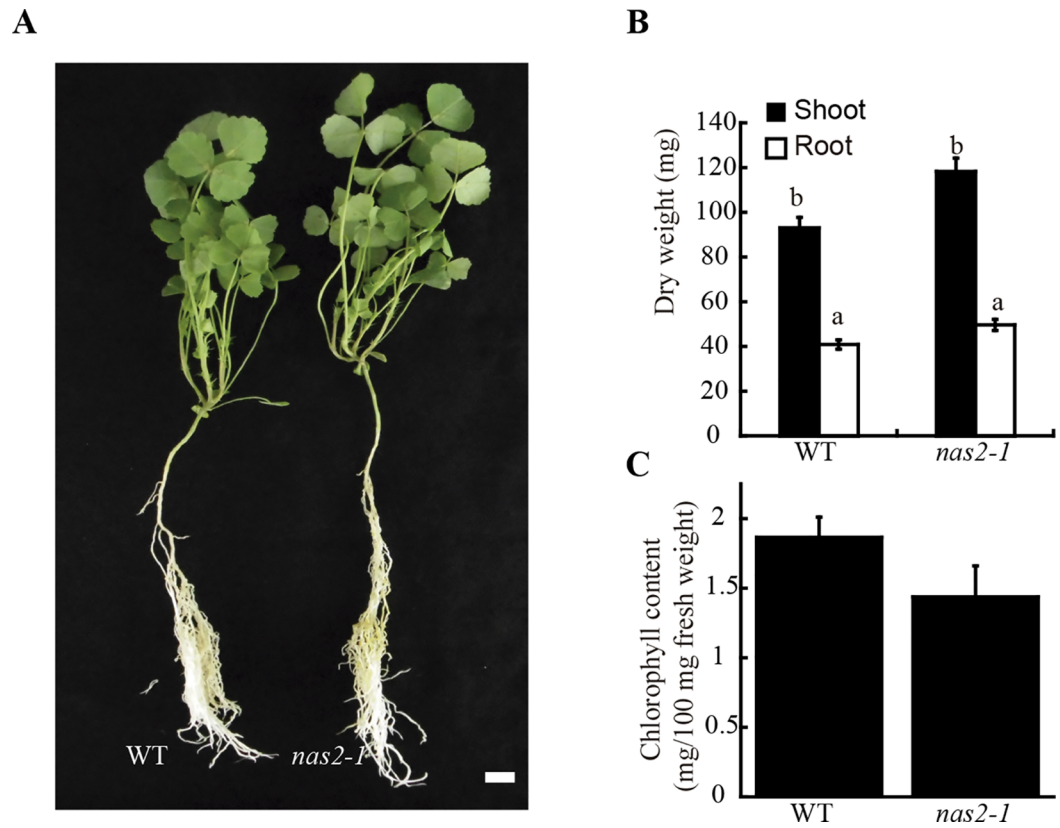

FIGURE 3 | *MtNAS2* is not required for plant growth under non-symbiotic conditions. **(A)** Growth of representative wild-type (WT) and *nas2-1* plants when watered with a nutrient solution supplemented with ammonium nitrate and not inoculated with *Sinorhizobium meliloti* (n = 10–15 plants). Bar = 1.5 cm. **(B)** Dry weight of WT and *nas2-1* plants. Data are the mean ± SE (n = 10 plants). Different letters indicate statistical differences at $P < 0.05$ (Tukey t-test). **(C)** Chlorophyll concentration of wild-type and *nas2-1* plants. Data are the mean ± SE of three sets of five pooled plants. No differences at $P < 0.05$ were observed (Student t-test).

late zone II, interzone, and fixation zone (**Figure 5A**). At higher magnification, we could observe that MtNAS2-HA had a homogenous distribution within the cells, and it did not seem to cluster in any particular location (**Figure 5B**). Analysis of nodule vasculature showed MtNAS2-HA in endodermal cells (**Figure 5C**). However, in the root vasculature, MtNAS2-HA was detected at the center of the root, in the region comprised between the endodermis and the xylem (**Figure 5D**). At higher magnification, the root MtNAS2-HA signal was detected in small cells associated to the xylem (**Supplementary Figure 5**). Controls were carried out to ensure that the data did not stem from autofluorescence (**Supplementary Figure 6**). In addition, the antibodies used for immunolocalization do not cross react with *M. truncatula* proteins (Tejada-Jiménez et al., 2015).

MtNAS2 Is Required for Efficient Metal Allocation for Symbiotic Nitrogen Fixation

Nicotianamine is required for metal allocation from source to sink tissues (Schuler et al., 2012). Alterations in nicotianamine synthesis typically lead to reduced metal delivery to sink tissues. To determine whether this was the case for *nas2-1*, iron, copper, and zinc levels in roots, shoots, and nodules from 28 days-post-inoculation (dpi) plants were determined. No significant changes in these levels were observed (**Figure 6A**). However, metal allocation might be altered while not affecting total nodule metal content. To assess this possibility, synchrotron-based X-ray fluorescence studies were carried out to determine iron distribution in *nas2-1* compared to wild type (**Figure 6B**). These experiments showed that iron distribution was altered in *nas2-1* mutants, which presented a lower percentage of iron in the fixation zone than wild type nodules (**Figure 6C**). To further confirm that mutation of *MtNAS2* affected iron distribution in nodules as a consequence of changes of iron speciation, X-ray Absorption Near-Edge Spectroscopy (XANES) analyses of iron speciation in the different nodule developmental zones were carried out (**Figure 6D**). Principal component analyses of these spectra showed that the iron complexes in the fixation zone were quite different (**Figure 6E**). Fitting of the obtained spectra to known standards showed that the proportion of Fe-S complexes had a dramatic drop in *nas2-1* compared to wild-type plants, while the proportion of O/N complexes with iron had a larger increase (**Table 1**).

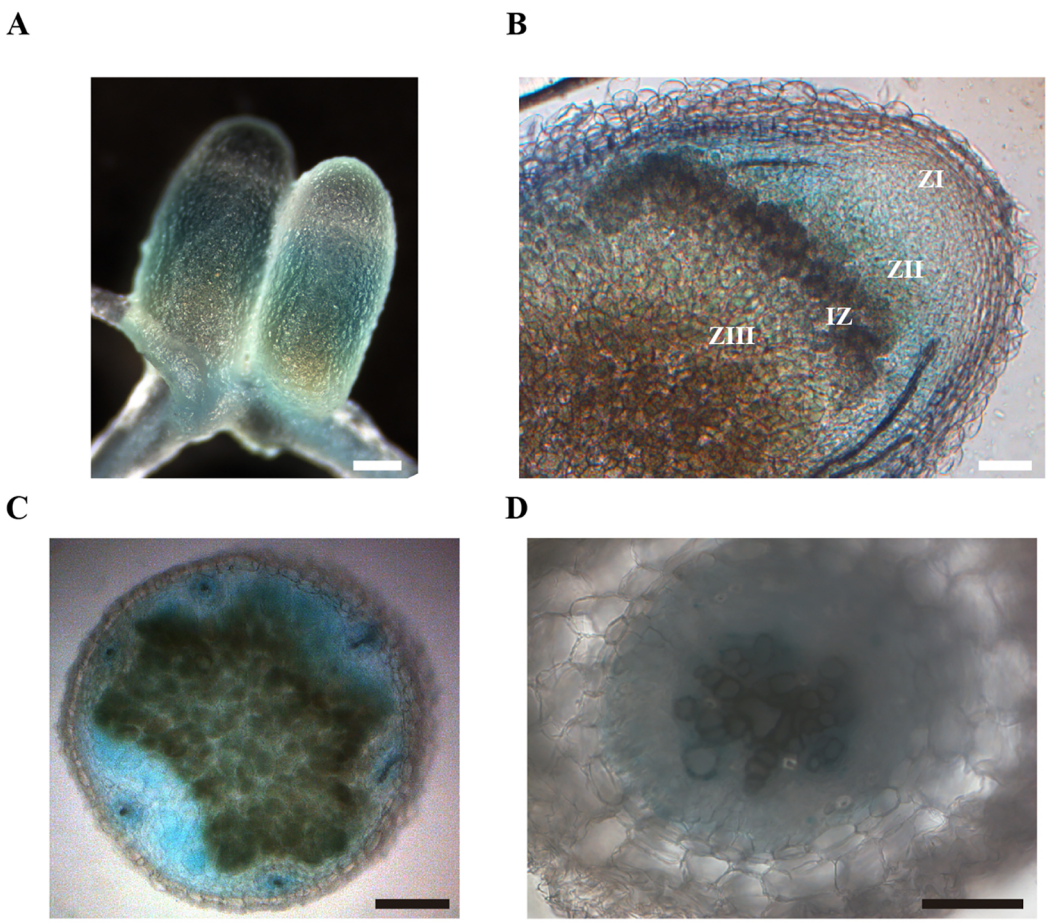

FIGURE 4 | *MtNAS2* is expressed in the root vasculature and in the late zone II, interzone, zone III, and vessels in nodules. **(A)** β-glucuronidase (GUS) staining of 28 dpi *Medicago truncatula* roots and nodules expressing the *gus* gene under the control of *MtNAS2* promoter region (n = 10–20 plants). Bar = 100 μm. **(B)** Longitudinal section of a GUS-stained 28 dpi *M. truncatula* nodule expressing the *gus* gene under the control of *MtNAS2* promoter region (n = 30 sections from 10 to 20 plants). ZI indicates zone I; ZII, zone II; IZ, interzone; and ZIII, zone III. Bar = 100 μm. **(C)** Cross section of the fixation zone of a GUS-stained 28 dpi *M. truncatula* nodule expressing the *gus* gene under the control of *MtNAS2* promoter region (n = 30 sections from 10 to 20 plants). Bar = 200 μm. **(D)** Cross section of a GUS-stained 28 dpi *M. truncatula* root expressing the *gus* gene under the control of *MtNAS2* promoter region (n = 30 sections from 10 to 20 plants). Bar = 100 μm.

DISCUSSION

Metallic micronutrient delivery to nodules is essential for symbiotic nitrogen fixation, as they are cofactors in many of the involved enzymes (Brear et al., 2013; González-Guerrero et al., 2014). In recent years, studies have shown how metals are exported to the apoplast in the infection/differentiation zone of *M. truncatula* nodules (Rodríguez-Haas et al., 2013), and transmembrane transporters introduce metals into rhizobia-infected cells (Tejada-Jiménez et al., 2015; Abreu et al., 2017; Tejada-Jiménez et al., 2017; Senovilla et al., 2018), or deliver iron to the bacteroids (Escudero et al., 2019b). In this transport, citrate participates in maintaining iron solubility in the apoplast, and as the preferred iron source for bacteroids (Moreau et al., 1995; LeVier et al., 1996; Kryvoruchko et al., 2018). Here we show that nicotianamine synthesis is also important for correct iron allocation to *M. truncatula* nodules.

Interrupting *MtNAS2* expression with a transposon insertion led to reduced plant growth in symbiotic conditions, a consequence of lower nitrogenase activity. Although several genes were affected in the studied *Tnt1* line, reintroduction of a wild-type copy of *MtNAS2* was sufficient to restore wild-type growth. Consequently, the mutation of this gene was mainly responsible for the observed phenotype. While important under symbiotic conditions, *MtNAS2* seemed to be playing a secondary role when plants were not inoculated but watered with an ammonium nitrate-supplemented nutrient solution instead. This is in contrast to the substantially higher expression levels of *MtNAS2* in roots than in nodules. This observation would suggest a predominant role in nicotianamine synthesis in roots. However, studies in *A. thaliana* reveal the existence of a high redundancy rate in the NAS family, where a quadruple *nas* mutant was required to observe a substantial phenotype, including limited growth (Klatte et al., 2009). Similarly, no

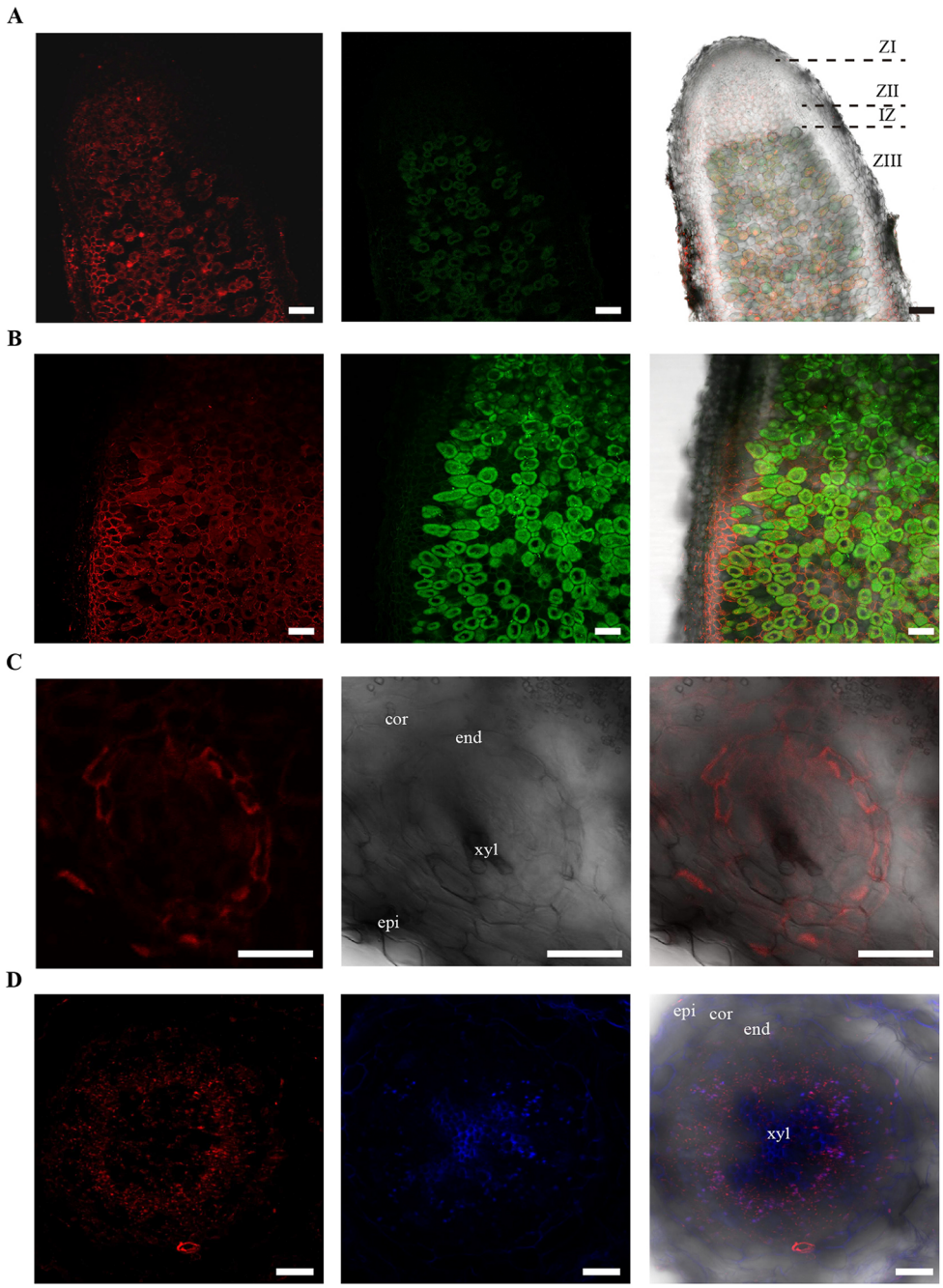

FIGURE 5 | MtNAS2 is located in the nodule core cells, in the endodermis of the nodule vessels, and in cells surrounding the xylem in the root vasculature. **(A)** Longitudinal section of a 28 dpi *M. truncatula* nodule expressing *MtNAS2-HA* under its own promoter (n = 30 sections from 10 to 20 plants). The three C-terminal HA epitopes were detected using an Alexa594-conjugated antibody (red, left panel). Transformed plants were inoculated with a GFP-expressing *Sinorhizobium meliloti* (green, middle panel). Both images were overlaid with the transillumination image (right panel). ZI indicates zone I; ZII, zone II; IZ, interzone; and ZIII, zone III. Bars = 100 μm. **(B)** Detail of the zone III of a 28 dpi *M. truncatula* nodule expressing *MtNAS2-HA* under its own promoter. Left panel corresponds to the Alexa594 signal used to detect the HA-tag, middle panel corresponds to the GFP channel showing *S. meliloti*, and the two were overlaid with the bright field channel in the right panel (n = 30 sections from 10 to 20 plants). Bars = 50 μm **(C)** Cross section of a nodule vessel from a 28 dpi *M. truncatula* nodule expressing *MtNAS2-HA* under its own promoter. Left panel corresponds to the Alexa594 signal used to detect the HA-tag, middle panel corresponds to the bright field channel, and the two were overlaid in the right panel (n = 30 sections from 10 to 20 plants). epi indicates nodule epidermis; cor, nodule cortex; end, nodule vascular endodermis; and xyl, nodule vascular xylem. Bars = 50 μm. **(D)** Cross section from a 28 dpi *M. truncatula* root expressing *MtNAS2-HA* under its own promoter. Left panel corresponds to the Alexa594 signal used to detect the HA-tag, middle panel corresponds to autofluorescence signal of xylem, and the two were overlaid with the bright field channel in the right panel (n = 30 sections from 10 to 20 plants). epi indicates root epidermis; cor, root cortex; end, root endodermis; and xyl, xylem. Bars = 100 μm.

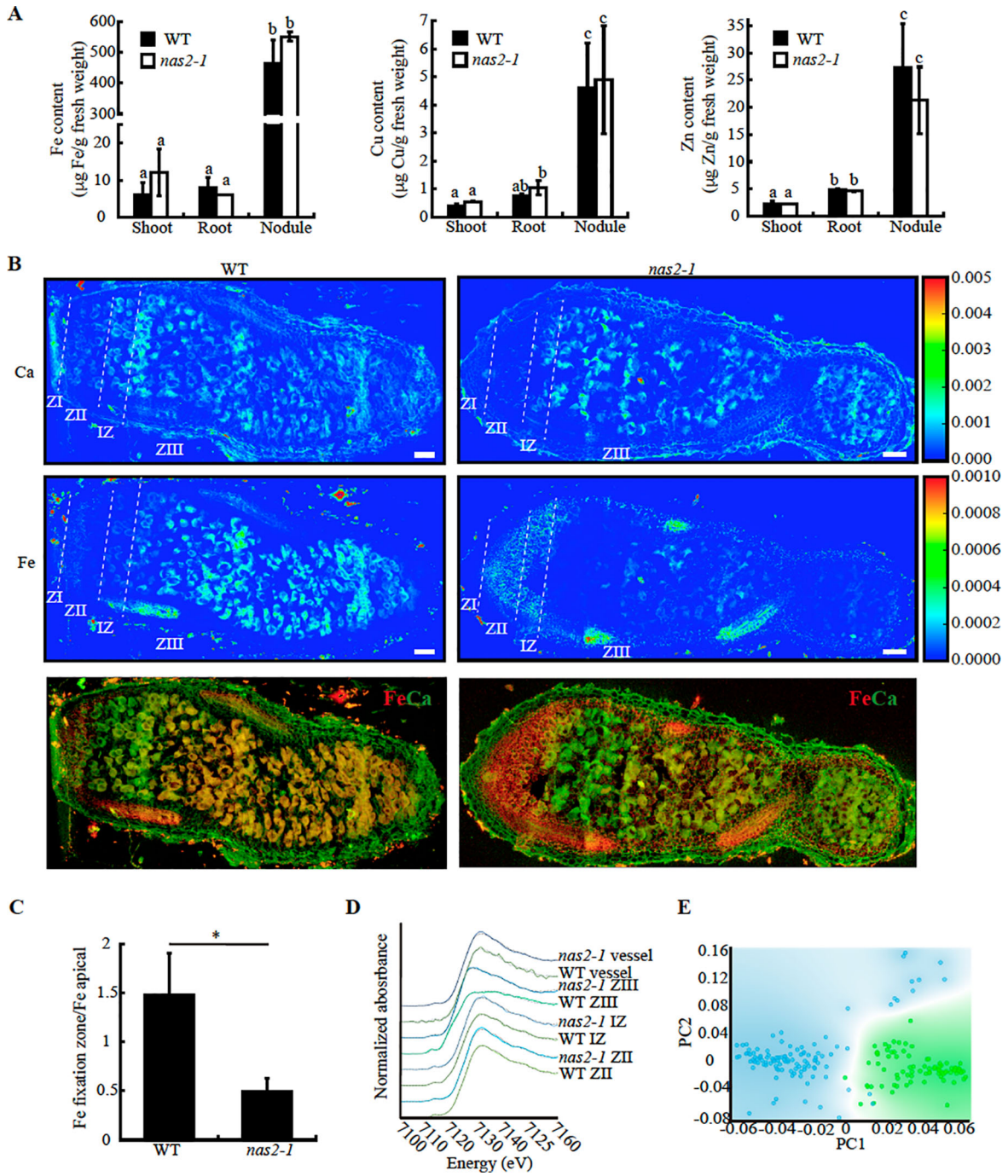

FIGURE 6 | *MtNAS2* is required for iron distribution and speciation in nodules. **(A)** Iron (left panel), copper (middle panel), and zinc (right panel) concentration in shoots, roots, and nodules from 28 dpi wild-type (WT) and *nas2-1* plants. Data are the mean ± SE of three sets of three-four pooled organs. Different letters indicate statistical differences at $P < 0.05$ (Tukey t-test). **(B)** Synchrotron-based X-ray fluorescence images of WT (left panels) or *nas2-1* (right panels) showing calcium (top panels) or iron (center panels) distribution in 28 dpi nodules. Lower panels are the overlaid iron and calcium distribution (iron is indicated in red and calcium in green). ZI indicates zone I; ZII, zone II; IZ, interzone; and ZIII, zone III (n = 5–7 nodules). Bars = 100 µm. **(C)** Iron content in fixation zone relative to the apical zone in wild type and *nas2-1* nodules. Data are the mean ± SE (n = 3). * indicates statistical differences at $P < 0.05$ (Student t-test). **(D)** XANES spectra obtained from different regions of WT and *nas2-1* nodules. **(E)** Decomposition of the zone III signal into its two principal components.

TABLE 1 | Iron speciation (%) in wild type (WT) and *nas2-1* nodules. n.d., not detected.

Region	WT				*nas2-1*			
	Fe(II)-S	Fe(II)-O/N	Fe(III)-O	R^2	Fe(II)-S	Fe(II)-O/N	Fe(III)-O	R^2
ZII	4	12	83	00004	n.d.	14	86	0.0008
IZ	13	19	69	0.0004	5	17	78	0.0006
ZIII	50	24	27	0.001	14	49	37	0.0005
Vessels	n.d.	22	79	0.0008	n.d.	22	78	0.001

significant changes in nicotianamine content were observed in single *nas A. thaliana* lines, as neither was observed in *M. truncatula nas2-1*. Two possible causes might explain the symbiosis-specific phenotype of *nas2-1* plants. One of them is that MtNAS2 would be required to compensate for the enhanced iron requirements of nodulated plants. This additional nutritional pressure would trigger the observed *nas2-1* phenotype. If so, we should have also observed a similar phenotype when plants were watered with an iron-restricted nutrient solution, which has been shown in the past to elicit the iron deficiency response in *M. truncatula* (Andaluz et al., 2009; Tejada-Jiménez et al., 2015). However, this was not observed. Alternatively, in a more parsimonious mechanism, neofunctionalization of pre-existing genes during the development of symbiotic nitrogen fixation might have led to the loss of functional redundancy. Similar observations have been made when studying other *M. truncatula* metal homeostasis genes that, although expressed in roots and in nodules, exhibit phenotypes limited to nodulation and nitrogen fixation (Tejada-Jiménez et al., 2015; Abreu et al., 2017; León-Mediavilla et al., 2018).

In roots, *MtNAS2* was expressed at high levels in xylem parenchyma cells, similarly to rice *NAS2* (Inoue et al., 2003). Vascular localization of NAS proteins is not unusual, since they have been associated to long distance metal trafficking (von Wiren et al., 1999; Kumar et al., 2017). In nodules, MtNAS2 was also associated to the vessels. However, the cellular localization of the protein is different to what was observed in roots; in nodules, most of vascular MtNAS2 was confined to the endodermis. This alternative distribution of MtNAS2 in vessels could be indicative of differential functions. Root vascular localization could indicate a role in metal loading of the vascular fluids, while endodermal localization in nodules might mediate either uptake from saps or intracellular metal trafficking. In any case, it seems unlikely that the nicotianamine synthesized by nodule endodermal cells would end up in the apoplast, since citrate-iron complexes seem to be formed in this compartment at a pH that does not facilitate iron-nicotianamine association (Rellán-Álvarez et al., 2008).

MtNAS2 expression in nodule core cells in the late zone II, interzone, and zone III also indicates a role of nicotianamine in metal homeostasis of nitrogen fixing cells. It has been previously described that nicotianamine can participate in intracellular metal trafficking and in cell-to-cell metal delivery, as well as serve as intracellular storage of metals (Haydon et al., 2012). Mutation of *MtNAS2* did not significantly alter iron, copper, or zinc levels in any of the plant organs analyzed, but a major shift in iron distribution was observed in nodules, with a significant decrease of iron accumulation in the interzone and early fixation zone. This would indicate that iron trafficking in these cells is altered. However, MtNAS2-mediated iron trafficking would only affect a subset of the nodule iron-proteome, since delivery to the fixation zone was not completely blocked as attested by the red color of nodules, indicative that leghemoglobin (an important iron sink) was being produced in addition to a residual nitrogenase activity. This could suggest the existence of differential metalation pathways in nodules that might serve different subsets of proteins, which could partially complement each other under stress conditions. Supporting this hypothesis, mutation of *MtNAS2* did not equally affect all the iron species in the fixation zone. While the percentage of iron-sulfur complexes detected by XANES was significantly lower than in control plants, iron coordinated by nitrogen or oxygen atoms was increased. Considering the high demand for iron-sulfur clusters for nitrogenase assembly (Rubio and Ludden, 2005), its decrease could explain the reduction of nitrogenase activity observed. The changes in iron speciation were particularly severe in the fixation zone, which is consistent with *MtNAS2* distribution, with the observed reduction of nitrogenase activity, and with the iron distribution data. It is important to indicate that we cannot rule out similar effects on copper or zinc speciation and distribution, since the synchrotron setup available to us at the European Synchrotron Radiation Facility prevented us to carry out similar analyses on those two elements.

This work highlights the importance of MtNAS2 in iron delivery for symbiotic nitrogen fixation. This is not the only NAS gene that might be involved in the process, since total nicotianamine production is sustained in nodules, and other family members have been shown to be expressed in these organs, such as *MtNAS1* (Avenhaus et al., 2016) or *MtNAS3* (*Medtr7g112130*) according to the Symbimics database (Roux et al., 2014). However, no *MtNAS4* (*Medtr2g034240*) expression in roots or nodules is reported in this database. The localization of MtNAS2 indicates that nicotianamine would be involved in intracellular iron trafficking that is highly important for nitrogenase functioning. This role would not be directly providing the element to the bacteroid, since iron-citrate seems to be the key here, but perhaps would shuttle this element in the cytosol. However, to better define this possibility, new tools in elemental imaging and speciation with higher resolution within a cell need to be established to track iron and other elements. In addition, the roles of zinc-induced facilitator (ZIF)-like (Haydon et al., 2012) and yellow stripe-like (YSL) proteins (Waters et al., 2006) in symbiotic nitrogen fixation must be determined. Finally,

other NAS proteins might facilitate iron recycling in *M. truncatula* nodules, as it occurs in *L. japonicus* (Hakoyama et al., 2009).

DATA AVAILABILITY STATEMENT

All datasets generated for this study are included in the article/ **Supplementary Material**.

AUTHOR CONTRIBUTIONS

VE carried out most of the experimental work. IA, CL, and HC-M carried out the synchrotron-based work. IA, JC-G, JA, and AÁ-F were responsible for the nicotianamine content determination. ES performed the phenotypic analyses under changing metal concentrations and participated in the complementation assays. MT-J carried out the initial expression analyses. JW and KM obtained the *nas2-1* mutant. LN-A and JMA determined metal concentrations. JI and MG-G were responsible for experimental design, data analyses, and wrote the manuscript with contributions from all authors.

FUNDING

This research was funded by a European Research Council Starting Grant (ERC-2013-StG-335284) and a Ministerio de Economía y Competitividad (MINECO) grant (AGL2015-65866-P), to MG-G, and a MINECO grant (AGL2016-75226-R) to JA and AÁ-F. VE was partially funded by the Severo Ochoa Programme for Centres of Excellence in R&D from Agencia Estatal de Investigación of Spain (grant SEV-2016-0672) to CBGP. IA is recipient of a Juan de la Cierva- Formación postodoctoral fellowship from Ministerio de Ciencia, Innovación y Universidades (FJCI-2017-33222). Development of *M. truncatula Tnt1* mutant population was, in part, funded by the National Science Foundation, USA (DBI-0703285) to KM.

ACKNOWLEDGMENTS

We would like to thank Dr. Marine Cotte and Dr Juan Reyes-Herrera for assistance in using beamline ID21 during experiments EV246 and EV323. We would also like to acknowledge the other members of laboratory 281 at Centro de Biotecnología y Genómica de Plantas (UPM-INIA) for their support and feedback in preparing this manuscript. This manuscript has been released as a pre-print at BioRxiv (Escudero et al. BioRxiv doi 10.1101/717983).

SUPPLEMENTARY MATERIAL

The Supplementary Material for this article can be found online at: https://www.frontiersin.org/articles/10.3389/fpls.2019.01780/full#supplementary-material

REFERENCES

Abreu, I., Saez, A., Castro-Rodríguez, R., Escudero, V., Rodríguez-Haas, B., Senovilla, M., et al. (2017). *Medicago truncatula* Zinc-Iron Permease6 provides zinc to rhizobia-infected nodule cells. *Plant Cell Environ.* 40, 2706–2719. doi: 10.1111/pce.13035

Andaluz, S., Rodríguez-Celma, J., Abadía, A., Abadía, J., and López-Millán, A.-F. (2009). Time course induction of several key enzymes in *Medicago truncatula* roots in response to Fe deficiency. *Plant Physiol. Biochem.* 47, 1082–1088. doi: 10.1016/j.plaphy.2009.07.009

Appleby, C. A. (1984). Leghemoglobin and *Rhizobium* respiration. *Annu. Rev. Plant Physiol.* 35, 443–478. doi: 10.1146/annurev.pp.35.060184.002303

Avenhaus, U., Cabeza, R. A., Liese, R., Lingner, A., Dittert, K., Salinas-Riester, G., et al. (2016). Short-term molecular acclimation processes of legume nodules to increased external oxygen concentration. *Front. Plant Sci.* 6, 1012. doi: 10.3389/fpls.2015.01133

Boisson-Dernier, A., Chabaud, M., Garcia, F., Bécard, G., Rosenberg, C., and Barker, D. G. (2001). *Agrobacterium rhizogenes*-transformed roots of *Medicago truncatula* for the study of nitrogen-fixing and endomycorrhizal symbiotic associations. *Mol. Plant Microbe Interact.* 14, 695–700. doi: 10.1094/MPMI.2001.14.6.695

Boyd, E. S., and Peters, J. W. (2013). New insights into the evolutionary history of biological nitrogen fixation. *Front. Microbiol.* 4, 201. doi: 10.3389/fmicb.2013.00201

Brear, E. M., Day, D. A., and Smith, P. M. C. (2013). Iron: an essential micronutrient for the legume–rhizobium symbiosis. *Front. Plant Sci.* 4, 359. doi: 10.3389/fpls.2013.00359

Brewin, N. J. (1991). Development of the legume root nodule. *Annu. Rev. Cell Biol.* 7, 191–226. doi: 10.1146/annurev.cb.07.110191.001203

Brito, B., Palacios, J. M., Hidalgo, E., Imperial, J., and Ruíz-Argüeso, T. (1994). Nickel availability to pea (*Pisum sativum* L.) plants limits hydrogenase activity of *Rhizobium leguminosarum* bv. *viciae* bacteroids by affecting the processing of the hydrogenase structural subunits. *J. Bacteriol.* 176, 5297–5303. doi: 10.1128/jb.176.17.5297-5303.1994

Burgess, B., and Lowe, D. (1996). Mechanism of molybdenum nitrogenase. *Chem. Rev.* 96, 2983–3011. doi: 10.1021/cr950055x

Burk, D. (1934). Azotase and nitrogenase in *Azotobacter*. *Enzymforschung* 3, 23–56.

Burton, J. W., Harlow, C., and Theil, E. C. (1998). Evidence for reutilization of nodule iron in soybean seed development. *J. Plant Nutr.* 5, 913–927. doi: 10.1080/01904169809365453

Catalano, C. M., Czymmek, K. J., Gann, J. G., and Sherrier, D. J. (2006). *Medicago truncatula* syntaxin SYP132 defines the symbiosome membrane and infection droplet membrane in root nodules. *Planta* 225, 541–550. doi: 10.1007/s00425-006-0369-y

Cheng, H. P., and Walker, G. C. (1998). Succinoglycan is required for initiation and elongation of infection threads during nodulation of alfalfa by *Rhizobium meliloti*. *J. Bacteriol.* 180, 5183–5191.

Cheng, X., Wang, M., Lee, H. K., Tadege, M., Ratet, P., Udvardi, M., et al. (2014). An efficient reverse genetics platform in the model legume *Medicago truncatula*. *New Phytol.* 201, 1065–1076. doi: 10.1111/nph.12575

Cotte, M. P. E., Salomé, M., Rivard, C., Nolf, W. D., Castillo-Michel, H., Fabris, T., et al. (2017). The ID21 X-ray and infrared microscopy beamline at the ESRF: status and recent applications to artistic materials. *J. Anal. Atom. Spect.* 32, 477–493. doi: 10.1039/C6JA00356G

Curie, C., and Mari, S. (2017). New routes for plant iron mining. *New Phytol.* 214, 521–525. doi: 10.1111/nph.14364

Dalton, D. A., Joyner, S. L., Becana, M., Iturbe-Ormaetxe, I., and Chatfield, J. M. (1998). Antioxidant defenses in the peripheral cell layers of legume root nodules. *Plant Physiol.* 116, 37–43. doi: 10.1104/pp.116.1.37

Demsar, J., Curk, T., Erjavec, A., Gorup, C., Hocevar, T., Milutinovic, M., et al. (2013). Orange: data mining toolbox in Python. *J. Mach. Learn. Res.* 14, 2349–2353.

Downie, J. A. (2014). Legume nodulation. *Curr. Biol.* 24, R184–R190. doi: 10.1016/j.cub.2014.01.028

Durrett, T. P., Gassmann, W., and Rogers, E. E. (2007). The FRD3-mediated efflux of citrate into the root vasculature is necessary for efficient iron translocation. *Plant Physiol.* 144, 197–205. doi: 10.1104/pp.107.097162

Escudero, V., Abeu, I., del Sastre, E., Tejada-Jiménez, M., Larue, C., Novoa-Aponte, L., et al. (2019a). Nicotianamine synthase2 is required for symbiotic nitrogen fixation in *Medicago truncatula* nodules. *bioRxiv*. 717983. doi: 10.1101/717983

Escudero, V., Abreu, I., Tejada-Jiménez, M., Rosa-Núñez, E., Quintana, J., Isabel Prieto, R., et al. (2019b). *Medicago truncatula* Ferroportin2 mediates iron import into nodule symbiosomes. *bioRxiv*. 630699. doi: 10.1101/630699

Fahraeus, G. (1957). The infection of clover root hairs by nodule bacteria studied by a simple glass slide technique. *J. Gen. Microbiol.* 16, 374–381. doi: 10.1099/00221287-16-2-374

Finney, L. A., and Halloran, T. V. (2003). Transition metal speciation in the cell: Insights from the chemistry of metal ion receptors. *Science* 300, 931. doi: 10.1126/science.1085049

Flis, P., Ouerdane, L., Grillet, L., Curie, C., Mari, S., and Lobinski, R. (2016). Inventory of metal complexes circulating in plant fluids: a reliable method based on HPLC coupled with dual elemental and high-resolution molecular mass spectrometric detection. *New Phytol.* 211, 1129–1141. doi: 10.1111/nph.13964

Gage, D. J. (2002). Analysis of infection thread development using Gfp- and DsRed-expressing *Sinorhizobium meliloti*. *J. Bacteriol.* 184, 7042–7046. doi: 10.1128/jb.184.24.7042-7046.2002

Gil-Díez, P., Tejada-Jiménez, M., León-Mediavilla, J., Wen, J., Mysore, K. S., Imperial, J., et al. (2019). MtMOT1.2 is responsible for molybdate supply to *Medicago truncatula* nodules. *Plant Cell Environ.* 42, 310–320. doi: 10.1111/pce.13388

González-Guerrero, M., Raimunda, D., Cheng, X., and Argüello, J. M. (2010). Distinct functional roles of homologous Cu^+ efflux ATPases in *Pseudomonas aeuginosa*. *Mol. Microbiol.* 78, 1246–1258. doi: 10.1111/j.1365-2958.2010.07402.x

González-Guerrero, M., Matthiadis, A., Sáez, Á., and Long, T. A. (2014). Fixating on metals: new insights into the role of metals in nodulation and symbiotic nitrogen fixation. *Front. Plant Sci.* 5, 45. doi: 10.3389/fpls.2014.00045

González-Guerrero, M., V., E., Sáez, Á., and Tejada-Jiménez, M. (2016). Transition metal transport in plants and associated endosymbionts. Arbuscular mycorrhizal fungi and rhizobia. *Front. Plant Sci.* 7, 1088. doi: 10.3389/fpls.2016.01088

Hakoyama, T., Watanabe, H., Tomita, J., Yamamoto, A., Sato, S., Mori, Y., et al. (2009). Nicotianamine synthase specifically expressed in root nodules of *Lotus japonicus*. *Planta* 230, 309–317. doi: 10.1007/s00425-009-0944-0

Hakoyama, T., Niimi, K., Yamamoto, T., Isobe, S., Sato, S., Nakamura, Y., et al. (2012). The integral membrane protein SEN1 is required for symbiotic nitrogen fixation in *Lotus japonicus* nodules. *Plant Cell Physiol.* 53, 225–236. doi: 10.1093/pcp/pcr167

Hardy, R. W., Holsten, R. D., Jackson, E. K., and Burns, R. C. (1968). The acetylene-ethylene assay for n(2) fixation: laboratory and field evaluation. *Plant Physiol.* 43, 1185–1207. doi: 10.1104/pp.43.8.1185

Haydon, M. J., Kawachi, M., Wirtz, M., Hillmer, S., Hell, R., and Krämer, U. (2012). Vacuolar nicotianamine has critical and distinct roles under iron deficiency and for zinc sequestration in Arabidopsis. *Plant Cell* 24, 724–737. doi: 10.1105/tpc.111.095042

Higuchi, K., Suzuki, K., Nakanishi, H., Yamaguchi, H., Nishizawa, N. K., and Mori, S. (1999). Cloning of nicotianamine synthase genes, novel genes involved in the biosynthesis of phytosiderophores. *Plant Physiol.* 119, 471–480. doi: 10.1104/pp.119.2.471

Hoffman, B. M., Lukoyanov, D., Yang, Z. Y., Dean, D. R., and Seefeldt, L. C. (2014). Mechanism of nitrogen fixation by nitrogenase: The next stage. *Chem. Rev.* 114, 4041–4062. doi: 10.1021/cr400641x

Inoue, H., Higuchi, K., Takahashi, M., Nakanishi, H., Mori, S., and Nishizawa, N. K. (2003). Three rice nicotianamine synthase genes, OsNAS1, OsNAS2, and OsNAS3 are expressed in cells involved in long-distance transport of iron and differentially regulated by iron. *Plant J.* 36, 366–381. doi: 10.1046/j.1365-313x.2003.01878.x

Inskeep, W. P., and Bloom, P. R. (1985). Extinction coefficients of chlorophyll a and b in N,N-dimethylformamide and 80% acetone. *Plant Physiol.* 77, 483–485. doi: 10.1104/pp.77.2.483

Jain, A., Wilson, G. T., and Connolly, E. L. (2014). The diverse roles of FRO family metalloreductases in iron and copper homeostasis. *Front. Plant Sci.* 5, 100. doi: 10.3389/fpls.2014.00100

Johnson, S. E., and Mohler, C. L. (2009). *Crop rotation on organic farms: A planning manual* (Ithaca, NY: National Resource, Agricultrue and Engineering Services).

Klatte, M., Schuler, M., Wirtz, M., Fink-Straube, C., Hell, R., and Bauer, P. (2009). The analysis of Arabidopsis nicotianamine synthase mutants reveals functions for nicotianamine in seed iron loading and iron deficiency responses. *Plant Physiol.* 150, 257–271. doi: 10.1104/pp.109.136374

Kobayashi, T., and Nishizawa, N. K. (2012). Iron uptake, translocation, and regulation in higher plants. *Annu. Rev. Plant Biol.* 63, 131–152. doi: 10.1146/annurev-arplant-042811-105522

Kondorosi, E., Mergaert, P., and Kereszt, A. (2013). A paradigm for endosymbiotic life: cell differentiation of *Rhizobium* bacteria provoked by host plant factors. *Annu. Rev. Microbiol.* 67, 611–628. doi: 10.1146/annurev-micro-092412-155630

Kryvoruchko, I. S., Routray, P., Sinharoy, S., Torres-Jerez, I., Tejada-Jiménez, M., Finney, L. A., et al. (2018). An iron-activated citrate transporter, MtMATE67, is required for symbiotic nitrogen fixation. *Plant Physiol.* 176, 2315–2329. doi: 10.1104/pp.17.01538

Kumar, R. K., Chu, H. H., Abundis, C., Vasques, K., Rodriguez, D. C., Chia, J.-C., et al. (2017). Iron-nicotianamine transporters are required for proper long distance iron signaling. *Plant Physiol.* 175, 1254. doi: 10.1104/pp.17.00821

Larue, C., Castilo-Michel, H., Sobanska, S., Cécillon, L., Bureau, S., Barthès, V., et al. (2014). Foliar exposure of the crop *Lactuca sativa* to silver nanoparticles: evidence for internalization and changes in Ag speciation. *J. Hazard. Mat.* 264, 98–106. doi: 10.1016/j.jhazmat.2013.10.053

León-Mediavilla, J., Senovilla, M., Montiel, J., Gil-Díez, P., Saez, Á., Kryvoruchko, I. S., et al. (2018). MtMTP2-facilitated zinc transport into intracellular compartments is essential for nodule development in *Medicago truncatula*. *Front. Plant Sci.* 9, 990. doi: 10.3389/fpls.2018.00990

LeVier, K., Day, D. A., and Guerinot, M. L. (1996). Iron uptake by symbisomes from soybean root nodules. *Plant Physiol.* 111, 893–900. doi: 10.1104/pp.111.3.893

Montiel, J., Arthikala, M. K., Cárdenas, L., and Quinto, C. (2016). Legume NADPH oxidases have crucial roles at different stages of nodulation. *Int. J. Mol. Sci.* 17, 680. doi: 10.3390/ijms17050680

Moreau, S., Meyer, J. M., and Puppo, A. (1995). Uptake of iron by symbiosomes and bacteroids from soybean nodules. *FEBS Lett.* 361, 225–228. doi: 10.1016/0014-5793(95)00155-3

Mus, F., Crook, M. B., Garcia, K., Garcia Costas, A., Geddes, B. A., Kouri, E. D., et al. (2016). Symbiotic nitrogen fixation and the challenges to its extension to non-legumes. *Appl. Environ. Microbiol.* 82, 3698–3710. doi: 10.1128/AEM.01055-16

Nakagawa, T., Kurose, T., Hino, T., Tanaka, K., Kawamukai, M., Niwa, Y., et al. (2007). Development of series of gateway binary vectors, pGWBs, for realizing efficient construction of fusion genes for plant transformation. *J. Biosci. Bioeng.* 104, 34–41. doi: 10.1263/jbb.104.34

O'Hara, G. W. (2001). Nutritional constraints on root nodule bacteria affecting symbiotic nitrogen fixation: a review. *Austr. J. Exp. Agr.* 41, 417–433. doi: 10.1071/EA00087

Oldroyd, G. E. D. (2013). Speak, friend, and enter: signalling systems that promote beneficial symbiotic associations in plants. *Nat. Rev. Microbiol.* 11, 252–263. doi: 10.1038/nrmicro2990

Preisig, O., Zufferey, R., Thony-Meyer, L., Appleby, C., and Hennecke, H. (1996). A high-affinity cbb3-type cytochrome oxidase terminates the symbiosis-specific respiratory chain of *Bradyrhizobium japonicum*. *J. Bacteriol.* 178, 1532–1538. doi: 10.1128/jb.178.6.1532-1538.1996

Ravel, B., and Newville, M. (2005). Athena, artemis, hephaestus: data analysis for X-ray absorption spectroscopy using IFEFFIT. *J. Synchr. Rad.* 12, 537–541. doi: 10.1107/S0909049505012719

Rellán-Álvarez, R., Abadía, J., and Álvarez-Fernández, A. (2008). Formation of metal-nicotianamine complexes as affected by pH, ligand exchange with citrate and metal exchange. A study by electrospray ionization time-of-flight mass spectrometry. *Rapid Commun. Mass Spectrom.* 22, 1553–1562. doi: 10.1002/rcm.3523

Rellán-Álvarez, R., Giner-Martínez-Sierra, J., Orduna, J., Orera, I., Rodríguez-Castrillón, J.Á., García-Alonso, J. I., et al. (2010). Identification of a tri-iron (III), tri-citrate complex in the xylem sap of iron-deficient tomato resupplied with iron: new insights into plant iron long-distance transport. *Plant Cell Physiol.* 51, 91–102. doi: 10.1093/pcp/pcp170

Rodríguez-Haas, B., Finney, L., Vogt, S., González-Melendi, P., Imperial, J., and González-Guerrero, M. (2013). Iron distribution through the developmental stages of *Medicago truncatula* nodules. *Metallomics* 5, 1247–1253. doi: 10.1039/c3mt00060e

Roschzttardtz, H., Séguéla-Arnaud, M., Briat, J.-F., Vert, G., and Curie, C. (2011). The FRD3 citrate effluxer promotes iron nutrition between symplastically disconnected tissues throughout Arabidopsis development. *Plant Cell* 23, 2725–2737. doi: 10.1105/tpc.111.088088

Roth, L. E., and Stacey, G. (1989). Bacterium release into host cells of nitrogen-fixing soybean nodules: the symbiosome membrane comes from three sources. *Eur. J. Cell Biol.* 49, 13–23.

Roux, B., Rodde, N., Jardinaud, M.-F., Timmers, T., Sauviac, L., Cottret, L., et al. (2014). An integrated analysis of plant and bacterial gene expression in symbiotic root nodules using laser-capture microdissection coupled to RNA sequencing. *Plant J.* 77, 817–837. doi: 10.1111/tpj.12442

Rubio, L. M., and Ludden, P. W. (2005). Maturation of nitrogenase: a biochemical puzzle. *J. Bacteriol.* 187, 405–414. doi: 10.1128/JB.187.2.405-414.2005

Rubio, M. C., Becana, M., Sato, S., James, E. K., Tabata, S., and Spaink, H. P. (2007). Characterization of genomic clones and expression analysis of the three types of superoxide dismutases during nodule development in *Lotus japonicus*. *Mol. Plant Microbe Interact.* 20, 262–275. doi: 10.1094/MPMI-20-3-0262

Santos, R., Hérouart, D., Puppo, A., and Touati, D. (2000). Critical protective role of bacterial superoxide dismutase in Rhizobium–legume symbiosis. *Mol. Microbiol.* 38, 750–759. doi: 10.1046/j.1365-2958.2000.02178.x

Schneider, S., Schintlmeister, A., Becana, M., Wagner, M., Woebken, D., and Wienkoop, S. (2019). Sulfate is transported at significant rates through the symbiosome membrane and is crucial for nitrogenase biosynthesis. *Plant Cell Environ.* 42, 1180–1189. doi: 10.1111/pce.13481

Schuler, M., Rellán-Álvarez, R., Fink-Straube, C., Abadía, J., and Bauer, P. (2012). Nicotianamine functions in the phloem-based transport of iron to sink organs, in pollen development and pollen tube growth in Arabidopsis. *Plant Cell* 24, 2380–2400. doi: 10.1105/tpc.112.099077

Senovilla, M., Castro-Rodríguez, R., Abreu, I., Escudero, V., Kryvoruchko, I., Udvardi, M. K., et al. (2018). *Medicago truncatula* Copper Transporter1 (MtCOPT1) delivers copper for symbiotic nitrogen fixation. *New Phytol.* 218, 696–709. doi: 10.1111/nph.14992

Singleton, P. W., and van Kessel, C. (1987). Effect of localized nitrogen availability to soybean half-root systems on photosynthate partitioning to roots and nodules. *Plant Physiol.* 83, 552. doi: 10.1104/pp.83.3.552

Smil, V. (1999). Nitrogen in crop production: an account of global flows. *Global Biogeochem. Cycles* 13, 647–662. doi: 10.1029/1999GB900015

Solé, V. A., Papillon, E., Cotte, M., Walter, P., and Susini, J. A. (2007). A multiplatform code for the analysis of energy-dispersive X-ray fluorescence spectra. *Spectrochim. Acta B* 62, 63–68. doi: 10.1016/j.sab.2006.12.002

Streeter, J. G. (1987). Carbohydrate, organic acid, and amino acid composition of bacteroids and cytosol from soybean nodules. *Plant Physiol.* 85, 768–773. doi: 10.1104/pp.85.3.768

Sun, L., Gill, U. S., Nandety, R. S., Kwon, S., Mehta, P., Dickstein, R., et al. (2019). Genome-wide analyses of flanking sequences reveals that *Tnt1* insertion is positively correlated with gene methylation in *Medicago truncatula*. *Plant J.* 98, 1016–1119. doi: 10.1111/tpj.14291

Takanashi, K., Yokosho, K., Saeki, K., Sugiyama, A., Sato, S., Tabata, S., et al. (2013). LjMATE1: a citrate transporter responsible for iron supply to the nodule infection zone of *Lotus japonicus*. *Plant Cell Physiol.* 54, 585–594. doi: 10.1093/pcp/pct019

Tang, C., Robson, A. D., and Dilworth, M. J. (1991). Which stage of nodule initiation in *Lupinus angustifolius* L. is sensitive to iron deficiency? *New Phytol.* 117, 243–250. doi: 10.1111/j.1469-8137.1991.tb04905.x

Tejada-Jiménez, M., Castro-Rodríguez, R., Kryvoruchko, I., Lucas, M. M., Udvardi, M., Imperial, J., et al. (2015). *Medicago truncatula* natural resistance-associated macrophage protein1 is required for iron uptake by rhizobia-infected nodule cells. *Plant Physiol.* 168, 258–272. doi: 10.1104/pp.114.254672

Tejada-Jiménez, M., Gil-Diez, P., Leon-Mediavilla, J., Wen, J., Mysore, K. S., Imperial, J., et al. (2017). *Medicago truncatula* molybdate transporter type 1 (MOT1.3) is a plasma membrane molybdenum transporter required for nitrogenase activity in root nodules under molybdenum deficiency. *New Phytol.* 216, 1223–1235. doi: 10.1111/nph.14739

Terry, R. E., Soerensen, K. U., Jolley, V. D., and Brown, J. C. (1991). The role of active *Bradyrhizobium japonicum* in iron stress response of soy-beans. *Plant Soil* 130, 225–230. doi: 10.1007/BF00011877

Udvardi, M., and Poole, P. S. (2013). Transport and metabolism in legume-rhizobia symbioses. *Annu. Rev. Plant Biol.* 64, 781–805. doi: 10.1146/annurev-arplant-050312-120235

Valentine, A. J., Kleinert, A., and Benedito, V. A. (2017). Adaptive strategies for nitrogen metabolism in phosphate deficient legume nodules. *Plant Sci.* 256, 46–52. doi: 10.1016/j.plantsci.2016.12.010

Vasse, J., de Billy, F., Camut, S., and Truchet, G. (1990). Correlation between ultrastructural differentiation of bacteroids and nitrogen fixation in alfalfa nodules. *J. Bacteriol.* 172, 4295–4306. doi: 10.1128/jb.172.8.4295-4306.1990

Vernoud, V., Journet, E. P., and Barker, D. G. (1999). *MtENOD20*, a Nod factor-inducible molecular marker for root cortical cell activation. *Mol. Plant Microbe Interact.* 12, 604–614. doi: 10.1094/MPMI.1999.12.7.604

von Wiren, N., Klair, S., Bansal, S., Briat, J.-F., Khodr, H., Shioiri, T., et al. (1999). Nicotianamine chelates both FeIII and FeII. Implications for metal transport in plants. *Plant Physiol.* 119, 1107–1114. doi: 10.1104/pp.119.3.1107

Waters, B. M., Chu, H.-H., DiDonato, R. J., Roberts, L. A., Eisley, R. B., Lahner, B., et al. (2006). Mutations in *Arabidopsis Yellow Stripe-Like1* and *Yellow Stripe-Like3* reveal their roles in metal ion homeostasis and loading of metal ions in seeds. *Plant Physiol.* 141, 1446–1458. doi: 10.1104/pp.106.082586

Xiao, T. T., Schilderink, S., Moling, S., Deinum, E. E., Kondorosi, E., Franssen,, et al. (2014). Fate map of *Medicago truncatula* root nodules. *Development* 141, 3517–3528. doi: 10.1242/dev.110775

Conflict of Interest: The authors declare that the research was conducted in the absence of any commercial or financial relationships that could be construed as a potential conflict of interest.

frontiers in Plant Science

REVIEW
published: 13 May 2020
doi: 10.3389/fpls.2020.00528

The Dynamics of Radio-Cesium in Soils and Mechanism of Cesium Uptake Into Higher Plants: Newly Elucidated Mechanism of Cesium Uptake Into Rice Plants

Hiroki Rai and Miku Kawabata*

Department of Biological Production, Faculty of Bioresource Sciences, Akita Prefectural University, Akita, Japan

Soil radio-cesium (Cs) contamination caused by nuclear accidents is a major public concern. In this review, we presented the behavior of radio-Cs in soils, the relationship between Cs^+ and potassium (K) ion uptake from soils, and the Cs^+ uptake model proposed previously. Finally, we introduced the newly elucidated mechanism of Cs^+ uptake in rice plants and compared it with the previously proposed Cs^+ uptake model. Cs is a trace element in soil. It is toxic to plants when absorbed at high concentrations, although this rarely occurs under normal environmental conditions. Nevertheless, radio-Cs released during nuclear weapon tests or nuclear power plant accidents is absorbed by plants, thus entering the food chain. As Cs^+ strongly binds to the frayed edge sites of illitic clays in soil, it is hardly moved by the infiltration of rainwater. However, plants have a strong ability for inorganic ions uptake, causing re-diffusion of radio-Cs^+ into ecosystems and radioactive contamination of food. It is hypothesized that Cs^+ is absorbed by plants through the same mechanism implemented in K^+ uptake. However, the dynamics of the two elements do not always coincide in their transition from soil to plants and inside the plants. A previously proposed model of Cs uptake by higher plants stated that Cs^+ is absorbed through high affinity potassium (HAK) family of transporters and voltage-insensitive cation (VIC) channels. A knockout line of a HAK transporter gene (*oshak1*) in rice revealed that the HAK transporter OsHAK1 is the main route of Cs^+ influx into rice plants, especially in low-potassium conditions. The K^+ uptake rates did not differ greatly between the *oshak1* and wildtype. On the surface of rice roots, potassium-transport systems other than OsHAK1 make little or no contribution to Cs^+ uptake. It is almost certain that OsAKT1 does not mediate the Cs uptake. Under normal soil conditions, 80–90% of Cs uptake into the roots is mediated by OsHAK1 and the rest by VIC channels. Except for the difference between the contribution ratio of HAK and VIC channels in Cs uptake, these results are consistent with the conventional model.

Keywords: cesium, potassium transporters, HAK, KIR channels, VIC channels, radio-cesium, rice, Fukushima

OPEN ACCESS

Edited by:
Tomoko Nozoye,
Meiji Gakuin University, Japan

Reviewed by:
Neil J. Willey,
University of the West of England, Bristol, United Kingdom
Chul Min Kim,
Wonkwang University, South Korea

****Correspondence:***
Hiroki Rai
raihiro@akita-pu.ac.jp

Specialty section:
This article was submitted to Plant Traffic and Transport, a section of the journal Frontiers in Plant Science

Received: *31 January 2020*
Accepted: *07 April 2020*
Published: *13 May 2020*

Citation:
Rai H and Kawabata M (2020) The Dynamics of Radio-Cesium in Soils and Mechanism of Cesium Uptake Into Higher Plants: Newly Elucidated Mechanism of Cesium Uptake Into Rice Plants. Front. Plant Sci. 11:528. doi: 10.3389/fpls.2020.00528

INTRODUCTION

Cesium (Cs) is a Group I alkali metal along with sodium (Na) and potassium (K). Its chemical properties are very similar to those of K, which is one of the macronutrient elements of plants. Generally, the solubility of K and Cs salts is very high, and both are always present as monovalent ions in the natural environment. The concentration of K^+ is in the range from 100 to 150 mM in the cytoplasm of plant cells, where it regulates the osmotic pressure of the cells. The controlled osmotic fields are essential for enzymatic reactions and maintaining the structure of nucleic acids. Although Cs^+ has physical properties similar to K^+, Cs^+ does not provide the same as K^+ in vital cell activities. As Cs concentration of the cells increases, the cytotoxicity increases due to the decrease in or inhibition of the enzyme activity (White and Broadley, 2000; Hampton et al., 2004; Maathuis, 2009).

The concentration of stable Cs isotope (^{133}Cs) in the environment is generally low (up to 25 μg/g soil) and not harmful to plants or human health. However, Cs uptake by plants may become a public concern when radio-Cs (^{134}Cs, ^{137}Cs) is released by nuclear weapons tests or nuclear power plant accidents. Plants can absorb the radio-Cs in soil and incorporate it into the food chain, where it may cause internal exposure to β and γ radiation during its radioactive decay (White and Broadley, 2000).

The research on the absorption of Cs^+ from soil by plants has been intensive over the past several decades. Cs^+ and K^+ compete during uptake by plants and a Cs^+ uptake model has been proposed based on the analysis of K^+ transporters. After the nuclear accident caused by the Great East Japan Earthquake in 2011, research on Cs^+ absorption in rice has been advanced in Japan. This helped to elucidate the mechanism of Cs^+ absorption by rice roots.

In this review, we introduce the outline of Cs^+ dynamics in soil and the results of research on the absorption mechanism in plants. Then, we compare the conventional Cs^+ absorption model of plants with the newly elucidated mechanism of Cs^+ uptake into rice.

CESIUM AND RADIO-CESIUM EXISTENCE IN THE ENVIRONMENT

The concentration of Cs (^{133}Cs) in soil is low. Although Cs is toxic to plants when absorbed in high concentration as its intracellular concentration becomes high, such a phenomenon rarely occurs under normal environmental conditions. The toxicity of Cs to living organisms is not from the stable isotope (^{133}Cs), but from the artificially produced radioactive Cs (^{134}Cs, ^{137}Cs). Atmospheric nuclear tests have already been prohibited, but the commercial nuclear power reactors account for 10% of electricity produced in the world.

We have experienced widespread radionuclide contaminations caused by the nuclear power plant accidents in the Chernobyl Nuclear Power Plant, Ukraine, in 1986 and in the Fukushima Daiichi Nuclear Power Plant, Japan, in 2011. Radio-Cs was a common problem in both nuclear accidents.

In the Chernobyl accident, the containment vessel exploded, exposing the reactor core to the atmosphere and releasing numerous radionuclides such as radioactive xenon (^{133}Xe), iodine (^{131}I), Cs (^{134,137}Cs), strontium (^{90}Sr), zirconium (^{95}Zr), ruthenium (^{103,106}Ru), and plutonium (^{239}Pu) (International Atomic Energy Agency [IAEA], 2003–2005; Imanaka, 2016). Among these nuclides, radio-Cs contaminated a large area and became a major source of radioactive contamination of the food chain (Fesenko et al., 2007).

In the Fukushima disaster, the containment vessel itself was not severely damaged, but ^{133}X, ^{131}I, and ^{134,137}Cs leaked from the containment vessel and were released into the atmosphere by venting or by hydrogen explosion of the building. ^{133}Xe, which is a gas, and ^{131}I and ^{134,137}Cs, both with low boiling points, were released in large amounts and widely dispersed. Of these three elements, ^{133}Xe diffused into the atmosphere, and ^{131}I was not detected in a few months after the accident because of its short half-life (8.04 days). However, the half-life of radio-Cs is long (2.06 years for ^{134}Cs; 30.17 years for ^{137}Cs), and it tends to strongly adsorb to the soil, thus polluting the fallout area for a long time (Chino et al., 2011; Beresford et al., 2016; Imanaka, 2016).

There are two problems related to radio-Cs pollution of the environment. One is elicited through external exposure, in which β and γ rays are emitted by the decay of radio-Cs, so air dose increases, exposing people to these harmful rays. The other problem is related to internal exposure generated through absorption of radio-Cs by crops and its transfer into the food chain, contaminating food and posing health problems (Fesenko et al., 2007; Beresford et al., 2016). The rate of radio-Cs absorption from ingested contaminated food is extremely high; the transfer factor is 65–90% (Henrichs et al., 1989; Beresford et al., 2000). In mammals, radio-Cs, similar to K, is taken up into the blood and transferred into tissues such as muscles, but its fecal and urinary excretion is low. In the body, radio-Cs has a considerably long half-life (45–200 days, with an average of 90 days), exposing the internal organs to radiation from radio-Cs (Henrichs et al., 1989). In addition, herbivores absorb radio-Cs from pasture fields, which results in contamination of dairy products and meat. In Chernobyl, the consumption of foods containing radio-Cs was the major source of public exposure via milk and other animal products (Beresford et al., 2000; Fesenko et al., 2007; Fesenko et al., 2015; **Figure 1**). In Fukushima, the provisional guideline levels for radio-Cs were specified immediately after the accident and all agricultural products were measured for radioactivity before shipment. The products contaminated with excess radiation have not been circulated (Nihei, 2013). Internal exposure by foods originates from the absorption of radio-Cs by plants, so it is important to know the dynamics of Cs from soils to plants.

DYNAMICS OF CESIUM AND RADIO-Cs IN THE ENVIRONMENT

Cesium has a strong ionization tendency, and its salts generally have high solubility. The radio-Cs released from nuclear power

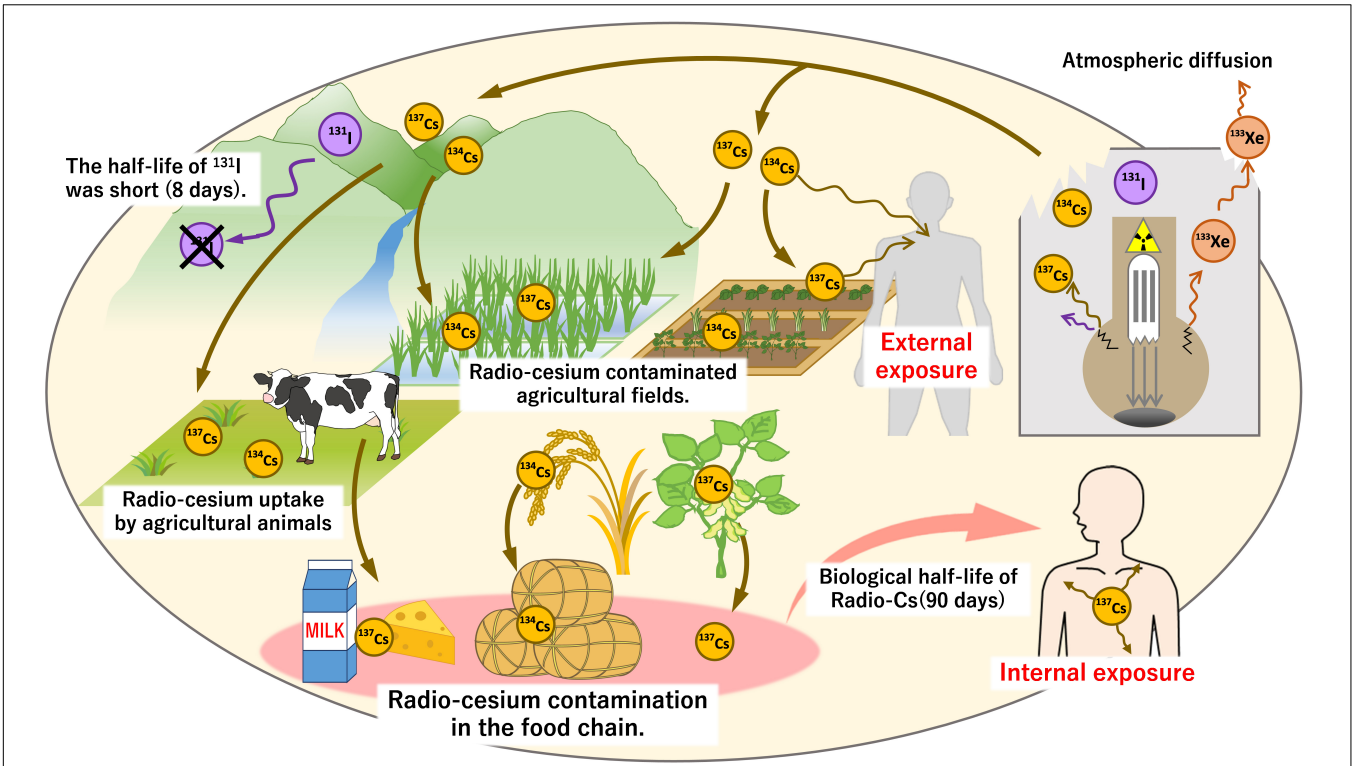

FIGURE 1 | Diffusion of radio-Cs and contamination of soil and food due to the Fukushima nuclear plant accident. At the time of the nuclear power plant accident, gaseous ^{133}Xe as well as ^{131}I, ^{134}Cs, and ^{137}Cs with low boiling point easily leaked. These nuclides were released and spread widely when a hydrogen explosion damaged the plant building. ^{133}Xe diffused quickly into the atmosphere, and ^{131}I could not be detected within a few months due to its short half-life. In contrast, the half-lives of ^{134,137}Cs are long, allowing its persistence in the environment for long periods. The decay of ^{134,137}Cs caused external exposure to emitted γ-rays. Internal exposure also occurred through the ingestion of contaminated food. Absorption of ^{134,137}Cs by plants (agricultural crops) allowed its entry into the food chain resulting in the contamination of grains, vegetables, dairy products, and many more food sources. Due to the long biological half-life of Cs in humans (approximately 90 days), it is necessary to monitor these isotopes in soil, plants, and foods.

plants is deposited from the atmosphere onto the ground. The particles containing radio-Cs fall on the soil surface in crop fields or on the leaves and bark of forest trees, and eventually enter the organic matter layer with rainfall. Ultimately, as the organic matter decomposes, radio-Cs migrates into the A layer containing clay minerals, where it behaves differently from K^+ and Na^+ (Takahashi et al., 2019).

Clay and humus contained in soil are negatively charged and have cation exchangeable sites that commonly adsorb cations such as Cs^+ and K^+ (**Figure 2**, left panel). Furthermore, there are sites in the soil that specifically adsorb Cs^+ (Cremers et al., 1988). Clay minerals in the soil have a layered structure of aluminosilicates, with the layers whose surfaces are negatively charged and held together by cations such as K^+ and Mg^{2+}. As soil weathers, aluminosilicates are precipitated, the ions between the layers are gradually released from the outer edge, and the layers slightly open at the edge of the clay mineral. In illitic clays, this edge is named frayed edge site, and it shows a specific adsorption affinity for Cs^+ whose ionic radius is large and hydration radius is small. The adsorption of Cs^+ by frayed edge sites is more than 1000-fold greater than that for K^+, and it is almost irreversible (Yamaguchi, 2014; **Figure 2**, right panel).

However, soils lacking illitic clays have much higher Cs availability for plant uptake. Thus, Radio-Cs Interception Potential (RIP) was proposed as the quantitative measure of radio-Cs retention in soils (Cremers et al., 1988). In typical clay soils containing illitic clays, the number of this frayed edge sites is much higher than that required for the immobilization of radio-Cs (Cremers et al., 1988; Vandebroek et al., 2012). It is assumed that most of the stable isotope Cs^+ is trapped by this frayed edge sites. Newly supplied Cs^+, such as radio-Cs, is hardly moved in the soil because it is captured by these sites and thereby immobilized. In the absence of human disturbance, most of the radioactive Cs^+ from the nuclear accidents has been concentrated in the top several centimeters of the soil (Almgren and Isaksson, 2006; Takahashi et al., 2019).

The concentration of stable isotope Cs (^{133}Cs) in a typical soil is 2.5 mg kg^{-1} and the concentration of Cs^+ in soil solution is lower than 10 μg L^{-1} (75 nM) (Tsukada et al., 2002; Rai et al., 2017). The soil concentration of radio-Cs is considerably lower than the concentration of ^{133}Cs.

In Japan, a reference value was set for protection during the continuous consumption of radioactive contaminated food after the Fukushima nuclear accident. The concentration of radio-Cs in soil where radioactive contamination of crops would exceed

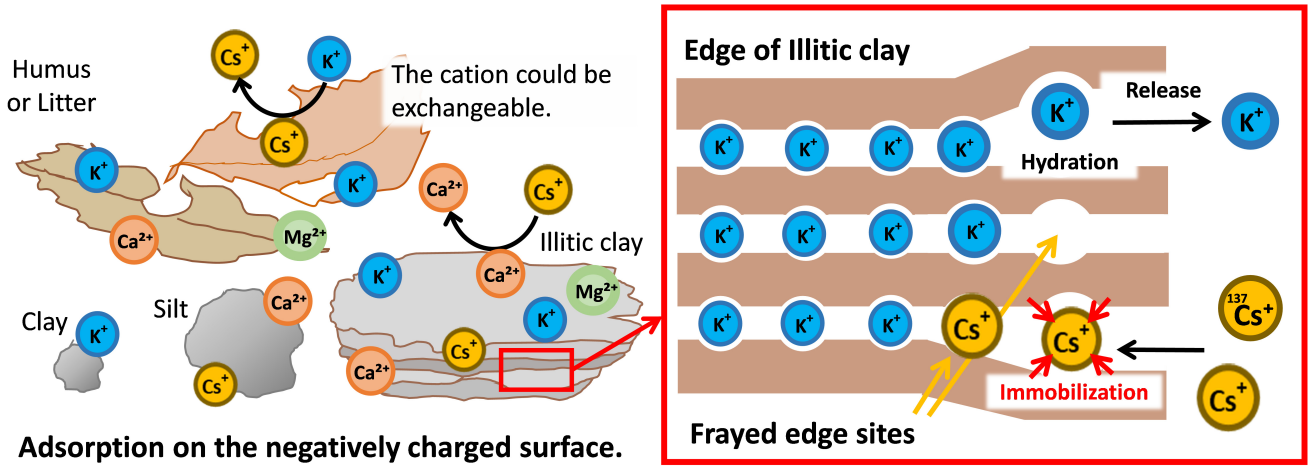

FIGURE 2 | Dynamics of radio-Cs in soil and the quantitative relationship between potassium and Cs. In soil, radio Cs^+ is adsorbed through the negative charges of organic substances such as humus or clay similarly to other cations such as K^+ and Ca^2. In addition, Cs^+ is strongly immobilized (captured) on the mica's frayed edge sites over time. As a result, radio Cs^+ is vertically immobile and mostly accumulates on the top soil.

the reference value could be estimated from the transfer factor and the reference value of crops (100 Bq kg^{-1} in rice). In the case of rice, the transfer factor for brown rice from the soil is from 0.004 to 0.065 (Kondo et al., 2015). At 0.065 as transfer factor, the radio-Cs concentration in the soil is estimated to 1540 Bq kg^{-1} soil. The concentration of radio-Cs in soils where agriculture could resume is expected to be less than a several thousand Bq kg^{-1} soil.

In soils contaminated with ^{134}Cs or ^{137}Cs at 10,000 Bq kg^{-1} soil, the weight of Cs can be calculated using the following formula.

$$10{,}000\ \text{Bq};^{134}\text{Cs in soil (Bq kg}^{-1}) = 10{,}000 \times 60 \times 60 \times 24 \times 365 \times 2.06 \times 2\hat{}(1/2)/(6.02 \times 10^{23})$$
$$= 1.54\ \text{pmol kg}^{-1} = 206\ \text{pg kg}^{-1}$$

$$10{,}000\ \text{Bq};^{137}\text{Cs in soil (Bq kg}^{-1}) = 10{,}000 \times 60 \times 60 \times 24 \times 365 \times 30.2 \times 2\hat{}(1/2)/(6.02 \times 10^{23})$$
$$= 23\ \text{pmol kg}^{-1} = 3.15\ \text{ng kg}^{-1}$$

Even if the concentration of radioactive Cs in the soil is 10,000 Bq/kg, the amount of ^{134}Cs and ^{137}Cs is 206 pg kg^{-1} and 3.15 ng kg^{-1}, respectively, which is negligible for the amount of stable isotope Cs. Cs that is the focus of this review is ^{133}Cs radioactively labeled with a considerably lower concentration of $^{134,137}Cs$ (**Figure 3**, bottom right panel).

It is well known that Cs^+ competes with K^+ during plant uptake and it is absorbed by plants through the same mechanism as K^+. The quantitative relationship between K^+ and Cs^+ controls for the Cs^+ uptake of plants (**Figure 3**, left panel).

K is the fourth most abundant element in the lithosphere, and its ion, K^+, is supplied by the soil clay minerals. The total K concentration in paddy fields is approximately 8000 mg kg^{-1} (5000–13,000 mg kg^{-1}) (Tsukada et al., 2002). The concentration of exchangeable K^+ is an indicator of plant available K^+. The exchangeable K^+ concentration in 178 agricultural soils (95 paddy fields and 83 upland fields in Japan) ranged from 43 to 1304 mg kg^{-1}, with a median of 209 mg kg^{-1} (Kitagawa et al., 2017). The concentration of K^+ in soil solution is less than 10% of exchangeable K^+ concentration. Furthermore, the concentration of K^+ in soil solution is variable in the rhizosphere as the rate of exchangeable K^+ release is slower than the rate of K^+ uptake by plants; 10–100 μM K^+ is contained in soil solution (Sparks and Huang, 1985; Ashley et al., 2005; Gomez-Porras et al., 2012; **Figure 3**, upper right panel).

As described above, K^+ concentration in soil solutions is 10–100 μM and that of Cs^+ is less than 100 nM. The difference between the K^+ and Cs^+ concentrations in soil solution is large and the K/Cs ratio is approximately 10^3 in the soil solution (**Figure 3**, bottom right panel). Some studies on Cs^+ uptake by plants for functional analysis, such as a selectivity of ions of the K^+ transporter, were conducted at equal concentration of Cs^+ and K^+, which therefore differed greatly from the concentration of Cs^+ in the environment. In the dynamics of radio-Cs between soils and plants, this difference should be considered.

THE MECHANISM OF K^+ UPTAKE IN HIGHER PLANTS

Since the time Collander (1941) proposed his theory that K^+ and Cs^+ are absorbed by roots through the same pathway, the research on Cs^+ uptake has always been associated with the analysis of the K^+ uptake mechanism. As described in section "Introduction," K^+ mainly regulates the osmotic pressure of plant cells, and its concentration in a cell itself affects the activity of enzymes. Plants use various K^+ transporters on the cell membrane to adjust the intracellular K^+ concentration depending on the plant part or tissue. Thus, the mechanism

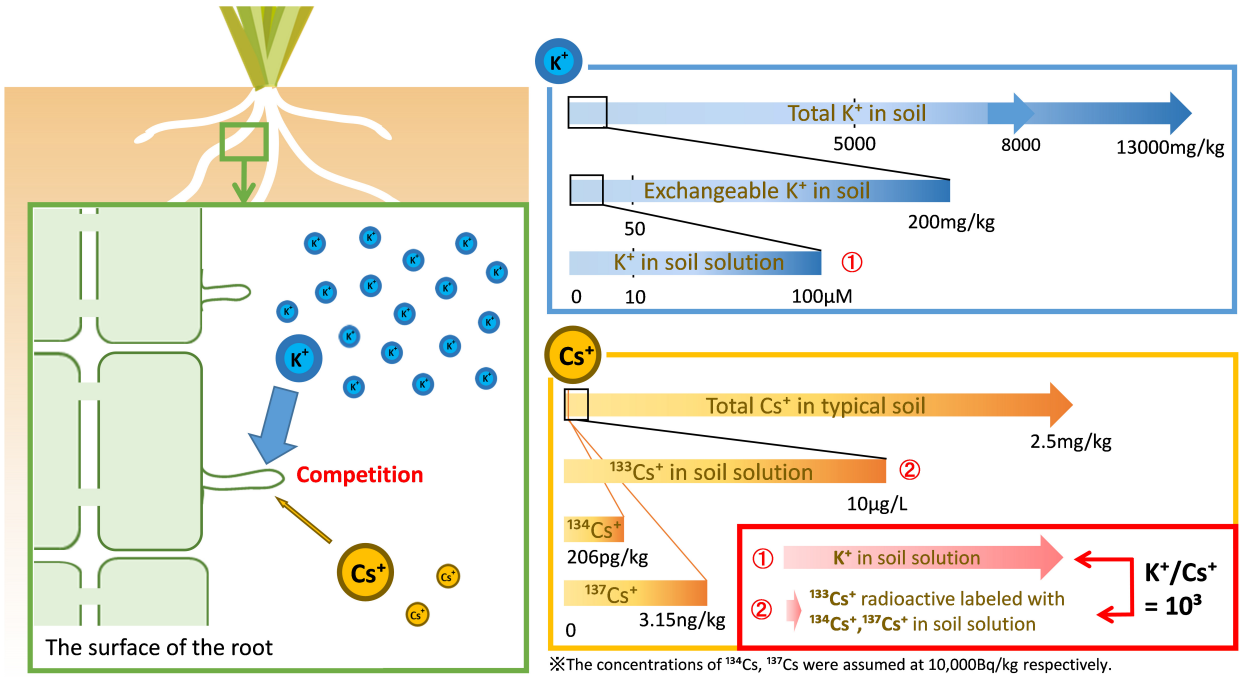

FIGURE 3 | The Cs targeted in this review. The amount of stable isotope Cs (^{133}Cs) in a typical soil is approximately 2.5 mg/kg but its concentration in soil solution is lower than 10 μg/L (75 nM) (Tsukada et al., 2002; Rai et al., 2017). Our target in this review is radioactively labeled ^{133}Cs and a much smaller amount of ^{134,137}Cs. In contrast to radio Cs^+, potassium is an environmentally abundant element supplied from soil clay minerals, at concentrations of 5000–13,000 mg/kg soil (Tsukada et al., 2002). The exchangeable K^+ available to plants is approximately 200 mg/kg soil, while 10–100 μM K^+ is retained in soil solution (Sparks and Huang, 1985; Gomez-Porras et al., 2012; Kitagawa et al., 2017). The actual K/Cs ratio is approximately 10^3 in the soil solution.

of intracellular K^+ concentration adjustment is intricate and involves a complex K^+ transport network in which a considerable number of K^+ transporters continuously cooperate to provide required concentrations of K^+ to all plant cells (Maathuis, 2009).

Genomic analyses identified 35 genes in Arabidopsis and 50 genes in rice controlling K^+ transporters and the uptake or excretion of K^+ across cell membranes (Amrutha et al., 2007; Yang et al., 2009). There are a large number of K^+ transporters, divided into five major K^+ transporter families based on their functional type (Mäser et al., 2001). To date, only a part of the K^+ uptake and transport pathways and their many transporters have been elucidated. One of them is K^+ uptake in roots.

The uptake of K^+ into plant cells using K^+ transporters is driven by the H^+ concentration gradient and electric potential difference caused by H^+ transport out of the cells. K^+ transporters that take K^+ into the cells are mainly divided into a carrier type and channel type. Carrier-type K^+ transporters include the KUP/HAK/KT (or shorter HAK) family of high affinity K^+ transporters, which transport K^+ into the cells by co-transport with H^+. The transport by HAK requires binding of K^+ and H^+ to the HAK protein itself; therefore, the absorption curve plotting the external K^+ concentration and the rate of K^+ carried into the cells fits the Michaelis–Menten equation (Maathuis and Sanders, 1994). Carrier-type K^+ transporters have high affinity for K^+ and can transfer K^+ into the cells even at low extracellular K^+ concentrations. The HAK family is the most numerous among the K^+ transporters, and it is encoded by genes such as *AtHAK1–AtHAK13* in Arabidopsis and *OsHAK1–OsHAK27* in rice (Gupta et al., 2008; Yang et al., 2009).

In contrast, the channel type of K^+ transporters carries K^+ into the cells when the extracellular K^+ concentration is relatively high. There are two types of K^+ channels: an inward rectifying K^+ (KIR) channel that transports K^+ into the cells, and an outward rectifying K^+ (KOR) channel that flows K^+ out of the cells (Rodríguez-Navarro, 2000; Szczerba et al., 2009).

Generally, the concentration of K^+ in plant cells is 100 mM or higher, while its concentration in soil solution is less than 1 mM even in K^+-rich soils. Therefore, the KIR channel functions (rectifying property) only when the membrane potential becomes more negative than the equilibrium potential of K^+ and the direction of K^+ transmission is predetermined. Channel-type K^+ transporters do not require the binding of K^+ to channel proteins and can pass more than 10^6 ions per second.

It has been shown that switching between the carrier type and channel type during K^+ uptake into plant roots depends on K^+ concentration in the soil. At low soil K^+ concentrations (less than 1 mM), HAK family such as OsHAK1 and OsHAK5 in rice and AtHAK5 and AtKUP7 in Arabidopsis is mainly activated (Pyo et al., 2010). However, at high soil K^+ concentrations (1 mM or more), channels such as OsAKT1 in rice and AtAKT1 in Arabidopsis, belonging to the KIR channel family, are the main transporters of K^+ (Nieves-Cordones et al., 2016; **Figure 4**). For example, the *K*m of AtHAK5 was 15–24 μM K^+, while that of AKT1 was 0.88 mM (Gierth et al., 2005).

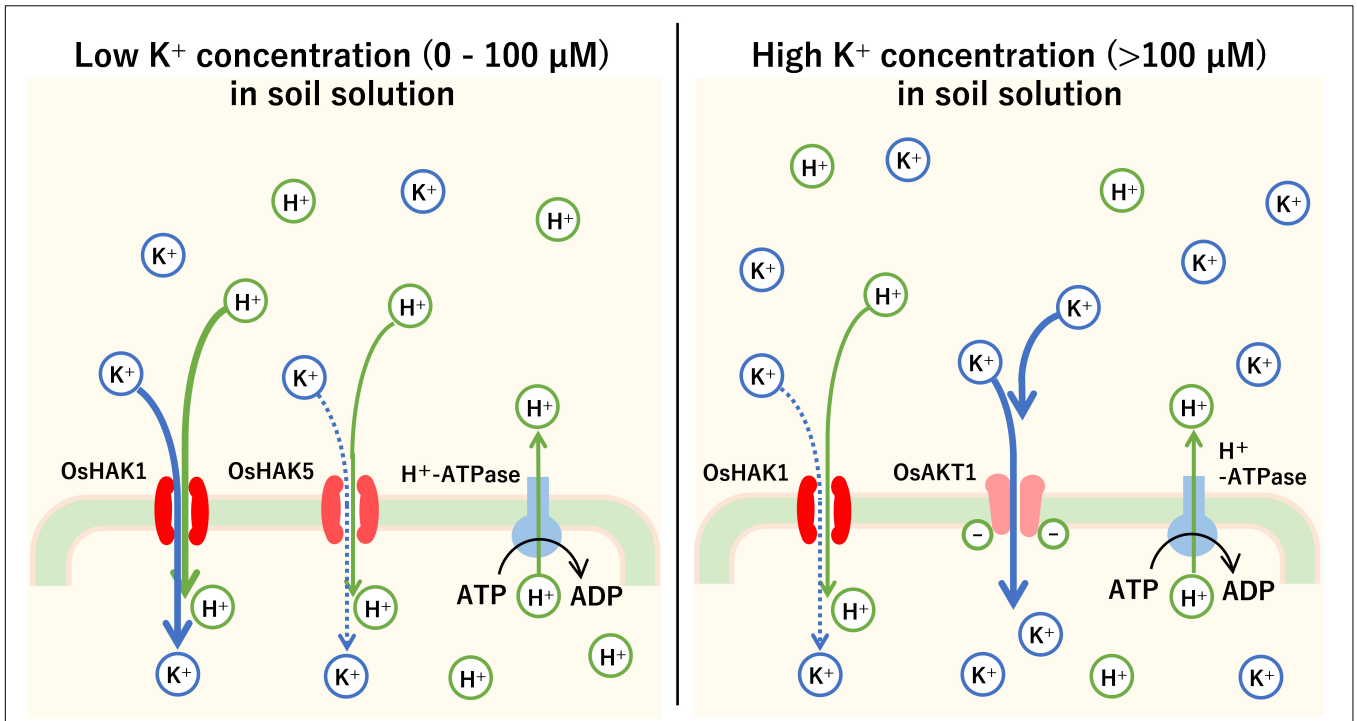

FIGURE 4 | The mechanism of K^+ uptake into the plant roots. Root cells in plants pump H^+ out of cells successively with H^+-ATPase. Using the H^+ concentration gradient and the electrical potential difference across the cell membrane as driving force, the root cells absorb K^+ by carrier or channel-type K^+ transporters. In rice, when the K^+ concentration is low (0–100 μM), high-affinity K^+ (HAK) transporters such as OsHAK1 and OsHAK5 mainly transport K^+ by symport with H^+. Above 100 μM, KIR channels such as OsAKT1 cause an influx of K^+ into root cells.

However, of the 27 HAK transporters in rice, the expression levels of OsHAK1, 7, and 16 are always high in rice roots, whereas the other HAK transporters are highly expressed during K^+ deficiency (Okada et al., 2008). Thus, not all routes of K^+ uptake are unknown. After absorption into root cells, K^+ is moved from epidermal cells into cambium via cytoplasmic communication, and then released from the adjacent vessel cells through the KOR channel.

CESIUM PERMEABILITY OF POTASSIUM TRANSPORTERS

Transport of Cs^+ by K^+ transporters has been investigated by competition analysis in various plants by altering the ionic composition of hydroponic solutions, by electrophysiological methods using microelectrodes, and by investigating Cs^+ uptake characteristics of knockout mutants for K^+ transporters in model plants such as Arabidopsis. Studies employing the first two types of experiments are detailed in a review by White and Broadley (2000).

Since the time Collander (1941) proposed his theory about K^+ and Cs^+ uptake by roots, the uptake of these alkali metal ions was analyzed in hydroponic cultivations of barley and wheat. A study found that the rate of Cs^+ influx under different Cs^+ concentrations can be described by the sum of two Michaelis–Menten hyperbolae (Epstein, 1972). This suggests that Cs^+ may be absorbed into the roots by two types of K^+ transporters (high affinity and low affinity) having different K_m. Shaw and Bell (1989) examined the concentration dependence of Cs^+ influx into excised wheat roots and proposed the existence of two distinct Cs^+ influx isotherms. These authors reported that at excessive Cs^+ concentrations, the Cs^+ influx into the roots increases linearly with increasing Cs^+ concentration in the hydroponic solution, and they suggested that this second uptake system had lower affinity (Shaw and Bell, 1989).

The inhibition of Cs^+ influx by other ions has also been analyzed. The inhibition increased in the following order: $Li^+ < Na^+ < NH_4^+ < Rb^+ \leq K^+$ (Bange and Overstreet, 1960; Handley and Overstreet, 1961; Shaw and Bell, 1991). For divalent ions, the inhibition increased in the following order: $Ca^{2+} < Mg^{2+} \leq Ba^{2+}$ (Handley and Overstreet, 1961), although the inhibition by divalent ions was incomplete. In spinach, an increase in the Ca^{2+} and Mg^{2+} concentrations significantly decreased Cs^+ uptake (Smolders et al., 1997).

Thus, it is possible that Cs^+ influx is associated with several K^+ transporters that may be inhibited by Ca^{2+} concentration. Cs is taken up by at least two types of transporters with different properties. However, it should be highlighted that in the studies utilizing hydroponics, the concentration of Cs^+ used in the experiments was sometimes much higher than that found in soil environments under normal conditions (less than 10 ppb; 75 nM Cs^+ in soil solution), since these studies focus on the difference in the uptake rate between K^+ and Cs^+.

Electrochemical studies have shown that high-affinity HAK, low-affinity KIR channels, KOR channels, and voltage-insensitive cation channels (VIC) are Cs^+ permeable (White and Broadley, 2000). The ratio of Cs^+ permeability to K^+ influx of KIR channel in barley is 0.39–0.43 and much lower, at 0.07, in Arabidopsis (Wegner and Raschke, 1994; Maathuis and Sanders, 1995). Cs permeability of KIR channels is lower than that of K^+. Furthermore, increasing Cs^+ concentration inhibits K^+ permeation of KIR channels (Bregante et al., 1997; White, 1997).

The genes for several KIR channels have been cloned and expressed in *Xenopus* oocytes, yeast, and other cell types to study the characteristics of KIR channels electrophysiologically (Dreyer et al., 1999). Cation influx through KIR channels is inhibited in a voltage-dependent manner by extracellular Cs^+ (Ichida and Schroeder, 1996; Dreyer et al., 1999). Therefore, although Cs^+ can physically diffuse through the KIR channels, practically it can hardly permeate from the soil solution in the natural environment (White and Broadley, 2000).

VIC channels have non-selective cation permeability and voltage independence (insensitivity). The permeability of Cs^+ through the VIC channels in rye roots was 0.85 when that of K^+ was defined as 1.0 (White and Tester, 1992). Cation influx through the VIC channels is insensitive to Cs^+, but is partly inhibited by Ca^{2+}, Ba^{2+}, and other divalent ions (Roberts and Tester, 1997; White, 1997, 1999; Davenport and Tester, 2000). These characteristics correspond to the inhibition of Cs^+ influx by divalent ions.

Finally, we introduce the results of the mutant analysis of the model plant *Arabidopsis thaliana*. In Arabidopsis, deletion mutant lines of K^+ transporters such as HAK and AKT have been obtained to study their contribution to Cs^+ influx.

AtHAK5 is a high-affinity K^+ transporter that mainly absorbs K^+ at low extracellular K^+ concentrations. The AtHAK5 deletion significantly reduced Cs^+ absorption, but Cs^+ absorption was not significantly changed in AtAKT1 deletion mutants (Broadley et al., 2001; Qi et al., 2008). However, Cs^+ uptake in *athak5* mutants during K^+ deficiency did not decrease significantly, suggesting that Cs^+ was absorbed by other K^+ transporters (Qi et al., 2008). Recently, it was reported that, when grown on radioactive Cs-contaminated soil, the amount of Cs^+ uptake by *athak5* is significantly lower than that of the wild type (Tanoi et al., 2019).

The rate of K^+ uptake was examined in *athak5* and *atakt1* single and double mutants. At K^+ concentrations lower than 0.01 mM, only AtHAK5 is involved in K^+ uptake, whereas at K^+ concentrations from 0.01 to 0.05 mM, both AtHAK5 and AtAKT1 are activated in K^+ uptake (Rubio et al., 2008, 2010). This suggested that AtAKT1 and other low-affinity K^+ transporters absorb K^+ at higher K^+ concentrations. In addition, the double *athak5* and *atakt1* mutants were able to grow at K^+ concentrations higher than 0.05 mM, suggesting that K^+ transporters other than AtHAK5 and AtAKT1 absorb K^+ and complement for the lack of the two K^+ transporters.

Caballero et al. (2012) reported that a Ca^{2+} sensitive transport system mediates low-affinity K^+ uptake in the *atakt1* plants. The low affinity system probably belonging to the VIC channels may mediate the K^+ uptake in *athak5*, *atakt1* plants.

In summary

I. Cs^+ is absorbed by the same mechanism as K^+, and their relationship is competitive.
II. Certain Cs^+ influx pathways are also inhibited by divalent ions such as Ca^{2+}.
III. Cs^+ and K^+ are not absorbed into the plant roots equally. It is also hypothesized that Cs^+ inhibits the K^+ influx through KIR channels. Cs^+ permeability differs for HAK, KIR, and VIC channels.
IV. There are at least two Cs^+ influx pathways into the roots (in wheat). The Cs^+ concentration dependence of Cs^+ influx into the roots could be drawn by the sum of two hyperbolae.
V. K^+ uptake systems have a high level of redundancy in plants. If one of K^+ transporters is inactivated, K^+ influx is complemented by other K^+ transporters (HAK, AKT, VIC). Similarly, Cs^+ uptake system may involve multiple K^+ transporters.

White and Broadley (2000) proposed the Cs^+ uptake model, which was based on the characteristics of each type of K^+ transporters (including VIC channels). The model predicted that the VIC channel and the HAK family mainly absorb Cs^+ into the root, and KIR channels, such as AKT1, are almost unrelated to the Cs^+ uptake (White and Broadley, 2000). However, in order to fully prove the model, it is necessary to create a plant in which each pathway has been deleted by techniques such as mutation or genome editing and examine the effect of gene deletions on Cs^+ influx. Ultimately, the goal would be to create a plant that does not absorb Cs^+. Unfortunately, this has not been achieved before Fukushima.

Cs UPTAKE MECHANISM INTO RICE ROOTS

In the post-Fukushima studies, cultivation tests of many rice varieties in Cs-contaminated soils were conducted promptly to examine the differences in Cs uptake between varieties (Ohmori et al., 2014; Ono et al., 2014). Cs accumulation in the straw and brown rice of numerous varieties was analyzed, and the results revealed wide differences in Cs accumulation between varieties and large fluctuations in a cultivation year. These studies could not identify the causative genes for low and high Cs accumulation.

The analyses conducted in rice fields established no correlation between the concentrations of radio-Cs in soils and the amount of radio-Cs absorbed by rice plants. However, there was a correlation between the amounts of exchangeable K^+ in the soils and the radio-Cs absorbed by rice plant (Kato et al., 2015; Kohyama et al., 2015; Kondo et al., 2015). The K^+ levels in the soils have a greater effect on the Cs uptake of plants than the concentration of radio-Cs in the soil.

Our research group separated the mutants with low Cs^+ uptake and identified the causative gene. Elemental analysis

of brown rice in 8027 mutants, which were induced by chemical mutation treatment, isolated a mutant with low Cs^+ uptake whose Cs concentration in brown rice was less than 10% of the wild type (Rai et al., 2017). OsHAK1, a member of the high-affinity HAK family expressed in roots, was identified as the causative gene. During hydroponic cultivation with multiple K^+ concentrations, the Cs^+ influx into the roots of *oshak1* was significantly reduced by less than 1/8 of the Cs^+ influx in wild type under low to normal soil K^+ concentrations. When this mutant was cultivated in a paddy field with high $^{134,137}Cs$ and low K^+ concentration, the ^{137}Cs of wild-type brown rice was 44 Bq/kg, whereas that of *oshak1* was lower than the detection limit (4.92 Bq/kg). Although the absorption of Cs^+ decreased, the absorption of K^+ was not significantly different from that of the wild type (Rai et al., 2017; **Figure 5**). This indicated that other K^+ transporters complemented the K^+ uptake of OsHAK1. It has been also suggested that K^+ transporters other than OsHAK1 expressed on the surface of rice roots (mainly OsAKT1) hardly absorb Cs^+. This is in agreement with the results of Cs^+ permeability analysis in higher plants (Wegner and Raschke, 1994; Maathuis and Sanders, 1995).

The contribution of OsHAK1 to K^+ absorption increases under low K^+ conditions (50–55% in the range of 50–100 μM K^+ and 30% at 1 mM K^+) (Chen et al., 2015). The expression of OsHAK1 is induced 8–12-fold under K^+ deficiency, but suppressed under increased external K^+ concentration (Okada et al., 2008; Chen et al., 2015). These findings suggest that the use of potassium fertilizer not only reduces the Cs^+ uptake rate by increasing the K^+:Cs^+ ratio, but also reduces the Cs^+ uptake by suppressing OsHAK1 expression.

The contribution of OsHAK1 for Cs^+ uptake has been also analyzed by reverse genetic techniques. The knockout lines that have lost the function of OsHAK1 created by CRISPR-Cas9 genome editing did not depolarize even when the roots were immersed in Cs^+ solutions with different concentrations (Nieves-Cordones et al., 2017). This indicated that Cs^+ was not absorbed into the root cells and the root membrane potential remained unaffected. It has also been reported that, when cultivated on K^+-deficient soil contaminated with radio-Cs, the amount of $^{134,137}Cs$ absorbed was significantly lower than that of the wild type (Nieves-Cordones et al., 2017).

Both the forward and reverse gene techniques identified the same causative gene, revealing that most of the Cs^+ uptake in rice plants takes place via OsHAK1. Cs absorption could be reduced by indirectly suppressing HAK expression (Ishikawa et al., 2017). From the mutants irradiated with accelerated carbon ions, a low-Cs mutant was obtained that could reduce the radio-Cs uptake to about 30% of that of the wild type. The causative gene in this mutant was *OsSOS2*. This gene encodes a kinase that phosphorylates OsSOS1 (Na^+/H^+ antiporter) in rice root cells. Considering that OsSOS1 is activated by phosphorylation, knockout of *OsSOS2* inactivates OsSOS1 and reduces the Na^+ extrusion from roots. Increased intracellular Na^+ concentration is sensed by the cell as an increase in osmotic pressure, which triggers the cell to suppresses the expression of K^+ transporters such as *HAK* (*OsHAK1*, *OsHAK5*), *OsAKT1*, and *OsHKT2*. It ultimately results in a decreased Cs^+ influx through these K^+ transporters. It has been shown that the stress caused by increasing Na^+ concentration in the root cells can also reduce Cs uptake in rice (Ishikawa et al., 2017). Thus, the mechanism of salt tolerance in rice can also be used to suppress Cs^+ uptake.

Cs ABSORPTION IN OTHER HIGHER PLANTS

Most of the radio-Cs that had fallen to land after the Fukushima nuclear accident entered the forest ecosystem. Therefore, it is also important to examine the absorption of radio-Cs in trees. An interesting dynamics of Cs^+ transport was revealed in the model forest tree poplar. The poplar does not change its K^+ absorption during both long-day period and short-day period. However, the rate of Cs^+ uptake by poplar treated for 6 weeks on short days decreased to about 1/4 of that in poplar treated for 9 days on a long day. Furthermore, the expression levels of major HAK and VIC channels did not change, suggesting that the tree may have an unknown Cs^+ absorption pathway (Noda et al., 2016).

After absorption into root cells, K^+ and Cs^+ are moved to cambium via cytoplasmic communication, and then released from the adjacent vessel cells via the KOR channels. One of the KOR channels, stelar K^+ outward rectifying channel (SKOR), has been identified in Arabidopsis. The SKOR is involved in the permeation of K^+, Rb^+, and Cs^+. However, as the results were obtained by heterologous expression, the pathway of Cs^+ in the plant body could not be elucidated (Gaymard et al., 1998; Johansson et al., 2006).

The molecular recognition of Cs^+ and K^+ in the K^+ transporter has also been reported. Mutations were randomly introduced by PCR in cDNA synthesized from AtHAK5 of *A. thaliana* and heterologously expressed in yeast. When amino acid substitution occurred between the second and third transmembrane regions containing the K^+ binding hole, the selectivity of K^+ was 100-fold higher than that for Na^+ or Cs^+ (Alemán et al., 2014). This points to a possibility that the selectivity of the high-affinity K^+ transporter for alkali metal ions can be further improved, and that only K^+ is incorporated into the cell by editing the amino acid sequence of HAK by mutagenesis. It may be possible to produce plants with K^+ transporters that are highly selective toward K^+ absorption (as well as plants that preferentially accumulate Cs^+). The plant K^+ transporter may have undergone evolutionary pressure for selective permeability of alkali metal ions.

COMPARING THE PATHWAY OF Cs^+ UPTAKE IN RICE ROOTS WITH THE MODEL PROPOSED BY WHITE AND BROADLEY

White and Broadley (2000) proposed a model for Cs^+ uptake, in which VIC channels contribute most of the Cs^+ influx under

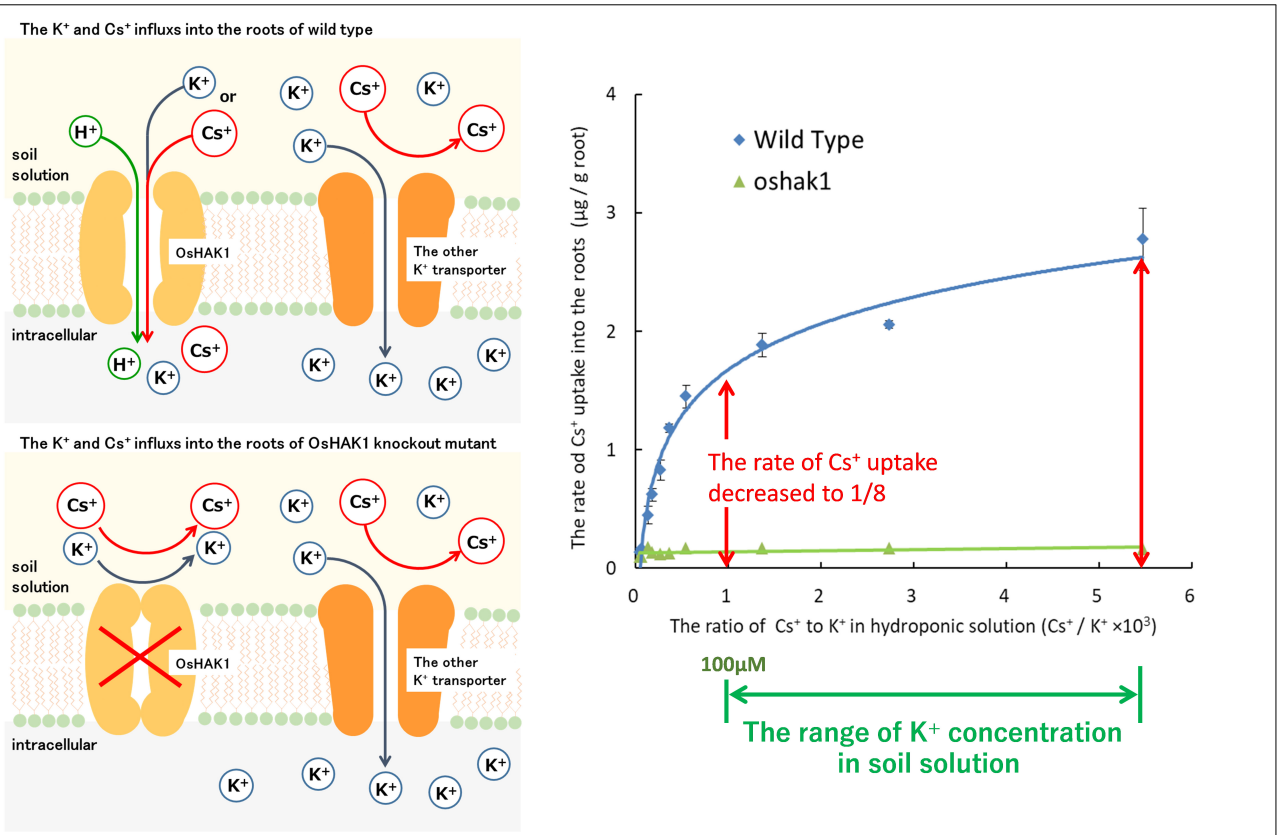

FIGURE 5 | The newly elucidated mechanism of Cs uptake in the rice plants. Upper left side: The root cells of rice (wild type) absorb K^+ and Cs^+ through OsHAK1 at extracellular K^+ concentration below 100 μM. Lower left side: OsHAK1 knockout mutants could not absorb K^+ and Cs^+ through OsHAK1. However, the rate of K^+ uptake was maintained and the uptake was complemented by K^+ transporters other than OsHAK1. Possibly, other K^+ transporters other than OsHAK1 in the membrane did not permeate Cs^+. Right figure: In typical soils, the concentration of K^+/the concentration of Cs^+ in soil solution is higher than 10^3. When the K^+ concentration in the hydroponic solution is 0–100 μM and the Cs^+ concentration is fixed at 75 nM, the rate of Cs^+ uptake into the root of the OsHAK1 mutant is reduced to 1/8 or less compared to the wild type. In addition, the rate of the slight Cs uptake is constant regardless of the K^+ concentration of the hydroponic solution.

realistic soil conditions and HAK transporters carry the residual Cs^+ influx. In this section, we verify whether the Cs^+ and K^+ uptake in rice fits this model, which involves HAK, KIR channels, and VIC channels.

Function of HAK in Cs^+ and K^+ Uptake by the Roots of Rice Plants

In rice grown in a hydroponic solution with normal soil K^+ concentration (0–100 μM), OsHAK1 absorbed most Cs^+ into the roots. When K^+ concentration in the hydroponic solution increased, the amount of Cs^+ uptake into the roots decreased drastically due to competition with K^+. At K^+ concentrations above 1 mM, there was no difference in Cs^+ uptake between wild-type and *OsHAK1* mutant (Rai et al., 2017). When the K^+ concentration was increased from 14 μM to 1.1 mM, the Cs^+ uptake was reduced from 2.8 to 0.13 μg g^{-1} roots, and it did not decrease further (**Figure 5** right panel). It is assumed that even at high K^+ concentrations, a small amount of Cs^+ is carried into the roots by transporters other than the K^+ transporter. The predicted mechanism of Cs^+ uptake under high K^+ condition is described in section "Function of VIC Channels in Cs^+ Uptake by the Roots of Rice Plants" (Rai et al., 2017).

In the simulation by White and Broadley (2000), at K^+ concentrations between 10 μM and 1 mM, the Cs^+ influx (Cs^+ concentration: 0.1 μM) is reduced to only about 1/4. Bossemeyer et al. (1989) reported that the KUP transporter in *Escherichia coli* has a K_m of 5 mM for Cs^+ transport and a K_m of 0.37 mM for K^+ transport. The simulation was based on the fact that K_m of HAK for Cs^+ transport is 10-fold higher than the K_m for K^+ transport.

However, Bañuelos et al. (2002) analyzed the Cs^+ transport functions of OsHAK1 in heterologous expression and revealed that the yeast-expressed chimeric OsHAK1 (a part of the barley HvHAK1 sequence was added to the incomplete OsHAK1 cDNA) can transport Cs^+ and K^+ with a K_m of 11 and 6 μM, respectively. Thus, the difference in K_m for Cs^+ and K^+ transport may be smaller (Cs: up to 2-fold, K^+: up to 11-fold) compared with the difference predicted by their model (White and Broadley, 2000; Bañuelos et al., 2002).

OsHAK1 is a high-affinity transporter that contributes to K^+ uptake mainly under low K^+ concentration, but under extracellular K^+ deficiency, the expression levels of this

transporter in the roots increase several-fold (Okada et al., 2008, 2018; Nieves-Cordones et al., 2016). Thus, the responses of rice plants indicate that the contribution of HAK (OsHAK1) to Cs^+ uptake may be higher than predicted by their model.

Function of KIR Channels (OsAKT1) in Cs^+ and K^+ Uptake by the Roots of Rice Plants

Deletion of *OsHAK1* drastically reduces Cs^+ uptake, but the K^+ uptake rates do not differ greatly between the OsHAK1 mutant and the wild type. This was attributed to other systems, which are involved in K^+ absorption into the roots, but contributed much less to Cs^+ uptake in OsHAK1 mutants. In rice roots, OsHAK1 and OsAKT1 mediate the K^+ uptake according to the extracellular K^+ concentration (Nieves-Cordones et al., 2016). In *oshak1*, probably most of K^+ that is typically absorbed by OsHAK1 is transported by OsAKT1. Although the KIR channel is a low affinity K^+ uptake system, the overexpression of OsAKT1 could improve the K^+ uptake under 100 μM K^+ conditions. OsAKT1-mediated K^+ flux may be small but can generate a sizeable contribution over prolonged periods (Ahmad et al., 2016).

The current of KAT1 in Arabidopsis, a kind of KIR, is blocked by Cs^+; it was reduced by 20% at Cs^+ concentration of 0.1 mM, and by 50% at 0.5 mM Cs^+ (Ichida and Schroeder, 1996). However, because the concentration of ^{133}Cs in the soil solution (below Cs^+: 10 ppb,75 nM) is considerably lower than the concentration of Cs^+ examined in these studies, it is likely that OsAKT1 is not blocked by Cs^+ and thus can complement for the loss of K^+ absorption caused by the absence of OsHAK1. In addition, as we discuss below, it is almost certain that OsAKT1 does not contribute to Cs^+ influx because the remaining Cs^+ uptake is not affected by K^+.

Function of VIC Channels in Cs^+ Uptake by the Roots of Rice Plants

Even with OsHAK1 knockout, a small amount of Cs^+ was incorporated into rice roots. The residual Cs^+ uptake in OsHAK1 mutant was not affected by the extracellular K^+ concentration. The model proposed by White and Broadley (2000) showed that a high amount of Cs^+ entered into the roots through the VIC channels. A relative permeability sequence of K^+:Rb^+:Cs^+:Na^+:Li^+ of 1.00:1.00:0.85:0.73:0.71 ($K^+ = Rb^+ > Cs^+ > Na^+ > Li^+$) was given by the electrical conductance measurements of the VIC channels on the plasma membrane in the rye roots (White and Tester, 1992). In wheat roots, the selectivity relative to Na^+ was NH_4^+ (2.06) > Rb^+ (1.38) > K^+ (1.23) = Cs^+ (1.18) > Li^+ (0.83) > TEA^+ (0.21) = Ca^{2+} (0.21) (Davenport and Tester, 2000). On the basis of the results, Cs^+ permeability via the VIC channels is much higher than that via KIR channels. Cation influx through the VIC channels is partly inhibited by Ca^{2+}, Ba^{2+}, and other divalent ions (Roberts and Tester, 1997; White, 1997, 1999; Davenport and Tester, 2000).

These characteristics of VIC channels correspond to the inhibition of Cs^+ influx of the plants by divalent ions (Handley and Overstreet, 1961; Smolders et al., 1997). Therefore, the uptake of residual Cs^+ in rice roots may have occurred through the VIC channels.

However, the contribution of the VIC channels in rice roots was considerably lower than that of OsHAK1, which was the opposite of what was predicted by their model. A possible reason is that the Cs^+ concentration in soil solution was lower than that assumed in their model. Given that the amount of Cs^+ uptake varies greatly depending on the extracellular K^+ concentration, the contribution of each transporter to Cs^+ uptake depends greatly on the value of extracellular K^+ concentration that is assumed standard. For example, if K^+ concentration is high, the contribution of HAK is lower and the contribution of other transporters (such as VIC channels) becomes high. Therefore, in this review, we discussed the contribution of each transporter to Cs^+ uptake under K^+ and Cs^+ concentrations typically found in actual soils.

The other reason for the discrepancy between the model and our results is that rice plants have remarkably high silica content. Rice plants actively absorb silicic acid, and its content in the stem and leaves ranges from 10 to 20%. In contrast, Ca^{2+} content of rice plants (0.3 to 0.4%, w/w) is lower than that recorded in other plants (average of 1.57%). Therefore, it was suggested that the Ca^{2+} concentration in the rhizosphere or apoplast of rice plants is higher than that in other plants because rice plants do not absorb high amounts of Ca^{2+}. Future research should analyze which VIC channels are involved in Cs^+ uptake into the roots by means of molecular techniques, mutations, or other methods.

Thus, the results of rice analysis indicated that, under normal soil conditions, OsHAK1 mediate 80–90% of Cs^+ uptake into the roots and the rest is mediated by VIC channels (Rai et al., 2017; **Figure 6**-⑤⑥). The proportion each transporter contributed to the Cs uptake was different, but they mostly agreed with the prediction by White and Broadley (2000).

SUMMARY OF THE DYNAMICS OF RADIO-Cs FROM SOIL TO PLANTS

The key point in the dynamics of radio-Cs in soils is its immobilization in soils. The amount of frayed edge sites in soils have significant effects on the radio-Cs uptake by plants. The free radio-Cs strongly binds to frayed edge sites in the soil, which decreases available radio-Cs for plants with time. This phenomenon is important for predicting the radio-Cs uptake of plants in addition to the decay of radioactivity of $^{134,137}Cs$ in soils (**Figure 6** ①).

In the dynamics of radio-Cs from soils to plants, the concentration of K^+ in soil solution affects the radio-Cs uptake into plants because K^+ and Cs^+ compete for absorption into plant roots. While the available K^+ concentration in soils increases, the Cs^+ uptake by plants decreases drastically (Zhu and Smolders, 2000; Kato et al., 2015; Kohyama et al., 2015; Kondo et al., 2015). Therefore, the application of potassium fertilizers is effective for preventing the agricultural crops from absorbing radio-Cs in contaminated fields (**Figure 6** ②).

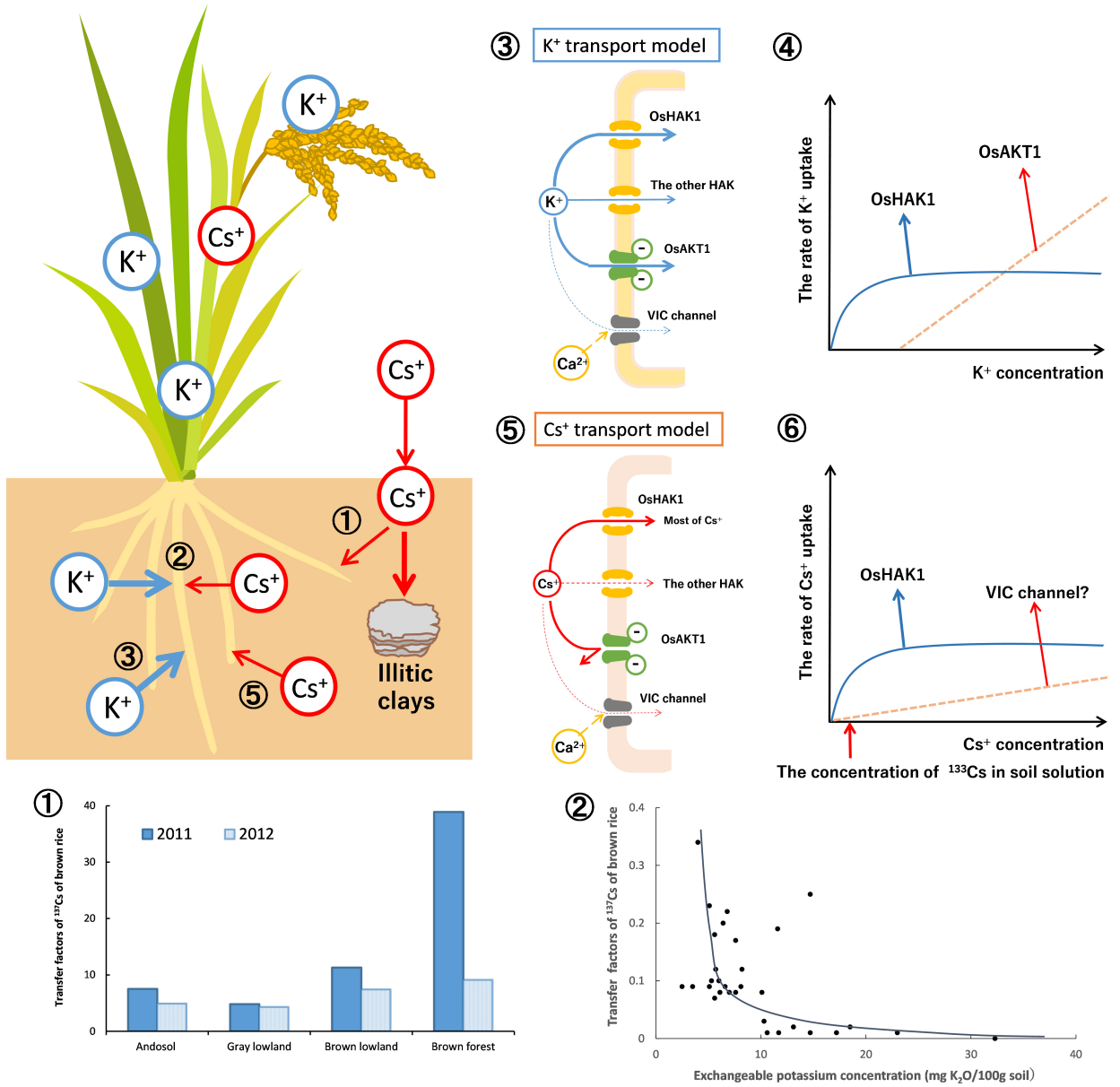

FIGURE 6 | Dynamics of radioactive Cs between soil and plant (using rice as an example). The dynamics of Cs^+ in soils was mainly affected by the specific adsorption to soil clay material (frayed edge sites of mica) and the competition with K^+ in the uptake by plants. As described in **Figure 2**, the newly entered Cs^+ (radio Cs^+) would be eventually immobilized. Therefore, available Cs^+ and its transfer factors in the rice grains decreased yearly (①). The graph is drawn from the data of Fujimura et al. (2015). The relationship between the soils-to-rice-plant transfer factors and the concentration of exchangeable potassium in soils was shown (②). The K^+ and Cs^+ compete for absorption by the rice roots. While exchangeable (plant-available) K^+ in soils increased, the Cs^+ concentrations in rice grains decreased drastically. The graph is drawn from the data of Kohyama et al. (2015). The K^+ and Cs^+ uptake in rice plants by the membrane transporters is estimated. In ③, the mode of K^+ uptake in the roots of rice plants is proposed. K^+ uptake is mainly through OsHAK1 and OsAKT1. In ④, the K^+ uptake curve is composed of two distinct transporter systems as shown by Epstein (1972). The solid line indicates the rate of K^+ uptake by OsHAK1 in rice while the dotted line indicates the K^+ influx through OsAKT1 channel. The rest of K^+ uptake is contributed by the other K^+ transporters. In ⑤, the mode of Cs^+ uptake is proposed. Cs^+ uptake is through OsHAK1 and the VIC channel. In ⑥, the Cs^+ uptake curve also consists of two Michaelis–Menten hyperbolae as shown by Shaw and Bell (1989). The solid line indicates the rate of Cs^+ uptake by OsHAK1 in rice and the dotted line indicates potential Cs^+ influx through the VIC channel. Since the Cs^+ concentration in typical soil solution is lower than 75 nM (10 ppb:^{133}Cs, as the red arrow indicates), it is estimated that most of the Cs^+ uptake in rice is absorbed by OsHAK1 and the rest through the VIC channel as the latter does not compete with K^+.

Increasing the K^+ concentration in the rhizosphere is also important because it regulates the expression of HAK, which absorb Cs^+ into the roots.

In rice roots, OsHAK1 and OsAKT1 mediate the K^+ uptake according to the extracellular K^+ concentration (Nieves-Cordones et al., 2016; **Figure 6** ③). The K^+ uptake curve is

divided into the two hyperbolae (Epstein, 1972). The K^+ uptake under low K^+ concentration depends upon OsHAK1, and the K^+ influx under high K^+ levels is mediated mainly by the OsAKT1 channel (**Figure 6** ④).

The Cs^+ uptake curve in wheat at 200 μM Cs^+ could also be described by the sum of two Michaelis–Menten hyperbolae (Shaw and Bell, 1989). It is estimated that most of the Cs^+ uptake in rice is via OsHAK1 under normal soil K^+ concentrations. Permeability of KIR channels to Cs^+ is lower than that to K^+; practically, Cs^+ can hardly permeate. The residual Cs^+ influx into roots does not compete with K^+, suggesting that it may be via transporters not involved in K^+ uptake (**Figure 6** ⑤). The uptake of low affinity Cs^+ is inhibited by divalent cations (Handley and Overstreet, 1961), whereas the permeability of monovalent cations through VIC channel is partly inhibited by Ca^{2+} (Davenport and Tester, 2000). It is reasonable to conclude that the residual Cs^+ influx is through VIC channels (**Figure 6** ⑥).

CONCLUSION

Humans have experienced extensive radionuclide contamination from atmospheric nuclear tests and the two nuclear power plant accidents. Nuclear tests in the atmosphere have already been prohibited, but the nuclear power accounts for 10% of global electricity production. Therefore, the risk of nuclear incidents must be considered and we must cope with the risks. Radio-Cs (^{134,137}Cs) described in this review, is produced in large amounts in the reactor core. It has a low boiling point and easily diffuses into the environment after accidents. Furthermore, it has a long half-life and strongly adsorbs to soil, remaining in the environment for a long time. In unforeseen circumstances, radio Cs can be absorbed by plants and enter the food chain.

Since Fukushima, numerous studies have been conducted in Japan, including those on radio-Cs dynamics in the environment, radionuclide testing of agricultural products, and the cultivation of various crops. In addition, our understanding of the mechanism of Cs^+ uptake in rice has rapidly progressed owing to the implementation of genetic and molecular techniques such as mutations and genome editing. As shown in this review, many researchers have conducted hydroponics experiments with various ion conditions, heterologous expression analysis of K^+ transporters using *Xenopus oocyte* and yeast, electrophysiological analysis using microelectrodes, and analysis of mutants by forward and reverse genetics. Thus, different pathways were implemented to elucidate the entire mechanism of Cs^+ (K^+) uptake and transport. These experimental results are expected to reveal the Cs^+ dynamics in soil, from soil to plant, and in individual plants. They will also lead to deeper understanding of the risks of nuclear power plants (problems caused by radio-Cs) to soil–plant ecosystems.

AUTHOR CONTRIBUTIONS

HR and MK made substantial direct and intellectual contribution to this work and approved the manuscript for publication.

FUNDING

This work was supported by the JSPS KAKENHI Grant Number JP19H04272.

REFERENCES

Ahmad, I., Mian, A., and Maathuis, F. M. J. (2016). Overexpression of the rice AKT1 potassium channel affects potassium nutrition and rice drought tolerance. *J. Exp. Bot.* 67, 2689–2698. doi: 10.1093/jxb/erw103

Alemán, F., Caballeo, F., Ródenas, R., Rivero, R. M., Martínez, V., and Rubio, F. (2014). The F130S point mutation in the Arabidopsis high-affinity K+ transporter AtHAK5 increases K+ over Na+ and Cs+ selectivity and confers Na+ and Cs+ tolerance to yeast under heterologous expression. *Front. Plant Sci.* 5:430. doi: 10.3389/fpls.2014.00430

Almgren, S., and Isaksson, M. (2006). Vertical migration studies of 137Cs from nuclear weapons fallout and the Chernobyl accident. *J. Environ. Radioact.* 91, 90–102. doi: 10.1016/j.jenvrad.2006.08.008

Amrutha, R. N., Sekhar, P. N., Varshney, R. K., and Kishor, P. B. K. (2007). Genome-wide analysis and identification of genes related to potassium transporter families in rice (*Oryza sativa* L.). *Plant Sci.* 172, 708–721.8.

Ashley, M. K., Grant, M., and Grabov,A. (2005). Plant responses to potassium deficiencies: a role for potassium transport proteins. *J. Exp. Bot.* 57, 425–436. doi: 10.1093/jxb/erj034

Bange, G. G. J., and Overstreet, R. (1960). Some observations on absorption of cesium by excised barley roots. *Plant Physiol.* 35, 605–608. doi: 10.1104/pp.35.5.605

Bañuelos, M. A., Garciadeblas, B., Cubero, B., and Rodríguez-Navarro, A. (2002). Inventory and functional characterization of the HAK potassium transporters of rice. *Plant Physiol.* 130, 784–795. doi: 10.1104/pp.007781

Beresford, N. A., Fesenko, S., Konoplev, A., Skuterudd, L., Smithe, J. T., and Voigt, G. (2016). Thirty years after the chernobyl accident: what lessons have we learnt? *J. Environ. Radioact.* 157, 77–89. doi: 10.1016/j.jenvrad.2016.02.003

Beresford, N. A., Robert, W., Mayes, R. W., Cooke, A. I., Barnett, C. L., Howard, B. J., et al. (2000). The Importance of source-dependent bioavailability in determining the transfer of Ingested radionuclides to ruminant-derived food products. *Am. Chem. Soc.* 34, 4455–4462. doi: 10.1021/es0000697

Bossemeyer, D., Schlösser, A., and Bakker, E. P. (1989). Specific cesium transport via the *Escherichia coli* kup (TrkD) K+ uptake system. *J. Bacteriol.* 171, 2219–2221. doi: 10.1128/jb.171.4.2219-2221.1989

Bregante, M., Carpaneto, A., Pastorino, F., and Gambale, F. (1997). Effects of mono- and multi-valent cations on the inward-rectifying potassium channel in isolated protoplasts from maize roots. *Eur. Biophys. J.* 26, 381–391. doi: 10.1007/s002490050092

Broadley, M. R., Escobar-Gutiérrez, A. J., Bowen, H. C., Willey, N. J., and White, P. J. (2001). Influx and accumulation of Cs+ by the *akt1* mutant of *Arabidopsis thaliana* (L.) Heynh. lacking a dominant K+ transport system. *J. Exp. Bot.* 52, 839–844. doi: 10.1093/jexbot/52.357.839

Caballero, F., Botella, M. A., Rubio, L., Fernández, J. A., Martínez, V., and Rubio, F. (2012). A Ca2+-sensitive system mediates low-affinity K+ uptake in the absence of AKT1 in Arabidopsis Plants. *Plant Cell Physiol.* 53, 2047–2059. doi: 10.1093/pcp/pcs140

Chen, G., Hu, Q., Luo, L., Yang, T., Zhang, S., Hu, Y., et al. (2015). Rice potassium transporter OsHAK1 is essential for maintaining potassium-mediated growth and functions in salt tolerance over low and high potassium concentration ranges. *Plant Cell Environ.* 38, 2747–2765. doi: 10.1111/pce.12585

Chino, M., Nakayama, H., Nagai, H., Terada, H., Katata, G., and Yamazawa, H. (2011). Preliminary estimation of release amounts of ^{131}I and ^{137}Cs accidentally discharged from the Fukushima Daiichi nuclear power plant into the atmosphere. *J. Nucl. Sci. Technol.* 48, 1129–1134. doi: 10.1080/18811248.2011.9711799

Collander, R. (1941). Selective absorption of cations by higher plants. *Plant Physiol.* 16, 691–720. doi: 10.1104/pp.16.4.691

Cremers, A., Elsen, A., Preter, P. D., and Maes, A. (1988). Quantitative analysis of radiocaesium retention in soils. *Nature* 335, 247–249. doi: 10.1038/335247a0

Davenport, R. J., and Tester, M. (2000). A weakly voltage-dependent, nonselective cation channel mediates toxic sodium influx in wheat. *Plant Physiol.* 122, 823–834. doi: 10.1104/pp.122.3.823

Dreyer, I., Horeau, C., Lemaillet, G., Zimmermann, S., Bush, D. R., Rodríguez-Navarro, A., et al. (1999). Identification and characterization of plant transporters using heterologous expression systems. *J. Exp. Bot.* 50, 1073–1087. doi: 10.1093/jexbot/50.suppl_1.1073

Epstein, E. (1972). *Mineral Nutrition of Plants : Principles and Perspectives*. New York, NY: Wiley.

Fesenko, S., Isamov, N., Barnett, C. L., Beresford, N. A., Howard, B. J., Sanzharova, N., et al. (2015). Review of Russian language studies on radionuclide behaviour in agricultural animals: biological half-lives. *J. Environ. Radioact.* 142, 136–151. doi: 10.1016/j.jenvrad.2015.01.015

Fesenko, S. V., Alexakhin, R. M., Balonov, M. I., Bogdevitch, I. M., Howard, B. J., Kashparov, V. A., et al. (2007). An extended critical review of twenty years of countermeasures used in agriculture after the Chernobyl accident. *Sci. Total Environ.* 383, 1–24. doi: 10.1016/j.scitotenv.2007.05.011

Fujimura, S., Muramatsu, Y., Ohno, T., Saitou, M., Suzuki, Y., Kobayashi, T., et al. (2015). Accumulation of 137Cs by rice grown in four types of soil contaminated by the Fukushima Dai-ichi nuclear power plant accident in 2011 and 2012. *J. Environ. Radioact.* 140, 59–64. doi: 10.1016/j.jenvrad.2014.10.018

Gaymard, F., Pilot, G., Lacombe, B., Bouchez, D., Bruneau, D., Boucherez, J., et al. (1998). Identification and disruption of a plant shaker-like outward channel involved in K+ release into the xylem sap. *Cell* 94, 647–655.

Gierth, M., Mäser, P., and Schroeder, J. I. (2005). The potassium transporter *AtHAK5* functions in K+ deprivation-induced high-affinity K+ uptake and *AKT1* K+ channel contribution to K+ uptake kinetics in Arabidopsis roots. *Plant Physiol.* 137, 1105–1114.

Gomez-Porras, J. L., Riaño-Pachón, D. M., Benito, B., Haro, R., Sklodowski, K., Rodríguez-Navarro, A., et al. (2012). Phylogenetic analysis of K+ transporters in bryophytes, lycophytes, and flowering plants indicates a specialization of vascular plants. *Front. Plant Sci.* 3:167. doi: 10.3389/fpls.2012.00167

Gupta, M., Qiu, X., Wang, L., Xie, W., Zhang, C., Xiong, L., et al. (2008). KT/HAK/KUP potassium transporters gene family and their whole-life cycle expression profile in rice (*Oryza sativa*). *Mol. Genet. Genomics* 280, 437–452. doi: 10.1007/s00438-008-0377-7

Hampton, C. R., Bowen, H. C., Broadley, M. R., Hammond, J. P., Mead, A., Payne, K. A., et al. (2004). Cesium toxicity in Arabidopsis. *Plant Physiol.* 136, 3824–3837. doi: 10.1104/pp.104.046672

Handley, R., and Overstreet, R. (1961). Effect of various cations upon absorption of carrier-free cesium. *Plant Physiol.* 36, 66–69. doi: 10.1104/pp.36.1.66

Henrichs, K., Paretzke, H. G., Voigt, G., and Berg, D. (1989). Measurements of Cs absorption and retention in man. *Health Phys.* 57, 571–578.

Ichida, A. M., and Schroeder, J. I. (1996). Increased resistance to extracellular cation block by mutation of the pore domain of the *Arabidopsis* inward-rectifying K+ channel KAT1. *J. Membrane Biol.* 151, 53–62.

Imanaka, T. (2016). Chernobyl and Fukushima: comparison of accident process and radioactive contamination. *Kagaku* 86, 252–257. doi: 10.1093/jrr/rrv074

International Atomic Energy Agency [IAEA] (2003–2005). Chernobyl's Legacy: Health, Environmental, and Socio-economic Impacts, and Recommendations to the Governments of Belarus, the Russian Federation, and Ukraine. The Chernobyl Forum. ed. Kinly III (Vienna: International Atomic Energy Agency [IAEA]).

Ishikawa, S., Hayashi, S., Abe, T., Igura, M., Kuramata, M., Tanikawa, H., et al. (2017). Low-cesium rice: mutation in OsSOS2 reduces radiocesium in rice grains. *Sci. Rep.* 7:2432. doi: 10.1038/s41598-017-02243-9

Johansson, I., Wulfetange, K., Porée, F., Michard, E., Gajdanowicz, P., Lacombe, B., et al. (2006). External K+ modulates the activity of the Arabidopsis potassium channels SKOR via an unusual mechanism. *Plant J.* 46, 269–281.

Kato, N., Kihou, N., Fujimura, S., Ikeba, M., Miyazaki, N., Saito, Y., et al. (2015). Potassium fertilizer and other materials as countermeasures to reduce radiocesium levels in rice: results of urgent experiments in 2011 responding to the Fukushima Daiichi Nuclear Power Plant accident. *Soil Sci. Plant Nutr.* 61, 179–190.

Kitagawa, Y., Yanai, J., and Nakao, A. (2017). Evaluation of nonexchangeable potassium content of agricultural soils in Japan by the boiling HNO3 extraction method in comparison with exchangeable potassium. *Soil Sci. Plant Nutr.* 64, 116–122.

Kohyama, K., Obara, H., Takata, Y., Saito, T., Sato, M., Yoshioka, K., et al. (2015). Soil properties for analyzing cause of high radiocesium concentration in brown rice produced. *Bull. Natl. Inst. Agroenviron. Sci.* 34, 63–73.

Kondo, M., Maeda, H., Goto, A., Nakano, H., Kiho, N., Makino, T., et al. (2015). Exchangeable Cs/K ratio in soil is an index to estimate accumulation of radioactive and stable Cs in rice plant. *Soil Sci. Plant Nutr.* 61, 133–143. doi: 10.1080/00380768.2014.973347

Maathuis, F. J. M. (2009). Physiological functions of mineral macronutrients. *Curr. Opin. Plant Biol.* 12, 250–258. doi: 10.1016/j.pbi.2009.04.003

Maathuis, F. J. M., and Sanders, D. (1994). Mechanism of high-affinity potassium uptake in roots of *Arabidopsis thaliana*. *Proc. Natl. Acad. Sci. U.S.A.* 91, 9272–9276.

Maathuis, F. J. M., and Sanders, D. (1995). Contrasting roles in ion transport of two K+-channel types in root cells of *Arabidopsis thaliana*. *Planta* 197, 456–464.

Mäser, P., Thomine, S., Schroeder, J. I., Ward, J. M., Hirschi, K., Sze, H., et al. (2001). Phylogenetic relationships within cation transporter families of Arabidopsis. *Plant Physiol.* 126, 1646–1667.

Nieves-Cordones, M., Martínez, V., Benito, B., and Rubio, F. (2016). Comparison between *Arabidopsis* and rice for main pathways of K+ and Na+ uptake by roots. *Front. Plant Sci.* 7:992. doi: 10.3389/fpls.2016.00992

Nieves-Cordones, M., Mohamed, S., Tanoi, K., Kobayashi, N. I., Takagi, K., Vernet, A., et al. (2017). Production of low-Cs+rice plants by inactivation of the K+transporter OsHAK1 with the CRISPR-Cas system. *Plant J.* 92, 43–56. doi: 10.1111/tpj.13632

Nihei, N. (2013). "Radioactivity in agricultural products in Fukushima," in *Agricultural Implications of the Fukushima Nuclear Accident*, eds T. M. Nakanishi and K. Tanoi (Tokyo: Springer), 73–85.

Noda, Y., Furukawa, J., Aohara, T., Nihei, N., Hirose, A., Tanoi, K., et al. (2016). Short day length-induced decrease of cesium uptake without altering potassium uptake manner in poplar. *Sci. Rep.* 6:38360. doi: 10.1038/srep38360

Ohmori, Y., Inui, Y., Kajiwara, M., Nakata, A., Sotta, N., Kasai, K., et al. (2014). Difference in cesium accumulation among rice cultivars grown in the paddy field in Fukushima Prefecture in 2011 and 2012. *J. Plant Res.* 127, 57–66. doi: 10.1007/s10265-013-0616-9

Okada, T., Nakayama, H., Shinmyo, A., and Yoshida, K. (2008). Expression of *OsHAK* genes encoding potassium ion transporters in rice. *Plant Biotechnol.* 25, 241–245.

Okada, T., Yamane, S., Yamaguchi, M., Kato, K., Shinmyo, A., Tsunemitsu, Y., et al. (2018). Characterization of rice KT/HAK/KUP potassium transporters and K+ uptake by HAK1 from Oryza sativa. *Plant Biotechnol.* 35, 101–111. doi: 10.5511/plantbiotechnology.18.0308a

Ono, Y., Sato, K., Sakuma, H., Nemoto, K., Tanoi, K., and Nakanishi, T. M. (2014). Variation in rice radiocesium absorption among different cultivars. *Bull. Fukushima Agric. Technol. Cent.* 48, 29–32.

Pyo, Y. J., Gierth, M., Schroeder, J. I., and Cho, M. H. (2010). High-affinity K+ transport in Arabidopsis: AtHAK5 and AKT1 are vital for seedling establishment and postgermination growth under low-potassium conditions. *Plant Physiol.* 153, 863–875. doi: 10.1104/pp.110.154369

Qi, Z., Hampton, C. R., Shin, R., Barkla, B. J., White, P. J., and Schachtman, D. P. (2008). The high affinity K+ transporter AtHAK5 plays a physiological role *in planta* at very low K+ concentrations and provides a caesium uptake pathway in *Arabidopsis*. *J. Exp. Bot.* 59, 595–607. doi: 10.1093/jxb/erm330

Rai, H., Yokoyama, S., Satoh-Nagasawa, N., Furukawa, J., Nomi, T., Ito, Y., et al. (2017). Cesium uptake by rice roots largely depends upon a single gene, HAK1, which encodes a potassium transporter. *Plant Cell Physiol.* 58, 1486–1493. doi: 10.1093/pcp/pcx137

Roberts, S. K., and Tester, M. (1997). A patch clamp study of Na+ transport in maize roots. *J. Exp. Bot.* 48, 431–440. doi: 10.1093/jxb/48.Special_Issue.431

Rodríguez-Navarro, A. (2000). Potassium transport in fungi and plants. *Biochim. Biophys. Acta* 1469, 1–30.

Rubio, F., Alemán, F., Nieves-Cordones, M., and Martínez, V. (2010). Studies on Arabidopsis *athak5, atakt1* double mutants disclose the range of concentrations

at which AtHAK5, AtAKT1 and unknown systems mediate K+ uptake. *Physiol. Plant.* 139, 220–228. doi: 10.1111/j.1399-3054.2010.01354.x

Rubio, F., Nieves-Cordones, M., Alemán, F., and Martínez, V. (2008). Relative contribution of AtHAK5 and AtAKT1 to K+ uptake in the high-affinity range of concentrations. *Physiol. Plant.* 134, 598–608. doi: 10.1111/j.1399-3054.2008.01168.x

Shaw, G., and Bell, J. N. B. (1989). The Kinetics of Caesium absorption by roots of winter wheat and the possible consequences for the derivation of soil-to-plant transfer factors for radiocaesium. *J. Environ. Radioact.* 10, 213–231.

Shaw, G., and Bell, J. N. B. (1991). Competitive effects of potassium and ammonium on caesium uptake kinetics in wheat. *J. Environ. Radioact.* 13, 283–296.

Smolders, E., Sweeck, L., Merckx, R., and Cremers, A. (1997). Cationic interactions in radiocaesium uptake from solution by spinach. *J. Environ. Radioact.* 34, 161–170.

Sparks, D. L., and Huang, P. M. (1985). "physical chemistry of soil potassium," in *Potassium in Agriculture*, ed. R. D. Munson (Madison, WI: American Society of Agronomy), 201–276. doi: 10.2134/1985.potassium.c9

Szczerba, M. W., Britto, D. T., and Kronzucker, H. J. (2009). K+ transport in plants: physiology and molecular biology. *J. Plant Physiol.* 166, 447–466. doi: 10.1016/j.jplph.2008.12.009

Takahashi, J., Onda, Y., Hihara, D., and Tamura, K. (2019). Six-year monitoring of the vertical distribution of radiocesium in three forest soils after the Fukushima Dai-ichi nuclear power plant accident. *J. Environ. Radioact.* 192, 172–180. doi: 10.1016/j.jenvrad.2018.06.015

Tanoi, K., Nobori, T., Shiomi, S., Saito, T., Kobayashi, N. I., Leonhardt, N., et al. (2019). *Cesium Translocation in Rice, Agricultural Implications of the Fukushima Nuclear Accident (III)*. Singapore: Springer, 15–25.

Tsukada, H., Hasegawa, H., Hisamatsu, S., and Yamasaki, S. (2002). Transfer of 137Cs and stable Cs from paddy soil to polished rice in Aomori, Japan. *J. Environ. Radioact.* 59, 351–363.

Vandebroek, L., Hees, M. V., Delvaux, B., Spaargaren, O., and Thiry, Y. (2012). Relevane of Radiocaesium Interception Potential (RIP) on a worldwide scale to assess soil vulnerability to 137Cs contamination. *J. Environ. Radioact.* 104, 87–93. doi: 10.1016/j.jenvrad.2011.09.002

Wegner, L. H., and Raschke, K. (1994). Ion channels in the xylem parenchyma of barley roots. *Plant Physiol.* 105, 799–813.

White, P. J. (1997). Cation channels in the plasma membrane of rye roots. *J. Exp. Bot.* 48, 499–514. doi: 10.1093/jxb/48.Special_Issue.499

White, P. J. (1999). The molecular mechanism of sodium influx to root cells. *Trends Plant Sci.* 4, 245–247.

White, P. J., and Broadley, M. R. (2000). Mechanisms of caesium uptake by plants. *New Phytol.* 147, 241–256.

White, P. J., and Tester, M. A. (1992). Potassium channels from the plasma membrane of rye roots characterized following incorporation into planar lipid bilayers. *Planta* 186, 188–202. doi: 10.1007/BF00196248

Yamaguchi, N. (2014). Adsorption mechanism of radiocesium on soil. *J. Jpn. Soc. Soilphys.* 126, 11–21.

Yang, Z., Gao, Q., Sun, C., Li, W., Gu, S., and Xu, C. (2009). Molecular evolution and functional divergence of HAK potassium transporter gene family in rice (*Oryza sativa L.*). *J. Genet. Genomics* 36, 161–172. doi: 10.1016/S1673-8527(08)60103-4

Zhu, Y. G., and Smolders, E. (2000). Plant uptake of radiocaesium: a review of mechanisms, regulation and application. *J. Exp. Bot.* 51, 1635–1645.

Conflict of Interest: The authors declare that the research was conducted in the absence of any commercial or financial relationships that could be construed as a potential conflict of interest.

frontiers in Plant Science

ORIGINAL RESEARCH
published: 15 May 2020
doi: 10.3389/fpls.2020.00503

Selection of Agar Reagents for Medium Solidification Is a Critical Factor for Metal(loid) Sensitivity and Ionomic Profiles of *Arabidopsis thaliana*

Shimpei Uraguchi, Yuka Ohshiro, Yuto Otsuka, Hikari Tsukioka, Nene Yoneyama, Haruka Sato, Momoko Hirakawa, Ryosuke Nakamura, Yasukazu Takanezawa and Masako Kiyono*

Department of Public Health, School of Pharmacy, Kitasato University, Tokyo, Japan

For researchers in the plant metal field, the agar reagent used for the solid plate medium is a problematic factor because application of different agar types and even a different lot of the same agar type can mask the plant metal-related phenotypes and impair the reproducibility. In this study, we systematically assessed effects of different agar reagents on metal(loid) sensitivity and element accumulation of the Arabidopsis metal sensitive mutants. Three established mutants (*cad1-3*, *cad1-6*, and *abcc1/2*), and three different types of purified agar reagents (Type A, Type E, and Nacalai) with two independent batches for each reagent were subjected to the analyses. First, we found that element concentrations in the agar reagents largely varied among the agar types. Then the effects of agar reagents on the mutant metal(loid)-sensitivity were examined under As(III), Hg(II), Cd(II), and excess Zn(II) conditions. A significant variation of the mutant metal(loid)-sensitivity was observed among the different agar plates but the variation depended on the combination of metal(loid) stress and agar reagents. Briefly, the type-dependent variation was more evident under As(III) and Hg(II) than Cd(II) or excess Zn(II) conditions. A lot-dependent variation was also observed for Type A and Type E but not for Nacalai: hypersensitive phenotypes of *cad1-3*, *cad1-6*, and *abcc1/2* under As(III) or Hg(II) treatments were diminished when different batches of the Type A or Type E agar types were used. We also found a significant variation of As and Hg accumulation in the wild-type and *cad1-3*. Plant As and Hg concentrations were remarkably higher and the difference between the genotypes was more evident when grown with Type A agar plates. We finally analyzed ionomic profiles in the plants exposed to As(III) stress. Agar-type specific ionomic changes in *cad1-3* were more observed with the Type A plates than with the Nacalai plates. The presented results overall suggest that suitability of agar reagents for metal(loid)-related phenotyping depends on the experimental design, and an inappropriate selection of agar reagents can mask even very clear phenotypes of the established mutant like *cad1-3*. We also discuss perspectives on the agar problem in the plant metal study.

Keywords: agar reagent, Arabidopsis, *cad1-3*, ionome, metal sensitivity, metal toxicity

OPEN ACCESS

Edited by:
Stephan Clemens,
University of Bayreuth, Germany

Reviewed by:
Mauro Commisso,
University of Verona, Italy
Timothy O. Jobe,
University of Cologne, Germany

***Correspondence:**
Masako Kiyono
kiyonom@pharm.kitasato-u.ac.jp

Specialty section:
This article was submitted to Plant Traffic and Transport, a section of the journal Frontiers in Plant Science

Received: *31 January 2020*
Accepted: *03 April 2020*
Published: *15 May 2020*

Citation:
Uraguchi S, Ohshiro Y, Otsuka Y, Tsukioka H, Yoneyama N, Sato H, Hirakawa M, Nakamura R, Takanezawa Y and Kiyono M (2020) Selection of Agar Reagents for Medium Solidification Is a Critical Factor for Metal(loid) Sensitivity and Ionomic Profiles of Arabidopsis thaliana. Front. Plant Sci. 11:503. doi: 10.3389/fpls.2020.00503

INTRODUCTION

Contamination of environments or foods by heavy metals and metalloids such as arsenic (As), cadmium (Cd), mercury (Hg), lead (Pb), and zinc (Zn) is a worldwide concern as environmental, agricultural or health risks (Järup, 2003; Clemens, 2019). As health risks, As, Cd, Hg, and Pb rank in the top 10 on the US Agency for Toxic Substances and Disease Registry (ATSDR) 2017 Priority List of Hazardous Substances.[1] Plant-derived foods (mainly cereal grains) are often major sources of the toxic elements like As and Cd among the general people (Tsukahara et al., 2003; Gilbert-Diamond et al., 2011). As for Hg, the methylated form is a well-known toxicant mainly accumulated in seafoods, but its inorganic form [Hg(II)] is also toxic and substantially detected from cereal grains and vegetables harvested from the contaminated environments (Li et al., 2017; Tang et al., 2018). Pb is also a toxic metal but its accumulation in plants hardly becomes a problem unlike the other elements. It is firstly because phytoavailability of Pb in soils is much lower compared to those of As, Cd, Hg, and Zn (of the inorganic forms) (Xian, 1987; Jing et al., 2008; Stroud et al., 2011) and secondary, probably due to the very low uptake and within-plant mobility of Pb (Kumar and Prasad, 2018). Zn is an essential element for both plant and human but its excess causes toxicity: excess Zn treatment leads to over-accumulation of Zn and inhibits plant growth by disrupting mineral homeostasis and vacuolar functions (Fukao and Ferjani, 2011; Fukao et al., 2011). With these reasons, the plant studies of toxic metal(loid)s rather focus on As, Cd, Hg, and excess Zn than Pb.

Molecular understanding of plant metal transport and tolerance is an important basis to control plant metal responses for further mitigating the various toxic element-related risks (Clemens, 2019). Genetic analyses of the model plants Arabidopsis and rice largely contribute to identifying molecules playing crucial roles in plant metal transport and tolerance (see reviews by Krämer et al., 2007; Uraguchi and Fujiwara, 2013; Ma et al., 2014; Clemens and Ma, 2016; Bashir et al., 2016; Yamaji and Ma, 2017). Phenotyping loss-of-function mutants of candidate player genes is the key to such genetic analyses elucidating the molecular functions *in planta*. Under the laboratory conditions, for both forward and reverse genetic experiments of Arabidopsis, in particular, artificial solid plate medium is a useful assay system to observe mutant plant responses against metal(loid) stress. Murashige-Skoog (MS) based solid medium is widely used for general plant experiments, however, for phenotyping assay under metal(loid) stress, diluted media with lower ionic strength are often preferred (Hou et al., 2005; Tazib et al., 2009; Huang et al., 2010; Yamaguchi et al., 2016). Medium dilution reduces the competitive interaction of the supplemented ions in the medium and sharpens the toxic effects of the target metal(loid). Among one-tenth strength modified Hoagland medium is one of the promising media for various metal(loid)-related phenotyping (Tennstedt et al., 2009; Fischer et al., 2014; Kühnlenz et al., 2014; Uraguchi et al., 2018, 2019a,b). The assay with this medium highlights the metal-sensitive phenotypes of several mutants, which are not visible under the MS-based conditions (Tennstedt et al., 2009; Fischer et al., 2014).

In addition to the medium composition, the selection of agar reagents for plate solidification is another medium-related factor affecting plant responses to mineral/metal stress. This point has been examined by a few previous studies in regard to nutrient deficiency responses of Arabidopsis: elemental composition of agar reagents largely varies among types or batches of agar reagents, which consequently affects plant responses and phenotypes to macro- and micro-nutrient starvation (Jain et al., 2009; Gruber et al., 2013). As for heavy metal toxicity assay, it would be also vaguely recognized among researchers in the plant-metal community that types and lots of agar reagents can influence metal-related phenotypes and impair the reproducibility of experiments. Indeed, we have occasionally experienced agar type- and lot-dependent variation of metal-sensitive phenotypes of Arabidopsis.

In this study, using a set of Arabidopsis metal-sensitive mutants, we systematically assessed variation of metal(loid)-related phenotypes attributed to different agar types and batches. The further aim of the study was to promoting awareness to the plant-metal community about the importance of agar reagents used for metal-related phenotyping. For this purpose, the established metal-sensitive Arabidopsis mutants were subjected to the assay: *cad1-3* and *cad1-6* are loss-of-function alleles of AtPCS1, the Arabidopsis major phytochelatin (PC) synthase (PCS). The two alleles respond differently to As(III), Cd(II) and excess Zn(II) stress (Tennstedt et al., 2009; Uraguchi et al., 2018). *abcc1*/*abcc2* (hereafter *abcc1/2*) is the double knock-out mutant of AtABCC1 and AtABCC2 that function as PC-metal(loid) complex transporters on tonoplast (Song et al., 2010; Park et al., 2012). We tested three types of agar reagents often used for metal-related phenotyping as well as two different lots for each type. A variation of plant growth under As(III), Hg(II), Cd(II), and excess Zn(II) attributed to agar reagents, and elemental profiles of plants and agar reagents were analyzed.

MATERIALS AND METHODS

Agar Reagents and Ionomic Profiles

Three types of agar reagents and two independent lots for each type were subjected to the study: agar Type A (Sigma-Aldrich, catalog no. A4550-500G, lot nos. SLBL4283V and SLBJ9623V, hereafter Type A-1 and Type A-2, respectively), agar Type E (Sigma-Aldrich, catalog no. A4675-500G, lot nos. SLBN1798V and SLBL0898V, hereafter Type E-1 and Type E-2, respectively) and purified agar (Nacalai Tesque, catalog no. 01162-15, lot nos. M7B5170 and M7K8912, hereafter Nacalai-1 and Nacalai-2, respectively). These agar reagents are often used for analyzing Arabidopsis responses to metal toxicity or mineral stress.

To obtain ionomic profiles of the agar reagents, elemental concentrations of the agar reagents (Type A-1, Type A-2, Type E-1, Type E-2, Nacalai-1, and Nacalai-2) were determined as described previously (Uraguchi et al., 2018, 2019a). 100 mg of each agar reagent was wet-digested

[1] https://www.atsdr.cdc.gov/SPL/

with 3ml of HNO_3. After filling up to 5 ml with 2% HNO_3, total Hg concentrations in the digested samples were quantified by a cold vapor atomic absorption spectrometer (CV-AAS, HG-400, Hiranuma). Concentrations of elements other than Hg were quantified by an inductively coupled plasma-optical emission spectroscopy (ICP-OES, iCAP7400Duo, Thermo Fisher Scientific).

Plant Materials and Growth Conditions

Arabidopsis thaliana wild type (Col-0), the *AtPCS1* null mutant *cad1-3* (Howden et al., 1995), the *AtPCS1* T-DNA insertion line *cad1-6* (Tennstedt et al., 2009) and the *AtABCC1* and *AtABCC2* double knockout mutant line *abcc1/2* (Song et al., 2010) were used for the growth assay. For elemental analyses, Col-0 and *cad1-3* were used.

One-tenth strength modified Hoagland medium was used for plant cultivation [100 μM $(NH_4)_2HPO_4$, 200 μM $MgSO_4$, 280 μM $Ca(NO_3)_2$, 600 μM KNO_3, 5 μM Fe- N, N′-di-(2-hydroxybenzoyl)-ethylenediamine-N,N′-diacetic acid (HBED), 1% (w/v) sucrose, 5 mM MES, pH 5.7] (Tennstedt et al., 2009; Kühnlenz et al., 2014). For metal(loid) sensitivity assay, essential microelements other than Fe were not added to the medium to avoid possible interaction between the metal(loid) added. To prepare the plants for elemental analyses, the following essential microelements were additionally supplemented to the medium (4.63 μM H_3BO_3, 32 nM $CuSO_4$, 915 nM $MnCl_2$, 77 nM $ZnSO_4$, 11 nM MoO_3). The concentration of agar reagents used for medium solidification was 1% (w/v) for Type A and Type E, and 1.5% (w/v) for Nacalai. The higher concentration of the Nacalai agar was determined to obtain sufficient gel strength to reduce root penetration into the medium. Plastic square plates (AW2000, Eiken Chemical) were used for the agar plate preparation.

Arabidopsis seeds were surface sterilized by 5 min-immersion with 70% (v/v) ethanol, followed by 1-min immersion with 99.5% ethanol (Sotta and Fujiwara, 2017). After air-drying, the sterilized seeds resuspended with 0.1% (w/v) agar were sown on agar plates (seven seeds of each genotype per plate for sensitivity assay, and 36 seeds of a single genotype per plate for ionome assay). After 2 days stratification at 4°C, plants were grown vertically in a growth chamber (16 h light/8 h dark, 22°C) as described elsewhere.

Metal(loid) Sensitivity Assay

To examine the effects of agar reagents on metal(loid) sensitivity of the Arabidopsis metal-hypersensitive mutants, the growth assay was conducted by modifying the method previously described for As and Cd treatment (Uraguchi et al., 2017, 2018). For this assay, Col-0, *cad1-3*, *cad1-6,* and *abcc1/2* were tested with all six agar reagents (Type A, Type E and Nacalai with two lots, respectively). Plants were grown for 12 days on agar plates containing different concentrations of As(III) as $NaAsO_2$ (1 and 1.5 μM), Hg(II) as $HgCl_2$ (10 and 15 μM), Zn (II) as $ZnSO_4$ (40 and 50 μM) or Cd(II) as $CdCl_2$ (2 and 3 μM). These metal(loid) concentrations were determined based on the previous reports (Tennstedt et al., 2009; Uraguchi et al., 2017, 2018, 2019b) as well as our preliminary experiments. The selected treatments were expected to maximize the phenotypic differences between the wild-type and the mutants (thus not lethal to the wild-type Col-0 during the experimental period). Two different levels for each metal(loid) were examined to cover possible variation of the plant growth derived from the "agar-effects." The plates without the addition of the metal(loid) served as control. After 12 days cultivation, plants were photographed, and plant growth was assessed by primary root length and seedling (roots and shoots) fresh weight measurements. For the respective genotypes, root length was measured for each plant, and seedling fresh weight was measured for each plate.

Elemental Accumulation in Plants

To examine the effects of agar reagents on plant elemental accumulation, elemental concentrations in the plants were compared among Type A-1, Type A-2, Nacalai-1, and Nacalai-2. The plant elemental analysis was conducted as described previously (Uraguchi et al., 2018, 2019a) with a slight modification. Col-0 and *cad1-3* were grown on the control plates for 10 days. Uniformly grown seedlings were then transferred to control plates or plates containing 5 μM As (III) or 10 μM Hg(II) and grown for additional 4 days. At harvest, roots and shoots from each plate (15 seedlings per genotype for control and Hg(II) treatment, and 30 seedlings per genotype for As(III) treatment) were separately pooled as a single sample. Shoot samples were washed with MilliQ water twice. Root samples were subjected to sequential washing procedures: roots were desorbed for 10 min each in ice-cold MilliQ water, 20 mM $CaCl_2$ (twice), 10 mM EDTA (pH 5.7) and MilliQ water. Harvested roots and shoots were dried at 50°C before acid digestion at least for a few days. Dried plant samples (3–10 mg for control and Hg(II) treatment samples, and 5–20 mg for As(III) treatment samples) were wet-digested with 3ml of HNO_3. After filling up to 5 ml with 2% HNO_3 in a plastic tube, total Hg concentrations in the digested samples obtained from the Hg(II) treatment were quantified by CV-AAS. For the As(III) treated plant samples, multiple elemental concentrations including As were quantified by ICP-OES.

Statistical Analyses

The R software (ver. 3.5.1) was used for statistical analyses. The root growth and seedling fresh weight data obtained from the growth assay was analyzed by one-way ANOVA, followed by Tukey's HSD ($p < 0.05$) to examine the significance of differences among the plant genotypes grown under respective metal(loid) stress and each agar reagent. The Hg and As concentrations in the plant were also analyzed by one-way ANOVA, followed by Tukey's HSD ($p < 0.05$) to examine the effects of the agar reagents and the plant genotypes. The plant ionomic data were analyzed by three-way ANOVA ($p < 0.05$) to verify the effects of genotypes, As(III) treatment and agar reagents, and the interaction of these factors. A *post-hoc* analysis by Tukey's HSD ($p < 0.05$) was conducted for each agar reagent to examine the *cad1-3* specific ionomic changes under As(III) stress.

RESULTS

Ionomic Profiles of the Agar Reagents

We expected a variation of ionomic profiles in the agar reagents used in this study, as previously reported for other agar reagents (Jain et al., 2009; Gruber et al., 2013). We first quantified total element concentrations in the agar reagents (**Figure 1**). The measured elements were briefly classified into two groups: the first group included sodium (Na), potassium (K), Fe, copper (Cu), Zn, phosphorus (P), sulfur (S), and As. These element concentrations were higher in Type A and Type E agars than in Nacalai agars. This tendency was drastic for Na, K, Fe, and P (up to 7-, 27-, 20-, and 100-fold higher in Type A or Type E than Nacalai, respectively). The second group included magnesium (Mg) and calcium (Ca), which concentrations were drastically higher in Nacalai agars. A pattern of manganese (Mn) was different from these two groups. Nacalai agars contained relatively higher Mn concentrations than Type A-1, and Type E agars but Type A-2 showed the highest concentration. Aluminum (Al) concentrations were almost 2-fold higher in Type A agars than the other agars.

We then calculated molar concentrations of the respective elements in the one-tenth strength modified Hoagland medium supplemented with all micronutrients (**Supplementary Figure S1**). The agar concentration used for the calculation was 1% (w/v) for Type A and Type E, and 1.5% (w/v) for Nacalai agars, which were the same concentrations used for the plate preparation in this study. This calculation did not take account

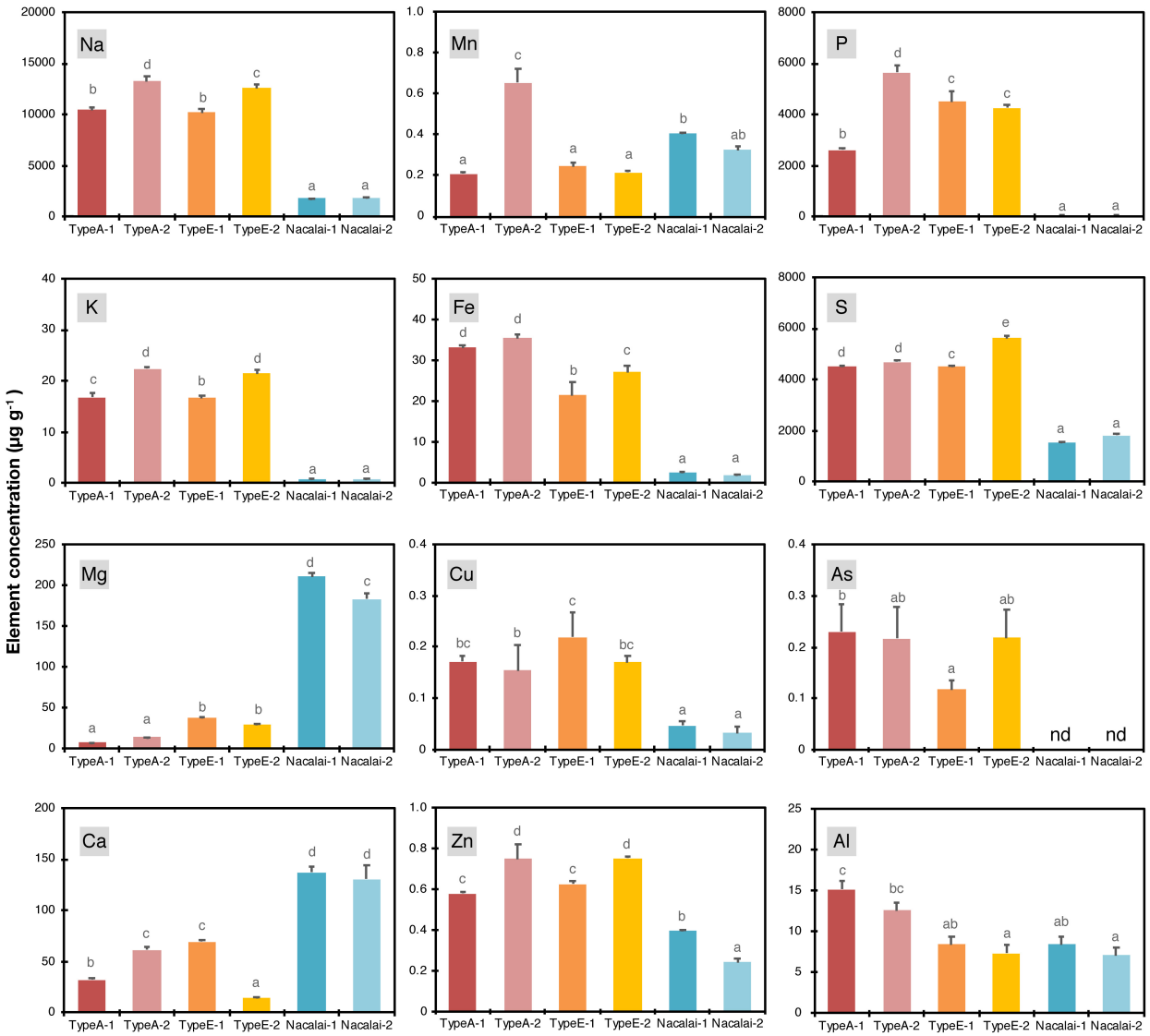

FIGURE 1 | Concentrations of Na, K, Mg, Ca, Mn, Fe, Cu, Zn, P, S, As, and Al in the agar regents (μg g^{-1}). Data represent means with standard deviation of at least three independent measurements. Means sharing the same letter are not significantly different within each panel ($P < 0.05$, Tukey's HSD). n.d., not detected.

of chemical forms and phytoavailability of the agar-derived elements, thus it evaluated maximum additive elemental load to the medium derived from the agar reagents. Proportions of the additive load to the basal medium were remarkably higher in Fe, Cu, Zn, P, and S. The agar-derived loads of Fe, Cu, and Zn were almost equal to the basal medium levels in the highest cases. The addition of Type A and Type E drastically increased total P and S concentrations in the medium (up to 20- and 10-fold increase, respectively). The increase of Fe, Cu, P, and S by Nacalai agar addition was much more moderate compared to the case of Type A and Type E agars. In contrast, the additive levels of Mg and Ca were estimated to be up to 65 and 18% of the respective basal concentrations in the medium for Nacalai agars but were much less for Type A and Type E agar reagents.

For non-essential elements, Na and As showed a similar pattern: higher contents in Type A and Type E and lower in Nacalai agars (**Figure 1**). But their molar concentrations in the medium were < 6 mM for Na and < 0.03 μM for As (**Supplementary Figure S1**). These values were way below the level to cause toxicity to plants. Al concentrations were ˜2-fold higher in Type A agars compared to Type E and Nacalai agar reagents (**Figure 1**). But molar concentrations of Al in the medium were in a range of 3–5 μM (**Supplementary Figure S1**), which was again below the toxic levels used in many experiments. In addition to the elements presented in **Figure 1** and **Supplementary Figure S1**, Cd, Hg, and Pb were also quantified but concentrations of these elements in the agar reagents were below the quantification limits of our ICP-OES (for Cd and Pb) and CV-AAS (for Hg) systems.

A lot-dependent variation of the elemental profiles was also found but not so drastic as the type-to-type variation mentioned above. A variation between Nacalai agars was overall very minor. In contrast, compared to Type A-1, Type A-2 contained higher levels of Na, K, Mg, Ca, Mn, Fe, Zn, and P (**Figure 1**), but the difference in the medium concentration basis was little except for P (**Supplementary Figure S1**). The total P concentration in the medium was 2-fold higher with Type A-2 than Type A-1 (**Supplementary Figure S1**). Type E-2 contained higher levels of Na, K, Fe, Zn, S, and As and lower levels of Mg and Ca than Type E-1 (**Figure 1**). However, comparing the concentrations in the medium, the difference between the Type E batches was not that much evident (**Supplementary Figure S1**).

Agar-Dependent Variation of As(III)-Sensitive Phenotypes

We then tested the metal(loid)-sensitive phenotypes of the established mutants (*cad1-3*, *cad1-6,* and *abcc1/2*) with six agar reagents (Type A-1, A-2, Type E-1, E-2, Nacalai-1, and Nacalai-2) and four metal(loid) species [As(III), Hg(II), Zn(II), and Cd(II)]. The plant growth under control conditions was little affected by the different agar reagents (**Supplementary Figures S2–S4**). On the other hand, an agar-dependent variation of the metal(loid)-sensitivity was prominently observed for As(III). As(III)-sensitivity assay was conducted under 1 μM (**Supplementary Figure S5**) and 1.5 μM As(III) treatments (**Figure 2**). We previously demonstrated comparable As(III)-hypersensitivity of *cad1-3*, *cad1-6,* and *abcc1/2* under these As(III) conditions (Uraguchi et al., 2018). The mutants stably exhibited the As(III)-hypersensitive phenotypes when grown on the plates prepared with Nacalai agars (**Figure 2A** and **Supplementary Figure S5A**). The primary root length (**Figure 2B** and **Supplementary Figure S5B**) and seedling fresh weight (**Figure 2C** and **Supplementary Figure S5C**) of the mutants were severely reduced by the As(III) treatments when either Nacalai-1 or Nacalai-2 was used for the plate preparation. Under 1.5 μM As(III) treatment, *abcc1/2* slightly showed intermediate As(III) sensitive phenotypes compared to the AtPCS1 mutants *cad1-3* and *cad1-6* and this trend was visible on the plates with both Nacalai-1 and Nacalai-2 agars.

In contrast, a lot-dependent variation of the As(III)-sensitivity was observed for Type A and Type E agar reagents. The application of Type A-2 for the medium preparation diminished the As(III) sensitivity of the mutants, whereas the phenotypes on the plates with Type A-1 were similar to those obtained from the Nacalai plates (**Figure 2** and **Supplementary Figure S5**). The lot-to-lot variation of Type E agar was more serious. The As(III)-sensitive phenotypes of *cad1-3*, *cad1-6,* and *abcc1/2* were clearly observed with Type E-2 agar plates even under 1μM As(III) treatment, however, the effects of As(III) exposure on the plant growth were barely visible when Type E-1 was used for the medium preparation (**Figure 2A** and **Supplementary Figure S5A**). There was no significant difference of the seedling fresh weight between Col-0 and the mutants under both As(III) conditions (**Figure 2C** and **Supplementary Figure S5C**) and the difference of the root length among the genotypes was significant but very little (**Figure 2B** and **Supplementary Figure S5B**).

Agar-Dependent Variation of Hg(II)-Sensitive Phenotypes

The plant growth was examined under 10 μM (**Supplementary Figure S6**) and 15 μM Hg(II) treatments (**Figure 3**). It has been demonstrated that *cad1-3* and *abcc1/2* are similarly hypersensitive to Hg(II) (Ha et al., 1999; Park et al., 2012). And we found that Hg(II) was the second metal species showing the agar-dependent variation of the mutant hypersensitivity. As a major difference from the case of As(III) treatment, the agar type-dependent variation under Hg(II) stress was more evident than the variation between the batches of the respective agar types. The mutants growth was less inhibited by the Hg(II) treatments on the Nacalai agar plates compared to those of other agar types, whereas the mutant plants grown on the plates with Type A or Type E agars showed severe growth reduction. A variation of the root length among the individuals of each genotype was also larger when the Nacalai agars were used (**Figures 3A,B**).

A lot-dependent variation was again observed between Type E-1 and E-2 as like the case of As(III), but in the opposite direction: under 15 μM Hg(II) treatment, the growth of *cad1-6* and *abcc1/2* was more severely inhibited on the Type E-1 plates than on the Type E-2 plates (**Figure 3**). The hypersensitive phenotypes of the tested mutants were remarkably and stably observed on the Type A plates. The root and shoot development

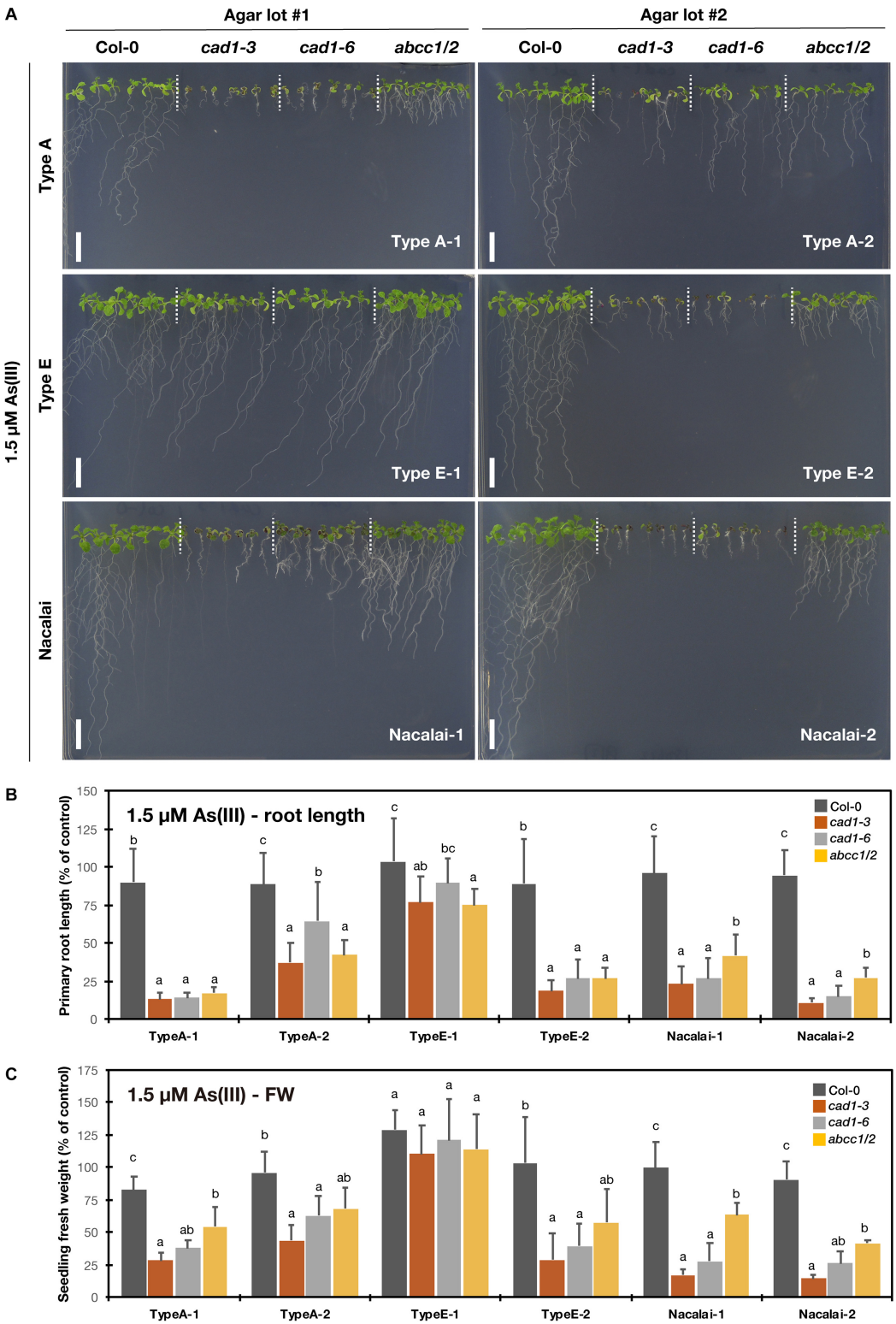

FIGURE 2 | As(III)-sensitivity of the phytochelatin-related Arabidopsis mutants on the agar plates prepared with different agar reagents. Three types of agar reagents with two independent lots for each type were tested. Col-0, *cad1-3*, *cad1-6* and *abcc1/2* were grown on the agar medium containing 1.5 µM As(III) for 12 days. **(A)** Phenotypes of Col-0, *cad1-3*, *cad1-6,* and *abcc1/2*. Scale bars = 1 cm. **(B,C)** Relative primary root length **(B)** and fresh weight of seedlings **(C)** of Col-0, *cad1-3*, *cad1-6,* and *abcc1/2*. Values are shown as percentage of each control. Data represent means with SD from at least three independent experiments (n = 19 – 28 for root length, and n = 3–4 for seedling fresh weight). Means sharing the same letter are not significantly different within each agar reagent ($P < 0.05$, Tukey's HSD).

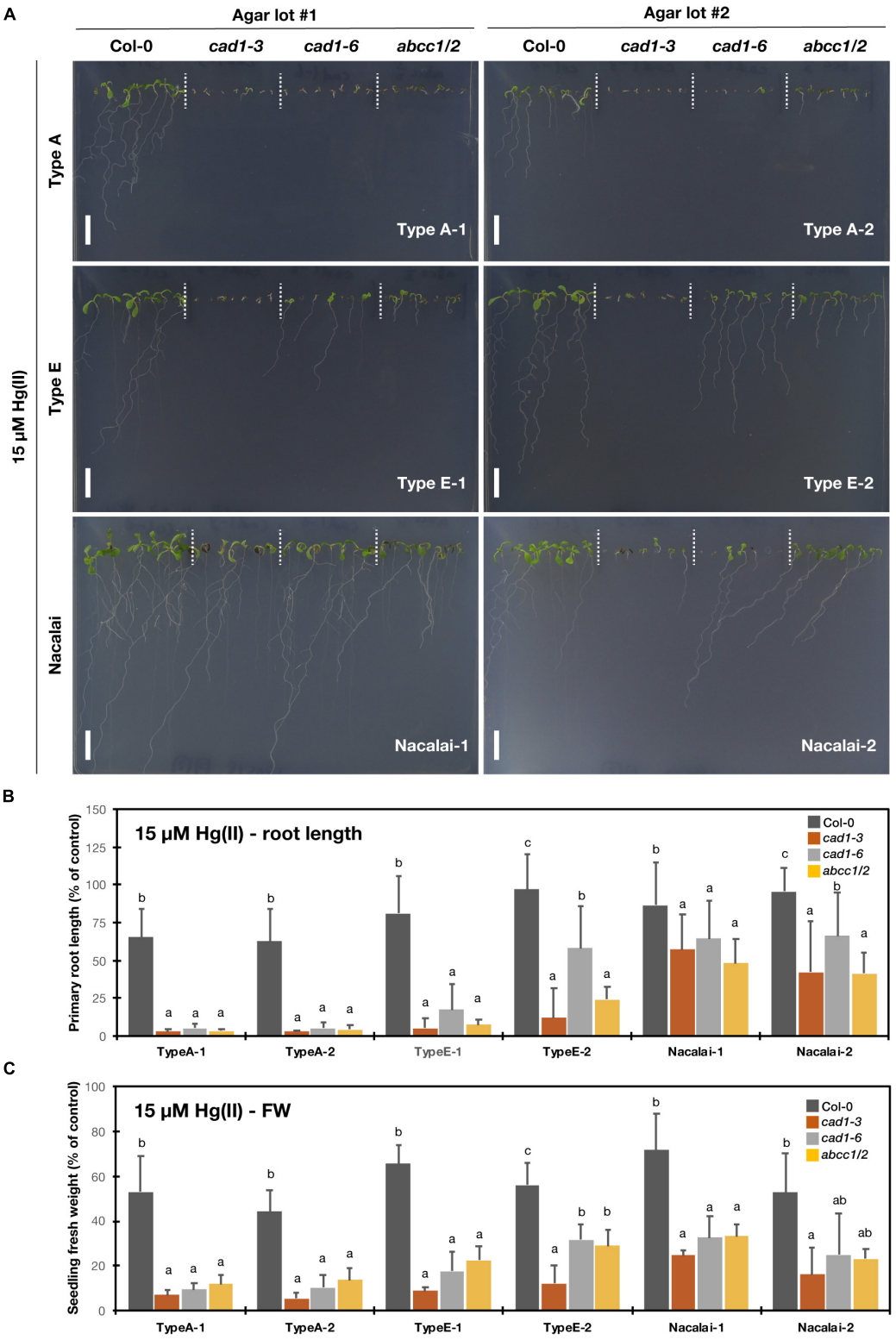

FIGURE 3 | Hg(II)-sensitivity of the phytochelatin-related Arabidopsis mutants on the agar plates prepared with different agar reagents. Three types of agar reagents with two independent lots for each type were tested. Col-0, *cad1-3*, *cad1-6,* and *abcc1/2* were grown on the agar medium containing 15 µM Hg(II) for 12 days. **(A)** Phenotypes of Col-0, *cad1-3*, *cad1-6,* and *abcc1/2*. Scale bars = 1 cm. **(B,C)** Relative primary root length **(B)** and fresh weight of seedlings **(C)** of Col-0, *cad1-3*, *cad1-6,* and *abcc1/2*. Values are shown as percentage of each control. Data represent means with SD from at least three independent experiments (n = 13–28 for root length, and n = 3–4 for seedling fresh weight). Means sharing the same letter are not significantly different within each agar reagent ($P < 0.05$, Tukey's HSD).

of the mutants was nearly completely impaired after germination even under lower Hg(II) treatment and the application of different lots of Type A agar did not change the phenotypes (**Figure 3** and **Supplementary Figure S6**).

Agar-Dependent Variation of Excess Zn(II)-Sensitive Phenotypes

To test excess Zn(II)-sensitivity of the mutants, the plants were grown under 40 μM (**Supplementary Figure S7**) and 50 μM Zn(II) treatments (**Figure 4**). AtPCS1 plays major roles in excess Zn tolerance: *cad1-3* and *cad1-6* exhibit enhanced sensitivity to the excess Zn stress (Tennstedt et al., 2009; Kühnlenz et al., 2016). But phenotypes of *abcc1/2* under excess Zn conditions have not been reported. The root growth and seedling fresh weight of *cad1-3* and *cad1-6* were similarly reduced by 50 μM Zn(II) treatment when the Nacalai agar reagents were used for the medium solidification (**Figures 4B,C**), as reported previously. Under this condition, the growth of *abcc1/2* was overall similar to that of Col-0. Similar results were obtained for 40 μM Zn(II) treatment (**Supplementary Figure S7**), suggesting that the sensitivity of *abcc1/2* to excess Zn stress was Col-0 like.

Agar type- and lot-dependent variation was detected for Type A and Type E especially for the root growth: the shorter root length phenotype of *cad1-3* and *cad1-6* under excess Zn(II) was also somewhat observed when grown on the plates prepared with Type A-1 and Type E-1 but less evident on the Type A-2 and Type E-2 plates (**Figure 4B** and **Supplementary Figure S7B**). Seedling fresh weight of *cad1-3* and *cad1-6* was also not significantly different from that of Col-0 under 40 μM Zn(II) treatment with Type A-2 and Type E-2 agars (**Supplementary Figure S7C**).

Agar-Dependent Variation of Cd(II)-Sensitive Phenotypes

Compared to the other tested metal(loid)s, the agar-dependent variation of the sensitivity of the mutants under Cd(II) stress was very small. Under both 2 μM (**Supplementary Figure S8**) and 3 μM Cd(II) treatments (**Figure 5**), *cad1-3* showed the highest Cd-sensitivity based on the root length and seedling fresh weight quantification irrespective of the agar reagents. *cad1-6* shows a weaker/intermediate Cd-sensitivity compared to *cad1-3* (Tennstedt et al., 2009; Kühnlenz et al., 2016) and indeed, the second allele exhibited the longer root length than *cad1-3* under all the tested agar conditions (**Figure 5B** and **Supplementary Figure S8B**). Larger seedling fresh weight of *cad1-6* was significantly observed on the Type A-1, Nacalai-1 and Nacalai-2 plates under both 2 and 3 μM Cd(II), whereas there was no significant difference between *cad1-3* and *cad1-6* when Type A-2, Type E-1, and Type E-2 were used for the medium (**Figure 5C** and **Supplementary Figure S8C**).

abcc1/2 is also a Cd-hypersensitive mutant but the phenotype is reported to be weaker than that of *cad1-3* (Park et al., 2012). In line with this previous result, seedling fresh weight of *abcc1/2* under our assay conditions was generally larger than that of *cad1-3* (**Figure 5C** and **Supplementary Figure S8C**). Intermediate root length phenotypes of *abcc1/2* as like *cad1-6* were also observed on the Nacalai plates, however, on the Type A and Type E plates, the *abcc1/2* root length was comparable to that of *cad1-3* (**Figure 5B** and **Supplementary Figure S8B**).

Agar-Dependent Variation of Plant As and Hg Accumulation

Because the growth assay demonstrated considerable agar-dependent variation of the mutant sensitivity especially against As(III) and Hg(II) stress, we hypothesized that the variation was attributed to different accumulation levels of As or Hg in the plants. Thus, we next examined As and Hg accumulation in Col-0 and *cad1-3* grown on the Type A and Nacalai agar plates. *cad1-3* was selected as the representative mutant due to the evident hypersensitive phenotypes under both As(III) and Hg(II) stress. Type E agars were not subjected to this experiment because the remaining Type E-1 was insufficient to complete the experiment. Unlike the sensitivity assay, the established 10-d-old seedlings grown on the control plates were transferred to the plates containing As(III) or Hg(II) to minimize the effects of different sensitivity to As(III) or Hg(II) stress between Col-0 and *cad1-3* on As or Hg uptake and accumulation.

A variation of As and Hg concentrations in plants was more prominent between agar types than batches (**Figure 6**). As and Hg concentrations in both shoots (**Figures 6A,C**) and roots (**Figures 6B,D**) were generally higher when the Type A agars were used for the medium than the Nacalai agars. Genotypic difference between Col-0 and *cad1-3* was significant for As concentrations in roots irrespective of the agar reagents (**Figure 6B**) and in shoots harvested from the Type A-1 and A-2 plates (**Figure 6A**). There was no significant difference between the genotypes for Hg concentrations in shoots and roots, except for that of roots harvested from the Type A-2 plates (**Figures 6C,D**). In every significant case, *cad1-3* accumulated less As or Hg compared to Col-0.

Agar-Dependent Variation of Ionomic Profiles of As(III)-Treated Plants

Because different As accumulation within the plants seemed not to be a cause for the agar-dependent As(III)-sensitivity variation, we next analyzed the ionomic profiles of the control and As(III)-treated plants grown on the Type A or Nacalai agar plates. Another motivation to conduct ionome analysis of the As(III)-treated plants was our previous result showing that As(III) treatment drastically altered Zn accumulation and distribution specifically in *cad1-3* (Uraguchi et al., 2018). Analyzed elemental concentrations in shoots and roots were shown in **Figure 7** and **Supplementary Figure S9**, respectively, and the obtained ionome data were analyzed by three-way ANOVA as presented in **Supplementary Table S1**. The effects of As(III) treatment, genotypes (Col-0 and *cad1-3*) and agar reagents (Type A-1, A-2, Nacalai-1, and Nacalai-2) were generally significant over the analyzed elements but were more clearly detected in shoots than in roots (**Supplementary Table S1**). The typical case was Cu concentrations in roots, which was not significantly affected by any factors. The interaction effects among As(III)-treatment, genotypes, and agar reagents were also tested (**Supplementary Table S1**): significant interaction between As(III)-treatment and

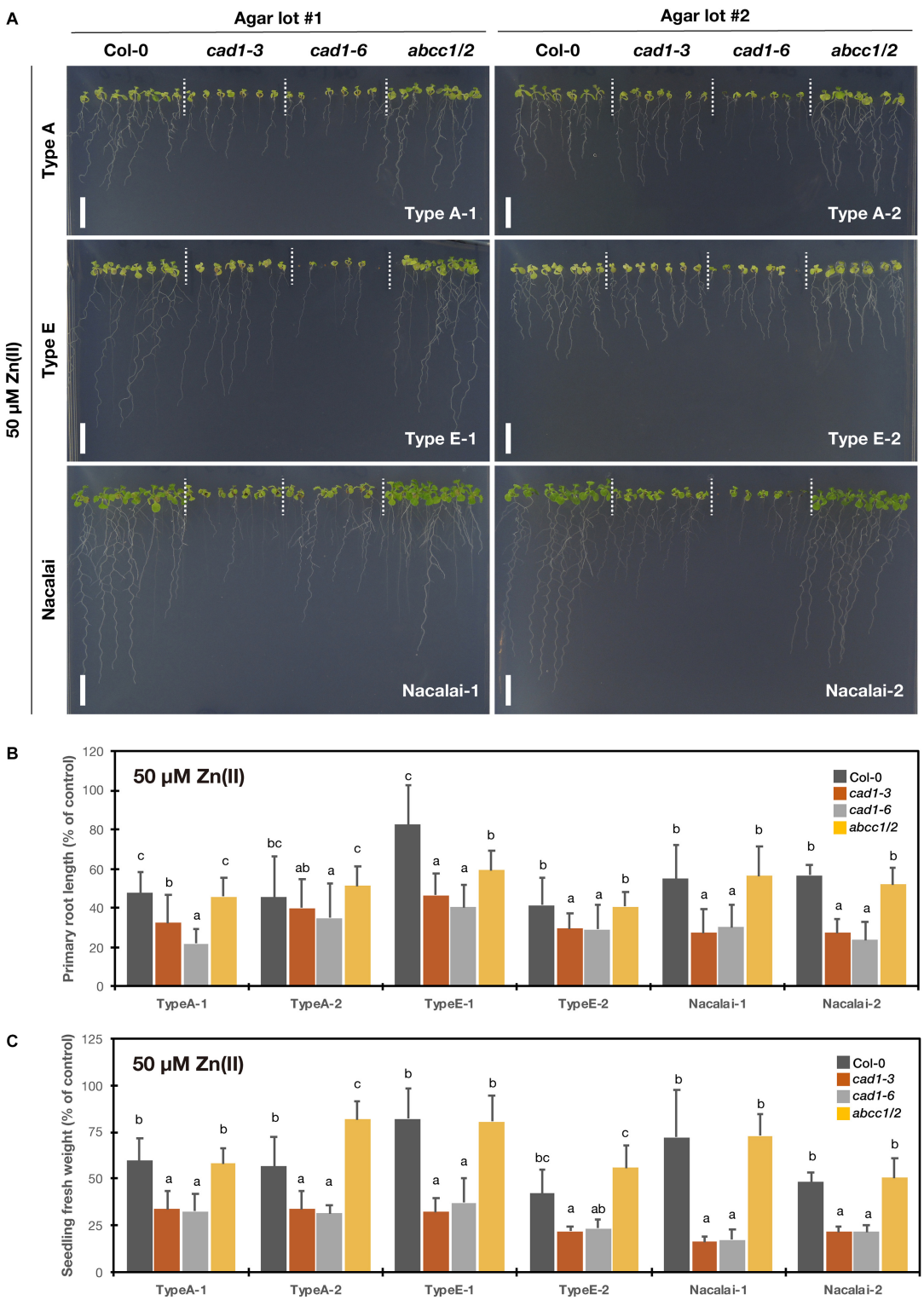

FIGURE 4 | Excess Zn(II)-sensitivity of the phytochelatin-related Arabidopsis mutants on the agar plates prepared with different agar reagents. Three types of agar reagents with two independent lots for each type were tested. Col-0, *cad1-3*, *cad1-6,* and *abcc1/2* were grown on the agar medium containing 50 µM Zn(II) for 12 days. **(A)** Phenotypes of Col-0, *cad1-3*, *cad1-6,* and *abcc1/2*. Scale bars = 1 cm. **(B,C)** Relative primary root length **(B)** and fresh weight of seedlings **(C)** of Col-0, *cad1-3*, *cad1-6,* and *abcc1/2*. Values are shown as percentage of each control. Data represent means with SD from at least three independent experiments (n = 22–28 for root length, and n = 3–4 for seedling fresh weight). Means sharing the same letter are not significantly different within each agar reagent ($P < 0.05$, Tukey's HSD).

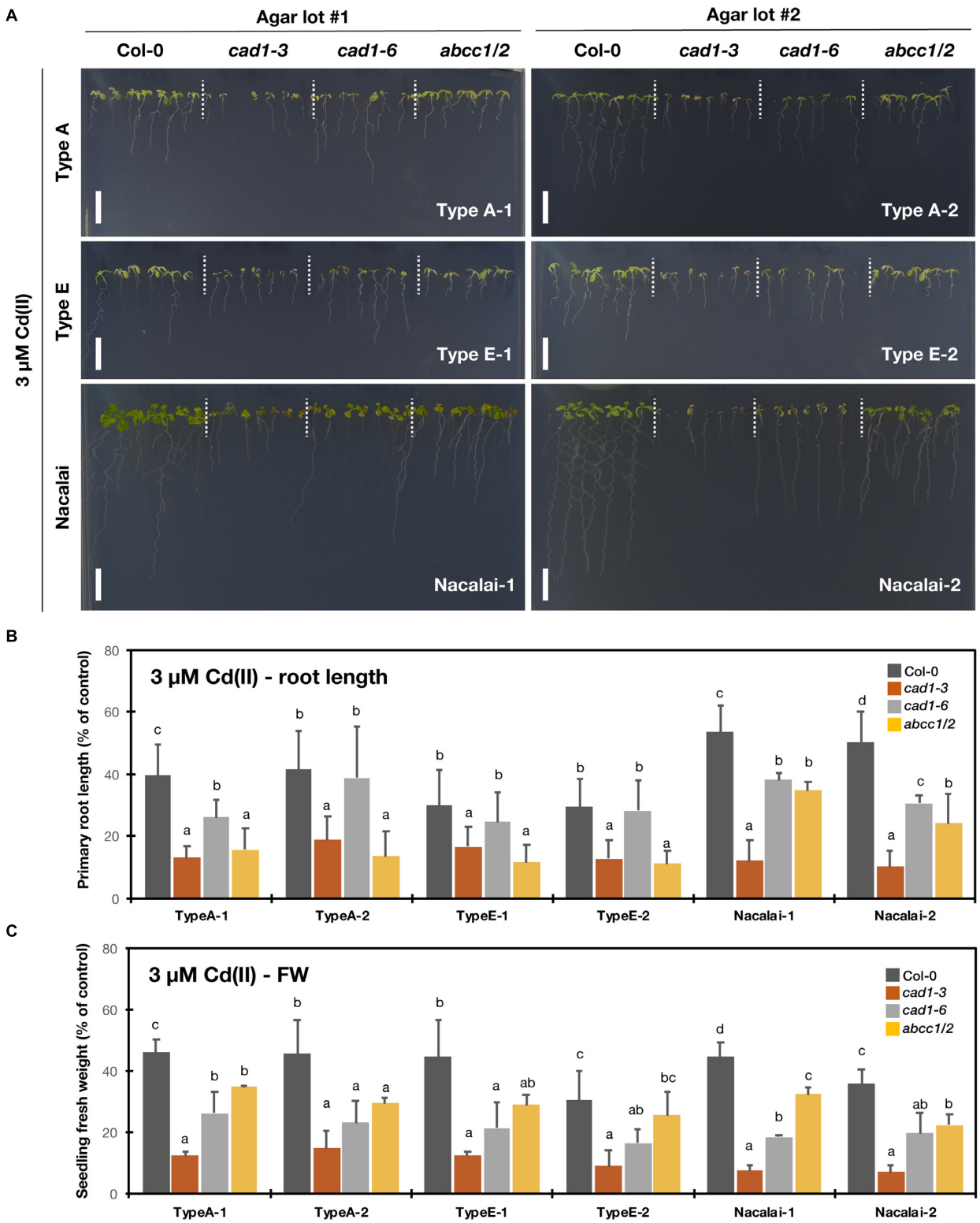

FIGURE 5 | Cd(II)-sensitivity of the phytochelatin-related Arabidopsis mutants on the agar plates prepared with different agar reagents. Three types of agar reagents with two independent lots for each type were tested. Col-0, *cad1-3*, *cad1-6,* and *abcc1/2* were grown on the agar medium containing 3 µM Cd(II) for 12 days. **(A)** Phenotypes of Col-0, *cad1-3*, *cad1-6,* and *abcc1/2*. Scale bars = 1 cm. **(B,C)** Relative primary root length **(B)** and fresh weight of seedlings **(C)** of Col-0, *cad1-3*, *cad1-6,* and *abcc1/2*. Values are shown as percentage of each control. Data represent means with SD from at least three independent experiments (n = 24–28 for root length, and n = 3–4 for seedling fresh weight). Means sharing the same letter are not significantly different within each agar reagent ($P < 0.05$, Tukey's HSD).

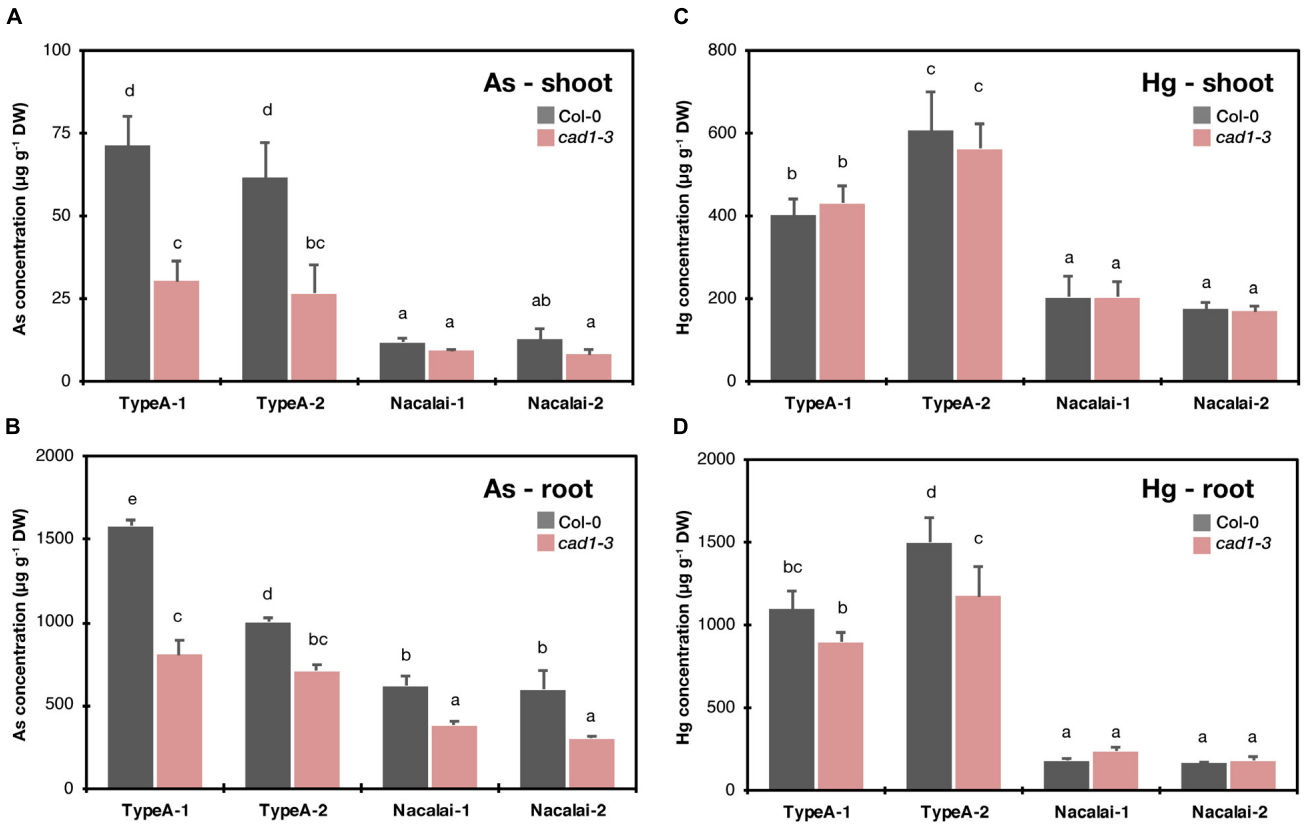

FIGURE 6 | Concentrations of As in shoots **(A)** and roots **(B)** and Hg in shoots **(C)** and roots **(D)** of Col-0 and *cad1-3*. Plants were grown on the control medium prepared with the respective agar reagents for 10 days and then transferred to the medium containing 5 μM As(III) or 10 μM As(III). After 4 days, plants were harvested and As and Hg concentrations in shoots and roots were separately quantified by ICP-OES and CV-AAS, respectively. Data represent means with SD from two independent experiments ($n = 4$). Means sharing the same letter are not significantly different within each panel ($P < 0.05$, Tukey's HSD).

genotypes was detected in most of the elements analyzed except for Fe, Cu, and P in shoots and Na, Mn and Cu in roots. In contrast, for Na, Mn, Fe, Cu, P, and S in shoots and Mn, Fe, Zn, and S in roots, interaction effects between As(III)-treatments and agar reagents were significant. Interaction effects between genotypes and agar reagents were strongly indicated for Na ($P < 0.001$), and weakly indicated for Mn, Zn, and P in shoots ($P < 0.05$). These statistical results indicate that As(III)-treatment induces genotype-specific changes in the accumulation of many elements, and selection of agar reagents influences the degree of the As(III)-induced changes of Na, Mn, Fe, Cu, P, and S in shoots and Mn, Fe, Zn, and S in roots.

We then conducted a *post-hoc* analysis to test significant differences attributed to As(III) treatment and genotypes (**Figure 7** and **Supplementary Figure S9**). As suggested by the three-way ANOVA (**Supplementary Table S1**), the accumulation of many elements in shoots was significantly altered by the As(III) treatment, especially in *cad1-3*. As(III)-induced reduction of shoot K, Mg, Ca, Zn, and S concentrations more largely in *cad1-3*, irrespective of agar reagents (**Figure 7**). With the Type A agars, As(III)-induced increase of Zn levels in *cad1-3* roots was larger (**Supplementary Figure S9**) and alteration of S concentrations by As(III) treatment was significant even in Col-0 (**Figure 7** and **Supplementary Figure S9**). In addition, as Type A agar-specific changes, Na, Mn, and P concentrations in shoots and Mn concentration in roots were significantly reduced by As(III) treatment in *cad1-3* (**Figure 7** and **Supplementary Figure S9**). In contrast, a very slight but significant reduction of Cu concentration under As(III) stress was detected as the only Nacalai agar specific pattern (**Figure 7**). In comparison to the agar type-dependent variation, a lot-dependent variation was minor. As(III)-dependent reduction in *cad1-3* shoot was significantly clear for Fe on the Type A-1 agar plates but not on the Type A-2 plates (**Figure 7**), and the effect of agar batches was minor for other cases.

DISCUSSION

Significance of Agar Reagents for Metal(loid)-Sensitivity Assay

Gelling agents including agar are one of the basic components of the solid medium for plant experiments, and most of the reports do not mention the details of the gelling reagent used for the experiment. However, a large variation of various element contents was previously reported among a number of

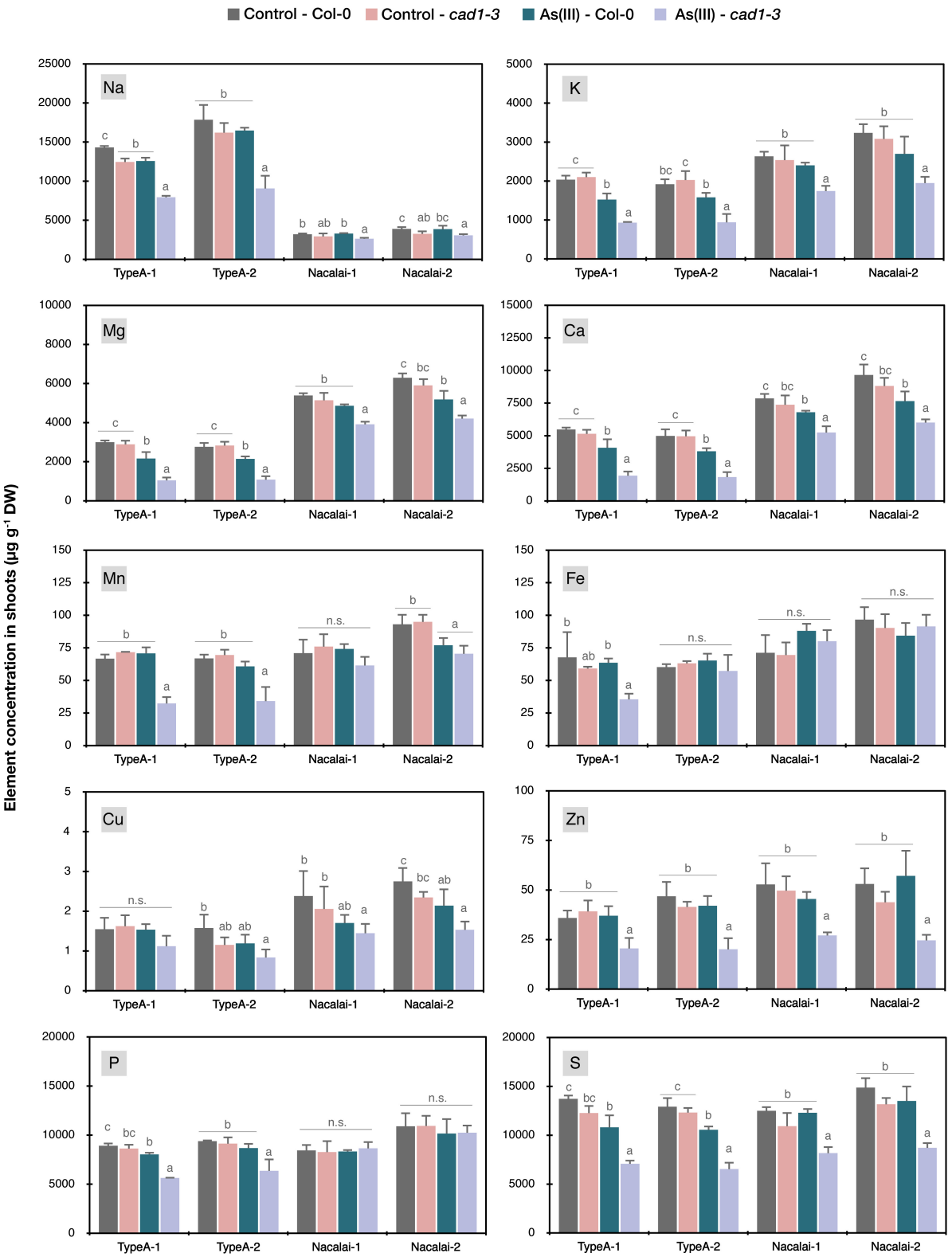

FIGURE 7 | Ionomic profiles in shoots of Col-0 and *cad1-3* under normal conditions and As(III) stressed conditions. Plants were grown on the control medium prepared with the respective agar reagents for 10 days and then transferred to the fresh control medium or the medium containing 5 μM As(III). After 4 days, plants were harvested and concentrations of Na, K, Mg, Ca, Mn, Fe, Cu, Zn, P, and S in shoots were quantified by ICP-OES. Data represent means with SD from two independent experiments ($n = 4$). Means sharing the same letter are not significantly different within each agar reagent ($P < 0.05$, Tukey's HSD).

different gelling reagents, and "carry-on" elemental load derived from gelling reagents is suggested to mask transcriptional and morphological responses of Arabidopsis plants under nutrient-deficient stress (Jain et al., 2009; Gruber et al., 2013). These studies suggest that the selection of proper gelling agents for each nutrient element is critical for analyzing plant responses to nutrient deficiency. Another suggestion by Jain et al. (2009) is switching a cultivation method from agar-plates to hydroponics. This can solve the problems imposed by elemental contamination from gelling reagents.

For studies of plant metal(loid) transport or toxicity, the importance of selecting appropriate gelling reagents seems to be implicitly recognized for similar reasons. Co-existing ions in the medium (and from the agar reagent) can affect root metal uptake through competitive interactions and therefore modulate levels of metal toxicity to plants. Indeed, several papers mentioned specific types of agar reagents used for analyzing plant metal responses (Thomine et al., 2000; Wong and Cobbett, 2009; Nishida et al., 2011; Weber et al., 2013; Lešková et al., 2017; Uraguchi et al., 2017, 2019b). Hydroponic systems are also used for phenotyping of plant metal responses, which are free from the agar-derived elemental contamination. However, especially for studying Arabidopsis plants, the solid plate system still has some advantages over the hydroponic system. In particular, the plate assay enables phenotyping of many Arabidopsis lines in parallel and analyzing young Arabidopsis seedlings even less than one-week-old. It should be noted that a standard hydroponic protocol of Arabidopsis requires a few weeks preculture to establish seedlings before the treatment. The plate-based metal treatment would also reduce the hazardous risks of handling toxic elements because it is a closed safer system and requires fewer volumes of the media compared to the hydroponic system. Thus optimizing the agar-based metal assay system for Arabidopsis especially in terms of agar reagents is significant.

Selection of Agar Reagents for Mutant Metal(loid) Sensitivity Assay

Three types of agars with two independent batches for each type were examined in this study. Type A (Nishida et al., 2011; Weber et al., 2013; Uraguchi et al., 2019b) and Type E agars (LeBlanc et al., 2012; Sone et al., 2017; Uraguchi et al., 2017) of Sigma-Aldrich, and purified agar of Nacalai Tesque (Uraguchi et al., 2017, 2018, 2019a,b) are agar reagents previously used for toxic metal treatment of Arabidopsis. It should be noted that this "Type-A" agar is different from other "Type A" agars of Sigma-Aldrich (catalog nos. A1296 and P8169) used in the previous studies (Jain et al., 2009; Gruber et al., 2013). The ionomic analysis of the agar reagents used in this study revealed different elemental backgrounds mainly between the agar types (**Figure 1**). And the agar-derived additive loads of each element to the medium were considerably higher for Mg and Ca in the Nacalai plates, and for Na, Fe, Cu, P, and S in the Type A and Type E plates (**Supplementary Figure S1**). With these medium conditions, the three established mutant lines of AtPCS1, AtABCC1 and AtABCC2 were tested as the model of hypersensitive mutants to metal(loid)s: AtPCS1 catalyzes synthesis of PCs, metal(loid)-binding peptides and promotes PC-metal(loid) complex formation in cytosol (Ha et al., 1999; Blum et al., 2010) and AtABCC1 and AtABCC2 coordinately pump the PC-metal(loid) complex into vacuoles (Song et al., 2010; Park et al., 2012).

The comprehensive growth assay demonstrated the significant agar-dependent variation of the mutant phenotypes. Overall, Nacalai agar was suggested as the first choice among the tested three types of agar reagents. Firstly, a lot-dependent variation of the mutant growth was little between the two tested lots (**Figures 2–5** and **Supplementary Figures S5–S8**). We also tested two other lots of the Nacalai agar under some conditions, and we found the similar phenotypes of the mutants regardless of the batches (data not shown). Another important advantage of employing Nacalai agar is that the growth of the wild-type Col-0 and the mutants were more clearly distinguishable than when the other agars were used, except for Hg(II) treatment (**Figures 2–5** and **Supplementary Figures S5–S8**). The representative result was of As(III) treatment. *cad1-3* and *cad1-6* are equally sensitive to As(III) treatment showing shorter roots and accumulation of anthocyanins in leaves, whereas *abcc1/2* exhibits slight but yet better shoot growth without apparent anthocyanin accumulation (Uraguchi et al., 2018). These genotypic differences were stably observed with the Nacalai plates but not with either of the two batches of Type A and Type E agars (**Figure 2**). For Cd(II) stress, the application of the Nacalai agars enabled stable and clear observation of the intermediate Cd-sensitive phenotypes of *cad1-6* (**Figure 5** and **Supplementary Figure S8**), which was previously reported (Tennstedt et al., 2009; Kühnlenz et al., 2016). The same goes for phenotyping of excess Zn(II) stress. The growth difference between Col-0 and the AtPCS1 mutants (*cad1-3* and *cad1-6*) was smaller than the cases of other metal(loid) stress but the equally sensitive phenotypes of *cad1-3* and *cad1-6* were more sharply and stably detected on the Nacalai plates (**Figure 4** and **Supplementary Figure S7**). Even under such conditions, the growth of *abcc1/2* was overall comparable to that of Col-0, without an apparent sign of Zn-hypersensitivity. AtABCC1 and AtABCC2 are crucial players in metal detoxification by mediating sequestration of the PC-metal(loid) complex into vacuoles (Song et al., 2010; Park et al., 2012). However, our results suggest for the first time that AtABCC1 and AtABCC2 do not significantly contribute to excess Zn detoxification. Another vacuolar Zn sequestration pathway is likely more dominant. AtMTP1, a member of the cation diffusion facilitator (CDF) family is a strong candidate (Kobae et al., 2004; Desbrosses-Fonrouge et al., 2005).

As discussed so far, Nacalai agar was suggested as a versatile gelling agent for the toxic metal(loid) sensitivity assay, however, the exception was Hg(II). The application of the Nacalai agar drastically diminished the Hg(II) sensitivity of the mutant plants (**Figure 3** and **Supplementary Figure S6**). Contrastingly the same Hg(II) treatment with Type A and Type E agars severely inhibited the mutant plant growth, thus these agars rather than Nacalai agar are suitable for Hg(II)-sensitivity phenotyping. For As(III), Cd(II), and Zn(II) stress, we found a considerable variation of the mutant growth between the lots of Type A or Type E agars, however, the hypersensitive phenotypes of the mutants were substantially observed when an appropriate batch was used

(**Figures 2**, **4**, **5** and **Supplementary Figures S5, S7, S8**). Thus, Type A or Type E agar would be the alternative choice of a gelling agent for the growth experiments testing various metal(loid) stress, especially when including Hg(II).

Agar-Dependent Variation of Plant As and Hg Accumulation and Toxicity

Because we observed the agar type-dependent or lot-dependent variation of the mutant phenotypes mainly under As(III) and Hg(II) treatments, we hypothesized that the agar affected uptake and accumulation of As or Hg in the plants, and different accumulation levels of As or Hg resulted in the different growth sensitivity of the mutant. The results of Hg measurement in Col-0 and *cad1-3* likely explain the agar type-dependent variation of Hg(II)-sensitivity (**Figure 3** and **Supplementary Figure S6**, severe toxicity was observed with the Type A plates but not with the Nacalai plates). Hg concentrations in plants were generally higher when Type A agars were used for the plate preparation than Nacalai agars (>2-fold in shoots, and > 4-fold in roots, **Figures 6C,D**). The enhanced Hg accumulation with the Type A plates would sharpen the toxic symptoms in the mutants which cannot handle Hg(II) ions in the cells due to the loss-of-function mutations of AtPCS1 or AtABCC1 and AtABCC2 (Ha et al., 1999; Park et al., 2012). A possible cause for the agar-dependent variation of plant Hg accumulation is higher Mg and Ca contents in the Nacalai agar plates (**Figure 1** and **Supplementary Figure S1**). Nacalai agars contained remarkably higher levels of Mg and Ca, which resulted in up to 65 and 20% increase of the medium Mg and Ca concentrations, respectively. It is generally believed that root transport systems for essential cations mediate uptake of non-essential divalent metals including Hg(II). Antagonistic inhibition of Hg(II) uptake was reported by co-existing essential cations including Ca (Esteban et al., 2013; Kis et al., 2017). Taken together, it is very likely that higher concentrations of Mg and/or Ca in the Nacalai plates antagonistically affect Hg uptake by the plants, which consequently diminishes the mutant sensitivity under Hg(II) stress when grown on the Nacalai agar plates.

Unlike the case of Hg(II), different As concentrations in plants are not likely the major factor causing the agar-dependent variation of the mutant As(III)-sensitivity, because the As concentration in the plants and growth sensitivity of the mutant were not correlated between Type A and Nacalai agars, and between Type A-1 and A-2. Plant As concentrations were overall lower when grown with the Nacalai plates than with the Type A plates (**Figures 6A,B**), although the mutant plants exhibited more severe hypersensitivity to As(III) on the Nacalai plates (**Figure 2** and **Supplementary Figure S5**). The lot-dependent variation of plant As accumulation was not found in *cad1-3* between the Type A plates (**Figure 6B**), although there was a lot-dependent difference of the As(III)-sensitivity with the Type A plates (**Figure 2** and **Supplementary Figure S5**). Similarly, no correlation between plant As accumulation and sensitivity was reported for *sel1-8*, a loss-of-function mutant of a sulfate transporter gene *SULTR1;2* (Nishida et al., 2016). The study suggests that total As concentrations in plants are not a reliable marker for As(III)-hypersensitivity of *sel1-8*, in which reduced sulfate uptake appears to disrupt GSH-based cellular redox maintenance under As(III) stress (Nishida et al., 2016). The agar-dependent variation of the mutant As(III)-sensitivity observed in this study would be also caused by different physiological conditions of the plants like redox activity. Another possibility is interaction between As(III) toxicity and supplied P levels in the medium as suggested by Lou-Hing et al. (2011). Increased P supply to the medium alleviated As(III) toxicity in rice cultivars, although the mechanism remained elusive. The higher P level in the Type A-2 agar compared to the Type A-1 (**Figure 1** and **Supplementary Figure S1**) could be a reason for the As(III)-sensitivity variation between the Type A lots. However, this hypothesis cannot explain the similar phenotypic variation between the Type E lots, because the P levels of Type E-1 and E-2 were equal (**Figure 1** and **Supplementary Figure S1**). Further molecular understanding of the As(III) toxicity in the plants would provide a clue for the growth condition-dependent variation of the As(III)-sensitivity.

Apart from the metal(loid) sensitivity variation, the agar-dependent variation of the plant As and Hg accumulation that we observed (**Figure 6**) suggests that the selection of agar reagents is also important for phenotyping metal(loid) accumulation. It should be considered that differences of metal(loid) accumulation between wild-type and mutant plants can be masked by a certain agar reagent as we observed for Type A and Nacalai agars. As far as comparing Type A and Nacalai agars, Type A would be a better selection for assessing plant metal(loid) accumulation because the Type A plates can provide higher plant As and Hg accumulation with clear genotypic differences (**Figure 6**). Moreover, Type A-specific ionomic alterations were indicated as the As(III) toxicity for Na, Mn, Fe, and P, and for Zn and S, the As(III)-induced changes were more evidently detected with the Type A plates (**Figure 7** and **Supplementary Figure S9**). These results suggest that the Type A medium is overall suitable for analyzing plant element accumulation under metal(loid) stress.

Perspectives on the Agar Matter of Plant Metal Study

The present study conducted a series of experiments using six different agar reagents and three established metal(loid)-sensitive Arabidopsis mutant plants to examine the effects of agar reagents in the medium on the plant responses against toxic metal(loid) stress. Based on the results presented, we can draw conclusions that (i) a "wrong" agar reagent can easily mask phenotypes (plant growth and metal accumulation) of the well-established Arabidopsis mutants, (ii) suitability of gelling agents for metal(loid) stress assay depends on the target metal(loid), and (iii) elemental profiles of agar reagents would help to predict possible "masking effects" derived from elemental contaminants in the agar regents.

Regarding (i), the agar effect is terrifying as we demonstrated that the growth inhibition of *cad1-3*, one of the most evident metal(loid)-sensitive mutants was completely masked by a certain type of agar reagents. Many of other metal(loid)-sensitive

mutants would exhibit more moderate phenotypes compared to *cad1-3*, and then phenotyping with an agar reagent causing even mild masking effects would result in "misphenotyping," and lead to a wrong conclusion. Similarly, the unsuitable medium composition was reported to cause "misphenotyping" of several mutants under Zn(II) and Pb(II) stress (Tennstedt et al., 2009; Fischer et al., 2014). Related to the second conclusion (ii), what makes the agar problem complicated is that it is almost impossible to find a "complete agar" which can be applied for any metal(loid) treatment. Therefore, one should be careful in the choice of gelling agents for their respective experiments. Conducting the phenotyping assay with at least two independent agar reagents would be a solution to avoid such agar-derived "misphenotyping," however, it is time-consuming. One alternative suggestion is including *cad1-3* for instance as a positive control to every assay. Suitability of the experimental conditions, including a selection of agar reagents, can be judged based on the *cad1-3* performance. Another possible solution to predict the suitability of agar reagents is an analysis of elemental profiles of the reagent to be used, as stated in the third remark (iii). Our data imply that less contaminated agars are less likely to cause "masking effects," although it is difficult in some cases to point out which element contamination would be critical. This is likely because such "masking effects" are attributed to chemical and physiological interactions between the elements (Lou-Hing et al., 2011; Lešková et al., 2017). Agarose, which is prepared from agar, can be another candidate for medium solidification, because it generally contains less elemental contaminants than agar reagents (Gruber et al., 2013), due to the removal of agaropectin fractions from agar. However, as reported (Gruber et al., 2013) and as we observed in preliminary experiments, the plant growth was not fine and uniform on agarose medium plates.

Incidentally, our ionomic data of agar reagents demonstrated a large variation of the agar-derived load of essential minerals to the medium, supporting the importance of agar selection for nutrient deficiency experiments (Jain et al., 2009; Gruber et al., 2013). Substantial increase of total element concentrations in the medium was expected for Mg, Ca, Fe, Cu, Zn, P, and S depending on the agar reagents (**Supplementary Figure S1**). As far as comparing plant ionomic data of control conditions (**Figure 7** and **Supplementary Figure S9**), positive correlations were only detected for Mg and Ca between total element concentrations in the medium and plants. For other elements, concentrations in the plants seemed rather unaffected by the elemental contents in the agar reagents. This would be because total concentrations in the agars do not represent phytoavailable fractions and/or uptake and utilization of these elements by plants are tightly regulated. Nevertheless, our ionomic analysis of the agar reagents indicates that Nacalai agars which have less elemental contamination would be a suitable gelling reagent for nutrient deficiency experiments among the agars tested in this study.

In conclusion, the present study demonstrates with a series of data obtained from several agar reagents that selecting a proper agar reagent is important for metal(loid) stress-related phenotypes and ionome of Arabidopsis. We propose to include a reference mutant such as *cad1-3* to the growth assay to avoid "misphenotyping" caused by agar and other experimental factors. We also propose to describe types and lot numbers of agar reagents in the method section when reporting results of metal-sensitivity growth assay or ionome obtained from agar plate culture.

DATA AVAILABILITY STATEMENT

All datasets generated for this study are included in the article/**Supplementary Material**.

AUTHOR CONTRIBUTIONS

SU conceived and designed the experiments. MK supervised the study. SU, YOt, HT, NY, HS, and MH conducted the experiments. SU, YOh, RN, YT, and MK analyzed the data. SU and MK prepared the manuscript with contributions from all authors.

FUNDING

This work was supported in part by the Japan Society for the Promotion of Science (Grant Nos. 18K05377 to SU and 18H03401 to MK) and Kitasato University Research Grant for Young Researchers to SU.

ACKNOWLEDGMENTS

We thank Youngsook Lee (POSTECH), Enrico Martinoia (University of Zurich), and Stephan Clemens (University of Bayreuth) for providing the seeds of the mutants. We also thank Sho Nishida (Saga University) for providing an agar reagent.

SUPPLEMENTARY MATERIAL

The Supplementary Material for this article can be found online at: https://www.frontiersin.org/articles/10.3389/fpls.2020.00503/full#supplementary-material

REFERENCES

Bashir, K., Rasheed, S., Kobayashi, T., Seki, M., and Nishizawa, N. K. (2016). Regulating subcellular metal homeostasis: the key to crop improvement. *Front. Plant Sci.* 7:1192. doi: 10.3389/fpls.2016.01192

Blum, R., Meyer, K. C., Wünschmann, J., Lendzian, K. J., and Grill, E. (2010). Cytosolic action of phytochelatin synthase. *Plant Physiol.* 153, 159–169. doi: 10.1104/pp.109.149922

Clemens, S. (2019). Safer food through plant science: reducing toxic element accumulation in crops. *J. Exp. Bot.* 70, 5537–5557. doi: 10.1093/jxb/erz366

Clemens, S., and Ma, J. F. (2016). Toxic heavy metal and metalloid accumulation in crop plants and foods. *Annu. Rev. Plant Biol.* 67, 489–512. doi: 10.1146/annurev-arplant-043015-112301

Desbrosses-Fonrouge, A. G. G., Voigt, K., Schröder, A., Arrivault, S., Thomine, S., and Krämer, U. (2005). Arabidopsis thaliana MTP1 is a Zn transporter in the vacuolar membrane which mediates Zn detoxification and drives leaf Zn accumulation. *FEBS Lett.* 579, 4165–4174. doi: 10.1016/j.febslet.2005.06.046

Esteban, E., Deza, M., and Zornoza, P. (2013). Kinetics of mercury uptake by oilseed rape and white lupin: influence of Mn and Cu. *Acta Physiol. Plant.* 35, 2339–2344. doi: 10.1007/s11738-013-1253-6

Fischer, S., Kühnlenz, T., Thieme, M., Schmidt, H., and Clemens, S. (2014). Analysis of plant Pb tolerance at realistic submicromolar concentrations demonstrates the role of phytochelatin synthesis for Pb detoxification. *Environ. Sci. Technol.* 48, 7552–7559. doi: 10.1021/es405234p

Fukao, Y., and Ferjani, A. (2011). V-ATPase dysfunction under excess zinc inhibits *Arabidopsis* cell expansion. *Plant Signal. Behav.* 6, 1253–1255. doi: 10.4161/psb.6.9.16529

Fukao, Y., Ferjani, A., Tomioka, R., Nagasaki, N., Kurata, R., Nishimori, Y., et al. (2011). iTRAQ analysis reveals mechanisms of growth defects due to excess zinc in *Arabidopsis*. *Plant Physiol.* 155, 1893–1907. doi: 10.1104/pp.110.169730

Gilbert-Diamond, D., Cottingham, K. L., Gruber, J. F., Punshon, T., Sayarath, V., Gandolfi, J. A., et al. (2011). Rice consumption contributes to arsenic exposure in US women. *Proc. Nat. Acad. Sci. U.S.A.* 108, 20656–20660. doi: 10.1073/pnas.1109127108

Gruber, B. D., Giehl, R. F., Friedel, S., and von Wirén, N. (2013). Plasticity of the *Arabidopsis* root system under nutrient deficiencies. *Plant Physiol.* 163, 161–179. doi: 10.1104/pp.113.218453

Ha, S., Smith, A., Howden, R., Dietrich, W., Bugg, S., O'Connell, M., et al. (1999). Phytochelatin synthase genes from *Arabidopsis* and the yeast *Schizosaccharomyces pombe*. *Plant Cell* 11, 1153–1164. doi: 10.1105/tpc.11.6.1153

Hou, X., Tong, H., Selby, J., DeWitt, J., Peng, X., and He, Z.-H. (2005). Involvement of a cell wall-associated kinase, WAKL4, in *Arabidopsis* mineral responses. *Plant Physiol.* 139, 1704–1716. doi: 10.1104/pp.105.066910

Howden, R., Goldsbrough, P., Andersen, C., and Cobbett, C. (1995). Cadmium-sensitive, cad1 mutants of *Arabidopsis thaliana* are phytochelatin deficient. *Plant Physiol.* 107, 1059–1066. doi: 10.1104/pp.107.4.1059

Huang, C.-F., Yamaji, N., and Ma, J. (2010). Knockout of a bacterial-type ATP-binding cassette transporter gene, AtSTAR1, results in increased aluminum sensitivity in *Arabidopsis*. . *Plant Physiol.* 153, 1669–1677. doi: 10.1104/pp.110.155028

Jain, A., Poling, M. D., Smith, A. P., Nagarajan, V. K., Lahner, B., Meagher, R. B., et al. (2009). Variations in the composition of gelling agents affect morphophysiological and molecular responses to deficiencies of phosphate and other nutrients. *Plant Physiol.* 150, 1033–1049. doi: 10.1104/pp.109.136184

Järup, L. (2003). Hazards of heavy metal contamination. *Br. Med. Bull.* 68, 167–182. doi: 10.1093/bmb/ldg032

Jing, Y., He, Z., Yang, X., and Sun, C. (2008). Evaluation of soil tests for plant available mercury in a soil–crop rotation system. *Commun. Soil Sci. Plant Anal.* 39, 3032–3046. doi: 10.1080/00103620802432907

Kis, M., Sipka, G., and Maróti, P. (2017). Stoichiometry and kinetics of mercury uptake by photosynthetic bacteria. *Photosynth. Res.* 132, 197–209. doi: 10.1007/s11120-017-0357-z

Kobae, Y., Uemura, T., Sato, M. H., Ohnishi, M., Mimura, T., Nakagawa, T., et al. (2004). Zinc transporter of *Arabidopsis thaliana* AtMTP1 is localized to vacuolar membranes and implicated in zinc homeostasis. *Plant Cell Physiol.* 45, 1749–1758. doi: 10.1093/pcp/pci015

Krämer, U., Talke, I. N., and Hanikenne, M. (2007). Transition metal transport. *FEBS Lett.* 581, 2263–2272. doi: 10.1016/j.febslet.2007.04.010

Kühnlenz, T., Hofmann, C., Uraguchi, S., Schmidt, H., Schempp, S., Weber, M., et al. (2016). Phytochelatin synthesis promotes leaf Zn accumulation of Arabidopsis thaliana plants grown in soil with adequate Zn supply and is essential for survival on Zn-contaminated soil. *Plant Cell Physiol.* 57, 2342–2352. doi: 10.1093/pcp/pcw148

Kühnlenz, T., Schmidt, H., Uraguchi, S., and Clemens, S. (2014). *Arabidopsis thaliana* phytochelatin synthase 2 is constitutively active in vivo and can rescue the growth defect of the PCS1-deficient cad1-3 mutant on Cd-contaminated soil. *J. Exp. Bot.* 65. 65, 4241–4253. doi: 10.1093/jxb/eru195

Kumar, A., and Prasad, M. N. V. (2018). Plant-lead interactions: transport, toxicity, tolerance, and detoxification mechanisms. *Ecotoxicol. Environ. Safe.* 166, 401–418. doi: 10.1016/j.ecoenv.2018.09.113

LeBlanc, M. S., McKinney, E. C., Meagher, R. B., and Smith, A. P. (2012). Hijacking membrane transporters for arsenic phytoextraction. *J. Biotechnol.* 163, 1–9. doi: 10.1016/j.jbiotec.2012.10.013

Lešková, A., Giehl, R. F., Hartmann, A., Fargašová, A., and von Wirén, N. (2017). Heavy metals induce iron deficiency responses at different hierarchic and regulatory levels. *Plant Physiol.* 174, 1648–1668. doi: 10.1104/pp.16.01916

Li, R., Wu, H., Ding, J., Fu, W., Gan, L., and Li, Y. (2017). Mercury pollution in vegetables, grains and soils from areas surrounding coal-fired power plants. *Sci. Rep.* 7:46545. doi: 10.1038/srep46545

Lou-Hing, D., Zhang, B., Price, A. H., and Meharg, A. A. (2011). Effects of phosphate on arsenate and arsenite sensitivity in two rice (*Oryza sativa* L.) cultivars of different sensitivity. *Environ. Exp. Bot.* 72, 47–52. doi: 10.1016/j.envexpbot.2010.11.003

Ma, J. F., Chen, Z. C., and Shen, R. F. (2014). Molecular mechanisms of Al tolerance in gramineous plants. *Plant Soil* 381, 1–12. doi: 10.1007/s11104-014-2073-1

Nishida, S., Duan, G., Ohkama-Ohtsu, N., Uraguchi, S., and Fujiwara, T. (2016). Enhanced arsenic sensitivity with excess phytochelatin accumulation in shoots of a SULTR1;2 knockout mutant of *Arabidopsis thaliana* (L.) Heynh. *Soil Sci. Plant Nutr.* 62, 1–6. doi: 10.1080/00380768.2016.1150790

Nishida, S., Tsuzuki, C., Kato, A., Aisu, A., Yoshida, J., and Mizuno, T. (2011). AtIRT1, the primary iron uptake transporter in the root, mediates excess nickel accumulation in *Arabidopsis thaliana*. *Plant Cell Physiol* 52, 1433–1442. doi: 10.1093/pcp/pcr089

Park, J., Song, W.-Y. Y., Ko, D., Eom, Y., Hansen, T. H., Schiller, M., et al. (2012). The phytochelatin transporters AtABCC1 and AtABCC2 mediate tolerance to cadmium and mercury. *Plant J.* 69, 278–288. doi: 10.1111/j.1365-313X.2011.04789.x

Sone, Y., Uraguchi, S., Takanezawa, Y., Nakamura, R., Pan-Hou, H., and Kiyono, M. (2017). A Novel role of MerC in methylmercury transport and phytoremediation of methylmercury contamination. *Biol. Pharm. Bull.* 40, 1125–1128. doi: 10.1248/bpb.b17-00213

Song, W.-Y. Y., Park, J., Mendoza-Cózatl, D. G., Suter-Grotemeyer, M., Shim, D., Hörtensteiner, S., et al. (2010). Arsenic tolerance in Arabidopsis is mediated by two ABCC-type phytochelatin transporters. *Proc. Nat. Acad. Sci. U.S.A.* 107, 21187–21192. doi: 10.1073/pnas.1013964107

Sotta, N., and Fujiwara, T. (2017). Preparing thin cross sections of *Arabidopsis* roots without embedding. *BioTechniques* 63, 281–283. doi: 10.2144/000114621

Stroud, J. L., Khan, A. M., Norton, G. J., Islam, R. M., Dasgupta, T., Zhu, Y.-G., et al. (2011). Assessing the labile arsenic pool in contaminated paddy soils by isotopic dilution techniques and simple extractions. *Environ. Sci. Technol.* 45, 4262–4269. doi: 10.1021/es104080s

Tang, Z., Fan, F., Wang, X., Shi, X., Deng, S., and Wang, D. (2018). Mercury in rice (*Oryza sativa* L.) and rice-paddy soils under long-term fertilizer and organic amendment. *Ecotox. Environ. Saf.* 150, 116–122. doi: 10.1016/j.ecoenv.2017.12.021

Tazib, T., Kobayashi, Y., Ikka, T., Zhao, C.-R., Iuchi, S., Kobayashi, M., et al. (2009). Association mapping of cadmium, copper and hydrogen peroxide tolerance of roots and translocation capacities of cadmium and copper in *Arabidopsis thaliana*. *Physiol. Plant* 137, 235–248. doi: 10.1111/j.1399-3054.2009.01286.x

Tennstedt, P., Peisker, D., Böttcher, C., Trampczynska, A., and Clemens, S. (2009). Phytochelatin synthesis is essential for the detoxification of excess zinc and contributes significantly to the accumulation of zinc. *Plant Physiol.* 149, 938–948. doi: 10.1104/pp.108.127472

Thomine, S., Wang, R., Ward, J., Crawford, N., and Schroeder, J. (2000). Cadmium and iron transport by members of a plant metal transporter family in *Arabidopsis* with homology to *Nramp* genes. *Proc. Nat. Acad. Sci. U.S.A.* 97, 4991–4996. doi: 10.1073/pnas.97.9.4991

Tsukahara, T., Ezaki, T., Moriguchi, J., Furuki, K., Shimbo, S., Matsuda-Inoguchi, N., et al. (2003). Rice as the most influential source of cadmium intake among general Japanese population. *Sci. Total Environ.* 305, 41–51. doi: 10.1016/S0048-9697(02)00475-8

Uraguchi, S., and Fujiwara, T. (2013). Rice breaks ground for cadmium-free cereals. *Curr. Opin. Plant Biol.* 16, 328–334. doi: 10.1016/j.pbi.2013.03.012

Uraguchi, S., Sone, Y., Kamezawa, M., Tanabe, M., Hirakawa, M., Nakamura, R., et al. (2019a). Ectopic expression of a bacterial mercury transporter MerC in root epidermis for efficient mercury accumulation in shoots of *Arabidopsis* plants. *Sci. Rep.* 9:4347. doi: 10.1038/s41598-019-40671-x

Uraguchi, S., Sone, Y., Ohta, Y., Ohkama-Ohtsu, N., Hofmann, C., Hess, N., et al. (2018). Identification of C-terminal regions in *Arabidopsis thaliana* Phytochelatin Synthase 1 specifically involved in activation by arsenite. *Plant Cell Physiol.* 59, 500–509. doi: 10.1093/pcp/pcx204

Uraguchi, S., Sone, Y., Yoshikawa, A., Tanabe, M., Sato, H., Otsuka, Y., et al. (2019b). SCARECROW promoter-driven expression of a bacterial mercury transporter MerC in root endodermal cells enhances mercury accumulation in *Arabidopsis* shoots. *Planta* 250, 667–674. doi: 10.1007/s00425-019-03186-3

Uraguchi, S., Tanaka, N., Hofmann, C., Abiko, K., Ohkama-Ohtsu, N., Weber, M., et al. (2017). Phytochelatin synthase has contrasting effects on cadmium and arsenic accumulation in rice grains. *Plant Cell Physiol.* 58, 1730–1742. doi: 10.1093/pcp/pcx114

Weber, M., Deinlein, U., Fischer, S., Rogowski, M., Geimer, S., Tenhaken, R., et al. (2013). A mutation in the *Arabidopsis thaliana* cell wall biosynthesis gene pectin methylesterase 3 as well as its aberrant expression cause hypersensitivity specifically to Zn. *Plant J.* 76, 151–164. doi: 10.1111/tpj.12279

Wong, C., and Cobbett, C. S. (2009). HMA P-type ATPases are the major mechanism for root-to-shoot Cd translocation in *Arabidopsis thaliana*. *New Phytol.* 181, 71–78. doi: 10.1111/j.1469-8137.2008.02638.x

Xian, X. (1987). Chemical partitioning of cadmium, zinc, lead, and copper in soils near smelter. *J. Environ. Sci. Health Part A* 22, 527–541. doi: 10.1080/10934528709375368

Yamaguchi, C., Takimoto, Y., Ohkama-Ohtsu, N., Hokura, A., Shinano, T., Nakamura, T., et al. (2016). Effects of cadmium treatment on the uptake and translocation of sulfate in *Arabidopsis thaliana*. *Plant Cell Physiol.* 57, 2353–2366. doi: 10.1093/pcp/pcw156

Yamaji, N., and Ma, J. (2017). Node-controlled allocation of mineral elements in Poaceae. *Curr. Opin. Plant Biol.* 39, 18–24. doi: 10.1016/j.pbi.2017.05.002

Conflict of Interest: The authors declare that the research was conducted in the absence of any commercial or financial relationships that could be construed as a potential conflict of interest.

frontiers in Plant Science

ORIGINAL RESEARCH
published: 26 May 2020
doi: 10.3389/fpls.2020.00560

di-Cysteine Residues of the *Arabidopsis thaliana* HMA4 C-Terminus Are Only Partially Required for Cadmium Transport

Stanislaus Antony Ceasar[1,2†], Gilles Lekeux[1,2], Patrick Motte[1], Zhiguang Xiao[3], Moreno Galleni[2] and Marc Hanikenne[1]*

[1] InBioS – PhytoSystems, Functional Genomics and Plant Molecular Imaging, University of Liège, Liège, Belgium, [2] InBioS – Center for Protein Engineering, Biological Macromolecules, University of Liège, Liège, Belgium, [3] Melbourne Dementia Research Centre, Florey Institute of Neuroscience and Mental Health, The University of Melbourne, Parkville, VIC, Australia

OPEN ACCESS

Edited by:
Seçkin Eroğlu,
Middle East Technical University, Turkey

Reviewed by:
Felipe Klein Ricachenevsky,
Universidade Estadual do Rio Grande do Sul, Brazil
Michael Palmgren,
University of Copenhagen, Denmark

***Correspondence:**
Marc Hanikenne
marc.hanikenne@uliege.be

†Present address:
Stanislaus Antony Ceasar,
Division of Plant Biotechnology, Entomology Research Institute, Loyola College, Chennai, India

Specialty section:
This article was submitted to Plant Traffic and Transport, a section of the journal Frontiers in Plant Science

Received: 03 January 2020
Accepted: 15 April 2020
Published: 26 May 2020

Citation:
Ceasar SA, Lekeux G, Motte P, Xiao Z, Galleni M and Hanikenne M (2020) di-Cysteine Residues of the Arabidopsis thaliana HMA4 C-Terminus Are Only Partially Required for Cadmium Transport. Front. Plant Sci. 11:560. doi: 10.3389/fpls.2020.00560

Cadmium (Cd) is highly toxic to the environment and humans. Plants are capable of absorbing Cd from the soil and of transporting part of this Cd to their shoot tissues. In Arabidopsis, the plasma membrane Heavy Metal ATPase 4 (HMA4) transporter mediates Cd xylem loading for export to shoots, in addition to zinc (Zn). A recent study showed that di-Cys motifs present in the HMA4 C-terminal extension (AtHMA4c) are essential for high-affinity Zn binding and transport *in planta*. In this study, we have characterized the role of the AtHMA4c di-Cys motifs in Cd transport *in planta* and in Cd-binding *in vitro*. In contrast to the case for Zn, the di-Cys motifs seem to be partly dispensable for Cd transport as evidenced by limited variation in Cd accumulation in shoot tissues of *hma2hma4* double mutant plants expressing native or di-Cys mutated variants of AtHMA4. Expression analysis of metal homeostasis marker genes, such as *AtIRT1*, excluded that maintained Cd accumulation in shoot tissues was the result of increased Cd uptake by roots. *In vitro* Cd-binding assays further revealed that mutating di-Cys motifs in AtHMA4c had a more limited impact on Cd-binding than it has on Zn-binding. The contributions of the AtHMA4 C-terminal domain to metal transport and binding therefore differ for Zn and Cd. Our data suggest that it is possible to identify HMA4 variants that discriminate Zn and Cd for transport.

Keywords: Arabidopsis, AtHMA4, Cadmium (Cd), Cd-binding, metal specificity, P-type ATPase

INTRODUCTION

Cadmium (Cd) is one of the most toxic substances present in the environment (Nriagu, 1988; Clemens et al., 2013) and represents a major health threat to humans, especially upon long-term exposure to low concentrations (Satarug et al., 2003, 2010). Although it may occasionally act as a prosthetic group in biologically active metalloproteins (Lane and Morel, 2000), Cd is usually considered to have no biological function.

Widespread low-level contamination of soil and water by Cd stems mostly from anthropogenic sources, e.g., mining, non-ferrous metal manufacturing, or the application of phosphate fertilizers

and sewage sludge on soils (Clemens et al., 2013; Tóth et al., 2016). Although Cd emissions into the environment have declined in many industrialized countries, it is still prevalent in emerging countries and low-level contamination of soils results in important contamination of the food chain. This calls for a comprehensive understanding of the Cd accumulation mechanisms in plants (Clemens et al., 2013).

The plasma membrane Heavy Metal ATPase 4 (HMA4) belongs to P_{IB}-type ATPases that transport heavy metal ions across cell membranes. Heavy Metal ATPase 4 is a main contributor to Cd xylem loading and root-to-shoot translocation in *Arabidopsis thaliana* (Arabidopsis) (Wong and Cobbett, 2009), although its primary function is to ensure, together with HMA2, sufficient zinc (Zn) supply to shoot tissues and to developing seeds (Mills et al., 2003; Hussain et al., 2004; Verret et al., 2004; Wong and Cobbett, 2009; Cun et al., 2014). An *hma2hma4* double mutant has a stunted growth phenotype, resulting from severe shoot Zn deficiency (Hussain et al., 2004). HMA4 is also a key factor in the Zn and Cd hyperaccumulation syndrome found in a number of calamine species such as *Arabidopsis halleri* or *Noccaea caerulescens*, i.e., species that can establish populations on zinc/cadmium/lead-rich, so-called calamine soils (Hanikenne et al., 2008; Krämer, 2010; Merlot et al., 2018).

Typical of P_{IB}-type ATPases, the HMA4 protein possesses eight transmembrane domains that play a key role in ion selectivity (Argüello, 2003; Argüello et al., 2007; Smith et al., 2014; Wang et al., 2014; Lekeux et al., 2019), multiple cytoplasmic catalytic domains, and N- and C-terminal cytosolic extensions rich in putative metal-binding amino acids such as Cys, His, Asp, and Glu (Williams and Mills, 2005; Argüello et al., 2007; Rosenzweig and Argüello, 2012). Hence, in the Arabidopsis HMA4 (AtHMA4) protein, a Cys–Cys–Thr–Ser–Glu motif in the N-terminal domain binds one Zn(II) atom with high affinity, and this interaction is essential for the function of the protein *in planta* (Zimmermann et al., 2009; Laurent et al., 2016). The long cytosolic C-terminal extension of AtHMA4 (AtHMA4c, 470 amino acids), which usually lacks in its bacterial homologs, exhibits 13 di-Cys motifs and an 11 His-stretch and is capable of binding 10-11 Zn(II) atoms with high affinity (Bækgaard et al., 2010; Lekeux et al., 2018). While the function of the His-stretch remains elusive (Verret et al., 2005; Lekeux et al., 2018), the di-Cys motifs were recently shown to confer nanomolar affinity for Zn(II) and to play a key role in the protein's function in Zn homeostasis *in planta* (Lekeux et al., 2018).

Although AtHMA4 is known to transport Cd in addition to Zn (Talke et al., 2006; Courbot et al., 2007; Wong and Cobbett, 2009), the role of AtHMA4c in Cd binding and transport has not been determined. It was, however, shown that expression of AtHMA4c alone in yeast conferred Cd tolerance (Bernard et al., 2004). Here, we examined the functional role of the multiple di-Cys motifs in AtHMA4c in Cd transport *in vivo* and Cd(II) binding properties *in vitro*. We show that, in contrast to the case of Zn, the di-Cys motifs are only partially required for Cd transport to shoot tissues and only partially contribute to the Cd(II)-binding capacity of the C-terminal domain of AtHMA4. Our data suggest that the contribution of the AtHMA4 C-terminal domain to metal transport differs for Zn and Cd.

MATERIALS AND METHODS

Plant Material and Growth Conditions

Arabidopsis thaliana L. Heynhold (accession Columbia, Col-0) and *hma2hma4* double mutant *A. thaliana* plants (Col-0 background) (Hussain et al., 2004) were used in all experiments. *hma2hma4* mutant plants expressing either a native *AtHMA4* or an *AtHMA4CCAA* (13 di-Cys→13 di-Ala motifs) variant under the control of the *AtHMA4* promoter were reported previously (Lekeux et al., 2018). Sterile seeds were germinated for 14 days under short days (22°C and 8 h day^{-1} photoperiod) on 1/2 Murashige and Skoog (MS) agar medium containing 1% sucrose. These two-week-old seedlings were then transferred in hydroponics [Araponics growth trays, Araponics, Belgium (Tocquin et al., 2003)] and supplied with modified Hoagland medium containing 1 μM $ZnSO_4$ (control condition) and grown for another 3 weeks in short days (Talke et al., 2006; Charlier et al., 2015; Nouet et al., 2015). The Cd treatment was initiated from the 4^{th} week by supplying 0.05 or 1 μM $CdSO_4$, still in the presence of 1 μM $ZnSO_4$. Nutrient solutions were changed weekly. After 3 weeks of Cd treatment, root and shoot tissues were harvested separately for elemental profiling and gene expression analysis. All experiments were conducted in three biological replicates, each including two independent T3 homozygous lines per genotype, representative of the lines described in Lekeux et al. (2018).

Elemental Profiling

Metal content in root and shoot tissues was analyzed as described (Lekeux et al., 2018).

Gene Expression Analysis

Total RNAs were isolated from shoot and root samples using the NucleoSpin RNA Plant Kit (Macherey-Nagel GmbH & Co., Germany). The samples were treated on column with DNAse. cDNAs were then synthesized using 1 μg of total RNA, oligo-dT and the RevertAid H Minus First Strand cDNA Synthesis Kit (Thermo Fisher Scientific, United States). Quantitative RT-PCR reactions were performed in 384-well plates with a QuantStudio 5 Real-Time PCR system (Thermo Fisher Scientific, United States) using Takyon Low Rox SYBR MasterMix (Eurogentec, Belgium). Three technical replicates were performed as described (Lekeux et al., 2018) for each sample/primer combinations. The quality of the quantitative PCR was checked by inspection of dissociation and amplification curves. For each primer pair (**Supplementary Table S1**), mean reaction efficiencies were calculated using the LinRegPCR software (Ruijter et al., 2009) and then used to quantify relative gene expression levels by normalization using three reference genes (At1g18050, *UBQ10*, and *EF1α*) (Czechowski et al., 2005) with the qBase software

(Biogazelle; Hellemans et al., 2007). The adequacy of the reference genes to normalize gene expression in the experimental conditions was checked using the geNorm module in qBase (Vandesompele et al., 2002).

Cadmium Binding Assay

The protocol and experimental conditions for the analysis of Cd(II) binding to the AtHMA4 C-terminal domain (AtHMA4c as wild-type and AtHMA4CCAAc as mutant versions) were as described in Lekeux et al. (2018) except for the use of the Mag-Fura-2 (MF2) probe (Invitrogen M1290) instead of the Par probe. The binding affinity of Par for Cd(II) is too weak to allow a quantitative analysis (Kocyła et al., 2015). The metal-free MF2 probe exhibits an absorbance maximum at 366 nm with $\varepsilon = 2.99 \times 10^4\ M^{-1}\ cm^{-1}$ which was used in this work to quantify MF2 concentration (Zimmermann et al., 2009). It was reported that MF2 can bind one equivalent of Cd(II) with a dissociation constant K_D = 126 nM and Cd(II) binding to MF2 led to a decrease in absorbance at 366 nm until the probe was saturated with one equivalent of Cd(II) (de Seny et al., 2001). Consequently, in this work, Cd(II) binding assay was performed by titration of the MF2 probe (16.2 μM) with $CdCl_2$ (taken from a 200 μM stock) in the presence of a target HMA4 protein domain (3.3–3.4 μM) with the titration process monitored by the absorbance change at 366 nm. Likewise, the concentration of the $CdCl_2$ stock used in this work was calibrated by the control titration of the MF2 probe by setting the titration turning point to Cd(II)/MF2 = 1.0. The experiments were conducted in MOPS buffer (50 mM, pH 7.3, 100 mM NaCl) with inclusion of TCEP (1 mM) to maintain the reduced protein form. Cd(II) binding stoichiometry and affinity to each protein domain were estimated by a quantitative comparison of the titration curve to the control titration curve without protein under the same condition (see section "Results and Discussion" for details). The protein samples were produced and purified in fusion to the Maltose-Binding Protein (MBP) as described (Lekeux et al., 2018).

Data Analysis

Data were analyzed, and statistics were performed using SPSS software.

RESULTS AND DISCUSSION

The di-Cys Motifs of the AtHMA4 C-Terminal Domain Are Only Partially Required for Cd Transport

To examine the function of the C-terminal domain of AtHMA4 (AtHMA4c) in Cd transport, *hma2hma4* double mutant plants expressing the native *AtHMA4* or a *AtHMA4CCAA* (13 di-Cys→13 di-Ala motifs) variant under the control of the *AtHMA4* promoter (Lekeux et al., 2018) were assessed for Cd accumulation. Col-0 and *hma2hma4* double mutant plants were also assessed as wild-type and mutant controls, respectively. In the AtHMA4CCAA variant, all 13 di-Cys motifs found in the AtHMA4c domain were mutated into di-Ala motifs (Lekeux et al., 2018). Both native and mutant protein variants were shown to localize to the plasma membrane and to be expressed at similar levels (Lekeux et al., 2018). When grown in control conditions (1 μM Zn), the *hma2hma4* mutant displayed a typical phenotype with lower shoot and higher root Zn accumulation compared to wild-type plants (**Figures 1A,B**; Hussain et al., 2004; Nouet et al., 2015; Lekeux et al., 2018). Whereas expression of the native AtHMA4 fully restored this phenotype, expression of AtHMA4CCAA resulted in only limited complementation indicating impaired Zn transport to shoot tissues, as described (Lekeux et al., 2018).

As Cd treatment, a low Cd concentration (0.05 μM Cd) was selected so as to enable Cd accumulation in tissues without causing toxicity, which may have triggered spurious effects on metal homeostasis and general plant fitness (Nouet et al., 2015; Lekeux et al., 2019). The Zn accumulation pattern in tissues of the different genotypes was only marginally altered upon Cd treatment, with a noticeable, but barely significant, increase in Zn root accumulation in all genotypes (**Figures 1A,B**).

Upon Cd treatment (0.05 μM Cd), the *hma2hma4* mutant displayed strongly increased Cd accumulation in roots (∼6.5-fold) and reduced Cd accumulation in shoots (∼3.7-fold), compared to wild-type plants. This phenotype was fully reversed by the expression of the native AtHMA4 in the mutant background (**Figures 1C,D**). However, in contrast to the case of Zn, the *hma2hma4* double mutant plants expressing the AtHMA4CCAA variant displayed shoot Cd concentrations similar to wild-type plants (**Figure 1C**). Cadmium accumulation in root tissues of the AtHMA4CCAA plants was intermediate between the high and low Cd concentrations accumulated in the *hma2hma4* and wild-type plants, respectively (**Figure 1D**), suggesting that Cd transport capacity of the AtHMA4CCAA is somehow impacted by the di-Cys motif mutation. While the shoot/root Zn concentration ratio was only marginally increased (1.2-fold) upon expression of AtHMA4CCAA in the *hma2hma4* background, the shoot/root Cd concentration ratio was increased 4.2-fold, indicative of a higher Cd transport to shoots. Similar results were obtained when plants were exposed to a higher, toxic, Cd concentration (1 μM Cd, **Supplementary Figure S1**). All genotypes displayed reduced growth and chlorosis (data not shown). Zn shoot accumulation remained low in AtHMA4CCAA-expressing plants, whereas Cd shoot accumulation was significantly higher in AtHMA4CCAA plants compared to the *hma2hma4* mutant (**Supplementary Figure S1**). These observations are striking as they suggest that while the di-Cys motifs present in the AtHMA4 C-terminal domain are key to enable Zn transport (Lekeux et al., 2018), they are at least partly dispensable for Cd transport to the shoot.

Finally, the plant genotype or the Cd treatment had limited effect on the accumulation of other elements in tissues (**Supplementary Table S2**). For instance, the iron (Fe) concentration was about 20% lower in shoots of the *hma2hma4*

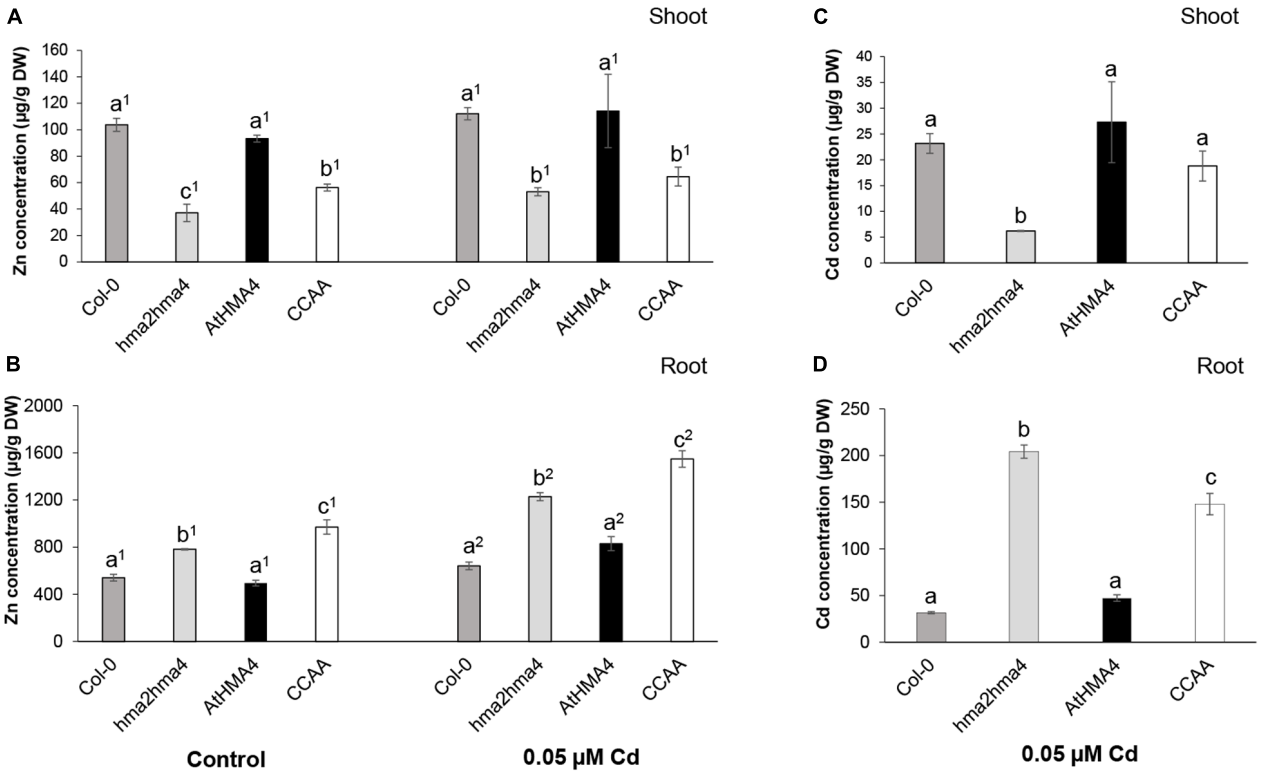

FIGURE 1 | Zinc and cadmium accumulation in shoot **(A,C)** and root **(B,D)** tissues of wild-type (Col-0), *hma2hma4* mutant, and *hma2hma4*-expressing AtHMA4 or AtHMA4CCAA plants upon hydroponic growth in control conditions (1 µM Zn, no Cd) or exposed for 3 weeks to 0.05 µM Cd. Values (in µg g^{-1} DW) are means ± SD of three biological replicates each consisting of pools of three plants from two independent lines per genotype. Statistically significant differences ($P < 0.05$) between genotypes within treatments (one-way ANOVA followed by Tukey's multiple comparison test) or between treatments within genotypes (*t*-test for independent means) are indicated by different letters or different superscript numbers, respectively. DW, dry weight; CCAA, di-Cys → di-Ala motifs.

double mutant and AtHMA4CCAA plants compared to wild-type plants upon Cd exposure.

The Expression of Metal Homeostasis Marker Genes Is Altered in Response to Cd

To further assess the physiology of the plants, the expression levels of metal-responsive genes were assessed and compared in root (*AtIRT3*, *AtZIP9*, and *AtIRT1*) and shoot (*AtIRT3* and *AtZIP9*) tissues of plants grown in both control and Cd-treated (0.05 µM) conditions (**Figure 2**).

First, *AtZIP9* and *AtIRT3* are Zn-responsive genes, induced upon Zn deficiency and repressed upon Zn excess (Talke et al., 2006). The two genes are regulated by the bZIP19 and bZIP23 transcription factors, which are key regulators of the Zn deficiency response in Arabidopsis (Assunção et al., 2010; Castro et al., 2017). As shown previously (Nouet et al., 2015; Lekeux et al., 2018), *AtZIP9* was strongly responding to Zn deficiency in the shoot of the *hma2hma4* mutant, whereas both genes were repressed in roots compared to the wild-type (**Figures 2A–D**). Again, the expression of AtHMA4CCAA in the *hma2hma4* background did not complement this phenotype (Lekeux et al., 2018). Cd exposure had contrasting effects on the expression of *AtZIP9* and *AtIRT3*. Indeed, Cd reduced the expression of *AtZIP9* in root tissues of all genotypes although the pattern of differential expression between wild-type and mutant plants remained visible (**Figure 2A**). Conversely, Cd induced the expression of *AtIRT3* in root tissues of *hma2hma4* and AtHMA4CCAA plants and among genotype differences were no longer observed (**Figure 2B**). This induction may be responsible for higher Zn in roots under Cd supply (**Figure 1B** and **Supplementary Table S2**). In shoot tissues, the Cd treatment overall reduced differences of *AtIRT3* and *AtZIP9* expression among genotypes (**Figures 2B,D**). The observed differences in expression of *AtIRT3* and *AtZIP9* in response to Cd are unlikely to be responsible for the contrasting Cd accumulation pattern between the *hma2hma4* mutant and the other genotypes (**Figures 1C,D**), but rather reflect their different contribution to metal homeostasis adjustment in response to Cd. Indeed, Cd may compete for uptake with other divalent cations, such as Zn or Fe. *AtIRT3*, encoding a Zn and Fe transporter (Lin et al., 2009), has been shown to be regulated by Zn deficiency (Talke et al., 2006; van de Mortel et al., 2006), but not by Fe deficiency (Buckhout et al., 2009; Yang et al., 2010). In contrast, *AtZIP9* is regulated by both Zn and Fe deficiency (Talke et al., 2006; Yang et al., 2010), under the control of bZIP19 mostly (Inaba et al., 2015), and FIT, a transcription factor with a major role in

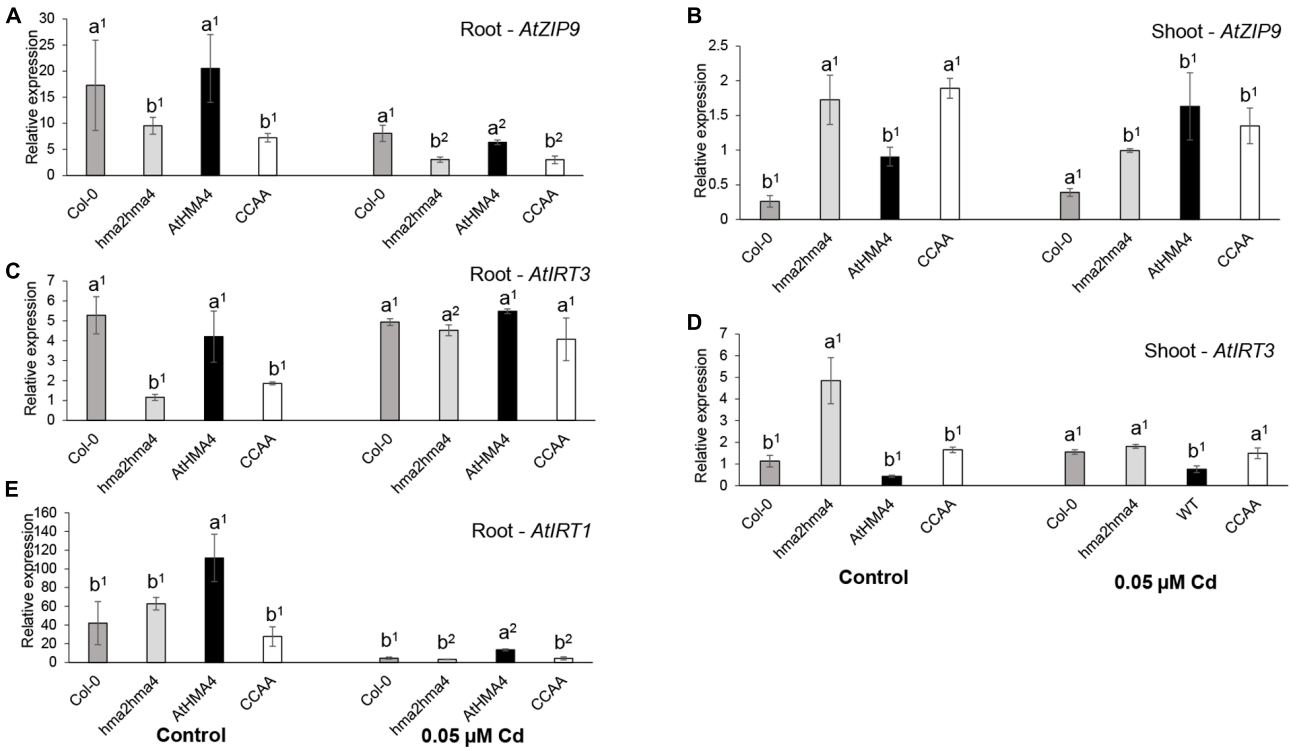

FIGURE 2 | Expression analysis of metal homeostasis genes. *AtZIP9* **(A,B)**, *AtIRT3* **(C,D)**, and *AtIRT1* **(E)** relative expression levels were measured in root **(A,C,E)** and shoot **(B,D)** tissues of wild-type (Col-0), *hma2hma4* mutant, and *hma2hma4*-expressing AtHMA4 or AtHMA4CCAA plants upon hydroponic growth in control conditions (1 µM Zn, no Cd) or exposed for 3 weeks to 0.05 µM Cd. Relative expression values are means ± SEM of three biological replicates each consisting of pools of three plants from two independent lines per genotype. Statistically significant differences ($P < 0.05$) between genotypes within treatments (one-way ANOVA followed by Tukey's multiple comparison test) or between treatments within genotypes (*t*-test for independent means) are indicated by different letters or different superscript numbers, respectively. CCAA: di-Cys → di-Ala motifs.

regulating the Fe deficiency response (Colangelo and Guerinot, 2004), respectively.

Second, *AtIRT1* encodes the main Fe uptake transporter at the root epidermis in Arabidopsis (Vert et al., 2002; Thomine and Vert, 2013). AtIRT1 has low ion selectivity and is also responsible for the uptake of additional divalent metal cations such as Zn or Cd (Vert et al., 2002; Barberon et al., 2011). AtIRT1 is subjected to a complex regulation by Fe availability but also by the presence of its other metal substrates, at both transcriptional and post-translational levels enabling fine-tuning of metal uptake (Connolly et al., 2002; Barberon et al., 2011; Barberon and Geldner, 2014; Dubeaux et al., 2018). In particular, *AtIRT1* expression is down-regulated upon Cd exposure at both transcript and protein levels (Connolly et al., 2002). Recent work suggested that differential transcription levels as well as functionality of IRT1 may contribute to among-population variation in Zn and/or Cd accumulation in the metal hyperaccumulators *A. halleri* (Corso et al., 2018; Schvartzman et al., 2018) and *N. caerulescens* (Halimaa et al., 2019). Altogether, there is ample evidence that IRT1 represents a major route of entry for Cd in plant tissues. Therefore, *AtIRT1* expression was assessed here in root tissues of all genotypes in both control and Cd conditions to determine whether the differential Cd accumulation observed among genotypes (**Figures 1C,D**) resulted from changes in *AtIRT1* expression. Upon Cd treatment, *AtIRT1* expression was down-regulated in roots of all genotypes compared to control conditions (**Figure 2E**) and there was very little variation among wild-type and mutant genotypes, except for the slightly higher expression of *AtIRT1* in *hma2hma4* lines complemented by the native AtHMA4 which is difficult to interpret. These observations suggested that higher Cd accumulation in shoots of AtHMA4CCAA plants compared to the *hma2hma4* mutant did not result from IRT1-driven differential Cd root uptake.

Mutating the di-Cysteine Residues in the AtHMA4 C-Terminus Only Partially Alters Cd Binding

To link the above *in vivo* observations to the possible impact of the di-Cys motifs in AtHMA4c to the Cd(II) binding property, Cd(II) binding assays were performed by titrations of the purified MBP-AtHMA4c or MBP-AtHMA4CCAAc fusion proteins with Cd^{2+} in the presence of the Cd(II)-responding probe MF2 (de Seny et al., 2001; Zimmermann et al., 2009). A control titration of Cd^{2+} into a MF2 solution (16.2 µM) without protein component led to a steady decrease in absorbance at 366 nm with an apparent turning point at Cd(II)/MF2 = 1.0 (**Figure 3**, curve

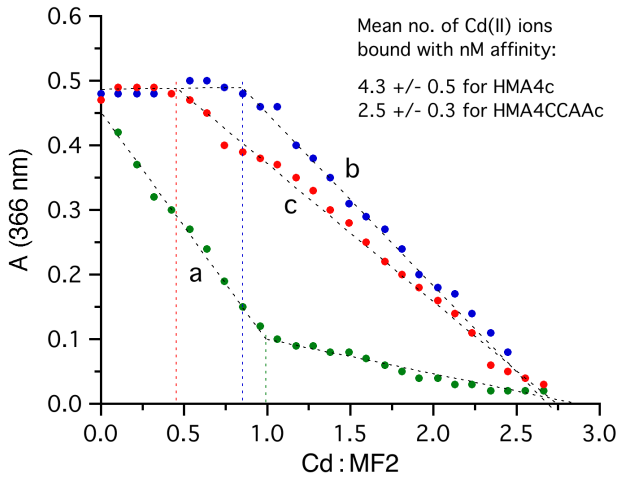

FIGURE 3 | Cd(II)-binding assay for the AtHMA4 C-terminal domains by competition with MF2 probe in MOPS buffer (pH 7.3, 100 mM NaCl, 1 mM TCEP): curve (a) titration of MF2 (16.2 μM) with $CdCl_2$ (200 μM); curve (b) titration of a mixture of MF2 (16.2 μM) and MBP-AtHMA4c (3.4 μM) with $CdCl_2$ (200 μM); curve (c) titration of a mixture of MF2 (16.2 μM) and MBP-AtHMA4CCAAc (3.3 μM) with $CdCl_2$ (200 μM). The apparent turning point for each titration curve is indicated by a vertical dashed line. The number of Cd(II) ions bound to each protein domain with affinities out-competing that of MF2 was estimated by the product of the molar ratio Cd(II)/MF2 at the titration turning point and the molar ratio MF2/protein in the titration mixture. Values in the chart represent data from one experiment representative of three independent experiments, whereas values in the table insert are means ± SD of the three independent experiments.

a), consistent with the formation of a 1:1 Cd(II)-MF2 complex with the reported sub-micromolar affinity (K_D = 126 nM) (de Seny et al., 2001). Inclusion of the purified MBP carrier protein in the same MF2 solution had little effect on the titration curve (data not shown), demonstrating that MBP lacked detectable Cd(II) binding sites by the MF2 probe. However, an equivalent titration with substitution of MBP by MBP-AtHMA4c (3.4 μM) in the same MF2 probe solution generated a very different titration curve (compare curve b to curve a in **Figure 3**). With titration of Cd^{2+}, the solution absorbance at 366 nm remained essentially unchanged until a molar ratio Cd(II)/MF2 = 0.9 ± 0.1 was reached for three independent titrations (**Figure 3**, curve b), indicating that the AtHMA4c protein domain out-competed MF2 for high-affinity Cd(II) binding before the titration turning point and can bind 4.3 ± 0.5 equivalents of Cd(II) with high affinities estimated at the nanomolar concentration range (ie, K_D < < 126 nM). The titration curve (b) after the turning point was somewhat flatter than the titration curve (a) before the titration turning point (**Figure 3**), suggesting the existence of further weaker Cd(II) binding sites with affinities comparable to that of MF2 at K_D = 126 nM.

On the other hand, another equivalent titration with inclusion of MBP-AtHMA4CCAAc (3.3 μM) instead of MBP-AtHMA4c led to a titration curve with an apparent turning point at a lower Cd(II)/MF2 of 0.50 ± 0.06 (**Figure 3**, curve c), suggesting that the AtHMA4CCAAc protein domain can bind 2.5 ± 0.3 equivalents on average of Cd(II) with nanomolar affinity. However, the titration curve (c) after the turning point was further flattened, suggesting that AtHMA4CCAAc featured somewhat much weaker Cd(II)-binding sites than did AtHMA4c. Overall, mutation of the 13 di-Cys motifs in the AtHMA4 C-terminal domain has led to a loss of ∼42% of high-affinity Cd(II) binding. This is in contrast to previous Zn-binding assays which showed that the CCAA mutations reduced high-affinity Zn(II) binding at K_D < 1 nM from ∼7 equivalents for AtHMA4c to only ∼2 equivalents for AtHMA4CCAAc, i.e., a loss of ∼70% high-affinity Zn(II) binding (Lekeux et al., 2018).

CONCLUSION

Cd(II) binding by AtHMA4c was thus lower than Zn(II) binding, with ∼4.3 equivalents for Cd(II) on average (**Figure 3**) and ∼11 equivalents for Zn(II) [7 with K_D < 1 nM and 4 with K_D = 1–10 nM (Lekeux et al., 2018)]. In the absence of the di-Cys motifs, the AtHMA4CCAAc domain retains 2.5 equivalents (>50%) of high-affinity Cd(II) binding which might result from either other non-di-Cys ligands such as single Cys and/or numerous His, Asp, and Glu residues also present in AtHMA4CCAAc. Alternatively, the retained Cd(II) binding in AtHMA4CCAAc might result from creation of new high-affinity binding sites caused by structural coordination rearrangement induced upon removal of di-Cys motifs, which may be facilitated by the fact that the AtHMA4c domain is intrinsically disordered. This remaining Cd(II)-binding capacity of AtHMA4CCAAc appeared to be sufficient, at low Cd(II) exposure, to at least partially enable Cd(II) transport and translocation to the plant shoot (**Figure 1**), whereas it was shown recently that the di-Cys motif of AtHMA4c is essential for Zn transport (Lekeux et al., 2018). In the past, several attempts have been made to identify mutations enabling metal transporters to discriminate between essential metals (e.g., Fe or Zn) and non-essential toxic metals (e.g., Cd) (Rogers et al., 2000; Pottier et al., 2015; Liedschulte et al., 2017), with the aim of favoring transport of specific metals for biofortification. For HMA4-related proteins in tobacco, modification of the protein sequence to reduce Cd accumulation in tobacco leaves resulted in drastically altered Zn homeostasis and consequently strongly impaired growth (Liedschulte et al., 2017). In contrast, plants expressing an AtHMA4 variant with a substitution of Phe_{177}, present in transmembrane domain 2, into a Leu displayed significantly decreased Cd accumulation in shoots while Zn accumulation was maintained to a level enabling normal growth of Arabidopsis (Lekeux et al., 2019). Here, the contribution of the multiple di-Cys motifs in the AtHMA4 C-terminal domain to metal transport appears to differ for Zn and Cd, which may be instrumental to discriminate between the two metals for biofortification or phytoremediation strategies.

DATA AVAILABILITY STATEMENT

All datasets generated for this study are included in the article/**Supplementary Material**.

AUTHOR CONTRIBUTIONS

MH and MG conceived and directed the study. MH, MG, SC, GL, and ZX designed the experiments. SC and GL performed the experiments. SC, MH, MG, and ZX analyzed the data. MH, MG, and PM contributed reagents, materials, and analysis tools. SC, MH, ZX, and MG wrote the manuscript. All authors commented on the manuscript.

FUNDING

Funding was provided by the "Fonds de la Recherche Scientifique–FNRS" (PDR-T.0206.13, CDR J.0009.17, and PDR T0120.18) (MH, MG), the University of Liège (SFRD-12/03) (MH), and the Belgian Program on Interuniversity Attraction Poles (IAP no. P7/44) (MG and MH). MH is Senior Research Associate of the FNRS. GL thanks the FRIA for his Ph.D. fellowship. SC was supported by a Non-European Post-doctoral research fellowship from the Belgian "Politique Scientifique Fédérale" (Belspo).

ACKNOWLEDGMENTS

We thank Arnaud Degueldre and Marie Schloesser for technical support.

SUPPLEMENTARY MATERIAL

The Supplementary Material for this article can be found online at: https://www.frontiersin.org/articles/10.3389/fpls.2020.00560/full#supplementary-material

REFERENCES

Argüello, J. M. (2003). Identification of ion-selectivity determinants in heavy-metal transport P1B-type ATPases. *J. Membr. Biol.* 195, 93–108. doi: 10.1007/s00232-003-2048-2

Argüello, J. M., Eren, E., and González-Guerrero, M. (2007). The structure and function of heavy metal transport P1B-ATPases. *BioMetals*20, 233–234. doi: 10.1007/s10534-006-9055-6

Assunção, A. G. L., Herrero, E., Lin, Y.-F., Huettel, B., Talukdar, S., Smaczniak, C., et al. (2010). *Arabidopsis thaliana* transcription factors bZIP19 and bZIP23 regulate the adaptation to zinc deficiency. *Proc. Natl. Acad. Sci. U.S.A.* 107, 10296–10301. doi: 10.1073/pnas.1004788107

Barberon, M., and Geldner, N. (2014). Radial transport of nutrients: the plant root as a polarized epithelium. *Plant Physiol.* 166, 528–537. doi: 10.1104/pp.114.246124

Barberon, M., Zelazny, E., Robert, S., Conéjéro, G., Curie, C., Friml, J., et al. (2011). Monoubiquitin-dependent endocytosis of the iron-regulated transporter 1 (IRT1) transporter controls iron uptake in plants. *Proc. Natl. Acad. Sci. U.S.A.* 108, E450–E458. doi: 10.1073/pnas.1100659108

Bernard, C., Roosens, N., Czernic, P., Lebrun, M., and Verbruggen, N. (2004). A novel CPx-ATPase from the cadmium hyperaccumulator *Thlaspi caerulescens*. *FEBS Lett.* 569, 140–148. doi: 10.1016/j.febslet.2004.05.036

Buckhout, T. J., Yang, T. J. W., and Schmidt, W. (2009). Early iron-deficiency-induced transcriptional changes in *Arabidopsis* roots as revealed by microarray analyses. *BMC Genomics* 10:147. doi: 10.1186/1471-2164-10-147

Bækgaard, L., Mikkelsen, M. D., Sørensen, D. M., Hegelund, J. N., Persson, D. P., Mills, R. F., et al. (2010). A combined Zinc/Cadmium sensor and Zinc/Cadmium export regulator in a heavy metal pump. *J. Biol. Chem.* 285, 31243–31252. doi: 10.1074/jbc.M110.111260

Castro, P. H., Lilay, G. H., Munoz-Merida, A., Schjoerring, J. K., Azevedo, H., and Assuncao, A. G. L. (2017). Phylogenetic analysis of F-bZIP transcription factors indicates conservation of the zinc deficiency response across land plants. *Sci. Rep.* 7:3806. doi: 10.1038/s41598-017-03903-6

Charlier, J.-B., Polese, C., Nouet, C., Carnol, M., Bosman, B., Krämer, U., et al. (2015). Zinc triggers a complex transcriptional and post-transcriptional regulation of the metal homeostasis gene FRD3 in *Arabidopsis* relatives. *J. Exp. Bot.* 66, 3865–3878. doi: 10.1093/jxb/erv188

Clemens, S., Aarts, M. G. M., Thomine, S., and Verbruggen, N. (2013). Plant science: the key to preventing slow cadmium poisoning. *Trends Plant Sci.* 18, 92–99. doi: 10.1016/j.tplants.2012.08.003

Colangelo, E. P., and Guerinot, M. L. (2004). The essential basic helix-loop-helix protein FIT1 is required for the iron deficiency response. *Plant Cell* 16, 3400–3412. doi: 10.1105/tpc.104.024315

Connolly, E. L., Fett, J. P., and Guerinot, M. L. (2002). Expression of the IRT1 metal transporter is controlled by metals at the levels of transcript and protein accumulation. *Plant Cell* 14, 1347–1357. doi: 10.1105/tpc.001263

Corso, M., Schvartzman, M. S., Guzzo, F., Souard, F., Malkowski, E., Hanikenne, M., et al. (2018). Contrasting cadmium resistance strategies in two metallicolous populations of *Arabidopsis halleri*. *New Phytol.* 218, 283–297. doi: 10.1111/nph.14948

Courbot, M., Willems, G., Motte, P., Arvidsson, S., Roosens, N., Saumitou-Laprade, P., et al. (2007). A major quantitative trait locus for cadmium tolerance in *Arabidopsis halleri* colocalizes with HMA4, a gene encoding a heavy metal ATPase. *Plant Physiol.* 144, 1052–1065. doi: 10.1104/pp.106.095133

Cun, P., Sarrobert, C., Richaud, P., Chevalier, A., Soreau, P., Auroy, P., et al. (2014). Modulation of Zn/Cd P1B2-ATPase activities in *Arabidopsis* impacts differently on Zn and Cd contents in shoots and seeds. *Metallomics* 6, 2109–2116. doi: 10.1039/c4mt00182f

Czechowski, T., Stitt, M., Altmann, T., Udvardi, M. K., and Scheible, W.-R. (2005). Genome-wide identification and testing of superior reference genes for transcript normalization in *Arabidopsis*. *Plant Physiol.* 139, 5–17. doi: 10.1104/pp.105.063743

de Seny, D., Heinz, U., Wommer, S., Kiefer, M., Meyer-Klaucke, W., Galleni, M., et al. (2001). Metal ion binding and coordination geometry for wild type and mutants of metallo-β-lactamase from *Bacillus cereus* 569/H/9 (BcII): a combined thermodynamic, kinetic, and spectroscopic approach. *J. Biol. Chem.* 276, 45065–45078. doi: 10.1074/jbc.M106447200

Dubeaux, G., Neveu, J., Zelazny, E., and Vert, G. (2018). Metal sensing by the IRT1 transporter-receptor orchestrates its own degradation and plant metal nutrition. *Mol. Cell* 69, 953.e5–964.e5. doi: 10.1016/j.molcel.2018.02.009

Halimaa, P., Blande, D., Baltzi, E., Aarts, M. G. M., Granlund, L., Keinänen, M., et al. (2019). Transcriptional effects of cadmium on iron homeostasis differ in calamine accessions of *Noccaea caerulescens*. *Plant J.* 97, 306–320. doi: 10.1111/tpj.14121

Hanikenne, M., Talke, I. N., Haydon, M. J., Lanz, C., Nolte, A., Motte, P., et al. (2008). Evolution of metal hyperaccumulation required cis-regulatory changes and triplication of HMA4. *Nature* 453, 391–395. doi: 10.1038/nature06877

Hellemans, J., Mortier, G., De Paepe, A., Speleman, F., and Vandesompele, J. (2007). qBase relative quantification framework and software for management and automated analysis of real-time quantitative PCR data. *Genome Biol.* 8:R19. doi: 10.1186/gb-2007-8-2-r19

Hussain, D., Haydon, M. J., Wang, Y., Wong, E., Sherson, S. M., Young, J., et al. (2004). P-type ATPase heavy metal transporters with roles in essential zinc homeostasis in *Arabidopsis*. *Plant Cell* 16, 1327–1339. doi: 10.1105/tpc.020487

Inaba, S., Kurata, R., Kobayashi, M., Yamagishi, Y., Mori, I., Ogata, Y., et al. (2015). Identification of putative target genes of bZIP19, a transcription factor essential for *Arabidopsis* adaptation to Zn deficiency in roots. *Plant J.* 84, 323–334. doi: 10.1111/tpj.12996

Kocyła, A., Pomorski, A., and Krêżel, A. (2015). Molar absorption coefficients and stability constants of metal complexes of 4-(2-pyridylazo)resorcinol (PAR): revisiting common chelating probe for the study of metalloproteins. *J. Inorg. Biochem.* 152, 82–92. doi: 10.1016/j.jinorgbio.2015.08.024

Krämer, U. (2010). Metal hyperaccumulation in plants. *Annu. Rev. Plant Biol.* 61, 517–534. doi: 10.1146/annurev-arplant-042809-112156

Lane, T. W., and Morel, F. M. (2000). A biological function for cadmium in marine diatoms. *Proc. Natl. Acad. Sci. U.S.A.* 97, 4627–4631. doi: 10.1073/pnas.090091397

Laurent, C., Lekeux, G., Ukuwela, A. A., Xiao, Z., Charlier, J.-B., Bosman, B., et al. (2016). Metal binding to the N-terminal cytoplasmic domain of the PIB ATPase HMA4 is required for metal transport in *Arabidopsis*. *Plant Mol. Biol.* 90, 453–466. doi: 10.1007/s11103-016-0429-z

Lekeux, G., Crowet, J.-M., Nouet, C., Joris, M., Jadoul, A., Bosman, B., et al. (2019). Homology modeling and *in vivo* functional characterization of the zinc permeation pathway in a heavy metal P-type ATPase. *J. Exp. Bot.* 70, 329–341. doi: 10.1093/jxb/ery353

Lekeux, G., Laurent, C., Joris, M., Jadoul, A., Jiang, D., Bosman, B., et al. (2018). di-Cysteine motifs in the C-terminus of plant HMA4 proteins confer nanomolar affinity for zinc and are essential for HMA4 function *in vivo*. *J. Exp. Bot.* 69, 5547–5560. doi: 10.1093/jxb/ery311

Liedschulte, V., Laparra, H., Battey, J. N. D., Schwaar, J. D., Broye, H., Mark, R., et al. (2017). Impairing both HMA4 homeologs is required for cadmium reduction in tobacco. *Plant. Cell Environ.* 40, 364–377. doi: 10.1111/pce.12870

Lin, Y.-F., Liang, H.-M., Yang, S.-Y., Boch, A., Clemens, S., Chen, C.-C., et al. (2009). *Arabidopsis* IRT3 is a zinc-regulated and plasma membrane localized zinc/iron transporter. *New Phytol.* 182, 392–404. doi: 10.1111/j.1469-8137.2009.02766.x

Merlot, S., de la Torre, V. S. G., and Hanikenne, M. (2018). "Physiology and molecular biology of trace element hyperaccumulation," in *Agromining: Farming for Metals*, eds A. Van der Ent, G. Echevarria, A. J. M. Baker, and J. L. Morel (Cham: Springer International Publishing), 93–116.

Mills, R. F., Krijger, G. C., Baccarini, P. J., Hall, J. L., and Williams, L. E. (2003). Functional expression of AtHMA4, a P1B-type ATPase of the Zn/Co/Cd/Pb subclass. *Plant J.* 35, 164–176. doi: 10.1046/j.1365-313x.2003.01790.x

Nouet, C., Charlier, J.-B., Carnol, M., Bosman, B., Farnir, F., Motte, P., et al. (2015). Functional analysis of the three HMA4 copies of the metal hyperaccumulator *Arabidopsis halleri*. *J. Exp. Bot.* 66, 5783–5795. doi: 10.1093/jxb/erv280

Nriagu, J. O. (1988). A silent epidemic of environmental metal poisoning? *Environ. Pollut.* 50, 139–161. doi: 10.1016/0269-7491(88)90189-3

Pottier, M., Oomen, R., Picco, C., Giraudat, J., Scholz-Starke, J., Richaud, P., et al. (2015). Identification of mutations allowing Natural Resistance associated macrophage proteins (NRAMP) to discriminate against cadmium. *Plant J.* 83, 625–637. doi: 10.1111/tpj.12914

Rogers, E. E., Eide, D. J., and Guerinot, M. L. (2000). Altered selectivity in an *Arabidopsis* metal transporter. *Proc. Natl. Acad. Sci. U.S.A.* 97, 12356–12360. doi: 10.1073/pnas.210214197

Rosenzweig, A. C., and Argüello, J. M. (2012). Toward a molecular understanding of metal transport by P1B-Type ATPases. *Curr. Top. Membr.* 69, 113–136. doi: 10.1016/B978-0-12-394390-3.00005-7

Ruijter, J. M., Ramakers, C., Hoogaars, W. M. H., Karlen, Y., Bakker, O., van den Hoff, M. J. B., et al. (2009). Amplification efficiency: linking baseline and bias in the analysis of quantitative PCR data. *Nucleic Acids Res.* 37:e45. doi: 10.1093/nar/gkp045

Satarug, S., Baker, J. R., Urbenjapol, S., Haswell-Elkins, M., Reilly, P. E. B., Williams, D. J., et al. (2003). A global perspective on cadmium pollution and toxicity in non-occupationally exposed population. *Toxicol. Lett.* 137, 65–83. doi: 10.1016/S0378-4274(02)00381-8

Satarug, S., Garrett, S. H., Sens, M. A., and Sens, D. A. (2010). Cadmium, environmental exposure, and health outcomes. *Environ. Health Perspect.* 118, 182–190. doi: 10.1289/ehp.0901234

Schvartzman, M. S., Corso, M., Fataftah, N., Scheepers, M., Nouet, C., Bosman, B., et al. (2018). Adaptation to high zinc depends on distinct mechanisms in metallicolous populations of *Arabidopsis* halleri. *New Phytol.* 218, 269–282. doi: 10.1111/nph.14949

Smith, A. T., Smith, K. P., and Rosenzweig, A. C. (2014). Diversity of the metal-transporting P1B-type ATPases. *J. Biol. Inorg. Chem.* 19, 947–960. doi: 10.1007/s00775-014-1129-2

Talke, I. N., Hanikenne, M., and Krämer, U. (2006). Zinc-dependent global transcriptional control, transcriptional deregulation, and higher gene copy number for genes in metal homeostasis of the hyperaccumulator *Arabidopsis halleri*. *Plant Physiol.* 142, 148–167. doi: 10.1104/pp.105.076232

Thomine, S., and Vert, G. (2013). Iron transport in plants: better be safe than sorry. *Curr. Opin. Plant Biol.* 16, 322–327. doi: 10.1016/j.pbi.2013.01.003

Tocquin, P., Corbesier, L., Havelange, A., Pieltain, A., Kurtem, E., Bernier, G., et al. (2003). A novel high efficiency, low maintenance, hydroponic system for synchronous growth and flowering of *Arabidopsis thaliana*. *BMC Plant Biol.* 3:2. doi: 10.1186/1471-2229-3-2

Tóth, G., Hermann, T., Da Silva, M. R., and Montanarella, L. (2016). Heavy metals in agricultural soils of the European Union with implications for food safety. *Environ. Int.* 88, 299–309. doi: 10.1016/j.envint.2015.12.017

van de Mortel, J. E., Almar Villanueva, L., Schat, H., Kwekkeboom, J., Coughlan, S., Moerland, P. D., et al. (2006). Large expression differences in genes for iron and zinc homeostasis, stress response, and lignin biosynthesis distinguish roots of *Arabidopsis thaliana* and the related metal hyperaccumulator *Thlaspi caerulescens*. *Plant Physiol.* 142, 1127–1147. doi: 10.1104/pp.106.082073

Vandesompele, J., De Preter, K., Pattyn, F., Poppe, B., Van Roy, N., De Paepe, A., et al. (2002). Accurate normalization of real-time quantitative RT-PCR data by geometric averaging of multiple internal control genes. *Genome Biol.* 3:research0034.1. doi: 10.1186/gb-2002-3-7-research0034

Verret, F., Gravot, A., Auroy, P., Leonhardt, N., David, P., Nussaume, L., et al. (2004). Overexpression of AtHMA4 enhances root-to-shoot translocation of zinc and cadmium and plant metal tolerance. *FEBS Lett.* 576, 306–312. doi: 10.1016/j.febslet.2004.09.023

Verret, F., Gravot, A., Auroy, P., Preveral, S., Forestier, C., Vavasseur, A., et al. (2005). Heavy metal transport by AtHMA4 involves the N-terminal degenerated metal binding domain and the C-terminal His11 stretch. *FEBS Lett.* 579, 1515–1522. doi: 10.1016/j.febslet.2005.01.065

Vert, G., Grotz, N., Dédaldéchamp, F., Gaymard, F., Guerinot, M. L., Briat, J.-F., et al. (2002). IRT1, an *Arabidopsis* transporter essential for iron uptake from the soil and for plant growth. *Plant Cell* 14, 1223–1233. doi: 10.1105/tpc.001388

Wang, K., Sitsel, O., Meloni, G., Autzen, H. E., Andersson, M., Klymchuk, T., et al. (2014). Structure and mechanism of Zn2+-transporting P-type ATPases. *Nature* 514, 518–522. doi: 10.1038/nature13618

Williams, L. E., and Mills, R. F. (2005). P1B-ATPases; an ancient family of transition metal pumps with diverse functions in plants. *Trends Plant Sci.* 10, 491–502. doi: 10.1016/j.tplants.2005.08.008

Wong, C. K., and Cobbett, C. S. (2009). HMA P-type ATPases are the major mechanism for root-to-shoot Cd translocation in *Arabidopsis thaliana*. *New Phytol.* 181, 71–78. doi: 10.1111/j.1469-8137.2008.02638.x

Yang, T. J. W., Lin, W.-D., and Schmidt, W. (2010). Transcriptional profiling of the *Arabidopsis* iron deficiency response reveals conserved transition metal homeostasis networks. *Plant Physiol.* 152, 2130–2141. doi: 10.1104/pp.109.152728

Zimmermann, M., Clarke, O., Gulbis, J. M., Keizer, D. W., Jarvis, R. S., Cobbett, C. S., et al. (2009). Metal binding affinities of *Arabidopsis* zinc and copper transporters: selectivities match the relative, but not the absolute, affinities of their amino-terminal domains. *Biochemistry* 48, 11640–11654. doi: 10.1021/bi901573b

Conflict of Interest: The authors declare that the research was conducted in the absence of any commercial or financial relationships that could be construed as a potential conflict of interest.

frontiers in Plant Science

ORIGINAL RESEARCH
published: 27 May 2020
doi: 10.3389/fpls.2020.00662

Structure, Function, Regulation and Phylogenetic Relationship of ZIP Family Transporters of Plants

*T.P. Ajeesh Krishna[1], T. Maharajan[1], G. Victor Roch[1], Savarimuthu Ignacimuthu[2] and Stanislaus Antony Ceasar[1]**

[1] Division of Plant Biotechnology, Entomology Research Institute, Loyola College, University of Madras, Chennai, India,
[2] Xavier Research Foundation, St. Xavier's College, Palayamkottai, India

Zinc (Zn) is an essential micronutrient for plants and humans. Nearly 50% of the agriculture soils of world are Zn-deficient. The low availability of Zn reduces the yield and quality of the crops. The zinc-regulated, iron-regulated transporter-like proteins (ZIP) family and iron-regulated transporters (IRTs) are involved in cellular uptake of Zn, its intracellular trafficking and detoxification in plants. In addition to Zn, ZIP family transporters also transport other divalent metal cations (such as Cd^{2+}, Fe^{2+}, and Cu^{2+}). ZIP transporters play a crucial role in biofortification of grains with Zn. Only a very limited information is available on structural features and mechanism of Zn transport of plant ZIP family transporters. In this article, we present a detailed account on structure, function, regulations and phylogenetic relationships of plant ZIP transporters. We give an insight to structure of plant ZIPs through homology modeling and multiple sequence alignment with *Bordetella bronchiseptica* ZIP (BbZIP) protein whose crystal structure has been solved recently. We also provide details on ZIP transporter genes identified and characterized in rice and other plants till date. Functional characterization of plant ZIP transporters will help for the better crop yield and human health in future.

Keywords: ZIP transporters, homology modeling, transcription factor, functional characterization, genetic modification

OPEN ACCESS

Edited by:
Louis Grillet,
Academia Sinica, Taiwan

Reviewed by:
Khurram Bashir,
Riken, Japan
Grmay Hailu Lilay,
University of Copenhagen, Denmark
Andrea Valeria Ochoa Tufino,
University of the Armed Forces (ESPE), Ecuador

****Correspondence:***
Stanislaus Antony Ceasar
antony_sm2003@yahoo.co.in

Specialty section:
This article was submitted to Plant Traffic and Transport, a section of the journal Frontiers in Plant Science

Received: *14 February 2020*
Accepted: *29 April 2020*
Published: *27 May 2020*

Citation:
Ajeesh Krishna TP, Maharajan T, Victor Roch G, Ignacimuthu S and Antony Ceasar S (2020) Structure, Function, Regulation and Phylogenetic Relationship of ZIP Family Transporters of Plants. Front. Plant Sci. 11:662. doi: 10.3389/fpls.2020.00662

INTRODUCTION

In agriculture, the low availability of nutrients has reduced the crop production. The optimal supply of micro-nutrients in soil solutions is vital for normal agriculture production. Zinc (Zn) is one of the most essential micronutrients; it is irreplaceable for plant growth and metabolism (Marschner, 1995, 2011). Both deficient and excess Zn has impaired the physiological and biochemical process of the plant (Cakmak, 2000; Marichali et al., 2014). Zn deficiency is one of the most serious problems worldwide reducing quality of crops (Ruel and Bouis, 1998; Sadeghzadeh, 2013), apart from yield loss and the reduced Zn content in grains (Krithika and Balachandar, 2016). Soil Zn deficiency and human Zn deficiency are often closely associated (Cakmak, 2008). Zn deficiency has been a major cause of death for children in many countries (Black et al., 2008). Regmi et al. (2010) reported that the lack of Zn was a major nutritional problem in humans; more than 3 billion world population were affected by various health problems due to low supply of Zn in their food. For example, approximately 50% of the paddy field is Zn deficient and rice grown on these soils usually produces very less yield with poor nutritional quality (Krithika and Balachandar, 2016). It was estimated that

the Zn sufficient rice plant had 40 mg/kg of Zn in its grains, whereas under Zn deficient condition it showed only 10 mg/kg of Zn (Wissuwa et al., 2008). All over the world, 50% of agriculture soils are Zn deficient (FAO, 2000). Zn deficiency was observed in a wide range of soil types such as high pH calcareous soils, sandy soils, and high phosphorus (P) fertilized soils (Marschner, 1995). In 1972, the United States considered Zn deficiency as the most common micronutrient deficiency in crops (Lindsay, 1972). Zn deficiency is one of the major limiting factors affecting crop production badly. So, improving crop varieties with Zn efficiency is helpful to overcome the Zn deficiency problem.

To overcome low Zn availability, plants have evolved a complex array of tightly controlled adaptive mechanisms. The Zinc-regulated, Iron-regulated transporter-like Protein (ZIP) family has been identified and characterized in prokaryotes, eukaryotes, and archaeotes and has been validated to be involved in metal uptake and transport including Zn^{2+} (Grotz and Guerinot, 2006; Kavitha et al., 2015). The presence of ZIP transporters in such a diverse organism indicates their pivotal role in Zn homeostasis. The ZIP family has a major role in Zn transport and metal homeostasis in plants. Besides Zn^{2+}, ZIP transporters are reported to be involved in the transport of other transition metal cations such as manganese (Mn^{2+}), iron (Fe^{2+}), cadmium (Cd^{2+}), cobalt (Co^{2+}), copper (Cu^{2+}), and nickel (Ni^{2+}) (Pedas and Husted, 2009). The iron-regulated transporters (IRTs) are the major Fe transporters; they are members of the ZIP family transporters (Eide et al., 1996; Conte and Walker, 2011). The AtIRT1 is identified as the key Fe^{2+} transporter in *Arabidopsis*. The AtIRT1 (Eide et al., 1996), AtIRT2 (Vert et al., 2001), and AtIRT3 (Lin et al., 2009) transporters are seem to be functioning for Fe^{2+} uptake and transport in *Arabidopsis*. IRTs of *Arabidopsis* has the ability to transport several divalent metal ions such as Zn^{2+}, Mn^{2+}, and Cd^{2+} (Eide et al., 1996; Vert et al., 2001; Chiang et al., 2006; Lee and An, 2009; Lin et al., 2009). The IRTs genes are found to be expressing under different metal stress conditions with increased expression levels under Fe deficiency. ZIP transporters balance the uptake, utilization, and storage of Zn^{2+} under Zn stress condition (Ramesh et al., 2003; Palmgren et al., 2008). The ZIP transporters are also located in various cell organelles and they are actively involved in Zn homeostasis and plant's adaptation to low and high Zn soils (Tiong et al., 2015). In crops, most of the ZIP transporters are poorly understood with only ZIPs of a few plants have been functionally characterized (Kavitha et al., 2015). The detailed analysis of the structure of the plant ZIP transporter is still lacking. Recently, the crystal structure of the ZIP protein was deduced from a bacterium *Bordetella bronchiseptica* and its metal transport mechanism was also predicted (Zhang et al., 2017). So, in this article, we present the details on the structure, mechanism and phylogenetic relationships of plant ZIP transporters. We provided insight into the structure of plant ZIPs through homology modeling and multiple sequence alignment using *B. bronchiseptica* ZIP (BbZIP) protein as a template. These findings would be a valuable theoretical knowledge for future studies on Zn transporters in crops. We also present details on ZIP transporter genes identified and characterized till date in various plants.

ROLE OF Zn IN CROPS

Zinc is one of the eight essential micronutrients in plants (Hänsch and Mendel, 2009). In crops, Zn deficiency was first identified in rice on calcareous soils in India (Nene, 1966; Yoshida and Tanaka, 1969). Plant cells require optimum levels of Zn for normal physiological functions. Zn is involved in the maintenance of the structural and functional integrity of biological membrane and facilitation of protein synthesis, gene expression and regulation and defense against disease (Cakmak, 2000; Andreini et al., 2006; Sadeghzadeh, 2013). Also, it is involved as a structural, catalytic, and intracellular and intercellular signaling component and Zn is the only metal required for the activity of all six classes of the enzymes (Sadeghzadeh, 2013). Especially Zn is essential for the activity of metallo-enzymes that are involved in protein and nucleic acid metabolism (Eide, 2006).

Zinc is needed by a small quantity (0.5–2 μM) from the soil for the normal plant function (Krishna et al., 2017), but yet crucial for many physiological and metabolic pathways (Chen et al., 2008). In rice, 1.5 μM Zn is an optimum level for growth on agar nutrient solution (Impa et al., 2013). Zn content less than 15–20 μg per gram of dry leaf tissues of the plant is a sign of Zn deficiency (Mitra, 2015). Zn is actively involved in specific reactions of metabolic pathways, such as tryptophan biosynthesis, which in turn is the precursor of indole-3-acetic acid (IAA) and other phytohormones. In plants, Zn^{2+} ions are directly involved in the synthesis of tryptophan and auxin (Horak and Trčka, 1976; Marschner, 2011). Zn deficiency decreases the level of phytohormones such as auxin, abscisic acid, gibberellins, and cytokinin's (Kumar et al., 2016). It significantly affects the plant cell division, cell enlargement, and differentiation (Skoog, 1940; Tsui, 1948). Cakmak et al. (1989) observed that under Zn deficient condition, the level of IAA in the shoot tips and young leaves of bean was reduced to 50% of that in Zn sufficient condition. Zn deficiency reduces the plant growth, yield, and quality in crops such as rice (Chen et al., 2008), mungbean (Samreen et al., 2017), and maize (Wang and Jin, 2005). Zn deficiency decreases the activity of key photosynthetic enzymes, namely carbonic anhydrase, (Brown et al., 1993) which is crucial for crop production (Ali et al., 2008; Mousavi, 2011; Xi-wen et al., 2011). The Zn deficiency induces male sterility in maize (Sharma et al., 1987) and wheat (Sharma et al., 1979). Ekiz et al. (1998) noticed that the crops such as wheat, oat, barley, and triticale show significant decrease in growth and grain yield under Zn-deficient conditions. Zn is a not replaceable micro-nutrient for crops. Zn deficiency is a common problem in all parts of the globe. Therefore, much more research is necessary for improving Zn use efficiency in crops for growth and higher yields under Zn deficient soils.

ROLE OF ZIP TRANSPORTERS IN Zn TRANSPORT

In plants, Zn is acquired and transported predominantly as Zn^{2+} (divalent). Zn ions can also be bound with root exudates like

malate, citrate, oxalate and other low molecular weight organic acids which aided to move toward the root surface area (Suzuki et al., 2006). The charged Zn^{2+} ion do not freely diffuse across the lipid bilayer membranes (Eide, 2005). Zn first enters the root cell wall's free space by a diffusion process from the soil solutions (Hacisalihoglu and Kochian, 2003). Transport of Zn^{2+} into the cortex takes place via symplastic or apoplastic pathway (Kumar et al., 2016). The Zn transporter proteins are required to carry Zn^{2+} into the cells and transport out of intracellular compartments. They include a low-affinity (K_m = 2–5 μM) and high-affinity (K_m = 0.6–2 nM) membrane transporter systems (Hacisalihoglu et al., 2001; Kumar et al., 2016). The high-affinity transporter system is dominantly active under low Zn soil (Hacisalihoglu et al., 2001). The ZIP and IRT transporters help to carry Zn^{2+} ions across cellular membranes into the cytoplasm (Eide et al., 1996; Eide, 2005; Krishna et al., 2017). After that Zn^{2+} ions pass the casparian band, endodermis and xylem parenchyma cells which subsequently loaded into the xylem. The heavy metal ATPase 2 (HMA2) and HMA4 transporters of P-type ATPase family are involved in xylem loading of Zn from the xylem parenchymatous cells (Hussain et al., 2004; Hanikenne et al., 2008). The ZIP family transporters are mainly involved in up take, transport and distribution of Zn in the whole plant. The presence of ZIP transporters in a diverse organism indicates their importance in Zn transport and homeostasis. Therefore, understanding of their expression levels, localization, and function in crops is essential. The functional genomics and biotechnological approaches can be used to develop Zn deficiency tolerant crops in the future. It assists in improving the quality and quantity of crops especially enrichment of Zn content in grains and to overcome Zn deficiency problems worldwide. The ZIP transporter families can be used for genetic modification in crops to improve the fortification of Zn.

STRUCTURE OF THE ZIP TRANSPORTER

Only a very limited information is available on structural features and mechanism of Zn transport of plant ZIP family transporters. Plant ZIP family transporters are predicted to have 6–9 transmembrane (TM) domains (α-helices) with 8 being the most prevalent form (Guerinot, 2000). The molecular weight of the Zn transporters ranged from 33.1 to 51.4 kDa and protein sequence ranged from 322 to 478 amino acids (Vatansever et al., 2016). Understanding the mechanism of ZIP transporters requires their high-resolution crystal structures. The crystal structure of the plant ZIP protein is not yet available. However, recently, a high-resolution crystal structure of prokaryotic ZIP protein was deduced from a bacterium *B. bronchiseptica* and its metal (Cd^{2+} and Zn^{2+}) transport mechanism was also predicted (Zhang et al., 2017). The crystal structure of BbZIP transporter protein showed eight TM domains (TM1–TM8). The structure of BbZIP was deduced with an inward-open confirmation and occluded at the extracellular side with a binuclear metal center located in the center. The eight TMs formed a closely associated α-helix bundle. The first three TMs (TM1–TM3) can be superimposed on the last three TMs (TM6–TM8) by rotating 180°, and TM4 and TM5 are symmetrically related and sandwiched by the two 3 TM repeats (Zhang et al., 2017). The binuclear metal center is formed by TM4 and TM5 with several conserved amino acid residues (His177, Asn178, Pro180, Glu181, and Gly182) and metal-binding motifs (Gln207, Asp/Asn208, Pro210, Glu211, and Gly212). The structure of the BbZIP showed four Cd^{2+} and seven Zn^{2+} metal-binding sites (Zhang et al., 2017). The topology of BbZIP shows that both the N and the C termini are exposed to the extracellular space and the putative metal transport pathway found at the extracellular side is blocked by hydrophobic residues of the TM2 (Met99 and Ala102), TM5 (Leu200 and Iso204), and TM7 (Met269) (Zhang et al., 2017). The invariant Ser106 on TM2 is situated on the bottom of the shallow and negatively charged entrance cavity, it is important for guiding metals into the transport pathway. Two invariant metal-chelating residues Asp113 and Asp305 present in the entrance cavity have been predicted to be crucial for recruiting metal substrates. The BbZIP structure shows multiple conserved metal-binding sites near the metal exit cavity, indicating that these constitute a route of metal release to the cytoplasm. The bound metal released into the cytoplasm through a chain of metal-chelating residues such as His177, Glu276, His275, Pro180, Pro210, and Asp144 (Zhang et al., 2017). The Zn^{2+} binding is penta coordinated by Glu181, Gln207, and Glu211 and two molecules of water (Zhang et al., 2017). This structure provides a model to analyze the plant ZIP transporters. So we have used this as a template to model and analyze the residues in plant ZIP transporters.

Comparison of Metal Binding Residues in BbZIP and Plant ZIPs

We have analyzed the BbZIP protein sequence with plant ZIP transporters such as *Arabidopsis* (12 ZIPs), rice (12 ZIPs), and maize (10 ZIPs) through a ClustalW alignment (Tamura et al., 2013). The functional residues of the BbZIP and their corresponding plant ZIP residues are presented in **Figure 1**. We have also included the complete alignment file (**Supplementary Figure S1**). Except a few, most of the functional residues of *Arabidopsis*, rice and maize ZIP protein sequences are not conserved/homologous with BbZIP. But it is interesting to see that all the plant ZIP protein sequences (expect AtZIP10 and OsZIP16) have conserved His117 residue found in BbZIP (**Figure 1**). In AtZIP10 (Gln222) and OsZIP13 (Gln140) BbZIP's His177 is replaced by Gln. Gly182 of BbZIP is conserved in all plant ZIPs (**Figure 1**). The His177 and Gly182 are involved in the metal release from the metal-binding site of the BbZIP. Similarly, Glu211 and Gly212 are metal-binding residues in BbZIP. Glu211 of BbZIP is conserved in all plant ZIP proteins expect for AtZIP2 (Ala243), AtZIP11 (Ala215), OsZIP1 (Ala242), and OsZIP2 (Ala247) where Glu is replaced by Ala. Similarly, expect AtZIP2 (Ala224), AtZIP11 (Ala216), OsZIP1 (Ala243), and OsZIP2 (Ala248), other plants ZIP transporter proteins possess conserved Gly212 of BbZIP. Another interesting observation is that metal-binding site residues such as Asn178, Pro180, and Pro210 are conserved only with OsZIP13,

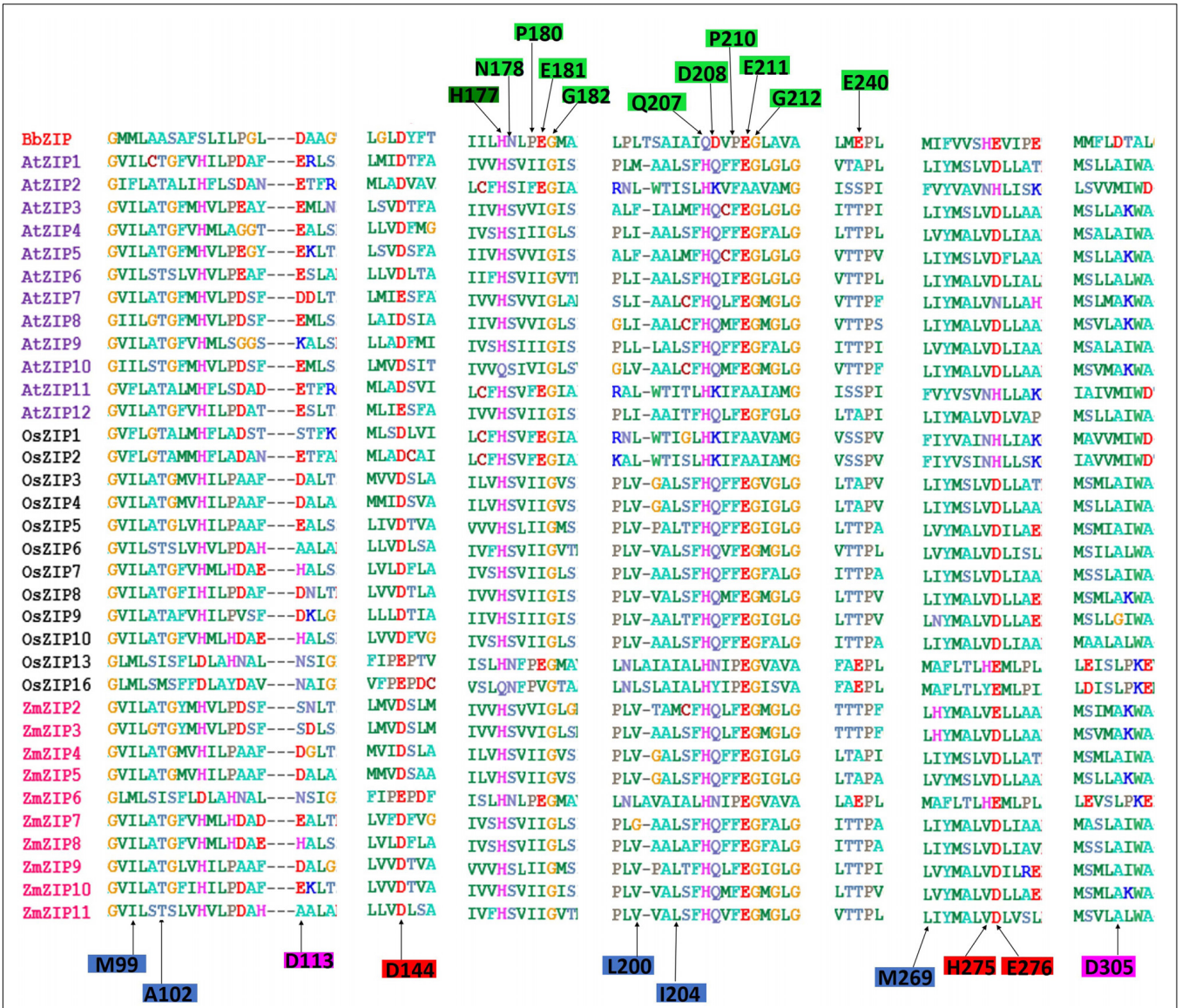

FIGURE 1 | Multiple sequence alignment of *Bordetella bronchiseptica* ZIP (BbZIP), *Arabidopsis* (AtZIP), rice (OsZIP), and maize (ZmZIP) transporters. The protein sequences were aligned by ClustalW alignment using molecular evolutionary genetics analysis, V 6.0 (MEGA6) tool (Tamura et al., 2013). The residues (BbZIP) involved in Cd/Zn binding and transport are highlighted in green and dark green. The His177 highlighted in dark green is involved in both metal recruiting and cytoplasmic transport of metal. The hydrophobic residues involved in blocking of metals at extracellular surface are highlighted in light blue. Metal recruiting residues are highlighted in pink. The residues involved in metal release into the cytoplasm are highlighted in red.

OsZIP16, and ZmZIP6 of plants (**Figure 1**). Metal binding site residues Gln207 and Asp208 and metal-chelating residue Asp305 are not conserved with any other plant ZIPs. The Gln207 is replaced by His residue in all plant ZIPs (**Figure 1**). An invariable Ser106 is an important residue for guiding metals into the transport pathway of the BbZIP. In plants, Ser is completely replaced by His or Asp residue with His being a dominant residue. Overall, the metal binding and transport residues of OsZIP13, OsZIP16, and ZmZIP6 are more conserved with BbZIP compared to other plant ZIPs. These variations indicated that plant ZIP transporters may have partially overlapping but distinct metal transport mechanism compared to BbZIP as some of the residues involved in metal binding and transport are not conserved in plant ZIPs. We have also done homology modeling of plant ZIPs whose details are discussed below.

Homology Modeling of Plant ZIP Transporters

In order to gain more insights to the structure of plant ZIP transporters, we have modeled some of the plant ZIP transporters by homology modeling using BbZIP (PDB Id: 5TSA) as a template with Zn^{2+} as a ligand. The models

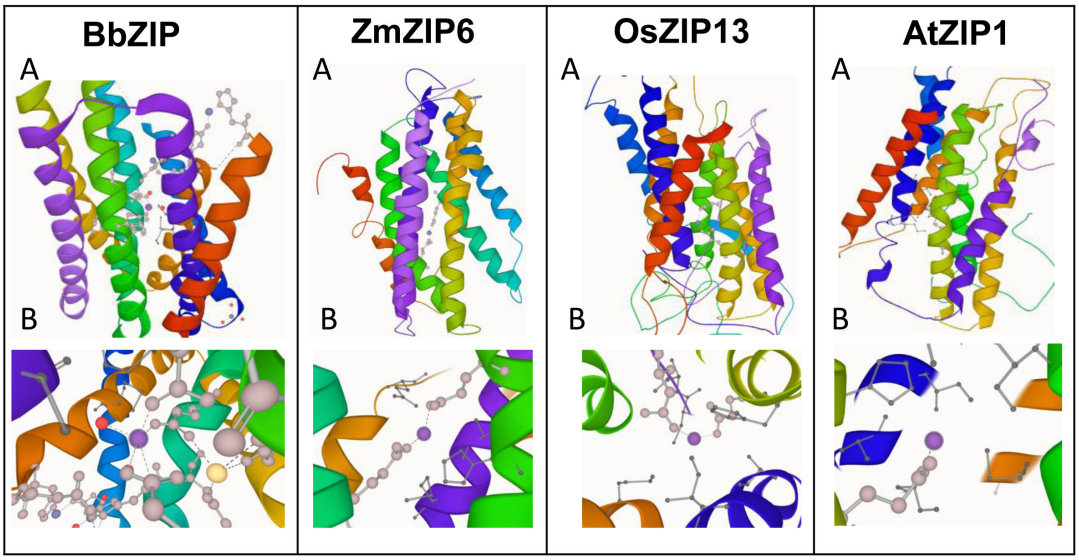

FIGURE 2 | Homology modeling of plant ZIP transporters using *Bordetella bronchiseptica* ZIP (BbZIP) (PDB ID: 5TSA) as a template. The BbZIP structure was visualized using LiteMol viewer (https://www.litemol.org/Viewer/). Both whole model **(A)** and its Zn^{2+} binding site **(B)** is shown for each ZIP. The protein sequences of plant ZIPs were obtained from phytozome website (https://phytozome.jgi.doe.gov/pz/portal.html). The homology models of the plant ZIP proteins were generated using Modeler v9.22 (Eswar et al., 2007), which created 100 models for each target protein. The models were then ranked based on their modeler objective function value. The five best models were analyzed using MolProbity (http://molprobity.biochem.duke.edu/), an online tool. Ramachandran plots were generated for these five models and finally the best model was chosen based on the% residues in the favored and allowed regions and the number of outliers. The models were then visualized by LiteMol viewer.

were then compared with the structure of BbZIP. In BbZIP, Zn^{2+} is coordinated by Glu181, Gln207, and Glu211 and water molecular at metal binding site as per our modeling (**Figure 2**; Zhang et al., 2017). The Zn^{2+} binding site is also covered by Glu276, His177, Met269, and Met99 which are involved in Zn transport (**Figure 2**). However, the plant ZIP transporters showed greater variation at Zn^{2+} binding site except for Glu181/211 (equivalent to BbZIP) based on the homology models (**Figure 2** and **Table 1**). Zn^{2+} binding is coordinated by Glu141 and Glu170 in ZmZIP6, Glu252 and Asp190 in ZmZIP11, Glu173 and Glu240 in OsZIP16, Glu253 and Asn30 in OsZIP13. Even Zn^{2+} is co-ordinated only by a single Glu residue in AtZIP1 and AtZIP2 and not co-ordinated by any residues in AtZIP8 (**Figure 2** and **Table 1**). The residues surrounding the Zn^{2+} binding site include Glu276, Met269, His177, and Met99 in BbZIP. These residues are partially conserved in some plant ZIPs and not at all conserved in other ZIPs modeled (**Table 1**). For e.g., His177 is conserved in OsZIP6 (His169) and ZmZIP6 (His166); shifting in the positioning of His is seen in AtZIP1 (His238), AtZIP2 (His239), OsZIP13 (His249), and ZmZIP11 (His278) as indicated in the alignment above (**Figures 1**, **2** and **Table 1**). Similar variation was seen for residues involved in Zn transport in the plant ZIPs analyzed (**Table 1**). It might be due to partially overlapping but distinct mechanism for binding and transport of Zn^{2+} by plant ZIPs which is also reflected in alignment (**Supplementary Figure S1**). This requires further studies to confirm the roles of functional residues especially by site directed mutagenesis with yeast mutants to gain more knowledge on residues involved in Zn^{2+} binding and transport in plant ZIPs. Also, the high-resolution crystal structure of plant ZIP is needed for understanding any specific Zn^{2+} transport mechanism in plants.

Phylogenetic Analysis of Plant ZIP Proteins

The phylogenetic tree was constructed from 113 ZIP protein sequences collected from 14 plant species. These include eight monocot plants and six dicot plants (**Supplementary File S1**). The phylogenetic tree consisted of eight major clusters (MCs) (MC1–MC8) and sub-divided into 1–2 sub-clusters (SCs) and each SC was again divided into small clusters (**Figure 3**). More ZIP transporters are clustered in MC-8. The MC-8 had 21 ZIP transporters and it is followed by MC-5 (20 ZIPs) and MC-2 (18 ZIPs). The ZIP proteins of *Brassica rapa* (BrZIP1), *Cucumis sativus* (CsZIP1), *Medicago truncatula* (MtZIP1), and *Glycine max* (GmZIP1) were clustered with AtZIP1; BrZIP3 is closely clustered with AtZIP3 (**Figure 3**). The AtZIP1 and AtZIP3 proteins are clustered closely which are characterized as low-affinity transporters (Grotz et al., 1998). In *Arabidopsis*, *AtZIP1*, and *AtZIP3* are highly expressed in roots in response to Zn deficiency condition suggesting their role in Zn uptake from soil (Grotz et al., 1998). OsZIP1 and OsZIP3 are characterized as low-affinity Zn transporters in rice plants (Ramesh et al., 2003) and these are placed distinctly in the phylogenetic tree. The OsZIP1 is clustered with monocot ZIP transporters such as TaZIP1, *Panicum hallii* ZIP1 (PhZIP1) and SbZIP1. The expression analysis showed the *OsZIP1* gene is induced in roots under Zn

TABLE 1 | Details on residues identified to be involved in Zn^{2+} transport through homology modeling using BbZIP as a template.

Name of the protein	UniProt Accession/Phytozome ID	Length (total amino acids)	Zn^{2+} coordinating residues	Zn^{2+} transporting residues
BbZIP	BB2405	309	Glu181; Glu211 Gln207	Glu276; Met 269 His177; Met 99
AtZIP1	O81123	355	Glu242	His238; Lys 89 Ile206; Met 312
AtZIP2	Q9LTH9	353	Glu216	His239; Leu77 Phe73
AtZIP8	Q8S3W4	347	–	Glu248; Asn251 Ile209; Ala247 Phe71
OsZIP13	LOC_Os07g12890 (Chen et al., 2008)	276	Asn30; Glu253	Ile59; Met321 His249; Ala85 Cys28
OsZIP16	LOC_Os08g01030 (Chen et al., 2008)	282	Glu173; Glu240	His169; Met48 Val144; Ala49
ZmZIP6	GRMZM2G050484_T01 (Mondal et al., 2013)	297	Glu141; Glu170	Glu237; Met51 His166; Ala47
ZmZIP11	GRMZM2G034551 (Mondal et al., 2013)	396	Glu282 Asp190	His278; Ile74 Lys198; Met159 Ala70

Name of the protein, its UniProt Id/Phytozome Id, length of the protein, residues involved in Zn^{2+} binding are listed for each protein.

starvation (Ramesh et al., 2003). Similarly, the OsZIP3 is closely clustered with HvZIP3, TaZIP3, BdZIP3, and SbZIP3. HvZIP3 was reported as a low-affinity transporter of barely (Pedas et al., 2009). Both *OsZIP3* and *HvZIP3* are highly expressed in both shoot and root under Zn deficient condition (Chen et al., 2008). AtZIP2 is a high-affinity transporter in *Arabidopsis* (Grotz et al., 1998), it is closely clustered with BrZIP2, SlZIP2 MtZIP2, TaZIP1, OsZIP1, PhZIP1, and SbZIP1 proteins. It is interesting to see that both low-affinity (OsZIP1) and high-affinity (AtZIP2) ZIPs are closely clustered. The monocot and dicot plant ZIPs are clustered in separate clusters. ZIP family member are mostly clustered together as per their numbers (**Figure 3**), for e.g., ZIP1s of *Arabidopsis*, mustard, barrel clover, soybean and sweet orange are closely clustered. The identification and characterization of the ZIP gene family are still lacking for many crops. More molecular and functional genomic studies will aid for the characterization of ZIP transporter in other plants in future.

REGULATION OF ZIP TRANSPORTERS IN PLANTS

All living organisms need to maintain optimum concentrations of nutrients including Zn to sustain cellular functions (Shaul et al., 1999). Plants possess the homeostatic networks to maintain Zn levels in a narrow concentration to avoid either deficiency or toxicity. Zn homeostasis needs a complex network of cellular functions such as Zn uptake, accumulation, trafficking, sequestration, remobilization, and detoxification (Clemens, 2001; Krishna et al., 2017). ZIP transporters are regulated to provide a suitable quantity of Zn into all cell types and at all stages of development (Clemens, 2001). The Zn homeostasis equilibrium was considered for external and internal requirements of Zn (Claus and Chavarría-Krauser, 2012). Unfortunately, very little information is available on the regulation of plant ZIP transporters and mechanism of Zn homeostasis. Transport of divalent metal ions like Zn^{2+} by different transporters may pose some difficulty for high resolution studies to understand the role of plant ZIPs in Zn homeostasis. Expression levels of genes are increased for some ZIP transporters under Zn deficiency to facilitate the higher uptake of Zn from the soil. For e.g., in barley, *HvZIP3*, *HvZIP5*, and *HvZIP8* genes are highly induced in roots and are involved in Zn uptake under Zn deficient condition (Pedas et al., 2009).

Till date plant's sensing and transferring the signal of Zn deficiency remains poorly understood. However, based on the available data, some transcription factors (TFs) are found to be essential for regulation of target genes and maintaining Zn homeostasis. Two TFs identified in model plant *Arabidopsis* are shown to be crucial in the adaptation response to Zn deficiency. The basic-region leucine zipper (bZIP) is a TF involved in the regulation of many physiological processes including abiotic and biotic stress responses (Corrêa et al., 2008). These TFs belong to the F group of bZIP and showed histidine-rich motifs at the basic N-terminal region (Nijhawan et al., 2008; Assunção et al., 2010). bZIP TFs are also involved in the up-regulation of ZIP transporters in *Arabidopsis* during Zn deficiency (Assunção et al., 2013). The TFs bZIP19 and bZIP23 are considered to be the essential regulators of candidate genes including ZIPs under Zn deficiency. In plants, bZIP19 and bZIP23 proteins exist as monomers under Zn sufficient condition. The Zn deficiency leads to the activation (binding) of bZIP9 and bZIP23 (dimerization) which induces the expression of ZIP genes. The bZIP19 and bZIP23 dimer bind to 10bp Zn-deficiency responsive elements (RTGTCGACAY) present in the promoter region of target genes (Assunção et al., 2010; Lilay et al., 2018). The histidine-rich motif is conserved among group F bZIP TFs (Jakoby et al., 2002; Castro et al., 2017) and suggested to play key role as a Zn-sensor (Assunção et al., 2013; Henriques et al., 2017). Totally, 33 *bZIP19* genes are identified and characterized in cereal crops using *in silico* approaches and histidine-rich motifs are found in most of these bZIP19 TFs (Henriques et al., 2017).

In *Arabidopsis*, the TFs AtbZIP19 and AtbZIP23 induce the expression of *AtZIP4* gene under Zn deficiency (Assunção et al., 2010). These TFs are also involved in the activation (up-regulation) of a specific subset of genes such as *AtZIP1, AtZIP2, AtZIP4, AtZIP5, AtZIP9, AtZIP10*, and *AtZIP12* (Assunção et al., 2010; Inaba et al., 2015; Lilay et al., 2018). Similarly, three bZIP TFs such as bZIP1, bZIP2, and bZIP3 were identified in common bean which are similar to *Arabidopsis* TFs bZIP19, bZIP23, and bZIP24 (Astudillo et al., 2013). In whole-genome transcriptome analysis, 3 bZIP TFs (*PvbZIP1*, *PvbZIP2*, and *PvbZIP3*) are found to be expressed under Zn deficiency condition in common bean (Astudillo-Reyes et al., 2015). But

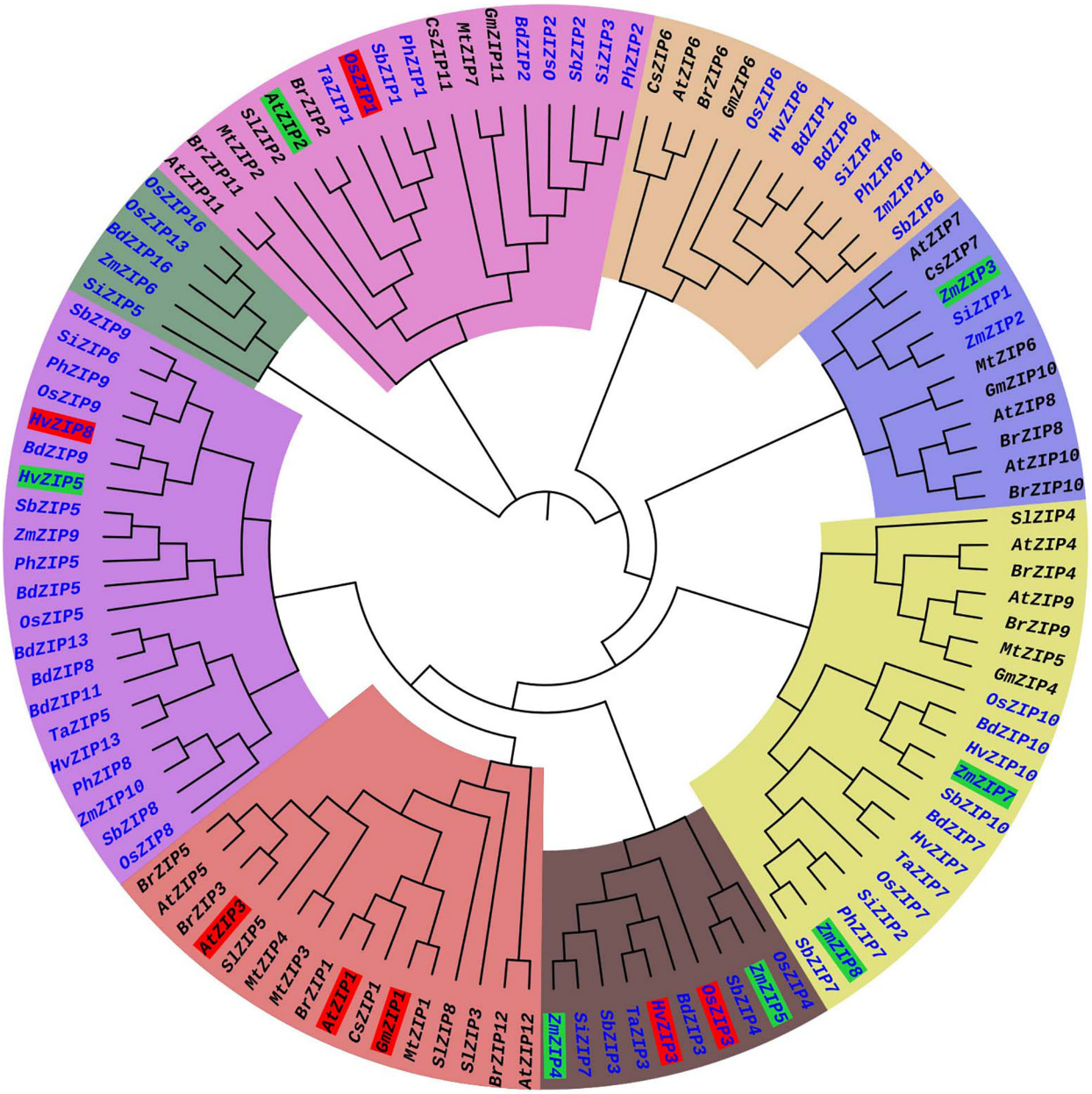

FIGURE 3 | Phylogenetic tree of ZIP transporter family proteins of plants. The ZIP phylogenetic tree was constructed from 113 ZIP transporter protein sequences collected from 14 plant species. These included 8 monocot (Blue) and 6 dicot plants (Black). Each major cluster (MC1-MC8) is highlighted with different color. The low-affinity and high-affinity ZIP transporters are highlighted in red and green, respectively. The protein sequences of ZIP transporter family members were collected from Phytozome (www.phytozome.net) website. The phylogenetic tree was constructed by MEGA version 6 software with the maximum likelihood method based on the Jones-Taylor-Thornton matrix-based model. The bootstrap values are from 1000 replicates. The phylogeny tree was visualized by iTOL (https://itol.embl.de/).

no information is available on target genes of these TFs. Similarly, seven bZIP TFs were identified in the wheat genome. Seven out of four TabZIP TFs such as TabZIPF1-7DL, TabZIPF3b-7BL, TabZIPF4-7AL, and TabZIPF4-7DL of wheat were used for functional complementation assay (Evens et al., 2017). The role of these four TabZIP TFs in the Zn homeostatic mechanism was determined by expression in the *Arabidopsis* double mutant line *bzip19-4 bzip23-2* under Zn deficient condition. The TabZIPF1-7DL and TabZIPF4-7AL could partially complement the double mutant line (*bzip19-4 bzip23-2*) under Zn-deficient condition. TabZIPF3b-7BL have slightly increased the growth of the double mutant line under Zn-deficient condition whereas TabZIPF4-7DL did not complement the double mutant lines (Evens et al., 2017). Similarly, seven bZIP TFs HvbZIP1, HvbZIP10, HvbZIP55, HvbZIP56, HvbZIP57, HvbZIP58, and HvbZIP62 were identified

in barely (Nazri et al., 2017). Among these, the TFs HvbZIP56 and HvbZIP62 could restore the growth of *bzip19* and *bzip23* double mutant of *Arabidopsis* under Zn deficiency condition (Nazri et al., 2017). Recently, Lilay et al. (2020) identified and characterized three bZIP TFs in rice such as OsbZIP48, OsbZIP49, and OsbZIP50. The OsbZIP48 and OsbZIP50 complemented the *Arabidopsis* double mutant (*bzip19/bzip23*) under Zn deficient condition but the OsbZIP49 does not compliment the *Arabidopsis* double mutant (*bzip19/bzip23*) (Lilay et al., 2020).

In plants, concentrations of both the macro- and micro-nutrients influence each other through molecular cross-talks. Signals of P nutrition interact with those of the micronutrients like Zn and Fe. The TFs such as phosphate starvation response 1 (PHR1) (Rubio et al., 2001), ZAT6 (Devaiah et al., 2007b), WRKY75 (Devaiah et al., 2007a), and MYB62 (Devaiah et al., 2009) are involved in P deficiency response. The PHR1 acts as a positive regulator of inorganic phosphate (Pi) starvation responsive genes and PHR1 along with *Phosphate 1* (*PHO1*) are involved in Zn and Fe homeostasis in *Arabidopsis* (Khan et al., 2014; Rai et al., 2015). Zn deficiency also induced the expression of P stress-responsive genes through *PHR1* and increased the uptake of Pi (Bouain et al., 2014). PHR1 seems to be a positive regulator of the ZIP transporters (AtZIP2 and AtZIP4) under Pi deficiency in *Arabidopsis* (Briat et al., 2015). The cross-talk of signals between P, Zn, and Fe were highlighted by many articles (Briat et al., 2015; Xie et al., 2019). Only a very little research is done on the characterization Zn responsive and ZIP related TFs in crops and most of the reports are also confined only to plants like *Arabidopsis*. Therefore, more studies are needed on the identification and characterization of Zn responsive TFs in crops. This could help to understand the molecular mechanism of Zn deficiency tolerance and may aid in developing Zn deficiency tolerant crops.

ZIP FAMILY TRANSPORTERS IDENTIFIED IN VARIOUS CROPS

We have enlisted the ZIP family members identified so far in crops (**Supplementary Table S1**), and the details are discussed below. ZIP family transporter genes have been identified and functions characterized majorly in model plants like *Arabidopsis* and rice. Identification and characterization of the ZIP family genes are still lacking for many crops. Expression levels of ZIP family genes showed dynamic pattern in crops. For e.g., a few ZIP transporters are expressed only under deplete Zn conditions, so their expression is declined within 2 h when Zn is added to the medium (Van de Mortel et al., 2006). The ZIP transporters are localized to plasma membrane and membranes of many intracellular organelles (**Figure 4**). It is proved that the plant ZIP transporters are involved in Zn uptake at the cellular level when tested in yeast complementation test (Fu et al., 2017). In model plant *Arabidopsis*, the ZIP transporters such as AtZIP1, AtZIP2, AtZIP3, and AtZIP4 have been functionally characterized to be the transporters with different affinities (Grotz et al., 1998; Mäser et al., 2001; Assunção et al., 2010). Evidence also shows the direct involvement of ZIP transporter in enhancing Zn accumulation at edible parts of the plants (Ramegowda et al., 2013; Gaitán-Solís et al., 2015). Rice has been the only cereal model crop whose ZIP family transporters have been studied to a reasonable extend when compared to other crops. So, the details on rice ZIP and IRT transporters are discussed in detail in the following section which could serve as a model to study the ZIP and IRT transporters of other crops especially cereals. We also discussed the details on ZIP family transporters identified in other crops.

Rice

Rice is a staple food for more than 560 million people in the world; it is one of the highly sensitive crops to Zn deficiency (Krithika and Balachandar, 2016). Many works were conducted on rice to understand the Zn transport mechanism and rice seems to be a good model for other crops to study the Zn transport. Totally 16 ZIP transporter members were identified in rice (Ramesh et al., 2003; Ishimaru et al., 2005; Chen et al., 2008). Some *OsZIP* genes are expressed in both roots and shoots and others are expressed in whole parts of the plant such as root, culms, leaves, and spikelets under Zn deficiency as reported by different authors (**Figure 5A**). In rice, several ZIPs such as OsZIP1, OsZIP3, OsZIP4, OsZIP5, OsZIP7, and OsZIP8 were reported to be responsible for Zn uptake from soil, translocation from root to shoot as well as for grain filling (Ramesh et al., 2003; Ishimaru et al., 2005, 2007; Lee et al., 2010b; Meng et al., 2018). In rice, understanding the molecular mechanisms of Zn transport is important for improving the Zn content in the edible part. Ishimaru et al. (2011) highlighted the mechanism of Zn uptake and translocation in rice. The OsZIP1 and OsZIP3 seem to be important for Zn uptake from the soil, OsZIP4, OsZIP5, and OsZIP8 for root to shoot translocation, while OsZIP4 and OsZIP8 played a role in grain filling (Bashir et al., 2012). The expression levels of *OsZIP3* and *OsZIP4* are higher in the roots of Zn-efficient genotype (IR8192) than those of in-efficient genotype (Erjiufeng) suggesting that these genes could contribute to high Zn efficiency (Chen et al., 2008).

Under Zn deficient condition, *OsZIP1*, *OsZIP3*, and *OsZIP4* are up-regulated in the roots and *OsZIP4* over-expressed in the shoot of both genotypes (Chen et al., 2008). These transporters are localized to the vascular bundles in shoots and in the vascular bundles and epidermal cells in roots of rice (Ramesh et al., 2003; Ishimaru et al., 2006). The expression analysis shows that *OsZIP4* is highly expressed under Zn deficient conditions in roots and shoots in rice (Ishimaru et al., 2005). It is expressed in the meristem of the roots and shoots, and also in vascular bundles of the roots and shoots under Zn deficient condition (Ishimaru et al., 2005; Ishimaru et al., 2011). The expression of *OsZIP1* gene is seen only in root tissues under Zn starvation, but *OsZIP3* is expressed in both roots and shoots under both Zn sufficient and deficient conditions (Ramesh et al., 2003). *OsZIP7* and *OsZIP8* are expressed in roots and shoots under Zn deficient condition (Yang et al., 2009; Tan et al., 2019). The *OsZIP3* and *OsZIP4* are highly expressed in the nodal regions under Zn deficiency condition (Sasaki et al., 2015). *OsZIP1* is expressed in the epidermis and vascular tissues of roots and leaves of rice (Ramesh et al., 2003; Bashir et al., 2012). The OsZIP4, OsZIP5,

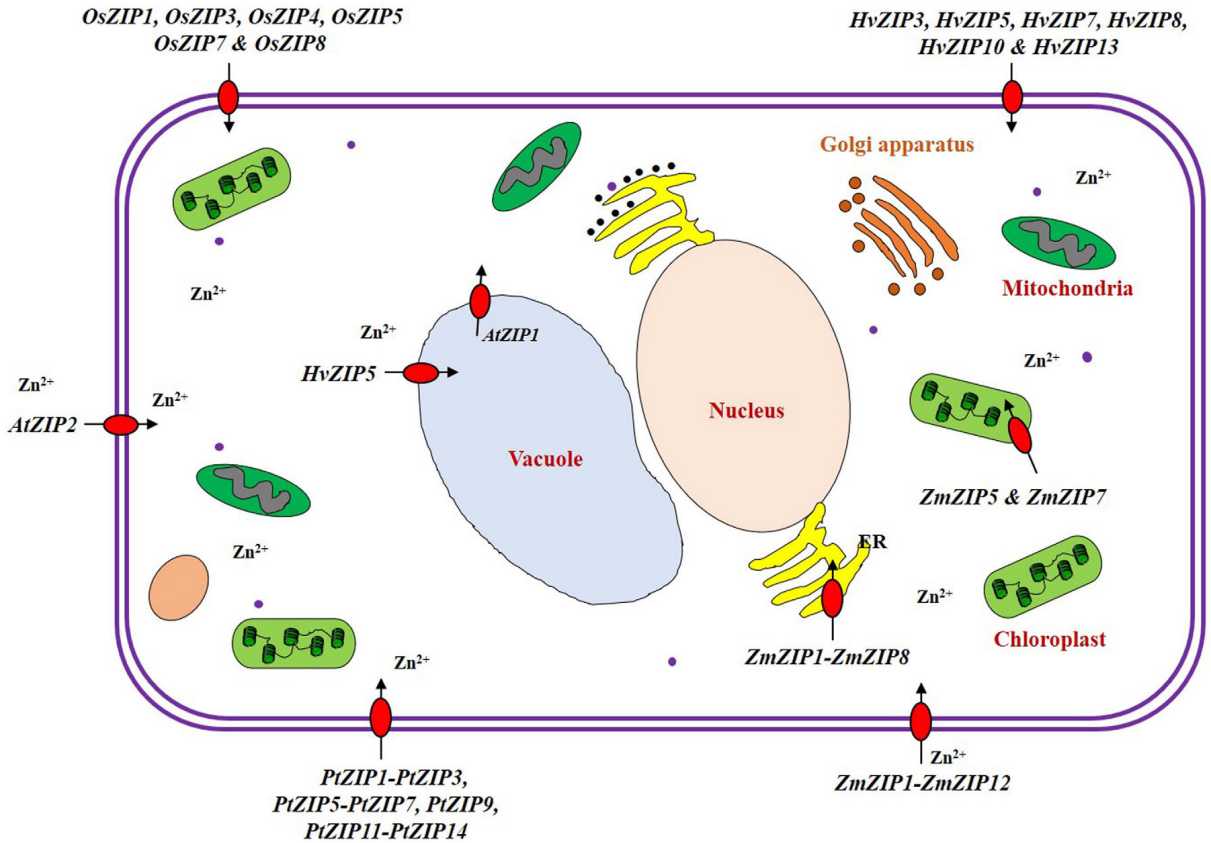

FIGURE 4 | Localization of ZIP transporter family proteins in the plant cell. The ZIP transporter family proteins are actively involved in uptake, transport, detoxification and homeostasis of Zn within plant cells (Li et al., 2013). Under low Zn condition, many ZIP transporters (ZIP1-ZIP12) are expressed and are localized in plasma membrane of the cell in rice, (Ramesh et al., 2003; Ishimaru et al., 2005; Yang et al., 2009; Lee et al., 2010a,b) hardy orange (Fu et al., 2017), maize (Li et al., 2013; Mondal et al., 2013), *Arabidopsis* (Milner et al., 2013), and barley (Pedas et al., 2009; Tiong et al., 2015). Some of the ZIP transporters are also localized to the membranes of intracellular organelles such as chloroplast [ZmZIP5 and ZmZIP7 (Li et al., 2013)], vacuole [HvZIP5 (Tiong et al., 2015) and AtZIP1 (Milner et al., 2013)], and endoplasmic reticulum [ZmZIP1-ZmZIP8 (Li et al., 2013)].

and OsZIP8 transporters are localized to plasma membrane and are involved in Zn influx (Ishimaru et al., 2005; Lee et al., 2010a,b). The *OsZIP3* gene was expressed in the nodal region which is responsible for unloading Zn from the xylem (Sasaki et al., 2015). OsZIP7 is located in the parenchyma cells of vascular bundles in nodal region, and in the stele in the roots of rice (Tan et al., 2019). OsZIPs might be actively involved in the uptake and transport of Zn in rice. Similarly, Ishimaru et al. (2011) suggest that OsZIP4 may be responsible for Zn translocation to aerial parts.

The OsIRTs are similar to OsZIP metal transporters; these are the members of ZIP family transporters (Guerinot, 2000). Especially OsZIP4, OsZIP5, OsZIP6, and OsZIP7 showed sequence similarity to OsIRT1 (Ishimaru et al., 2005). The expression analysis revealed that *OsIRT1* and *OsIRT2* are mainly expressed in roots of rice under low Fe conditions (Bughio et al., 2002; Ishimaru et al., 2006; Lee et al., 2009). The expression level *OsIRT1* was much higher than *OsIRT2* in the Fe deficient root of rice (Ishimaru et al., 2006). *OsIRT1* and *OsIRT2* have been cloned and characterized in yeast (Bughio et al., 2002; Ishimaru et al., 2006). The OsIRT1 and OsIRT2 proteins localize to the plasma membrane and have been shown to complement the growth defect of a yeast Fe uptake mutant, confirming that they are functional Fe^{2+} transporters under low Fe condition (Bughio et al., 2002; Ishimaru et al., 2006). The OsIRT transporters also capable of transporting other divalent metal cations such as Cd^{2+}, Zn^{2+}, Cu^{2+}, and Mn^{2+} (Bughio et al., 2002; Nakanishi et al., 2006). Cellular and sub-cellular metal homeostasis is very crucial for maintaining the optimal metabolic process and cellular functioning (Bashir et al., 2016). Therefore, identification and characterization of IRT transporters are essential for understanding the mechanism of Fe homeostasis in rice and other plants.

The information available on Zn transporters of rice plants are high when compared to other crops such as maize, wheat, barley, foxtail millet, orange, and common bean, etc. This large information is helpful for understanding the expression pattern of Zn transporters, their localization and metal homeostasis in other crops. Apart from these reports we need further studies on the biofortification of rice with Zn in order to increase the

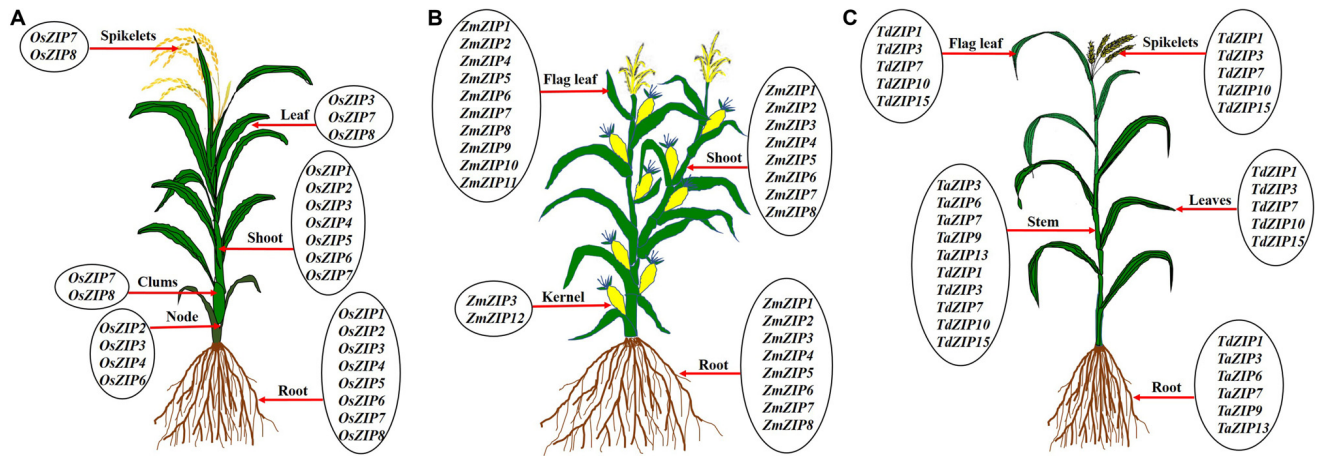

FIGURE 5 | Expression of ZIP transporter genes in different parts of rice **(A)**, maize **(B)**, and wheat **(C)**. The ZIP transporters are expressed in root, nodes, clumps, shoot/stem, leaf, flag leaf, kernel, and spikelets under Zn deficient levels. Under low Zn condition, root tissues show the expression of ZIP genes in rice (Ramesh et al., 2003; Ishimaru et al., 2005; Chen et al., 2008; Yang et al., 2009; Suzuki et al., 2012), maize (Li et al., 2013; Mondal et al., 2013) and wheat (Durmaz et al., 2011; Evens et al., 2017; Deshpande et al., 2018), clumps in rice (Yang et al., 2009), shoot/stem in rice (Ramesh et al., 2003; Ishimaru et al., 2005; Chen et al., 2008; Yang et al., 2009; Suzuki et al., 2012), maize (Li et al., 2013; Mondal et al., 2013), and wheat (Durmaz et al., 2011; Evens et al., 2017). Leaf tissue also showed the over expression of ZIP genes under low Zn soil in rice (Ramesh et al., 2003; Ishimaru et al., 2005; Chen et al., 2008) and wheat (Evens et al., 2017; Deshpande et al., 2018), flag leaf tissues in maize (Mondal et al., 2013) and wheat (Deshpande et al., 2018), kernel tissue in maize (Li et al., 2013) and spikelets tissue in rice (Yang et al., 2009) and wheat (Deshpande et al., 2018).

yield and quality of rice as it helps to improve the nutritional status of humans.

Maize

Maize is one of the most widely cultivated and important cereal crops for human and animal food (Shiferaw et al., 2011). Zn is the most common limiting micronutrient in maize yield worldwide (Alloway, 2009). The maize genome has been sequenced and assembled (Palmer et al., 2003). Li et al. (2013) identified eight ZIP transporters (*ZmZIP1–ZmZIP8*) in maize genome. All eight ZmZIP proteins are localized to the plasma membrane (Li et al., 2013). The expression analysis indicated that *ZmZIP3*, *ZmZIP4*, *ZmZIP5*, *ZmZIP7*, and *ZmZIP*8 are sensitive to Zn status during the seedlings stage of maize (Li et al., 2013). Under Zn deficient condition, *ZmZIP5* and *ZmZIP8* are induced in shoot and *ZmZIP3* is up-regulated in both root and shoot (Li et al., 2013). The expression of *ZmZIP4, ZmZIP5, ZmZIP7*, and *ZmZIP8* decreased in shoots and *ZmZIP3* is down-regulated in roots of maize under excess Zn supply (Li et al., 2013). Similarly, 12 *ZmZIP* genes (*ZmZIP1–ZmZIP12*) were identified by Mondal et al. (2013) in maize. Ten *ZmZIP* genes (*ZmZIP1, ZmZIP2,* and *ZmZIP4–ZmZIP11*) are tissue-specific and are highly expressed in flag leaf except *ZmZIP3* and *ZmZIP12,* under Zn deficient condition (Mondal et al., 2013). The *ZmZIP2*, *ZmZIP5*, *ZmZIP6*, *ZmZIP8*, and *ZmZIP11* are expressed in the kernel under Zn deficient condition (Mondal et al., 2013). ZmZIP4, ZmZIP5, ZmZIP7, and ZmZIP9 proteins are located in cytoplasm and chloroplast (Mondal et al., 2013; **Figure 4**). It is well known that some ZIP transporters are involved in Zn biofortification in other crops. For example, the OsZIP4 and OsZIP8 are actively involved in the grain filling of Zn in rice (Ishimaru et al., 2007; Lee et al., 2010b). The *ZmZIP5* and *ZmZIP11* are highly expressed in the flag leaf, which might play a vital role in the mobilization of Zn from flag leaf to developing kernel for the accumulation of the large amount of Zn in the kernel (Mondal et al., 2013; **Figure 5B**). These ZmZIPs (ZmZIP5 and ZmZIP11) might contribute to the biofortification of maize with Zn to improve the quality (Mondal et al., 2013). Since maize is highly sensitive to Zn deficiency, more high resolution studies are needed to improve the quality of maize grown under low Zn soils.

Wheat

Wheat is a major cereal crop for whole world and it provides about one-half of humans' food calories and a large part of their nutrient requirements (Shiferaw et al., 2013). Complete assembly of the hexaploid bread wheat genome is available now (Zimin et al., 2017). Previously, very little was known about ZIP family transporters except for TdZIP1 from wild emmer wheat (*Triticum turgidum* ssp. *dicoccoides*), a Zn transporter with higher expression under Zn deficiency (Durmaz et al., 2011). Recently, 14 *TaZIP* genes were identified in bread wheat (*Triticum aestivum*) (Evens et al., 2017). Out of 14 ZIPs, five (*TaZIP3, TaZIP5, TaZIP6, TaZIP7*, and *TaZIP13*) were analyzed for the expression level in shoot and root under Zn starvation. In shoot, expression of all five *TaZIPs* increased under low Zn conditions but the timing varied between individual genes. In roots, *TaZIP3*, *TaZIP5*, *TaZIP7*, and *TaZIP13* showed increased expression under Zn starvation with expression of only *TaZIP6* gene remains fairly stable (Evens et al., 2017). Similarly, Deshpande et al. (2018) analyzed the relative expression of five selective ZIP genes in durum wheat (*Triticum durum*) genotypes UC 1114 and MACS 3125 under three different foliar application of Zn (Deshpande et al., 2018). In flag leaves, expression level of three *TdZIP* genes (*TdZIP1, TdZIP3*, and *TdZIP7*) decreased and two genes

(*TdZIP10* and *TdZIP15*) increased during grain development (Deshpande et al., 2018). Time-dependent expression patterns of these *ZIP* transporters revealed that the expression pattern varies with tissues viz., flag leaves, non-flag leaves, stem, and spike (Deshpande et al., 2018). These studies revealed that most of the *TaZIP* transporter genes are expressed in all parts and are involved in Zn uptake and translocation under Zn starvation (**Figure 5C**). Till now, totally 16 *ZIP* genes are identified in the wheat genome and only a few works have been carried out on the expression analysis with these when compared to rice. No reports are available on localization and functional characterization of TaZIP transporters which may help to understand further on the Zn transport mechanism.

Barley

Barley is a nutritionally and economically important cereal crop. Till date, only a few *ZIP* family genes have been identified and characterized in barely. Pedas et al. (2009) reported that *HvZIP3*, *HvZIP5*, and *HvZIP8* are induced in root tissues under Zn deficient condition. These three HvZIP transporters might be involved in Zn uptake under low Zn conditions. *HvZIP7* is highly induced in the vascular tissues of roots and leaves under Zn deficiency condition and its protein is localized to plasma membrane (Tiong et al., 2014). In another report, 13 *HvZIP* genes were identified and their tissue-specific expression was also determined under Zn deficiency condition. Out of 13 *HvZIP* genes, six (*HvZIP3*, *HvZIP5*, *HvZIP7*, *HvZIP8*, *HvZIP10*, and *HvZIP13*) were highly induced in Zn deficient barely (Tiong et al., 2015). The expression levels of these six *HvZIP* genes are significantly increased (3-fold) in roots under Zn deficient condition (0.005 μM Zn) compared to Zn sufficient condition (0.5 μM Zn) (Tiong et al., 2015). All the six HvZIP proteins are localized to plasma membrane (Tiong et al., 2015). The *HvZIP2*, *HvZIP3*, *HvZIP5*, *HvZIP7, HvZIP8*, *HvZIP10*, and *HvZIP13* are also induced in shoot of barley under Zn deficient condition. Recently, five *HvZIP* family genes such as *HvZIP3*, *HvZIP7*, *HvZIP8*, *HvZIP9*, and *HvZIP13* were screened for their expression under the arbuscular mycorrhizal fungi (AMF) medium with low and high Zn treatments (Watts-Williams and Cavagnaro, 2018). Under low Zn condition, the *HvZIP* genes were up-regulated in the root of barley in the non-AMF condition. But, the activity of AMF has altered the expression of *HvZIP* family genes. The *HvZIP13* gene was significantly overexpressed in the mycorrhizal plant than non-mycorrhizal plants under low Zn condition. Two *HvZIP* genes (*HvZIP3* and *HvZIP8*) are down-regulated in mycorrhizal roots at low Zn soil (Watts-Williams and Cavagnaro, 2018). Therefore, ZIP genes may be directly or indirectly involved in the transport of Zn between the AMF and plant under low Zn conditions. Apart from this, no other information is available on the effect of AMF on the ZIP gene expression in other crops. AMF has the ability to improve the nutrition of the host plant through increased uptake of soil nutrients, especially immobile nutrients such as P, K, Zn, Fe, and Cu (Pellegrino and Bedini, 2014; Pellegrino et al., 2015; Watts-Williams and Cavagnaro, 2018). Kaiser et al. (2015) reported that the AMF (*Glomus contrictus* or *Glomus fasciculatus*) enhances the Zn up-take in barely. Further studies are needed to understand the molecular mechanism of AMF-mediated Zn transport and signals and TFs involved in this symbiotic Zn uptake.

Foxtail Millet

Foxtail millet is one of the food security minor cereal crops in low input regions. It is a domesticated diploid C4 crop having a small genome (∼515 Mb) with short life cycle (Doust et al., 2009). So, it is considered as a model crop for genetic and genomic studies of monocots (Lata et al., 2013; Ceasar et al., 2014). The whole-genome sequence is available for two different genotypes of foxtail millet (Bennetzen et al., 2012; Zhang et al., 2012). But, the information about ZIP genes is limited. Alagarasan et al. (2017) identified seven *SiZIP* genes (*SiZIP1*–*SiZIP7*) in foxtail millet. The expression pattern of seven *SiZIP* genes was analyzed in root, leaf, stem and spica tissues of foxtail millet grown under drought stress without any additional nutrient supplementation. All seven *SiZIP* genes were induced in all four tissues (root, leaf, stem, and spica) with various levels of expression. The *SiZIP2*, *SiZIP3*, *SiZIP4*, and *SiZIP5* showed relatively higher expression and low level of expression was observed with *SiZIP6*, in all tissues. *SiZIP1* gene is moderately expressed in root, shoot and spica and very least expression was seen in leaf (Alagarasan et al., 2017). The highly induced *SiZIP* genes (*SiZIP2*, *SiZIP3*, *SiZIP4*, and *SiZIP5*) could be used for the bio-fortification process for the enrichment of Zn into the seeds of foxtail millet. The functional characterization of ZIP genes in foxtail millet could aid to improve the Zn uptake in foxtail millet and other minor millets.

Orange

Orange is an important fruit crop with 60 million metric tonnes of annual production worldwide and has high nutritional values, vitamins and other nutrients (Etebu and Nwauzoma, 2014). Till date, orange is the only fruit crop in which ZIP transporters are identified. In navel orange (*Citrus sinensis*), four *ZIP* genes such as *CsZIP1*, *CsZIP2, CsZIP3,* and *CsZIP4* were identified and expression analysis show that *CsZIP3* and *CsZIP4* are highly expressed in mild, moderate and severely affected Zn deficient leaf. *CsZIP1* gene is down-regulated under mild Zn deficient leaf and up-regulated in moderate and severely Zn depleted leaf. There is no change in the expression of *CsZIP2* in all tissues when compared with control (Fei et al., 2016). Recently, 13 *ZIP* (*PtZIP1*–*PtZIP3* and *PtZIP5*–*PtZIP14*) genes were identified in trifoliate orange (*Poncirus trifoliata*), another variety of orange fruit crop. *PtZIP1*, *PtZIP2*, *PtZIP3*, *PtZIP5*, *PtZIP6*, and *PtZIP9* are highly induced in roots, whereas *PtZIP1*, *PtZIP2*, *PtZIP5*, *PtZIP6*, and *PtZIP7* are highly expressed in leaves, under Zn-deficient condition (Fu et al., 2017). In future, functional characterization of ZIP genes in orange is very important to improve the Zn content in the edible parts of orange. Therefore, it will help to reduce the Zn deficiency problems in humans. So, more studies are needed to improve the quality of orange in terms of biofortification.

Common Bean

Common bean is an important food crop for human as it contains a rich source of nutrients (Gepts et al., 2008), especially a source of dietary Zn (Astudillo-Reyes et al., 2015). Totally 19

PvZIP genes (*PvZIP1–PvZIP19*) were identified in common bean. But, only seven *PvZIP* genes such as *PvZIP2*, *PvZIP6*, *PvZIP7*, *PvZIP12*, *PvZIP13*, *PvZIP16,* and *PvZIP18* were analyzed for their expression dynamics. The selection of *PvZIP* genes is based on their location in the genome relative to the presence of QTLs for seed Zn content (Astudillo et al., 2013). *PvZIP12*, *PvZIP13,* and *PvZIP16* genes are expressed in root, leaf and pod of the common bean under Zn deficient condition (Astudillo et al., 2013). Other *PvZIP* genes are not expressed in any tissue types in Zn deficient condition. The *PvZIP12* is highly expressed in leaves at vegetative stage and *PvZIP13* is highly expressed in leaves at flowering stage. Hence, the *PvZIP12* gene could be involved in mobilizing the Zn to seeds of bean. The identification and characterization of the candidate genes related to *PvZIP* transporters may help to improve Zn uptake and nutrient content of seeds.

FUNCTIONAL CHARACTERIZATION OF ZIP TRANSPORTERS IN CROPS

Till date, only a little information is available on functional characterization of ZIP transporters in crops (Milner et al., 2013). Mostly, the investigations on the functions of plant ZIP transporters have been conducted by yeast complementation assays which revealed that ZIP transporters are capable of transporting various divalent cations (Guerinot, 2000). For functional characterization, Zn sensitive yeast mutant (*zrt1/zrt2*) which is defective in both the ZRT1 high−affinity and the ZRT2 low−affinity uptake transporters and is susceptible to Zn deficient conditions, was employed (Zhao and Eide, 1996a,b). In most of these studies, genes of model plant *A. thaliana* are used. The *AtZIP* genes such as *AtZIP1*, *AtZIP2*, and *AtZIP3*

TABLE 2 | Details on the ZIP family transporter genes identified in plants.

Name of the plant	Common name	Name of ZIP genes	Method of characterization	Affinity		References
				Low-affinity	High-affinity	
Arabidopsis thaliana	*Arabidopsis*	*AtZIP1-AtZIP4*	Yeast complementation assay	*AtZIP1* (*K*m = 13 μM) and *AtZIP3* (*K*m = 14 μM)	*AtZIP2* (*K*m = 2 μM)	Grotz et al., 1998
Poncirus trifoliate	Trifoliate orange	*PtZIP1-PtZIP3*, *PtZIP5-PtZIP7*, *PtZIP9* and *PtZIP10- PtZIP14*	qRT-PCR and yeast complementation assay	–	–	Fu et al., 2017
Setaria italica	Foxtail millet	*SiZIP1-SiZIP7*	RT-PCR	–	–	Alagarasan et al., 2017
Glycine max	Soybean	*GmZIP1*, *GmZIP4, GmZIP4, GmZIP6, GmZIP10* and *GmZIP11*	Yeast complementation assay	*GmZIP1* (*K*m = 13.8 μM)	–	Moreau et al., 2002
Oryza sativa	Rice	*OsZIP1- OsZIP16*	qRT-PCR complementation assay	*OsZIP1* (*K*m = 16.3 μM) *and OsZIP3* (*K*m = 18.5 μM)	–	Ramesh et al., 2003; Ishimaru et al., 2005; Chen et al., 2008; Yang et al., 2009
Phaseolus vulgaris	Common bean	*PvZIP1- PvZIP18*	qRT-PCR	–	–	Astudillo et al., 2013
Zea mays	Maize	*ZmZIP1- ZmZIP12*	qRT-PCR and yeast complementation assay	–	*ZmZIP3*, *ZmZIP4*, *ZmZIP5*, *ZmZIP7* and *ZmZIP8*	Li et al., 2013; Mondal et al., 2013
Triticum aestivum	Wheat	*TaZIP1-TaZIP3, TaZIP5-TaZIP7, TaZIP9-TaZIP11, TaZIP13, TaZIP14* and *TaZIP16*	qRT-PCR and yeast complementation assay	–	–	Evens et al., 2017
Citrus sinensis	Navel orange	*CsZIP1-CsZIP4*	qRT-PCR	–	–	Fei et al., 2016
Hordeum vulgare	Barley	*HvZIP1-HvZIP3, HvZIP5- HvZIP8, HvZIP10, HvZIP11, HvZIP13, HvZIP14* and *HvZIP16*	qRT-PCR and yeast complementation assay	*HvZIP3* and *HvZIP8*	*HvZIP5*	Pedas et al., 2009; Tiong et al., 2015
Triticum durum	Durum wheat	*TdZIP1, TdZIP3, TdZIP7 TdZIP10* and *TdZIP15*	qRT-PCR	–	–	Deshpande et al., 2018
Triticum dicoccoides	Emmer wheat	*TdZIP1*	qRT-PCR and yeast complementation assay	–	–	Durmaz et al., 2011

The details on name of the plant, name of ZIP genes, affinity of ZIP transporter and mode of characterization are provided.

enabled Zn transport based on the yeast complementation assay (Eide, 1998; Grotz et al., 1998; Guerinot, 2000). In another study, six ZIP genes such as *AtZIP1*, *AtZIP2*, *AtZIP3*, *AtZIP7*, *AtZIP11*, and *AtZIP12*, are able to complement the *zrt1/zrt2*Δ yeast mutant fully or partially under Zn deficient conditions (Milner et al., 2013). Recently, Fu et al. (2017) characterized the Zn transport specificities of the *PtZIP* genes and *PtZIP1*, *PtZIP2*, *PtZIP3*, and *PtZIP12* are also able to complement *zrt1zrt2* mutant (Fu et al., 2017).

In plants, the high-affinity ZIP transporter system was highly active under low Zn conditions. Based on a yeast complementation assay, the affinity values of AtZIP1 (K_m = 13 μM) and AtZIP3 (K_m = 14 μM) confirmed to be low-affinity transporters and AtZIP2 (K_m = 2 μM) as high-affinity transporter (Grotz et al., 1998). In rice, OsZIP1 (K_m = 16.3 μM) and OsZIP3 (K_m = 18.5 μM) are characterized as low-affinity Zn transporters (Ramesh et al., 2003). The GmZIP1 of soybean was identified to be a low-affinity transporter (K_m = 13.8 μM) (Moreau et al., 2002). The high affinity transporters ZmZIP3, ZmZIP4, ZmZIP5, ZmZIP7, and ZmZIP8 were identified in maize (Li et al., 2013; Mondal et al., 2013). Similarly, Pedas et al. (2009) found that HvZIP3 and HvZIP8 are low-affinity transporters and HvZIP5 is a high-affinity Zn transporter in barely based on yeast complementation assay. However, additional kinetic assay is essential for confirming this hypothesis. Till now, very little information is available on the affinities of ZIP transporters in crops (**Table 2**). Further, heterologous expression of plant ZIP transporters in yeast may not replicate the same function and may yield false results due to being a completely different system and lack of key signals involved in the regulation of Zn concentration. Testing the function of plant ZIPs in the same plant by knock-out studies may yield confident results. To this end, newly adopted genome editing tool CRISPR/Cas9 may help for the efficient generation of single, double and multiple mutants for plant ZIPs to test their function in the same system. Characterization of other ZIP transporters could help to understand the crucial roles of ZIP transporter family genes in crops.

MANIPULATION OF EXPRESSION LEVELS OF ZIP GENES THROUGH TRANSGENIC MODIFICATION

The plant ZIP genes were over expressed through transgenic modification in some studies. Till now, only a few genes such as *AtZIP1*, *OsZIP1*, *ZmZIP3*, *OsZIP4, OsZIP5*, and *HvZIP7* were used for over-expression analysis in crops (**Table 3**). For example, *OsZIP1* gene was transferred into finger millet using *pGreen0179* vector under the control of *Bx17* promoter through *Agrobacterium*-mediated transformation; the transgenic plants showed significantly improved accumulation of Zn in seeds (Ramegowda et al., 2013). Similarly, over-expression of *AtZIP1* gene in cassava showed an increase of 25% Zn content in the edible part of the plant (Gaitán-Solís et al., 2015). Over expression of *OsZIP4, OsZIP5*, and *OsZIP8* in transgenic rice decreased the Zn content in shoot and seed; but significantly increased the root Zn content (Ishimaru et al., 2007; Lee et al., 2010a,b). It clearly revealed that these OsZIP transporters play a crucial role in Zn uptake from the soil. Over-expression of *OsZIP4* in rice plants showed the reduction of plant growth under Zn deficient conditions (Ishimaru et al., 2007). Approximately, 50% reduction observed in plant height and root length in *OsZIP4* over-expressing transgenic rice plants (Ishimaru et al., 2007). At the flowering stage, *OsZIP5* and *OsZIP8* over-expressing transgenic rice plants are shorter and had fewer tillers (Lee et al., 2010a,b). Also, these transgenic plants produce very fewer grains (Lee et al., 2010a,b). Similarly, over-expression of *OsIRT1* in rice altered the plant architecture and increased the Fe and Zn contents in mature seeds and vegetative parts of the plant under Zn deficient condition (Lee and An, 2009). These studies indicate that the ZIP transporters are responsible for improving

TABLE 3 | Details on genetic manipulation of ZIP transporter genes reported in various plants.

Name of the ZIP gene	Source	Host	Name of vector used	Mode of transformation	Observation	References
ZmZIP3	*Zea mays*	*Arabidopsis thaliana*	pBI121	*Agrobacterium tumefaciens*	Improved Zn accumulation in the roots	Li et al., 2015
AtZIP1	*Arabidopsis thaliana*	*Manihot esculenta*	pCAMBIA2301	*Agrobacterium tumefaciens*	Higher Zn concentrations in the edible portion	Gaitán-Solís et al., 2015
HvZIP7	*Hordeum vulgare*	*Hordeum vulgare*	pMDC32	*Agrobacterium tumefaciens*	Increases root to shoot translocation of Zn	Tiong et al., 2014
OsZIP1	*Oryza sativa*	*Eleusine coracana* and *Nicotiana tabacum*	pGreen0179	*Agrobacterium tumefaciens*	Enhanced Zn concentration in seed and plant tissue	Ramegowda et al., 2013
OsZIP5	*Oryza sativa*	*Oryza sativa*	pCAMBIA1302	*Agrobacterium tumefaciens*	Decreased Zn concentration in shoot and increased in root	Lee et al., 2010a
OsZIP8	*Oryza sativa*	*Oryza sativa*	pCAMBIA1302	*Agrobacterium tumefaciens*	Decreased Zn concentration in shoot and seed; increased in root	Lee et al., 2010b
OsZIP4	*Oryza sativa*	Oryza sativa	pIG121Hm	*Agrobacterium tumefaciens*	Zn distribution	Ishimaru et al., 2007
AtZIP1	*Arabidopsis thaliana*	*Hordeum vulgare*	pWVec8	*Agrobacterium tumefaciens*	Increased Zn content in seed	Ramesh et al., 2004

The name of the plant, vectors and the role of ZIP genes are mentioned.

the nutritional quality in crops. So, more effort is needed to identify the specific function of all ZIP genes in crops and it could help to develop transgenic plants related to biofortification of edible parts with Zn/Fe in crops.

CONCLUSION AND FUTURE PROSPECTS

Zinc is not only essential for plant growth but also crucial for human health. It is estimated that nearly 50% of the world's population is at the risk of Zn deficiency problems (Pedas and Husted, 2009). In humans, Zn deficiency impairs growth and development, affects the nervous system, reduces immunity and can cause death (Ekweagwu et al., 2008; Menguer et al., 2018). Researchers need to pay more attention to the biofortification of food crops with priority to Zn. The ZIP transporters play a crucial role in biofortification with Zn. In soil, Zn deficiency problem is usually tackled by adding Zn containing fertilizers. But, it is only a temporary solution. Also, the subsistence farmers cannot afford to buy Zn fertilizers all the time due to high market price. Identification of candidate genes related to ZIP transporters, their characterization and tapping this information to develop crops via transgenic and/or the marker-assisted selection may help for developing Zn efficient crops. Genetic modification of crops with ZIP genes is also helpful in improving the crops related to Zn use efficiency. Therefore, the structural and functional insight of plant ZIP transporter are essential. The bioinformatics study showed that the plant ZIP transporters may have partially overlapping but distinct metal transport mechanism compared to BbZIP as some of the residues involved in metal binding and transport are not conserved in plant ZIPs. The plant ZIP transporters showed greater variation at the Zn^{2+} binding site when compared to BbZIP. The phylogenetic analysis of 113 plant ZIP proteins from 14 plant species revealed that the ZIP family members are mainly clustered together as per their numbers. Monocot and dicot plant ZIPs are clustered in separate clusters and both low-affinity and high-affinity ZIPs are closely clustered. These findings would be a valuable theoretical knowledge for future studies in terms of understanding the gene, protein, functional residues of Zn transporters in crops and might be helpful to overcome the problems associated with Zn deficiency. Many ZIP family genes involved in Zn transport have been characterized in model plants. Identification and functional characterization of certain ZIP genes, their relative expression and localization have been done only in a few crops such as rice and maize. More information on Zn transporters are available for rice plants when compared to other crops so this can serve as a model to study Zn transport in other cereal crops. ZIP family members involved in Zn transport and sequestration represent some of the clearest candidate genes for increased Zn content in crops. But very little information is available on how Zn is transported from leaf xylem to phloem of developing seeds and ultimately unloaded into seeds with the help of ZIP genes. This needs further research in the coming years. Identification and characterization of ZIP proteins and related TFs in many crops would help for the better understanding of Zn homeostasis. A more holistic and high-resolution studies on ZIP transporters in crops will help to overcome the problems associated with low Zn soils and to improve the human health.

DATA AVAILABILITY STATEMENT

All datasets generated for this study are included in the article/**Supplementary Material**.

AUTHOR CONTRIBUTIONS

TA, TM, and SA conceptualized and wrote the manuscript. TA and SA analyzed the protein sequences with alignment, modeling and phylogeny. GV and SI assisted, and TA, TM, GV, and SA edited, and updated the manuscript. SA and SI contributed critically in revising and improving the manuscript for publication.

FUNDING

The research in our lab is currently funded by the Department of Biotechnology, Government of India, India (No: BT/PR21321/GET/119/76/2016).

SUPPLEMENTARY MATERIAL

The Supplementary Material for this article can be found online at: https://www.frontiersin.org/articles/10.3389/fpls.2020.00662/full#supplementary-material

REFERENCES

Alagarasan, G., Dubey, M., Aswathy, K. S., and Chandel, G. (2017). Genome wide identification of orthologous ZIP genes associated with zinc and iron translocation in *Setaria italica*. *Front. Plant Sci.* 8:775. doi: 10.3389/fpls.2017.00775

Ali, S., Khan, A. R., Mairaj, G., Arif, M., Fida, M., and Bibi, S. (2008). Assessment of different crop nutrient management practices for yield improvement. *Aust. J. Crop Sci.* 2, 150–157.

Alloway, B. (2009). Soil factors associated with zinc deficiency in crops and humans. *Environ. Geochem. Health* 31, 537–548. doi: 10.1007/s10653-009-9255-4

Andreini, C., Banci, L., Bertini, I., and Rosato, A. (2006). Zinc through the three domains of life. *J. Proteome Res.* 5, 3173–3178. doi: 10.1021/pr0603699

Assunção, A., Persson, D., Husted, S., Schjørring, J., Alexander, R., and Aarts, M. (2013). Model of how plants sense zinc deficiency. *Metallomics* 5, 1110–1116. doi: 10.1039/c3mt00070b

Assunção, A. G., Herrero, E., Lin, Y. F., Huettel, B., Talukdar, S., Smaczniak, C., et al. (2010). *Arabidopsis thaliana* transcription factors bZIP19 and bZIP23 regulate the adaptation to zinc deficiency. *Proc. Natl. Acad. Sci. U.S.A.* 107, 10296–10301. doi: 10.1073/pnas.1004788107

Astudillo, C., Fernandez, A., Blair, M. W., and Cichy, K. A. (2013). The *Phaseolus vulgaris* ZIP gene family: identification, characterization, mapping, and gene expression. *Front. Plant Sci.* 4:286. doi: 10.3389/fpls.2013.00286

Astudillo-Reyes, C., Fernandez, A. C., and Cichy, K. A. (2015). Transcriptome characterization of developing bean (*Phaseolus vulgaris* L.) pods from two genotypes with contrasting seed zinc concentrations. *PLoS One* 10:e0137157. doi: 10.1371/journal.pone.0137157

Bashir, K., Ishimaru, Y., and Nishizawa, N. K. (2012). Molecular mechanisms of zinc uptake and translocation in rice. *Plant Soil* 36, 189–201. doi: 10.1007/s11104-012-1240-5

Bashir, K., Rasheed, S., Kobayashi, T., Seki, M., and Nishizawa, N. K. (2016). Regulating subcellular metal homeostasis: the key to crop improvement. *Front. Plant Sci.* 7:1192. doi: 10.3389/fpls.2016.01192

Bennetzen, J. L., Schmutz, J., Wang, H., Percifield, R., Hawkins, J., Pontaroli, A. C., et al. (2012). Reference genome sequence of the model plant *Setaria*. *Nat. Biotechnol.* 30, 555–561. doi: 10.1038/nbt.2196

Black, R. E., Allen, L. H., Bhutta, Z. A., Caulfield, L. E., De Onis, M., Ezzati, M., et al. (2008). Maternal and child undernutrition: global and regional exposures and health consequences. *Lancet* 371, 243–260. doi: 10.1016/S0140-6736(07)61690-0

Bouain, N., Shahzad, Z., Rouached, A., Khan, G. A., Berthomieu, P., Abdelly, C., et al. (2014). Phosphate and zinc transport and signalling in plants: toward a better understanding of their homeostasis interaction. *J. Exp. Bot.* 30, 5725–5741. doi: 10.1093/jxb/eru314

Briat, J. F., Rouached, H., Tissot, N., Gaymard, F., and Dubos, C. (2015). Integration of P, S, Fe, and Zn nutrition signals in *Arabidopsis thaliana*: potential involvement of phosphate starvation response 1 (PHR1). *Front. Plant Sci.* 28:290. doi: 10.3389/fpls.2015.00290

Brown, P. H., Cakmak, I., and Zhang, Q. (1993). "Form and function of zinc plants," in *Zinc in Soils and Plants. Developments in Plant and Soil Sciences*, Vol. 55, ed. A. D. Robson (Dordrecht: Springer), 93–106. doi: 10.1007/978-94-011-0878-2_7

Bughio, N., Yamaguchi, H., Nishizawa, N. K., Nakanishi, H., and Mori, S. (2002). Cloning an iron−regulated metal transporter from rice. *J. Exp. Bot.* 53, 1677–1682. doi: 10.1093/jxb/erf004

Cakmak, I. (2000). Tansley review no. 111 Possible roles of zinc in protecting plant cells from damage by reactive oxygen species. *New Phytol.* 146, 185–205. doi: 10.1046/j.1469-8137.2000.00630.x

Cakmak, I. (2008). Enrichment of cereal grains with zinc: agronomic or genetic biofortification? *Plant Soil* 302, 1–17. doi: 10.1007/s11104-007-9466-3

Cakmak, I., Marschner, H., and Bangerth, F. (1989). Effect of zinc nutritional status on growth, protein metabolism and levels of indole-3-acetic acid and other phytohormones in bean (*Phaseolus vulgaris* L.). *J. Exp. Bot.* 40, 405–412. doi: 10.1093/jxb/40.3.405

Castro, P. H., Lilay, G. H., Muñoz-Mérida, A., Schjoerring, J. K., Azevedo, H., and Assunção, A. G. (2017). Phylogenetic analysis of F-bZIP transcription factors indicates conservation of the zinc deficiency response across land plants. *Sci. Rep.* 7, 1–14. doi: 10.1038/s41598-017-03903-6

Ceasar, S. A., Hodge, A., Baker, A., and Baldwin, S. A. (2014). Phosphate concentration and arbuscular mycorrhizal colonisation influence the growth, yield and expression of twelve PHT1 family phosphate transporters in foxtail millet (*Setaria italica*). *PLoS One* 9:e108459. doi: 10.1371/journal.pone.0108459

Chen, W., Feng, Y., and Chao, Y. (2008). Genomic analysis and expression pattern of OsZIP1, OsZIP3, and OsZIP4 in two rice (*Oryza sativa* L.) genotypes with different zinc efficiency. *Russ. J. Plant Physiol.* 55, 400–409. doi: 10.1134/S1021443708030175

Chiang, H. C., Lo, J. C., and Yeh, K. C. (2006). Genes associated with heavy metal tolerance and accumulation in Zn/Cd hyperaccumulator *Arabidopsis halleri*: a genomic survey with cDNA microarray. *Environ. Sci. Technol.* 40, 6792–6798. doi: 10.1021/es061432y

Claus, J., and Chavarría-Krauser, A. (2012). Modeling regulation of zinc uptake via ZIP transporters in yeast and plant roots. *PLoS One* 8:e37193. doi: 10.1371/journal.pone.0037193

Clemens, S. (2001). Molecular mechanisms of plant metal tolerance and homeostasis. *Planta* 212, 475–486. doi: 10.1007/s004250000458

Conte, S. S., and Walker, E. L. (2011). Transporters contributing to iron trafficking in plants. *Mol. Plant* 4, 464–476. doi: 10.1093/mp/ssr015

Corrêa, L. G. G., Riaño-Pachón, D. M., Schrago, C. G., dos Santos, R. V., Mueller-Roeber, B., and Vincentz, M. (2008). The role of bZIP transcription factors in green plant evolution: adaptive features emerging from four founder genes. *PLoS One* 3:e2944. doi: 10.1371/journal.pone.0002944

Deshpande, P., Dapkekar, A., Oak, M., Paknikar, K., and Rajwade, J. (2018). Nanocarrier-mediated foliar zinc fertilization influences expression of metal homeostasis related genes in flag leaves and enhances gluten content in durum wheat. *PLoS One* 13:e0191035. doi: 10.1371/journal.pone.0191035

Devaiah, B. N., Karthikeyan, A. S., and Raghothama, K. G. (2007a). WRKY75 transcription factor is a modulator of phosphate acquisition and root development in *Arabidopsis*. *Plant Physiol.* 143, 1789–1801. doi: 10.1104/pp.106.093971

Devaiah, B. N., Madhuvanthi, R., Karthikeyan, A. S., and Raghothama, K. G. (2009). Phosphate starvation responses and gibberellic acid biosynthesis are regulated by the MYB62 transcription factor in *Arabidopsis*. *Mol. Plant* 2, 43–58. doi: 10.1093/mp/ssn081

Devaiah, B. N., Nagarajan, V. K., and Raghothama, K. G. (2007b). Phosphate homeostasis and root development in *Arabidopsis* are synchronized by the zinc finger transcription factor ZAT6. *Plant Physiol.* 145, 147–159. doi: 10.1104/pp.107.101691

Doust, A. N., Kellogg, E. A., Devos, K. M., and Bennetzen, J. L. (2009). Foxtail millet: a sequence-driven grass model system. *Plant Physiol.* 149, 137–141. doi: 10.1104/pp.108.129627

Durmaz, E., Coruh, C., Dinler, G., Grusak, M. A., Peleg, Z., Saranga, Y., et al. (2011). Expression and cellular localization of ZIP1 transporter under zinc deficiency in wild emmer wheat. *Plant Mol. Biol. Rep.* 29, 582–596. doi: 10.1007/s11105-010-0264-3

Eide, D., Broderius, M., Fett, J., and Guerinot, M. L. (1996). A novel iron-regulated metal transporter from plants identified by functional expression in yeast. *Proc. Natl. Acad. Sci. U.S.A.* 93, 5624–5628. doi: 10.1073/pnas.93.11.5624

Eide, D. J. (1998). The molecular biology of metal ion transport in *Saccharomyces cerevisiae*. *Annu. Rev. Nutr.* 18, 441–469. doi: 10.1146/annurev.nutr.18.1.441

Eide, D. J. (2005). "The zip family of zinc transporters," in *Zinc Finger Proteins. Molecular Biology Intelligence Unit*, eds S. Iuchi, and N. Kuldell (Boston, MA: Springer), 261–264. doi: 10.1007/0-387-27421-9_35

Eide, D. J. (2006). Zinc transporters and the cellular trafficking of zinc. *BBA Mol. Cell Res.* 1763, 711–722. doi: 10.1016/j.bbamcr.2006.03.005

Ekiz, H., Bagci, S., Kiral, A., Eker, S., Gültekin, I., Alkan, A., et al. (1998). Effects of zinc fertilization and irrigation on grain yield and zinc concentration of various cereals grown in zinc−deficient calcareous soils. *J. Plant Nutr.* 21, 2245–2256. doi: 10.1080/01904169809365558

Ekweagwu, E., Agwu, A., and Madukwe, E. (2008). The role of micronutrients in child health: a review of the literature. *Afr. J. Biotechnol.* 7, 3805–3810.

Eswar, N., Webb, B., Marti−Renom, M. A., Madhusudhan, M. S., Eramian, D., Shen, M. Y., et al. (2007). Comparative protein structure modeling using MODELLER. *Curr. Protoc. Protein Sci.* 50, 2–9. doi: 10.1002/0471140864.ps0209s50

Etebu, E., and Nwauzoma, A. (2014). A review on sweet orange (*Citrus sinensis* L Osbeck): health, diseases and management. *Am. J. Res. Commun.* 2, 33–70.

Evens, N. P., Buchner, P., Williams, L. E., and Hawkesford, M. J. (2017). The role of ZIP transporters and group F bZIP transcription factors in the Zn−deficiency response of wheat (*Triticum aestivum*). *Plant J.* 92, 291–304. doi: 10.1111/tpj.13655

FAO (2000). *Calcareous Soils. FAO AGL Land and Plant Nutrition Management Services*. Available online at: www.fao.org/ag/agl/agll/prosoil/calc.htm (accessed February 24, 2009).

Fei, X., Fu, X. Z., Wang, N. Q., Xi, J. L., Huang, Y., Wei, Z., et al. (2016). Physiological changes and expression characteristics of ZIP family genes under zinc deficiency in navel orange (*Citrus sinensis*). *J. Integr. Agric.* 15, 803–811. doi: 10.1016/S2095-3119(15)61276-X

Fu, X. Z., Zhou, X., Xing, F., Ling, L. L., Chun, C. P., Cao, L., et al. (2017). Genome-wide identification, cloning and functional analysis of the zinc/iron-regulated transporter-like protein (ZIP) gene family in trifoliate orange (*Poncirus trifoliata* L. Raf.). *Front. Plant Sci.* 8:588. doi: 10.3389/fpls.2017.00588

Gaitán-Solís, E., Taylor, N. J., Siritunga, D., Stevens, W., and Schachtman, D. P. (2015). Overexpression of the transporters AtZIP1 and AtMTP1 in cassava changes zinc accumulation and partitioning. *Front. Plant Sci.* 6:492. doi: 10.3389/fpls.2015.00492

Gepts, P., Aragão, F. J., De Barros, E., Blair, M. W., Brondani, R., Broughton, W., et al. (2008). "Genomics of phaseolus beans, a major source of dietary protein and micronutrients in the tropics," in *Genomics of Tropical Crop Plants. Plant*

Genetics and Genomics: Crops and Models, Vol. 1, eds P. H. Moore, and R. Ming (New York, NY: Springer), 113–143. doi: 10.1007/978-0-387-71219-2_5

Grotz, N., Fox, T., Connolly, E., Park, W., Guerinot, M. L., and Eide, D. (1998). Identification of a family of zinc transporter genes from *Arabidopsis* that respond to zinc deficiency. *Proc. Natl. Acad. Sci.U.S.A.* 95, 7220–7224. doi: 10.1073/pnas.95.12.7220

Grotz, N., and Guerinot, M. L. (2006). Molecular aspects of Cu, Fe and Zn homeostasis in plants. *BBA Mol. Cell. Res.* 1763, 595–608. doi: 10.1016/j.bbamcr.2006.05.014

Guerinot, M. L. (2000). The ZIP family of metal transporters. *BBA Biomembranes* 1465, 190–198. doi: 10.1016/s0005-2736(00)00138-3

Hacisalihoglu, G., Hart, J. J., and Kochian, L. V. (2001). High-and low-affinity zinc transport systems and their possible role in zinc efficiency in bread wheat. *Plant Physiol.* 125, 456–463. doi: 10.1104/pp.125.1.456

Hacisalihoglu, G., and Kochian, L. V. (2003). How do some plants tolerate low levels of soil zinc? Mechanisms of zinc efficiency in crop plants. *New Phytol.* 159, 341–350. doi: 10.1046/j.1469-8137.2003.00826.x

Hanikenne, M., Talke, I. N., Haydon, M. J., Lanz, C., Nolte, A., Motte, P., et al. (2008). Evolution of metal hyperaccumulation required cis-regulatory changes and triplication of HMA4. *Nature* 453:391. doi: 10.1038/nature06877

Hänsch, R., and Mendel, R. R. (2009). Physiological functions of mineral micronutrients (Cu, Zn, Mn, Fe, Ni, Mo, B, Cl). *Curr. Opin. Plant Biol.* 12, 259–266. doi: 10.1016/j.pbi.2009.05.006

Henriques, A., Farias, D., and de Oliveira Costa, A. (2017). Identification and characterization of the bZIP transcription factor involved in zinc homeostasis in cereals. *Genet. Mol. Res.* 16, 1–10. doi: 10.4238/gmr16029558

Horak, V., and Trčka, I. (1976). The influence of Zn^{2+} ions on the tryptophan biosynthesis in plants. *Biol. Plant.* 18, 393–396. doi: 10.1007/BF02922471

Hussain, D., Haydon, M. J., Wang, Y., Wong, E., Sherson, S. M., Young, J., et al. (2004). P-type ATPase heavy metal transporters with roles in essential zinc homeostasis in *Arabidopsis*. *Plant Cell* 16, 1327–1339. doi: 10.1105/tpc.020487

Impa, S. M., Morete, M. J., Ismail, A. M., Schulin, R., and Johnson-Beebout, S. E. (2013). Zn uptake, translocation and grain Zn loading in rice (*Oryza sativa* L.) genotypes selected for Zn deficiency tolerance and high grain Zn. *J. Exp. Bot.* 22, 2739–2751. doi: 10.1093/jxb/ert118

Inaba, S., Kurata, R., Kobayashi, M., Yamagishi, Y., Mori, I., Ogata, Y., et al. (2015). Identification of putative target genes of bZIP19, a transcription factor essential for *Arabidopsis* adaptation to Zn deficiency in roots. *Plant J.* 84, 323–334. doi: 10.1111/tpj.12996

Ishimaru, Y., Masuda, H., Suzuki, M., Bashir, K., Takahashi, M., Nakanishi, H., et al. (2007). Overexpression of the OsZIP4 zinc transporter confers disarrangement of zinc distribution in rice plants. *J. Exp. Bot.* 58, 2909–2915. doi: 10.1093/jxb/erm147

Ishimaru, Y., Suzuki, M., Kobayashi, T., Takahashi, M., Nakanishi, H., Mori, S., et al. (2005). OsZIP4, a novel zinc-regulated zinc transporter in rice. *J. Exp. Bot.* 56, 3207–3214. doi: 10.1093/jxb/eri317

Ishimaru, Y., Suzuki, M., Tsukamoto, T., Suzuki, K., Nakazono, M., Kobayashi, T., et al. (2006). Rice plants take up iron as an Fe^{3+}−phytosiderophore and as Fe^{2+}. *Plant J.* 45, 335–346. doi: 10.1111/j.1365-313X.2005.02624.x

Ishimaru, Y., Bashir, K., and Nishizawa, N. K. (2011). Zn uptake and translocation in rice plants. *Rice* 4, 21–27. doi: 10.1007/s12284-011-9061-3

Jakoby, M., Weisshaar, B., Dröge-Laser, W., Vicente-Carbajosa, J., Tiedemann, J., Kroj, T., et al. (2002). bZIP transcription factors in *Arabidopsis*. *Trends Plant Sci.* 7, 106–111. doi: 10.1016/s1360-1385(01)02223-3

Kaiser, C., Kilburn, M. R., Clode, P. L., Fuchslueger, L., Koranda, M., Cliff, J. B., et al. (2015). Exploring the transfer of recent plant photosynthates to soil microbes: mycorrhizal pathway vs direct root exudation. *New Phytol.* 205, 1537–1551. doi: 10.1111/nph.13138

Kavitha, P., Kuruvilla, S., and Mathew, M. (2015). Functional characterization of a transition metal ion transporter, OsZIP6 from rice (*Oryza sativa* L.). *Plant Physiol. Biochem.* 97, 165–174. doi: 10.1016/j.plaphy.2015.10.005

Khan, G. A., Bouraine, S., Wege, S., Li, Y., de Carbonnel, M., Berthomieu, P., et al. (2014). Coordination between zinc and phosphate homeostasis involves the transcription factor PHR1, the phosphate exporter PHO1, and its homologue PHO1; H3 in *Arabidopsis*. *J. Exp. Bot.* 13, 871–884. doi: 10.1093/jxb/ert444

Krishna, T. P. A., Ceasar, S. A., Maharajan, T., Ramakrishnan, M., Duraipandiyan, V., Al-Dhabi, N., et al. (2017). Improving the zinc-use efficiency in plants: a review. *SABRAO J. Breed. Genet.* 49, 221–230.

Krithika, S., and Balachandar, D. (2016). Expression of zinc transporter genes in rice as influenced by zinc-solubilizing *Enterobacter cloacae* strain ZSB14. *Front. Plant Sci.* 7:446. doi: 10.3389/fpls.2016.00446

Kumar, L., Meena, N. L., Singh, U., Singh, U., Praharaj, C., Singh, S., et al. (eds) (2016). "Zinc transporter: mechanism for improving Zn availability," in *Biofortification of Food Crops* (New Delhi: Springer), 129–146. doi: 10.1007/978-81-322-2716-8_11

Lata, C., Gupta, S., and Prasad, M. (2013). Foxtail millet: a model crop for genetic and genomic studies in bioenergy grasses. *Crit. Rev. Biotechnol.* 33, 328–343. doi: 10.3109/07388551.2012.716809

Lee, S., and An, G. (2009). Over−expression of OsIRT1 leads to increased iron and zinc accumulations in rice. *Plant Cell Environ.* 32, 408–416. doi: 10.1111/j.1365-3040.2009.01935.x

Lee, S., Jeong, H. J., Kim, S. A., Lee, J., Guerinot, M. L., and An, G. (2010a). OsZIP5 is a plasma membrane zinc transporter in rice. *Plant Mol. Biol.* 73, 507–517. doi: 10.1007/s11103-010-9637-0

Lee, S., Kim, S. A., Lee, J., Guerinot, M. L., and An, G. (2010b). Zinc deficiency-inducible OsZIP8 encodes a plasma membrane-localized zinc transporter in rice. *Mol. Cells* 29, 551–558. doi: 10.1007/s10059-010-0069-0

Li, S., Zhou, X., Huang, Y., Zhu, L., Zhang, S., Zhao, Y., et al. (2013). Identification and characterization of the zinc-regulated transporters, iron-regulated transporter-like protein (ZIP) gene family in maize. *BMC Plant Biol.* 13:114. doi: 10.1186/1471-2229-13-114

Li, S., Zhou, X., Li, H., Liu, Y., Zhu, L., Guo, J., et al. (2015). Overexpression of ZmIRT1 and ZmZIP3 enhances iron and zinc accumulation in transgenic *Arabidopsis*. *PLoS One* 10:e0136647. doi: 10.1371/journal.pone.0136647

Lilay, G. H., Castro, P. H., Campilho, A., and Assunção, A. G. (2018). The *Arabidopsis* bZIP19 and bZIP23 activity requires zinc deficiency–insight on regulation from complementation lines. *Front. Plant Sci.* 9:1955. doi: 10.3389/fpls.2018.01955

Lilay, G. H., Castro, P. H., Guedes, J. G., Almeida, D. M., Campilho, A., Azevedo, H., et al. (2020). Rice F-bZIP transcription factors regulate the zinc deficiency response. *J. Exp. Bot.* 71, 1–14. doi: 10.1093/jxb/eraa115

Lin, Y. F., Liang, H. M., Yang, S. Y., Boch, A., Clemens, S., Chen, C. C., et al. (2009). *Arabidopsis* IRT3 is a zinc−regulated and plasma membrane localized zinc/iron transporter. *New Phytol.* 182, 392–404. doi: 10.1111/j.1469-8137.2009.02766.x

Lindsay, W. (1972). Zinc in soils and plant nutrition. *Adv. Agron.* 24, 147–186. doi: 10.1016/S0065-2113(08)60635-5

Marichali, A., Dallali, S., Ouerghemmi, S., Sebei, H., and Hosni, K. (2014). Germination, morpho-physiological and biochemical responses of coriander (*Coriandrum sativum* L.) to zinc excess. *Ind. Crops Prod.* 55, 248–257. doi: 10.1016/j.indcrop.2014.02.033

Marschner, H. (1995). *Marschner's Mineral Nutrition of Higher Plants*. Cambridge, MA: Academic press.

Marschner, H. (2011). *Marschner's Mineral Nutrition of Higher Plants*. Cambridge, MA: Academic press.

Mäser, P., Thomine, S., Schroeder, J. I., Ward, J. M., Hirschi, K., Sze, H., et al. (2001). Phylogenetic relationships within cation transporter families of *Arabidopsis*. *Plant Physiol.* 126, 1646–1667. doi: 10.1104/pp.126.4.1646

Meng, L., Sun, L., and Tan, L. (2018). Progress in ZIP transporter gene family in rice. *Yi Chuan* 40, 33–43. doi: 10.16288/j.yczz.17-238

Menguer, P. K., Vincent, T., Miller, A. J., Brown, J. K., Vincze, E., Borg, S., et al. (2018). Improving zinc accumulation in cereal endosperm using HvMTP1, a transition metal transporter. *Plant Biotechnol. J.* 16, 63–71. doi: 10.1111/pbi.12749

Milner, M. J., Seamon, J., Craft, E., and Kochian, L. V. (2013). Transport properties of members of the ZIP family in plants and their role in Zn and Mn homeostasis. *J. Exp. Bot.* 64, 369–381. doi: 10.1093/jxb/ers315

Mitra, G. N. (2015). "Zinc (Zn) uptake," in *Regulation of Nutrient Uptake by Plants – A Biochemical and Molecular Approach* (New Delhi: Springer), 127–133.

Mondal, T. K., Ganie, S. A., Rana, M. K., and Sharma, T. R. (2013). Genome-wide analysis of zinc transporter genes of maize (*Zea mays*). *Plant Mol. Biol. Rep.* 32, 605–616. doi: 10.1007/s11105-013-0664-2

Moreau, S., Thomson, R. M., Kaiser, B. N., Trevaskis, B., Guerinot, M. L., Udvardi, M. K., et al. (2002). GmZIP1 encodes a symbiosis-specific zinc transporter in soybean. *J. Biol. Chem.* 277, 4738–4746. doi: 10.1074/jbc.M106754200

Mousavi, S. R. (2011). Zinc in crop production and interaction with phosphorus. *Aust. J. Basic Appl. Sci.* 5, 1503–1509.

Nakanishi, H., Ogawa, I., Ishimaru, Y., Mori, S., and Nishizawa, N. K. (2006). Iron deficiency enhances cadmium uptake and translocation mediated by the Fe^{2+} transporters OsIRT1 and OsIRT2 in rice. *Soil Sci. Plant Nutr.* 52, 464–469. doi: 10.1111/j.1747-0765.2006.00055.x

Nazri, A. Z., Griffin, J. H., Peaston, K. A., Alexander−Webber, D. G., and Williams, L. E. (2017). F−group bZIPs in barley–a role in Zn deficiency. *Plant Cell Environ.* 40, 2754–2770. doi: 10.1111/pce.13045

Nene, Y. (1966). Symptoms, cause and control of Khaira disease of paddy. *Bull. Indian Phytopathol. Soc.* 3, 97–191.

Nijhawan, A., Jain, M., Tyagi, A. K., and Khurana, J. P. (2008). Genomic survey and gene expression analysis of the basic leucine zipper transcription factor family in rice. *Plant Physiol.* 146, 333–350. doi: 10.1104/pp.107.112821

Palmer, L. E., Rabinowicz, P. D., Shaughnessy, A. L., Balija, V. S., Nascimento, L. U., Dike, S., et al. (2003). Maize genome sequencing by methylation filtration. *Science* 302, 2115–2117.

Palmgren, M. G., Clemens, S., Williams, L. E., Krämer, U., Borg, S., Schjørring, J. K., et al. (2008). Zinc biofortification of cereals: problems and solutions. *Trends Plant Sci.* 13, 464–473. doi: 10.1016/j.tplants.2008.06.005

Pedas, P., and Husted, S. (2009). Zinc transport mediated by barley ZIP proteins are induced by low pH. *Plant Signal. Behav.* 4, 842–845. doi: 10.4161/psb.4.9.9375

Pedas, P., Schjoerring, J. K., and Husted, S. (2009). Identification and characterization of zinc-starvation-induced ZIP transporters from barley roots. *Plant Physiol. Biochem.* 47, 377–383. doi: 10.1016/j.plaphy.2009.01.006

Pellegrino, E., and Bedini, S. (2014). Enhancing ecosystem services in sustainable agriculture: biofertilization and biofortification of chickpea (*Cicer arietinum* L.) by arbuscular mycorrhizal fungi. *Soil Biol. Biochem.* 68, 429–439. doi: 10.1016/j.soilbio.2013.09.030

Pellegrino, E., Bosco, S., Ciccolini, V., Pistocchi, C., Sabbatini, T., Silvestri, N., et al. (2015). Agricultural abandonment in Mediterranean reclaimed peaty soils: long-term effects on soil chemical properties, arbuscular mycorrhizas and CO2 flux. *Agric. Ecosyst. Environ.* 199, 164–175. doi: 10.1016/j.agee.2014.09.004

Rai, V., Sanagala, R., Sinilal, B., Yadav, S., Sarkar, A. K., Dantu, P. K., et al. (2015). Iron availability affects phosphate deficiency-mediated responses, and evidence of cross-talk with auxin and zinc in *Arabidopsis*. *Plant Cell Physiol.* 56, 1107–1123. doi: 10.1093/pcp/pcv035

Ramegowda, Y., Venkategowda, R., Jagadish, P., Govind, G., Hanumanthareddy, R. R., Makarla, U., et al. (2013). Expression of a rice Zn transporter, OsZIP1, increases Zn concentration in tobacco and finger millet transgenic plants. *Plant Biotechnol. Rep.* 7, 309–319. doi: 10.1007/s11816-012-0264-x

Ramesh, S. A., Choimes, S., and Schachtman, D. P. (2004). Over-expression of an *Arabidopsis* zinc transporter in *Hordeum vulgare* increases short-term zinc uptake after zinc deprivation and seed zinc content. *Plant Mol. Biol.* 54, 373–385. doi: 10.1023/B:PLAN.0000036370.70912.34

Ramesh, S. A., Shin, R., Eide, D. J., and Schachtman, D. P. (2003). Differential metal selectivity and gene expression of two zinc transporters from rice. *Plant Physiol.* 133, 126–134. doi: 10.1104/pp.103.026815

Regmi, B. D., Rengel, Z., and Khabaz-Saberi, H. O. (2010). Zinc deficiency in agricultural systems and its implication to human health. *Int. J. Environ. Rural Dev.* 1, 98–103.

Rubio, V., Linhares, F., Solano, R., Martín, A. C., Iglesias, J., Leyva, A., et al. (2001). A conserved MYB transcription factor involved in phosphate starvation signaling both in vascular plants and in unicellular algae. *Genes Dev.* 15, 2122–2133. doi: 10.1101/gad.204401

Ruel, M. T., and Bouis, H. E. (1998). Plant breeding: a long-term strategy for the control of zinc deficiency in vulnerable populations. *Am. J. Clin. Nutr.* 68, 488–494. doi: 10.1093/ajcn/68.2.488S

Sadeghzadeh, B. (2013). A review of zinc nutrition and plant breeding. *J. Soil Sci. Plant Nutr.* 13, 905–927. doi: 10.4067/S0718-95162013005000072

Samreen, T., Shah, H. U., Ullah, S., and Javid, M. (2017). Zinc effect on growth rate, chlorophyll, protein and mineral contents of hydroponically grown mungbeans plant (*Vigna radiata*). *Arab. J. Chem.* 10, S1802–S1807. doi: 10.1016/j.arabjc.2013.07.005

Sasaki, A., Yamaji, N., Mitani−Ueno, N., Kashino, M., and Ma, J. F. (2015). A node−localized transporter OsZIP3 is responsible for the preferential distribution of Zn to developing tissues in rice. *Plant J* 84, 374–384. doi: 10.1111/tpj.13005

Sharma, P., Chatterjee, C., Sharma, C., Nautiyal, N., and Agarwala, S. (1979). Effect of zinc deficiency on the development and physiology of wheat pollen. *J. Indian Bot. Soc.* 58, 330–334.

Sharma, P. N., Chatterjee, C., Sharma, C. P., and Agarwala, S. C. (1987). Zinc deficiency and anther development in maize. *Plant Cell Physiol.* 28, 11–18. doi: 10.1093/oxfordjournals.pcp.a077265

Shaul, O., Hilgemann, D. W., Almeida−Engler, J., Van Montagu, M., Inzé, D., and Galili, G. (1999). Cloning and characterization of a novel $Mg^{2+/}H^{+}$ exchanger. *EMBO J.* 15, 3973–3980. doi: 10.1093/emboj/18.14.3973

Shiferaw, B., Prasanna, B. M., Hellin, J., and Bänziger, M. (2011). Crops that feed the world 6. Past successes and future challenges to the role played by maize in global food security. *Food Secur.* 3, 307–327. doi: 10.1007/s12571-011-0140-5

Shiferaw, B., Smale, M., Braun, H. J., Duveiller, E., Reynolds, M., and Muricho, G. (2013). Crops that feed the world 10. Past successes and future challenges to the role played by wheat in global food security. *Food Secur.* 5, 291–317. doi: 10.1007/s12571-013-0263-y

Skoog, F. (1940). Relationships between zinc and auxin in the growth of higher plants. *Am. J. Bot.* 27, 939–951. doi: 10.1002/j.1537-2197.1940.tb13958.x

Suzuki, M., Bashir, K., Inoue, H., Takahashi, M., Nakanishi, H., and Nishizawa, N. K. (2012). Accumulation of starch in Zn-deficient rice. *Rice* 5, 1–8. doi: 10.1186/1939-8433-5-9

Suzuki, M., Takahashi, M., Tsukamoto, T., Watanabe, S., Matsuhashi, S., Yazaki, J., et al. (2006). Biosynthesis and secretion of mugineic acid family phytosiderophores in zinc−deficient barley. *Plant J.* 48, 85–97. doi: 10.1111/j.1365-313X.2006.02853.x

Tamura, K., Stecher, G., Peterson, D., Filipski, A., and Kumar, S. (2013). MEGA6: molecular evolutionary genetics analysis version 6.0. *Mol. Biol. Evol.* 16, 2725–2729. doi: 10.1093/molbev/mst197

Tan, L., Zhu, Y., Fan, T., Peng, C., Wang, J., Sun, L., et al. (2019). OsZIP7 functions in xylem loading in roots and inter-vascular transfer in nodes to deliver Zn/Cd to grain in rice. *Biochem. Biophys. Res. Commun.* 512, 112–118. doi: 10.1016/j.bbrc.2019.03.024

Tiong, J., McDonald, G., Genc, Y., Shirley, N., Langridge, P., and Huang, C. Y. (2015). Increased expression of six ZIP family genes by zinc (Zn) deficiency is associated with enhanced uptake and root−to−shoot translocation of Zn in barley (*Hordeum vulgare*). *New Phytol.* 207, 1097–1109. doi: 10.1111/nph.13413

Tiong, J., McDonald, G. K., Genc, Y., Pedas, P., Hayes, J. E., Toubia, J., et al. (2014). HvZIP7 mediates zinc accumulation in barley (*Hordeum vulgare*) at moderately high zinc supply. *New Phytol.* 201, 131–143. doi: 10.1111/nph.12468

Tsui, C. (1948). The role of zinc in auxin synthesis in the tomato plant. *Am. J. Bot.* 35, 172–179.

Van de Mortel, J. E., Villanueva, L. A., Schat, H., Kwekkeboom, J., Coughlan, S., Moerland, P. D., et al. (2006). Large expression differences in genes for iron and zinc homeostasis, stress response, and lignin biosynthesis distinguish roots of *Arabidopsis thaliana* and the related metal hyperaccumulator *Thlaspi caerulescens*. *Plant Physiol.* 142, 1127–1147. doi: 10.1104/pp.106.082073

Vatansever, R., Özyigit, I. I., and Filiz, E. (2016). Comparative and phylogenetic analysis of zinc transporter genes/proteins in plants. *Turk. J. Biol.* 40, 600–611. doi: 10.3906/biy-1501-91

Vert, G., Briat, J. F., and Curie, C. (2001). *Arabidopsis* IRT2 gene encodes a root−periphery iron transporter. *Plant J.* 26, 181–189. doi: 10.1046/j.1365-313x.2001.01018.x

Wang, H., and Jin, J. (2005). Photosynthetic rate, chlorophyll fluorescence parameters, and lipid peroxidation of maize leaves as affected by zinc deficiency. *Photosynthetica* 43, 591–596. doi: 10.1007/s11099-005-0092-0

Watts-Williams, S. J., and Cavagnaro, T. R. (2018). Arbuscular mycorrhizal fungi increase grain zinc concentration and modify the expression of root ZIP transporter genes in a modern barley (*Hordeum vulgare*) cultivar. *Plant Sci.* 274, 163–170. doi: 10.1016/j.plantsci.2018.05.015

Wissuwa, M., Ismail, A. M., and Graham, R. D. (2008). Rice grain zinc concentrations as affected by genotype, native soil-zinc availability, and zinc fertilization. *Plant Soil* 306, 37–48. doi: 10.1007/s11104-007-9368-4

Xie, X., Hu, W., Fan, X., Chen, H., and Tang, M. (2019). Interactions between phosphorus, zinc, and iron homeostasis in non mycorrhizal and mycorrhizal plants. *Front. Plant Sci.* 10:1172. doi: 10.3389/fpls.2019.01172

Xi-wen, Y., Xiao-hong, T., Xin-chun, L., William, G., and Yu-xian, C. (2011). Foliar zinc fertilization improves the zinc nutritional value of wheat (*Triticum aestivum* L.) grain. *Afri. J. Biotechnol.* 10, 14778–14785. doi: 10.5897/AJB11.780

Yang, X., Huang, J., Jiang, Y., and Zhang, H. S. (2009). Cloning and functional identification of two members of the ZIP (Zrt, Irt-like protein) gene family

in rice (*Oryza sativa* L.). *Mol. Bio. Rep.* 36, 281–287. doi: 10.1007/s11033-007-9177-0

Yoshida, S., and Tanaka, A. (1969). Zinc deficiency of the rice plant in calcareous soils. *Soil Sci. Plant Nutr.* 15, 75–80. doi: 10.1080/00380768.1969.10432783

Zhang, G., Liu, X., Quan, Z., Cheng, S., Xu, X., Pan, S., et al. (2012). Genome sequence of foxtail millet (*Setaria italica*) provides insights into grass evolution and biofuel potential. *Nat. Biotechnol.* 30, 549–553. doi: 10.1038/nbt.2195

Zhang, T., Liu, J., Fellner, M., Zhang, C., Sui, D., and Hu, J. (2017). Crystal structures of a ZIP zinc transporter reveal a binuclear metal center in the transport pathway. *Sci. Adv.* 3:e1700344. doi: 10.1126/sciadv.1700344

Zhao, H., and Eide, D. (1996a). The yeast ZRT1 gene encodes the zinc transporter protein of a high-affinity uptake system induced by zinc limitation. *Proc. Natl. Acad. Sci. U.S.A.* 93, 2454–2458. doi: 10.1073/pnas.93.6.2454

Zhao, H., and Eide, D. (1996b). The ZRT2 gene encodes the low affinity zinc transporter in *Saccharomyces cerevisiae*. *J. Biol. Chem.* 271, 23203–23210. doi: 10.1074/jbc.271.38.23203

Zimin, A. V., Puiu, D., Hall, R., Kingan, S., Clavijo, B. J., and Salzberg, S. L. (2017). The first near-complete assembly of the hexaploid bread wheat genome, *Triticum aestivum*. *GigaScience* 6, 1–7. doi: 10.1093/gigascience/gix097

Conflict of Interest: The authors declare that the research was conducted in the absence of any commercial or financial relationships that could be construed as a potential conflict of interest.

frontiers in Plant Science

PERSPECTIVE
published: 29 May 2020
doi: 10.3389/fpls.2020.00725

Transcriptional Regulation of Iron Distribution in Seeds: A Perspective

Hannetz Roschzttardtz[1], Frederic Gaymard[2] and Christian Dubos[2]*

[1]Faculty of Biological Sciences, Pontificia Universidad Católica de Chile, Santiago, Chile, [2]BPMP, University of Montpellier, CNRS, INRAE, SupAgro, Montpellier, France

Several transcription factors have been involved in the regulation of gene expression during seed development. Nutritional reserves, including iron, are principally accumulated during seed maturation stages. Using the model plant *Arabidopsis thaliana*, it has been shown that iron is stored during seed development in vacuoles of the endodermis cell layer. During seed germination, these iron reserves are remobilized and used by the seedling during the heterotrophic to autotrophic metabolism switch. To date, no information about how iron distribution is genetically regulated has been reported.

Keywords: seed, embryo, iron, transcription factors, regulation

OPEN ACCESS

Edited by:
Tomoko Nozoye, Meiji Gakuin University, Japan

Reviewed by:
Rumen Ivanov, Heinrich Heine University of Düsseldorf, Germany
Eduardo Zabaleta, CONICET Mar del Plata, Argentina

****Correspondence:***
Hannetz Roschzttardtz
hroschzttardtz@bio.puc.cl

Specialty section:
This article was submitted to Plant Traffic and Transport, a section of the journal Frontiers in Plant Science

Received: *20 February 2020*
Accepted: *06 May 2020*
Published: *29 May 2020*

Citation:
Roschzttardtz H, Gaymard F and Dubos C (2020) Transcriptional Regulation of Iron Distribution in Seeds: A Perspective. Front. Plant Sci. 11:725. doi: 10.3389/fpls.2020.00725

INTRODUCTION

Among the mineral nutrients required for plant metabolism, iron plays a central role as it is necessary for the activity of several proteins involved in various cellular processes such as photosynthesis, respiration, or the biosynthesis of primary and secondary metabolites (Couturier et al., 2013; Lu et al., 2013; Briat et al., 2015). Therefore, iron is a key element for crop yield and seed quality (Briat et al., 2015). Considering that metals' (such as iron or zinc) content has decreased since the 1960s (Fan et al., 2008; DeFries et al., 2015), it appears obvious that increasing (bio-fortification), or at least maintaining, iron content in seeds is a challenge that must be met in order to combat the growing public health problem that is iron dependent anemia.

When developing bio-fortification strategies for grains, knowing the total amount of nutrient in seeds is not sufficient. Modulating the intracellular partitioning of iron or the chemical iron complex nature that can modify its bioavailability is a part of the tools that can be used to reach such goal (Zielińska-Dawidziak, 2015; Moore et al., 2018). It is also important to determine the localization of nutrients present at the tissue and cell type levels within the seed, as well as identifying the intracellular structures in which iron is stored. Such knowledge is of importance as, in addition to, enhancing the flux of nutrients toward the seeds, one strategy could be extending the number of cells, cell types, or tissues displaying iron storage capacity in the embryos (Roschzttardtz et al., 2017).

IRON LOCALIZATION IN SEED PLANTS

Traditionally, seed iron metabolism has been studied in the model plant *Arabidopsis thaliana* (Brassicaceae). Using synchrotron-based micro X-ray fluorescence and the Perls/DAB stain method, it has been possible to show that iron is loaded solely in the endodermis cell layer of the embryo during *Arabidopsis* seed maturation (Kim et al., 2006; Roschzttardtz et al., 2009). In contrast, a recent publication indicates that quinoa (*Chenopodium quinoa*, Chenopodiaceae) seed embryos have a different and larger iron distribution compared to *Arabidopsis* (Ibeas et al., 2019).

In quinoa embryos, iron is detected, by synchrotron-based micro X-ray fluorescence and Perls/DAB stain, in cortex and endodermis cells, showing that this specific pattern of iron accumulation in quinoa embryos may explain why quinoa seeds contain more iron than the ones of *Arabidopsis*. This discovery highlights that iron distribution in seeds may vary depending on the plant species, in a way that could be different from *Arabidopsis* defining – from a phylogenetic point of view – this accumulation pattern as an apomorphic character (Ibeas et al., 2019).

At the intracellular level, the major fraction of total iron contained in *Arabidopsis* seeds is stored in vacuoles while ferritins play a minor role in this process, about 2% (Ravet et al., 2009). Interestingly, the relative amount of iron stored in vacuoles versus ferritins in seeds has been shown to depend on the plant species. For instance, in legumes, the fraction of total iron contained in ferritins is ranges from 15% in red kidney beans up to 70% in lentils (Hoppler et al., 2009; Moore et al., 2018). This observation is of importance as it emphasizes the necessity of determining the nature of iron storage in crop seeds, as plant ferritin is one of the main targets for iron bio-fortification, because of the intrinsic structural and biochemical properties of these proteins (Zielińska-Dawidziak, 2015). Ferritins form nano-cages that are able to transiently store iron (up to 4,500 atoms) in a non-toxic form, playing a central role in the maintenance of cell integrity by limiting the production of reactive oxygen species (ROS) (Ravet et al., 2009). Ferritin expression and stability is tightly related to iron availability, participating to the control of iron homeostasis (Ravet et al., 2012). Ferritins, by isolating iron from the surrounding environment, allow enhancing the amount of iron in the edible part of the plants while reducing the production of ROS and avoid iron-induced oxidative change in food, thus reducing the risk of gastric problems in consumers (Zielińska-Dawidziak, 2015). Lastly, it has been demonstrated that the bioavailability of the iron present in ferritins, for human's and animal's metabolism, is high. Therefore, favoring iron storage in ferritins rather than in vacuoles, together with expending the number of cells that accumulate iron in the embryo, is a promising strategy in order to sustain iron content in crop seeds (Roschzttardtz et al., 2014, 2017; Zielińska-Dawidziak, 2015). This will indeed necessitate optimizing, in a coordinated manner, iron loading and storage in seeds together with the development and differentiation of the embryos.

GENETIC REGULATION OF SEED IRON LOADING

Embryo development and seed maturation is a complex mechanism involving several genes whose expression is tightly controlled by the activity of key transcription factors (TFs) (North et al., 2010). Among the TFs that have been identified as involved in this process, some are dedicated to the control of embryo development (Hardtke and Berleth, 1998), the size of the seeds (Garcia et al., 2005), the accumulation of secondary metabolites (Xu et al., 2015), or the maturation of the seed (Santos-Mendoza et al., 2008; Verdier and Thompson, 2008). The seed-filling step, allowing the accumulation of key nutrients such as lipids and storage proteins, is essentially controlled by a set of transcription factors named "master regulators." It includes an atypical NF-Y TF named LEC1 (LEAFY COTYLEDON1) and LEC2, FUS3 (FUSCA3) and ABI3 (ABSCISIC ACID INSENSITIVE3), and three TFs belonging to the plant specific B3 family (Santos-Mendoza et al., 2008). Because B3 TFs have functions in seed development and reserves accumulation (Boulard et al., 2017), it is likely that these master regulators could directly or indirectly be involved in different stages of iron loading in the seed. In support of this hypothesis, Roschzttardtz et al. (2009) described that an embryo specific-gene encoding one iron-sulfur subunit of mitochondrial complex II is regulated by B3 transcription factors. B3 TFs target RY *cis*-regulatory sequences. The presence of RY motif in the promoters of genes encoding proteins involved in iron homeostasis may suggest a direct regulation of these genes by B3 TFs (Boulard et al., 2017). Whether B3 TFs are regulating the unknown machinery involved in the iron delivery to the endodermis cells (involving genes related to the synthesis of iron ligands, transporters, or storage proteins) is still an open question that should be investigated since only a reduced number of genes involved in iron homeostasis in seed (Kim et al., 2006; Ravet et al., 2009) have been identified so far. This is in contrast to what is known at the seedlings and adult plant stages where several TFs involved in iron deficiency responses have been identified and characterized (Gao et al., 2019).

Several embryo master regulators act in concert with additional regulators belonging to other family of transcription factors such as WRI1 (WRINKLED1; AP2 family), bZIP10, bZIP25, bZIP53, and ABI5 (BASIC LEUCINE ZIPPER family) (Santos-Mendoza et al., 2008; Alonso et al., 2009; To et al., 2012). The transcriptional mechanisms that control the accumulation of lipids and storage proteins in embryos are relatively well described. However, no transcription factors have been directly associated with iron (or other micronutrients) loading into the seeds (**Figure 1**). Indeed, one may expect that key regulators of iron homeostasis in vegetative tissues (Gao et al., 2019) exert their function in seeds or embryos, since iron content defect were observed in the seeds of the corresponding loss-of-function

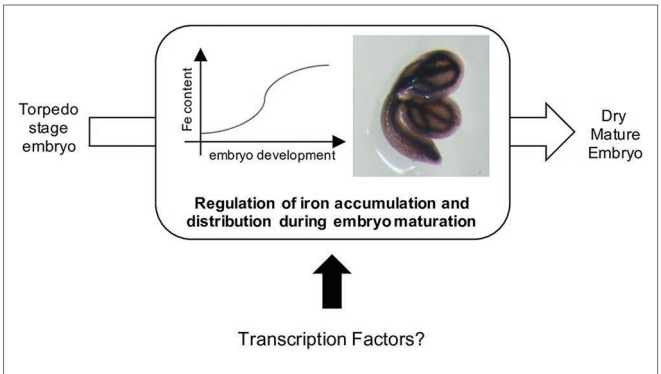

FIGURE 1 | Iron is accumulated in seed during the maturation of the embryo, from the torpedo stage (Ravet et al., 2009; Roschzttardtz et al., 2009). To date, no transcription factors involved in this process has been reported.

mutants (Li et al., 2016; Liang et al., 2017; Gao et al., 2020). However, to date, the data suggest that this is likely an indirect consequence of iron uptake defects at the root system level. On the other hand, one may expect that the abovementioned master regulators that regulate embryo development and seed maturation may be involved in the coordination of embryo lipids and reserve proteins accumulation together with other important (micro) nutrients such as iron.

PERSPECTIVE OR CONCLUSION

It is likely that plant species-specific molecular switches regulating iron storage in seeds have to be discovered and that "omic" driven strategies (e.g., large-scale expression studies) carried out on species differing in their iron storage strategy will allow their identification.

AUTHOR CONTRIBUTIONS

All authors participated in the writing of the manuscript.

FUNDING

FONDECYT 1160334, Chilean Government; ECOS-CONICYT C18C04.

REFERENCES

Alonso, R., Oñate-Sánchez, L., Weltmeier, F., Ehlert, A., Diaz, I., Dietrich, K., et al. (2009). A pivotal role of the basic leucine zipper transcription factor bZIP53 in the regulation of *Arabidopsis* seed maturation gene expression based on heterodimerization and protein complex formation. *Plant Cell* 21, 1747–1761. doi: 10.1105/tpc.108.062968

Boulard, C., Fatihi, A., Lepiniec, L., and Dubreucq, B. (2017). Regulation and evolution of the interaction of the seed B3 transcription factors with NF-Y subunits. *Biochim. Biophys. Acta Gene Regul. Mech.* 1860, 1069–1078. doi: 10.1016/j.bbagrm.2017.08.008

Briat, J. F., Dubos, C., and Gaymard, F. (2015). Iron nutrition, biomass production, and plant product quality. *Trends Plant Sci.* 20, 33–40. doi: 10.1016/j.tplants.2014.07.005

Couturier, J., Touraine, B., Briat, J. F., Gaymard, F., and Rouhier, N. (2013). The iron-sulfur cluster assembly machineries in plants: current knowledge and open questions. *Front. Plant Sci.* 4:259. doi: 10.3389/fpls.2013.00259

DeFries, R., Fanzo, J., Remans, R., Palm, C., Wood, S., and Anderman, T. L. (2015). Global nutrition. Metrics for land-scarce agriculture. *Science* 349, 238–240. doi: 10.1126/science.aaa5766

Fan, M. S., Zhao, F. J., Fairweather-Tait, S. J., Poulton, P. R., Dunham, S. J., and McGrath, S. P. (2008). Evidence of decreasing mineral density in wheat grain over the last 160 years. *J. Trace Elem. Med. Biol.* 22, 315–324. doi: 10.1016/j.jtemb.2008.07.002

Gao, F., Robe, K., Bettembourg, M., Navarro, N., Rofidal, V., Santoni, V., et al. (2020). The transcription factor bHLH121 interacts with bHLH105 (ILR3) and its closest homologs to regulate iron homeostasis in *Arabidopsis*. *Plant Cell* 32, 508–524. doi: 10.1105/tpc.19.00541

Gao, F., Robe, K., Gaymard, F., Izquierdo, E., and Dubos, C. (2019). The transcriptional control of iron homeostasis in plants: a tale of bHLH transcription factors? *Front. Plant Sci.* 10:6. doi: 10.3389/fpls.2019.00006

Garcia, D., Fitz Gerald, J. N., and Berger, F. (2005). Maternal control of integument cell elongation and zygotic control of endosperm growth are coordinated to determine seed size in *Arabidopsis*. *Plant Cell* 17, 52–60. doi: 10.1105/tpc.104.027136

Hardtke, C. S., and Berleth, T. (1998). The *Arabidopsis* gene MONOPTEROS encodes a transcription factor mediating embryo axis formation and vascular development. *EMBO J.* 17, 1405–1411. doi: 10.1093/emboj/17.5.1405

Hoppler, M., Zeder, C., and Walczyk, T. (2009). Quantification of ferritin-bound iron in plant samples by isotope tagging and species-specific isotope dilution mass spectrometry. *Anal. Chem.* 81, 7368–7372. doi: 10.1021/ac900885j

Ibeas, M., Grant-Grant, S., Coronas, M., Vargas-Pérez, J., Navarro, N., Abreu, I., et al. (2019). The diverse iron distribution in Eudicotyledoneae seeds: from *Arabidopsis* to quinoa. *Front. Plant Sci.* 9:1985. doi: 10.3389/fpls.2018.01985

Kim, S. A., Punshon, T., Lanzirotti, A., Li, L., Alonso, J. M., Ecker, J. R., et al. (2006). Localization of iron in *Arabidopsis* seed requires the vacuolar membrane transporter VIT1. *Science* 314, 1295–1298. doi: 10.1126/science.1132563

Li, X., Zhang, H., Ai, Q., Liang, G., and Yu, D. (2016). Two bHLH transcription factors, bHLH34 and bHLH104, regulate iron homeostasis in *Arabidopsis thaliana*. *Plant Physiol.* 170, 2478–2493. doi: 10.1104/pp.15.01827

Liang, G., Zhang, H., Li, X., Ai, Q., and Yu, D. (2017). bHLH transcription factor bHLH115 regulates iron homeostasis in *Arabidopsis thaliana*. *J. Exp. Bot.* 68, 1743–1755. doi: 10.1093/jxb/erx043

Lu, L., Tian, S., Liao, H., Zhang, J., Yang, X., Labavitch, J. M., et al. (2013). Analysis of metal element distributions in rice (*Oryza sativa* L.) seeds and relocation during germination based on X-ray fluorescence imaging of Zn, Fe, K, Ca, and Mn. *PLoS One* 8:e57360. doi: 10.1371/journal.pone.0057360

Moore, K. L., Rodríguez-Ramiro, I., Jones, E. R., Jones, E. J., Rodríguez-Celma, J., Halsey, K., et al. (2018). The stage of seed development influences iron bioavailability in pea (*Pisum sativum* L.). *Sci. Rep.* 8:6865. doi: 10.1038/s41598-018-25130-3

North, H., Baud, S., Debeaujon, I., Dubos, C., Dubreucq, B., Grappin, P., et al. (2010). *Arabidopsis* seed secrets unravelled after a decade of genetic and omics-driven research. *Plant J.* 61, 971–981. doi: 10.1111/j.1365-313X.2009.04095.x

Ravet, K., Reyt, G., Arnaud, N., Krouk, G., Djouani, el-B., Boucherez, J., et al. (2012). Iron and ROS control of the downstream mRNA decay pathway is essential for plant fitness. *EMBO J.* 31, 175–186. doi: 10.1038/emboj.2011.341

Ravet, K., Touraine, B., Kim, S. A., Cellier, F., Thomine, S., Guerinot, M. L., et al. (2009). Post-translational regulation of AtFER2 ferritin in response to intracellular iron trafficking during fruit development in *Arabidopsis*. *Mol. Plant* 2, 1095–1106. doi: 10.1093/mp/ssp041

Roschzttardtz, H., Bustos, S., Coronas, M. F., Ibeas, M. A., Grant-Grant, S., and Vargas-Pérez, J. (2017). Increasing provasculature complexity in the *Arabidopsis* embryo may increase total iron content in seeds: a hypothesis. *Front. Plant Sci.* 8:960. doi: 10.3389/fpls.2017.00960

Roschzttardtz, H., Conéjéro, G., Curie, C., and Mari, S. (2009). Identification of the endodermal vacuole as the iron storage compartment in the *Arabidopsis* embryo. *Plant Physiol.* 151, 1329–1338. doi: 10.1104/pp.109.144444

Roschzttardtz, H., Paez-Valencia, J., Dittakavi, T., Jali, S., Reyes, F. C., Baisa, G., et al. (2014). The vasculature complexity and connectivity gene encodes a plant-specific protein required for embryo provasculature development. *Plant Physiol.* 166, 889–902. doi: 10.1104/pp.114.246314

Santos-Mendoza, M., Dubreucq, B., Baud, S., Parcy, F., Caboche, M., and Lepiniec, L. (2008). Deciphering gene regulatory networks that control seed development and maturation in *Arabidopsis*. *Plant J.* 54, 608–620. doi: 10.1111/j.1365-313X.2008.03461.x

To, A., Joubès, J., Barthole, G., Lécureuil, A., Scagnelli, A., Jasinski, S., et al. (2012). Wrinkled transcription factors orchestrate tissue-specific regulation of fatty acid biosynthesis in *Arabidopsis*. *Plant Cell* 24, 5007–5023. doi: 10.1105/tpc.112.106120

Verdier, J., and Thompson, R. D. (2008). Transcriptional regulation of storage protein synthesis during dicotyledon seed filling. *Plant Cell Physiol.* 49, 1263–1271. doi: 10.1093/pcp/pcn116

Xu, W., Dubos, C., and Lepiniec, L. (2015). Transcriptional control of flavonoid biosynthesis by MYB-bHLH-WDR complexes. *Trends Plant Sci.* 20, 176–185. doi: 10.1016/j.tplants.2014.12.001

Zielińska-Dawidziak, M. (2015). Plant ferritin-a source of iron to prevent its deficiency. *Nutrients* 7, 1184–1201. doi: 10.3390/nu7021184

Conflict of Interest: The authors declare that the research was conducted in the absence of any commercial or financial relationships that could be construed as a potential conflict of interest.

frontiers in Plant Science

ORIGINAL RESEARCH
published: 03 June 2020
doi: 10.3389/fpls.2020.00610

Elevated Expression of Vacuolar Nickel Transporter Gene *IREG2* Is Associated With Reduced Root-to-Shoot Nickel Translocation in *Noccaea japonica*

Sho Nishida[1], Ryoji Tanikawa[2], Shota Ishida[2], Junko Yoshida[3], Takafumi Mizuno[3], Hiromi Nakanishi[4] and Naoki Furuta[2]**

[1] Laboratory of Plant Nutrition, Faculty of Agriculture, Saga University, Saga, Japan, [2] Laboratory of Environmental Chemistry, Faculty of Science and Engineering, Chuo University, Tokyo, Japan, [3] Laboratory of Soil Science and Plant Nutrition, Graduate School of Bioresources, Mie University, Tsu, Japan, [4] Laboratory of Plant Biotechnology, Graduate School of Agricultural and Life Sciences, The University of Tokyo, Tokyo, Japan

OPEN ACCESS

Edited by:
Tomoko Nozoye, Meiji Gakuin University, Japan

Reviewed by:
Fumihiko Sato, Kyoto University, Japan
Marc Hanikenne, University of Liège, Belgium

***Correspondence:**
Sho Nishida
shon@cc.saga-u.ac.jp
Naoki Furuta
nfuruta@chem.chuo-u.ac.jp

Specialty section:
This article was submitted to Plant Traffic and Transport, a section of the journal Frontiers in Plant Science

Received: *06 February 2020*
Accepted: *21 April 2020*
Published: *03 June 2020*

Citation:
Nishida S, Tanikawa R, Ishida S, Yoshida J, Mizuno T, Nakanishi H and Furuta N (2020) Elevated Expression of Vacuolar Nickel Transporter Gene IREG2 Is Associated With Reduced Root-to-Shoot Nickel Translocation in Noccaea japonica. Front. Plant Sci. 11:610. doi: 10.3389/fpls.2020.00610

A number of metal hyperaccumulator plants, including nickel (Ni) hyperaccumulators, have been identified in the genus *Noccaea*. The ability to accumulate Ni in shoots varies widely among species and ecotypes in this genus; however, little is known about the molecular mechanisms underlying this intra- and inter-specific variation. Here, in hydroponic culture, we compared Ni accumulation patterns between *Noccaea japonica*, which originated in Ni-enriched serpentine soils in Mt. Yubari (Hokkaido, Japan), and *Noccaea caerulescens* ecotype Ganges, which originated in zinc/lead-mine soils in Southern France. Both *Noccaea* species showed extremely high Ni tolerance compared with that of the non-accumulator *Arabidopsis thaliana*. But, following treatment with 200 μM Ni, *N. caerulescens* showed leaf chlorosis, whereas *N. japonica* did not show any stress symptoms. Shoot Ni concentration was higher in *N. caerulescens* than in *N. japonica*; this difference was due to higher efficiency of root-to-shoot Ni translocation in *N. caerulescens* than *N. japonica*. It is known that the vacuole Ni transporter IREG2 suppresses Ni translocation from roots to shoots by sequestering Ni in the root vacuoles. The expression level of the *IREG2* gene in the roots of *N. japonica* was 10-fold that in the roots of *N. caerulescens*. Moreover, the copy number of *IREG2* per genome was higher in *N. japonica* than in *N. caerulescens*, suggesting that *IREG2* expression is elevated by gene multiplication in *N. japonica*. The heterologous expression of *IREG2* of *N. japonica* and *N. caerulescens* in yeast and *A. thaliana* confirmed that both *IREG2* genes encode functional vacuole Ni transporters. Taking these results together, we hypothesize that the elevation of *IREG2* expression by gene multiplication causes the lower root-to-shoot Ni translocation in *N. japonica*.

Keywords: iron regulated 2, metal hyperaccumulator, nickel, nicotianamine, *Noccaea*, phytoremediation, transporter, zinc

INTRODUCTION

In plants, heavy metals absorbed from the soils by the roots accumulate in roots and shoots. Some heavy metals, such as zinc (Zn), manganese (Mn), and copper (Cu) are essential nutrients for plants, but excess accumulation of these metals can be toxic. Thus, plants found in natural environments contain heavy metals within certain ranges of concentrations, which can be defined as the "normal" ranges (Marschner, 1995). Some plant species, however, accumulate heavy metals in their aerial parts at unusually high levels without any stress symptoms. These species are called "metal hyperaccumulators" (Brooks et al., 1977). The threshold that defines metal hyperaccumulation depends on the element; for example, Zn/Mn hyperaccumulators contain >10,000 mg kg^{-1}, and nickel (Ni)/Cu hyperaccumulators contain >1,000 mg kg^{-1} on a dry weight basis (Reeves et al., 2018). More than 700 species have been identified as metal hyperaccumulators, and most of these have been discovered in metal-contaminated soils (Reeves et al., 2018). Metal hyperaccumulators have been studied both as rare species with unique molecular mechanisms for abnormal metal accumulation, and as model organisms for adaptation to extreme environments (Hanikenne and Nouet, 2011). Metal hyperaccumulators have also received attention from researchers developing technologies for decontaminating metal-polluted soils using plants, so-called "phytoremediation," or for harvesting rare metals from soils, so-called "phytomining" (Salt et al., 1998; Chaney et al., 2007).

Metal hyperaccumulators have several characteristic traits: enhanced metal absorption by roots, efficient metal translocation from roots to shoots, and elevated metal tolerance (Lasat et al., 1996; Kramer et al., 1997; Zhao et al., 2002; Caille et al., 2005). In recent years, the molecular mechanisms involved in those traits have been uncovered by molecular biological approaches. Zn/cadmium (Cd) transporter Heavy Metal ATPase 4 (HMA4), which plays a role in Zn/Cd loading into the xylem in roots, was shown to be involved in efficient Zn/Cd translocation from roots to shoots in the Zn/Cd hyperaccumulator *Arabidopsis halleri* using *HMA4*-knockdown plants (Hanikenne et al., 2008). HMA3 is thought to play a role in sequestering excess Cd in leaf vacuoles and contribute to high Cd tolerance and accumulation in shoots of the Zn/Cd/Ni hyperaccumulator *Noccaea caerulescens* (formerly *Thlaspi caerulescens*) ecotype Ganges (Ueno et al., 2011). Natural resistance-associated macrophage protein 1 (NRAMP1) is thought to mediate Cd influx across the endodermal plasma membrane in root vascular tissues and contribute to efficient root-to-shoot Cd translocation in *N. caerulescens* ecotype Ganges (Milner et al., 2014). The expression levels of *HMA4*, *HMA3* and *NRAMP1* are much higher in the metal hyperaccumulators than in the non-accumulators, and the elevated expression levels are required for metal hyperaccumulating abilities (Hammond et al., 2006; Hanikenne et al., 2008; Ueno et al., 2011; Milner et al., 2014). Hanikenne et al. (2008) attributed the elevated expression of *HMA4* in *A. halleri* to the triplication of *HMA4* in the genome and the mutation of *cis*-regulatory sequences. Elevated expression of *HMA4* caused by gene multiplication is also found in the Zn/Cd hyperaccumulating ecotypes of *N. caerulescens* (Lochlainn et al., 2011). Elevated *HMA3* and *NRAMP1* expression levels in *N. caerulescens* ecotype Ganges are also likely caused by gene multiplication (Ueno et al., 2011; Milner et al., 2014), indicating that the elevated expression of metal transporter genes caused by gene multiplication are key evolutionary events for metal hyperaccumulators. High expression of many other genes involved in metal transport and metal homeostasis is also thought to be implicated in metal hyperaccumulation (Hanikenne and Nouet, 2011).

Most metal hyperaccumulators (more than 500 species) are Ni hyperaccumulators (Reeves et al., 2018). Ni hyperaccumulators are found on serpentine soils, which contain Ni at a level excessive for normal plants. In the Ni hyperaccumulating ecotype of *N. caerulescens*, nicotianamine in root cells and xylem forms a complex with Ni and is involved in the long-distance translocation of Ni from roots to shoots (Vacchina et al., 2003; Mari et al., 2006). Expression of *Yellow-stripe like 3* (*YSL3*), encoding the Ni–nicotianamine complex transporter, is higher in the roots and shoots of *N. caerulescens* than in those of the non-accumulator *Arabidopsis thaliana* (Gendre et al., 2007), suggesting that elevated *YSL3* expression increases Ni–nicotianamine mobility and contributes to efficient root-to-shoot Ni translocation. In another *Noccaea* Ni hyperaccumulator, *N. goesingense*, elevated serine acetyltransferase activity and elevated glutathione concentration are essential for enhanced Ni tolerance (Freeman et al., 2004, 2005; Na and Salt, 2011).

Assunção et al. (2003) showed that accumulation patterns of Ni, Zn, and Cd vary among *N. caerulescens* ecotypes originating from different soil types, and that an ecotype growing in serpentine soils is superior in Ni tolerance and accumulation to ecotypes from other metalliferous or non-metalliferous soils. Peer et al. (2003, 2006) showed that there is a large variation in Ni accumulation patterns among the species or accessions of *Brassicaceae* metal hyperaccumulators including a number of *Noccaea* species. In their results, shoot Ni concentration was not always correlated with the shoot concentrations of other metals, suggesting that there is a genetic factor specifically determining Ni hyperaccumulation.

The molecular mechanism of Ni accumulation has been well studied in *A. thaliana*. Ni is absorbed by roots via iron (Fe) uptake transporter Iron-regulated transporter 1 (IRT1) and unknown transporters (Nishida et al., 2011, 2015), and then translocated to shoots via the xylem. Excessively absorbed Ni is sequestered in root vacuoles by Ni transporter Iron-regulated 2 (IREG2) (also known as Ferroportin 2; Schaaf et al., 2006; Morrissey et al., 2009). Excess Ni induces Fe deficiency due to competition between Ni and Fe (Nishida et al., 2012). Then, *IRT1* expression is induced by the Ni-induced Fe deficiency, resulting in accelerated Ni absorption via IRT1 (Nishida et al., 2012). *IREG2* is also induced by Ni-induced Fe deficiency and detoxifies excess Ni (Schaaf et al., 2006). This synchronized induction of *IREG2* and *IRT1*, which is regulated by FER-like Fe deficiency-induced transcription factor (FIT), is essential for the limited Ni tolerance

shown by *A. thaliana* (Schaaf et al., 2006). Knockdown of *IREG2* decreases root Ni and increases shoot Ni, indicating that *IREG2* can determine the efficiency of Ni translocation from roots to shoots (Schaaf et al., 2006; Merlot et al., 2014). IREG1, the ortholog of IREG2, plays a role in Fe/cobalt (Co) translocation from roots to shoots by loading Fe/Co into the xylem in roots, but the contribution of IREG1 to Ni translocation was not confirmed (Morrissey et al., 2009). Merlot et al. (2014) reported that the expression level of a *IREG* homolog is higher in the Ni hyperaccumulator *Psychotria gabriellae* than in the related non-accumulator *Psychotria semperflorens* and the overexpression of *P. gabriellae IREG* increases Ni tolerance in yeast and *A. thaliana*, suggesting that *IREG* contributes to high Ni tolerance in *P. gabriellae*.

The objective of the present study was to reveal a genetic factor associated with variation in shoot Ni accumulation in Ni hyperaccumulators. We assessed Ni accumulation patterns in roots and shoots in two related Ni hyperaccumulators: *Noccaea japonica*, which originated from a serpentine soil, and *N. caerulescens* ecotype Ganges, which originated from a Zn/Pb-mine soil. We also investigated the involvement of *IREG2* in the differential Ni accumulation patterns between the two *Noccaea* plant types.

MATERIALS AND METHODS

Plant Materials

Noccaea japonica growing in a serpentine soil in Mt. Yubari (Hokkaido, Japan), *N. caerulescens* ecotype Ganges growing in a Zn/Pb-mine soil in Southern France, and *A. thaliana* accession Col-0 were used. The *ireg2-1* T-DNA insertion line (SALK_74442; Schaaf et al., 2006) was obtained from the Arabidopsis Biological Resource Center (Ohio State University, United States). An *ireg2-1* homozygous line was identified using polymerase chain reaction (PCR) with primers flanking the insertion site and the left-border primer of T-DNA (**Supplementary Table S1**).

Growth Conditions

Half-strength Molecular Genetics Research Laboratory (MGRL) medium containing 8.6 μM Fe-EDTA at pH 5.5 was used as the hydroponic culture solution (Nishida et al., 2011). The procedure used for hydroponic culture was described previously (Nishida et al., 2011). Since *N. japonica* and *N. caerulescens* grow slower than *A. thaliana*, the preculture periods prior to metal exposure were 6 weeks for the *Noccaea* species and 4 weeks for *A. thaliana*. Two plants were cultured in every pot and pooled as one biological replicate. Plants were grown in a growth chamber at 22°C under a 10-h light/14-h dark cycle.

In agar-plate tests, half-strength MGRL medium containing 1.2% agar (agar type A, Sigma-Aldrich Co), 1% sucrose, 8.6 μM Fe-EDTA, and 5 mM 2-morpholinoethanesulfonic acid (MES) at pH 5.5 was used. Seeds were surface sterilized and sown on agar plates. Fifteen seedlings were pooled as one biological replicate. Plants were cultured in a growth chamber at 22°C under a 16-h light/8-h dark cycle.

Determination of Metal Tolerance and Accumulation in Hydroponic Culture

Plants were exposed to hydroponic culture solutions supplemented with 0–200 $NiCl_2$ or 0.5–1000 μM $ZnCl_2$ for a week. Hydroponic solutions were buffered with 5 mM MES (pH 5.5). After exposure, plants were separated into roots and shoots. Roots were washed with deionized water and 50 mM EDTA-Na_2 to remove metals bound to the cell walls, and then blotted. Harvested samples were weighed to determine the fresh weight, dried at 70°C, and weighted to determine the dry weight. Dried samples were digested with HNO_3 and H_2O_2 in a heat block and diluted with ultra-pure water. Elemental analysis was performed using inductively coupled plasma optical emission spectrometers (ICPS-7500, Shimadzu Co.; SPS5100, Hitachi High-Tech Science Co).

Cloning of *IREG2* From *Noccaea* Species

Noccaea japonica and *N. caerulescens* plants were cultured hydroponically as described above. Total RNA was extracted from their roots following the method of Suzuki et al. (2004). Residual DNA was digested by DNase I (Takara Bio Inc), and first-strand cDNA was synthesized using a PrimeScript RT-PCR kit (Takara Bio Inc) with oligo (dT) primers. The resulting cDNA was used for gene cloning as follows. The mRNA sequence of *NcIREG2*, which was previously obtained by the Transcriptome Shotgun Assembly project for *N. caerulescens*, is available at DDBJ/EMBL/GenBank as "Nc_isotig06993_isogroup03561" (Lin et al., 2014; **Supplementary Figure S3**). Full-length *IREG2* fragments from *N. japonica* and *N. caerulescens* were amplified using forward and reverse primers designed on regions corresponding to the 5' UTR and 3' UTR of *NcIREG2*, respectively, and a high-fidelity DNA polymerase (PrimeSTAR HS DNA Polymerase, Takara Bio Inc). PCR products were sequenced using primers designed on the internal regions of *IREG2* (**Supplementary Table S1**). Since single nucleotide polymorphisms were detected in *NjIREG2*, *NjIREG2* fragments were cloned separately in an *Escherichia coli* plasmid vector and sequenced as described later. *IREG2* sequences were aligned by using Clustal W[1]. *IREG2* sequences are deposited in the DNA Data Bank of Japan under the accession numbers LC522035 (*NcIREG2*) and LC522036 (*NjIREG2*).

Quantitative Reverse Transcription (RT)-PCR Assay

Plants pre-cultured in hydroponic solution were exposed to 200 μM $NiCl_2$ for a week. Total RNA was then extracted from the roots and treated with DNase I. cDNA was synthesized using a ReverTra Ace qPCR RT kit (Toyobo Co., Ltd), and quantitative RT-PCR (qRT-PCR) was performed using THUNDERBIRD SYBR qPCR Mix (Toyobo Co., Ltd). qPCR was performed in a real-time PCR system (LightCycler 96 System, Roche Diagnostics KK). The relative transcript level of *IREG2* was calculated using a calibration curve and normalized with the *EF1α* transcript level. The *IREG2*-specific primers were designed on sequences that are completely identical between *NcIREG2* and *NjIREG2*. To design *EF1α*-specific primers, a

portion of the *EF1α* sequence was amplified from genomic DNA of *N. japonica* and *N. caerulescens* by PCR with *EF1α* common primers, which were designed on a region conserved in higher plants. *EF1α* fragments were sequenced, and a forward primer and a reverse primer, spanning an intron, were designed on the sequences. The specificities of qPCR primers were confirmed by dissociation curve analysis and gel electrophoresis of PCR products. Primer information is summarized in **Supplementary Table S1**.

Estimation of *IREG2* Copy Number

Genomic DNA was extracted from young leaves of plants grown in a soil culture, and then *IREG2* copy number was estimated by qPCR as described previously (Ueno et al., 2011; Milner et al., 2014). The qPCR protocol was as described in the section "Quantitative Reverse Transcription (RT)-PCR Assay," except that the genomic DNA was used as the template instead of cDNA. Relative abundance of the *IREG2* gene was normalized with that of the *SHR* gene (AT4G37650), which is a putative single copy gene, or the expressed sequence tag–based indel marker RR11nr025, of *N. caerulescens* (Ueno et al., 2011; Milner et al., 2014). Primer sequences are summarized in **Supplementary Table S1**.

Plant Transformation

The open-reading frames of *NcIREG2* and *NjIREG2* were amplified from cDNA by PCR with PrimeSTAR HS DNA Polymerase using a 5′ primer with *Kpn*1 site and 3′ primer with *Xho*1 site (**Supplementary Table S1**). PCR products were cloned into the pMD20-T vector by TA cloning (Takara Bio. Inc). The resulting *IREG2*-pMD-T plasmids were extracted from three independent colonies of *E. coli* and then sequenced. *IREG2* fragments were subcloned into pENTR4 (Invitrogen) at the *Kpn*1–*Xho*1 sites, and subsequently subcloned into pGWB2 plant overexpression vector carrying the CaMV 35S promoter (Nakagawa et al., 2007) using Gateway LR Clonase II Enzyme mix (Invitrogen). The plasmid constructs were transferred into *Agrobacterium tumefaciens* strain GV3101 (pMP90), and the obtained transformants were used to transform the *ireg2-1* homozygous line using the standard floral dip method. T1 transformants were selected on agar plates containing 10 μg mL^{-1} hygromycin, and then transferred to a soil culture. T2 progenies of four independent T1 lines were used for the following experiments. Fifteen seedlings of each T2 line grown on agar plates for 2 weeks (without hygromycin) were pooled and subjected to qRT-PCR. The relative expression level of *IREG2* was calculated using *EF1α* as the internal reference gene.

Determination of Ni Tolerance and Accumulation in Transgenic Plants

Seeds were surface-sterilized and sown on agar plates supplemented with 0–70 μM $NiCl_2$ (without hygromycin) and cultured for 14 days. After exposure, seedlings were pooled for each line and growth and Ni concentrations in roots and shoots were determined as described above.

Yeast Transformation and Ni Tolerance Assay

The *IREG2*-pMD-T plasmids were digested with *Kpn*I, and the plasmid ends were blunted by T4 DNA polymerase. The resulting linear plasmids were digested with *Xho*I, and *IREG2* fragments were isolated by gel electrophoresis. The pKT10-Gal-HA-BS yeast expression vector was digested with *Eco*RI, and the plasmid ends were blunted by a Klenow fragment; the plasmid was then digested by *Sal*I. *IREG2* fragments were ligated to the blunt end and *Sal*I-digested end of pKT10-Gal-HA-BS. The obtained plasmids were transformed into *Saccharomyces cerevisiae* strain BY4741 (*MATa his3 leu2 met15 ura3*) by the standard method. The transformants were selected on a yeast nitrogen base (YNB) uracil minus medium, which consisted of 0.67% YNB, 2% glucose, and appropriate amino acids. The assay for Ni tolerance was performed as described by Nishida et al. (2011) using YNB uracil minus media containing 0 or 750 μM $NiCl_2$, and 2% galactose (pH 5.5).

Nicotianamine Analysis

Plants cultured hydroponically were exposed to 0 or 200 $NiCl_2$ for a week. After exposure, roots were harvested and subjected to nicotianamine extraction following Nozoye et al. (2014). Nicotianamine was measured using high-performance liquid chromatography (HPLC) as described previously (Mori and Nishizawa, 1987).

RESULTS

Difference in Ni Accumulation Between *N. japonica* and *N. caerulescens*

Noccaea japonica, *N. caerulescens* (ecotype Ganges), and *A. thaliana* were exposed to 0, 25, or 200 μM Ni for a week in hydroponic culture, and Ni accumulation and symptoms were compared; *A. thaliana* was not tested at 200 μM Ni because this high concentration was lethal for this species. Following 25 μM Ni treatment, *A. thaliana* showed severe chlorosis, a typical symptom of Ni-induced Fe deficiency, over the whole shoot, and the growth in roots and shoots was significantly reduced compared with the un-treated controls (**Figures 1A,B**). In contrast, both *N. japonica* and *N. caerulescens* showed no visible symptoms or growth reduction, confirming that these *Noccaea* plant types have extremely high tolerance to Ni. Following 200 μM Ni treatment, *N. caerulescens* but not *N. japonica* exhibited chlorosis between the veins of young leaves; neither plant types showed significant growth reduction (**Figures 1A,B** and **Supplementary Figure S1**). Ni-induced Fe deficiency induces *IRT1* expression in roots and accelerates Fe absorption. This means that Fe concentration in roots increases with Ni concentration in the medium (Nishida et al., 2011, 2012). Here, Fe concentration in roots was significantly increased by treatment with 25 μM Ni in *N. caerulescens* (**Supplementary Figure S1B**) but not *N. japonica*. Taken together, the data for chlorosis symptoms and root Fe concentration indicate that *N. caerulescens* shows higher Ni sensitivity than *N. japonica*.

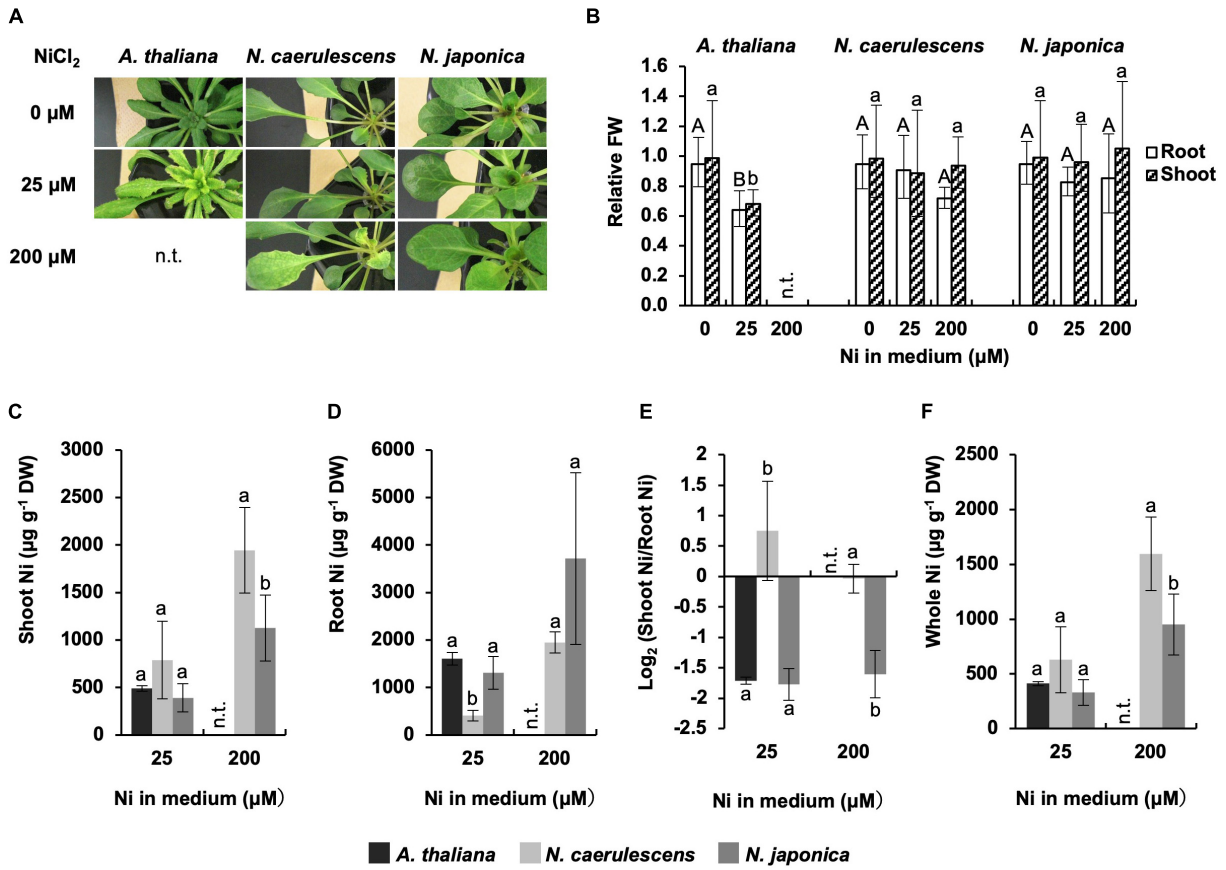

FIGURE 1 | Ni tolerance and accumulation. Plants were exposed to the indicated concentrations of $NiCl_2$ for 7 days in hydroponic culture. **(A)** Plants after Ni treatment. **(B)** Fresh weight (FW) relative to un-treated control. **(C,D)** Ni concentration expressed relative to dry weight (DW) in shoots **(C)** and roots **(D)**. **(E)** Ratio of shoot Ni to root Ni concentration. **(F)** Ni concentration in whole plants. Values are geometric **(B,E)** or arithmetic **(C,D,F)** means ± SD of four biological replicates. Different letters indicate a statistically significant difference ($P < 0.05$; ANOVA, Tukey–Kramer) between different Ni treatments in each part **(B)** or different species in each treatment **(C–F)**. n.t., not tested. Mean values of shoot FW/root FW under 0 μM Ni: 2.64 g/1.14 g (*A. thaliana*); 2. 02 g/1.01 g (*N. caerulescens*); 1.87 g/0.78 g (*N. japonica*).

Ni concentration in shoots was significantly higher in *N. caerulescens* than *N. japonica* following treatment with 200 μM Ni; the same tendency was observed for 25 μM Ni but the difference was not significant (**Figure 1C**). In contrast, Ni concentration in roots was significantly lower in *N. caerulescens* than *N. japonica* following treatment with either 25 or 200 μM Ni (**Figure 1D**). When the Ni levels in shoots and roots were compared, shoot Ni concentration was similar to or higher than root Ni concentration in *N. caerulescens* individuals, whereas shoot Ni concentration was lower than root Ni concentration in all *N. japonica* individuals tested. The ratio of shoot Ni to root Ni in *N. caerulescens* was significantly higher than that in *N. japonica* (**Figure 1E**). These results indicate that the activity of Ni translocation from roots to shoots was higher in *N. caerulescens* than in *N. japonica*. Following treatment with 200 μM Ni, the Ni concentration in whole plants was significantly higher in *N. caerulescens* than in *N. japonica* (**Figure 1F**) indicating that Ni absorption activity was higher in *N. caerulescens*.

We also investigated Zn accumulation and symptoms in *N. japonica*, *N. caerulescens*, and *A. thaliana* following treatment with a normal Zn concentration (0.5 μM Zn) or excess Zn (150 or 1000 μM Zn). Growth of *A. thaliana* was greatly inhibited by 150 μM Zn treatment compared with 0.5 μM Zn treatment, and serious necrosis developed in leaves following 1000 μM Zn treatment (**Figure 2A**). In contrast, both *N. japonica* and *N. caerulescens* showed high Zn tolerance, though there was a tendency for a slight decrease in growth under excess Zn conditions (**Figures 2A,B** and **Supplementary Figure S2**); this decrease was significant for 1000 μM Zn in *N. caerulescens* only. Shoot Zn concentrations in the *Noccaea* species were over twice that in *A. thaliana* under the normal Zn condition, while root Zn concentrations were lower in the *Noccaea* species than in *A. thaliana* (**Figure 2C**). These differences were statistically significant, confirming higher activity of root-to-shoot Zn translocation in the *Noccaea* species. In the comparison between *Noccaea* species, Zn concentrations in shoots and whole plants were significantly higher in *N. japonica* than in *N. caerulescens* under the normal Zn condition (**Figure 2C**), but no significant difference in Zn accumulation was observed under excess Zn conditions (**Figures 2D,E,G**). There was no difference in the ratio

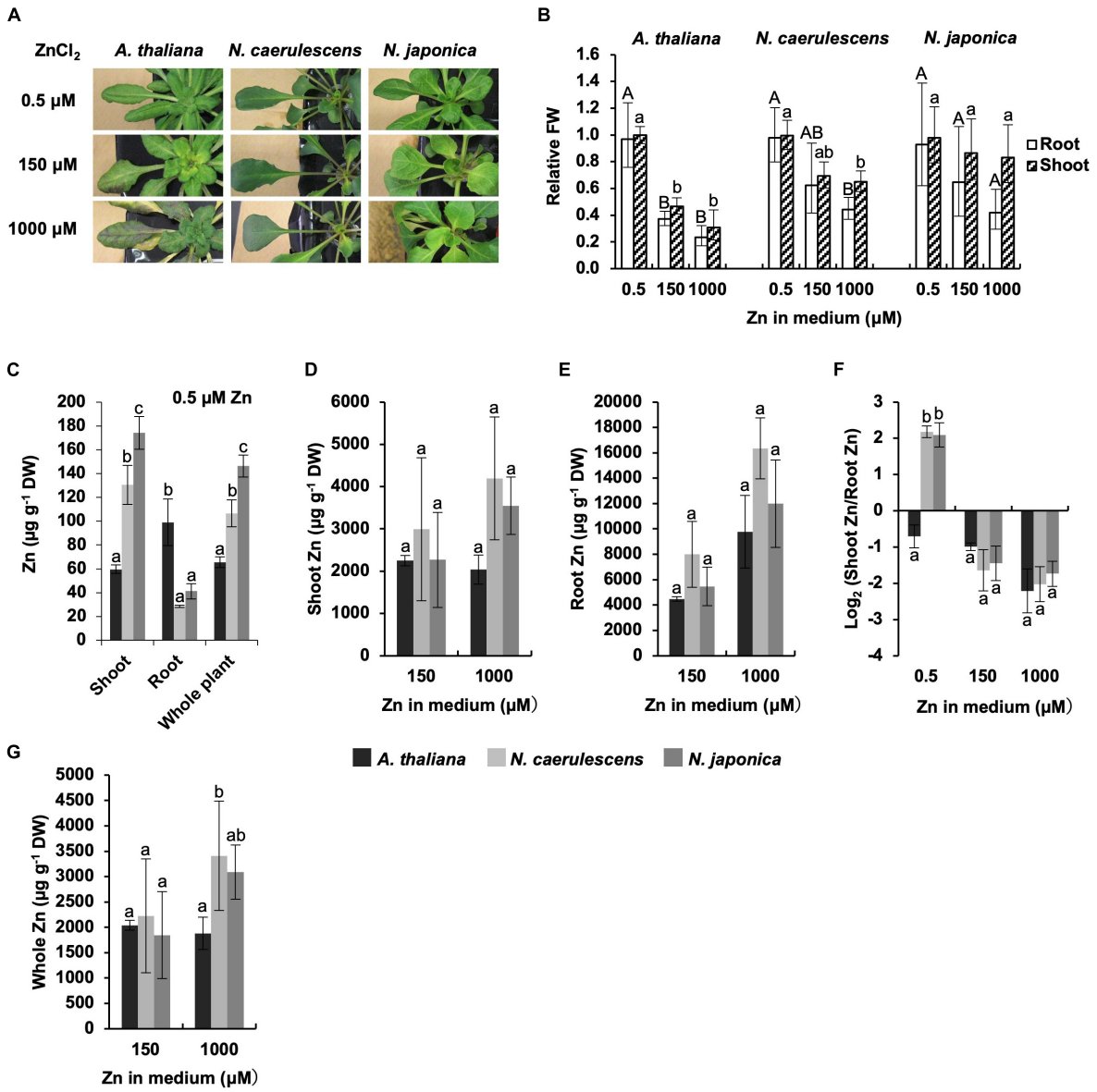

FIGURE 2 | Zn tolerance and accumulation. Plants were exposed to the indicated concentrations of $ZnCl_2$ for 7 days in hydroponic culture. **(A)** Plants after Zn treatments. **(B)** Fresh weight (FW) relative to un-treated control. **(C)** Zn concentration expressed relative to dry weight (DW) in shoots, roots, and whole plants under normal Zn condition (0.5 μM $ZnCl_2$). **(D,E)** Zn concentrations in shoots **(D)** and root **(E)** under excess Zn conditions (150 and 1000 μM $ZnCl_2$). **(F)** Ratio of shoot Zn to root Zn. **(G)** Zn concentration in whole plants. Values are geometric **(B,F)** or arithmetic **(C–E,G)** means ± SD of four biological replicates. Different letters indicate a statistically significant difference ($P < 0.05$; ANOVA, Tukey–Kramer) between different Zn treatments in each part **(B)**, different species in each part **(C)**, or different species in each treatment **(D–G)**. n.t., not tested. Mean values of shoot FW/root FW under 0.5 μM Zn: 3.04 g/1.08 g (*A. thaliana*); 2. 72 g/1.67 g (*N. caerulescens*); 1.36 g/0.67 g (*N. japonica*).

of shoot Zn to root Zn between *N. japonica* and *N. caerulescens* under excess Zn conditions (**Figure 2F**).

Differences in *IREG2* Expression Level and Gene Copy Number Between *N. japonica* and *N. caerulescens*

The observed significant difference between *N. japonica* and *N. caerulescens* in terms of Ni, but not Zn, translocation from roots to shoots, suggests that the inter-species difference in Ni translocation is due to a Ni-specific mechanism. The efficiency of Ni translocation from roots to shoots depends on the abundances of vacuolar Ni^{2+} transporter IREG2 and metal chelator nicotianamine in roots. Nicotianamine accumulation in roots affects translocation of both Ni and Zn (Mari et al., 2006; Uraguchi et al., 2019), whereas IREG2 transports Ni^{2+} but not Zn^{2+}. Therefore, we considered IREG2 to be the more likely candidate for the Ni-specific mechanism. We cloned the cDNAs

of *IREG2* from the roots of *N. japonica* and *N. caerulescens* (termed *NjIREG2* and *NcIREG2*, respectively), and determined their sequences (**Supplementary Figure S3**). From *N. japonica*, three different *IREG2* sequences were obtained (**Supplementary Figure S4**). These sequences were almost identical (>99.5% identity), and therefore one of them was used for further analysis. A single *IREG2* sequence was obtained from *N. caerulescens*. The polypeptides encoded by *NjIREG2* and *NcIREG2* were almost identical to each other (99.4% identity) and consisted of 501 aa residues (**Supplementary Figure S5**). NjIREG2 and NcIREG2 shared considerable sequence identity (79%) with AtIREG2 (512 aa), suggesting that the functional role of IREG2 is conserved between the two *Noccaea* plant types.

We compared the expression level of *IREG2* in roots between *N. caerulescens* and *N. japonica* using qRT-PCR. The expression level in *N. japonica* was over 10-fold that in *N. caerulescens* following treatment with 200 μM Ni (**Figure 3A**). This suggests that the *IREG2* activity that sequesters Ni in root vacuoles is higher and Ni translocation to shoots is lower in *N. japonica* than in *N. caerulescens*. We also compared the genomic copy number of *IREG2* between the two *Noccaea* plant types. The abundances of *IREG2* gene relative to the abundance of the putative single copy gene *SHR* or the indel marker site RR11nr025 were compared between the two plant types. The copy number of *IREG2* per genome in *N. japonica* was estimated to be 6–8 times that in *N. caerulescens* (**Figure 3B**). This suggests that the higher expression of *IREG2* in *N. japonica* than in *N. caerulescens* is due to a higher copy number of *IREG2* in *N. japonica*.

Confirmation of *NjIREG2* and *NcIREG2* Functions

According to Schaaf et al. (2006), heterologous expression of *AtIREG2* increases the Ni tolerances of *S. cerevisiae*, and also overexpression of *AtIREG2* increases the Ni tolerance of *A. thaliana*. Therefore, to determine whether *NjIREG2* and *NcIREG2* are functional homologs of *AtIREG2*, we first established *S. cerevisiae* strains expressing *NjIREG2* or *NcIREG2* and assayed their Ni tolerance. Both strains showed increased Ni tolerance compared with the vector control strain (**Figure 4A**). We then evaluated the Ni tolerance of *A. thaliana* transgenic lines expressing *NcIREG2* or *NjIREG2*. cDNA fragments of *NjIREG2* and *NcIREG2* driven by the 35S promoter were separately introduced into the *ireg2-1* homozygous line, and four independent lines constitutively expressing *NcIREG2* or *NjIREG2* were selected (**Figure 4B**). The Col-0 and *ireg2-1* lines showed severe growth inhibition under 70 μM Ni compared with untreated control, whereas the transgenic lines expressing *NjIREG2* or *NcIREG2* showed greatly increased Ni tolerance (**Figures 4C–E**). These results confirmed that *NjIREG2* and *NcIREG2* encode functional IREG2 proteins. Moreover, line *NcIREG2#5*, in which *IREG2* expression level was considerably lower than in the other *NcIREG2*- or *NjIREG2*-expressing lines (**Figure 4B**), showed significantly lower root Ni accumulation compared with the others (**Figure 4G**). In addition, the ratio of shoot Ni to root Ni in *NcIREG2#5* tended to be higher than that in the other lines (**Figures 4F–H**). These results indicate that the ability to sequester Ni in root vacuoles is lower in *NcIREG2#5* than in the other lines, and supports the notion that the expression level of *IREG2* determines the efficiency of root-to-shoot Ni translocation. Except for *NcIREG2#5*, there was no significant difference in Ni concentrations in roots and shoots between the *NjIREG2*-expressing lines and *NcIREG2*-expressing lines, suggesting that Ni sequestration activity is comparable between NcIREG2 and NjIREG2.

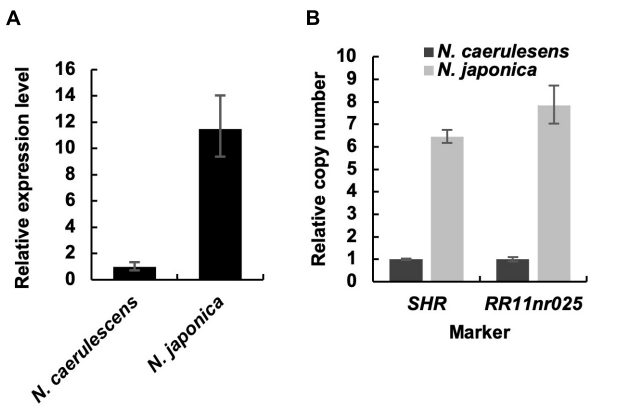

FIGURE 3 | Root expression level and genomic copy number of *IREG2* in the two *Noccaea* plant types. **(A)** Plants were exposed to 200 μM $NiCl_2$ for 7 days in hydroponic culture, and the roots were subjected to qRT-PCR. The relative expression levels of *IREG2* were calculated using *EF1α* as the internal reference gene. **(B)** The copy number of *IREG2* per genome was quantified by qPCR and normalized with the expressed sequence tag–based indel marker *RR11nr025* and the gene *SHR*. Values are means ± SD of three biological replicates.

DISCUSSION

Here, we showed that the efficiency of root-to-shoot Ni translocation is significantly lower in *N. japonica* than in *N. caerulescens* (ecotype Ganges), and that this is possibly due to higher *IREG2* expression in *N. japonica* than in *N. caerulescens*. Moreover, we showed that the genomic copy number of *IREG2* is much higher in *N. japonica* than in *N. caerulescens*, which likely causes the higher expression of *IREG2* in *N. japonica*. The multiple *IREG2* transcripts obtained from *N. japonica* (**Supplementary Figure S4**) could be derived from the multiplicated *IREG2*. These findings indicate that *IREG2* could be a genetic factor determining variation in shoot Ni hyperaccumulation. A hypothetical model of the IREG2-dependent mechanism causing differential shoot Ni accumulation in the two *Noccaea* plant types is shown in **Figure 5**: Ni is absorbed by IRT1 (or unknown Ni transporters) into root cells; a part of the Ni absorbed is sequestered in root vacuoles by IREG2, and the other part is loaded into the xylem and translocated from roots to shoots; in *N. japonica*, the elevated expression of *IREG2* in roots increases Ni accumulation in root vacuoles and decreases the amount of Ni to be loaded into xylem, thereby reducing the amount of Ni translocated from roots to shoots. A similar mechanism was shown for Cd

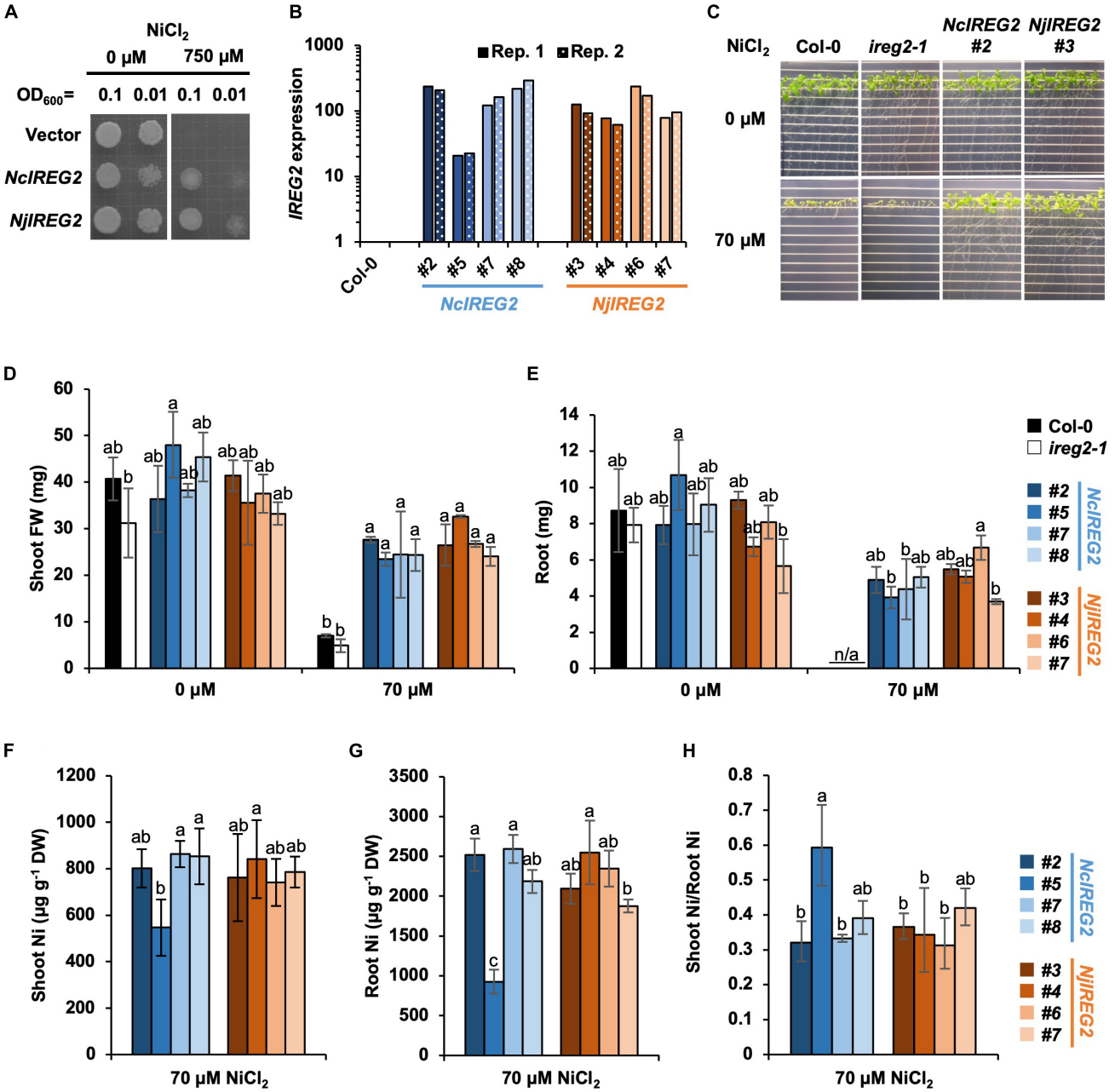

FIGURE 4 | Heterologous expression of *NcIREG2* and *NjIREG2* in yeast and *A. thaliana*. **(A)** *Saccharomyces cerevisiae* cells were transformed with *NcIREG2*, *NjIREG2*, or empty vector and then grown on YNB media containing 0 or 750 μM $NiCl_2$ at 30°C for 4 days. **(B)** Expression level of *IREG2* in the transgenic lines overexpressing *NcIREG2* or *NjIREG2*. The *ireg2-1* homozygous line was transformed with 35S:*NcIREG2* or 35S:*NjIREG2*, and four independent lines were selected for each construct. Relative expression levels of *IREG2* (Col-0 = 1) were determined by qRT-PCR. Data of each biological replicate (Rep. 1 and Rep. 2) are shown. **(C–E)** Growth of 14-day-old plants after the treatments. **(F,G)** Ni concentration expressed relative to dry weight (DW) in roots and shoots. **(H)** Ratio of shoot Ni to root Ni concentration. Values are means ± SD of four biological replicates. Different letters indicate a statistically significant difference ($P < 0.05$) among lines in each Ni treatment (ANOVA, Tukey–Kramer).

accumulation in rice and *A. thaliana*: HMA3 suppresses Cd translocation from roots to shoots by sequestering Cd in the root vacuoles and determines variation in shoot Cd accumulation among cultivars or accessions (Ueno et al., 2010; Chao et al., 2012). Metal sequestration in root vacuoles is probably a major trait determining the efficiency of metal translocation from roots to shoots. We observed that the Ni concentration in the whole plant was higher in *N. caerulescens* than *N. japonica* following 200 μM Ni treatment (**Figure 1F**), indicating that Ni absorption activity was higher in *N. caerulescens*. Both the

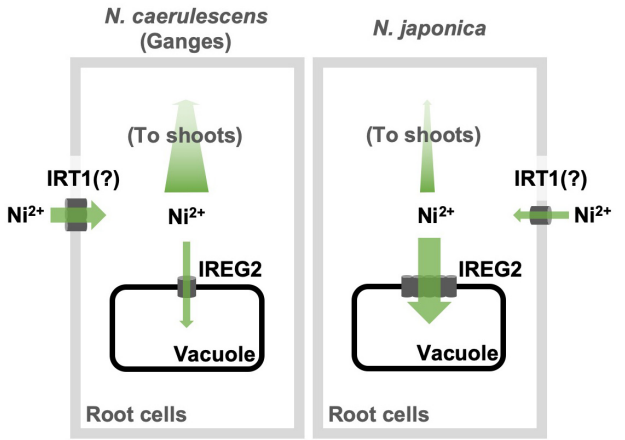

FIGURE 5 | Schematic model of IREG2-dependent mechanism causing differential Ni accumulation in *N. japonica* and *N. caerulescens*. The gray rectangles and black rectangles denote the root cell membranes and the vacuole membranes, respectively.

higher Ni absorption activity and the lower *IREG2* expression in *N. caerulescens* likely contribute to its higher sensitivity to Ni compared with *N. japonica* (**Figure 1A** and **Supplementary Figure S1**). *IRT1* expression is known to accelerate Ni absorption in *A. thaliana* (Nishida et al., 2012). We therefore hypothesize that more Ni is absorbed under excess Ni conditions in *N. caerulescens* than *N. japonica* because the induction of *IRT1* by Ni-induced Fe deficiency is higher in *N. caerulescens*. This hypothesis assumes that IRT1 is predominantly responsible for Ni absorption from soils. Further analyses are necessary to confirm the involvement of IRT1 in Ni hyperaccumulation in *N. caerulescens* and *N. japonica*.

In Ni hyperaccumulators, shoot Ni accumulation depends in part on nicotianamine accumulation in the roots: i.e., more nicotianamine accumulated in the roots increases the mobility of Ni in root cells and facilitates Ni translocation from roots to shoots (Curie et al., 2008). However, although the ratio of shoot Ni to root Ni concentration (an indicator of root-to-shoot translocation) was higher in *N. caerulescens* than *N. japonica*, we observed no significant difference in the ratio of shoot Zn to root Zn concentration between the two *Noccaea* plant types. If root nicotianamine were responsible for this difference, one might expect the root nicotianamine concentration to be higher in *N. caerulescens* than *N. japonica*, but this was not the case (**Supplementary Figure S6**). This finding provides further evidence that nicotianamine, which affects both Ni and Zn translocation, is not responsible for the difference in root-to-shoot Ni translocation between the two plant types. Richau et al. (2009) reported that shoot Ni accumulation in a Ni-hyperaccumulating *N. caerulescens* accession depends on the enhanced accumulation of free histidine in the roots: i.e., chelation of Ni by free histidine accumulated in the roots inhibits Ni sequestration into the root vacuoles and promotes Ni translocation from roots to shoots. However, Persans et al. (1999) denied the implication of root histidine accumulation in shoot Ni hyperaccumulation in the Ni hyperaccumulator *N. goesingenese*. Although the role of free histidine in Ni hyperaccumulation is still controversial, the possibility that free histidine is another factor determining variation in Ni hyperaccumulation in *Noccaea* cannot be ruled out.

It has been reported that *N. caerulescens* shows more efficient root-to-shoot Ni translocation compared with metal non-accumulator plants such as *A. thaliana* (Assunção et al., 2003; Mari et al., 2006). Here, we showed that the ratio of shoot Ni to root Ni concentration was significantly higher in *N. caerulescens* than in *A. thaliana* (**Figure 1**), confirming a higher Ni translocation in *N. caerulescens*. This difference is probably due to elevated nicotianamine accumulation in the roots of *N. caerulescens* as reported previously (Mari et al., 2006). A transcriptome analysis showing that *IREG2* is not differentially expressed between *N. caerulescens* (a Zn/Pb-mine ecotype) and *A. thaliana* Col-0 (van de Mortel et al., 2006) suggests that *IREG2* expression is not involved in the difference in Ni translocation. In contrast, our data suggest that the efficiency of Ni translocation from roots to shoots in *N. japonica* is similar to that of *A. thaliana* following treatment with 25 μM Ni (**Figure 1E**). Root nicotianamine accumulation in *N. japonica* was comparable with that in *N. caerulescens*, but the potential for efficient Ni translocation caused by elevated nicotianamine accumulation in roots might be offset by the elevated *IREG2* expression. Efficient translocation of metals from roots to shoots is generally found in metal hyperaccumulators. However, our results imply that efficient Ni translocation is not necessary for Ni hyperaccumulation. Shoot Ni concentrations could reach the hyperaccumulation level in *N. japonica* growing in serpentine soils for a long time (Mizuno et al., 2003).

The expression levels of metal transporter genes (e.g., *HMA3*, *HMA4*, and *NRAMP1*) involved in shoot metal hyperaccumulation are elevated by gene duplication in metal hyperaccumulator species, and gene duplication is recognized as a mechanism facilitating evolution of metal hyperaccumulators (Hanikenne et al., 2008; Ueno et al., 2011; Milner et al., 2014). *IREG2* is multiplicated in *N. japonica* and accordingly *IREG2* expression is elevated. But, the elevated *IREG2* reduces root-to-shoot Ni translocation by sequestering Ni in the root vacuoles (Schaaf et al., 2006; Morrissey et al., 2009) and so does not contribute to the trait of efficient Ni translocation from roots to shoots. *N. japonica* grows in serpentine soil areas, whereas *N. caerulescens* Ganges, the ecotype studied here, grows in Zn/Pb mine soil areas. *IREG2* expression in *N. caerulescens* is higher in an ecotype from serpentine soils than in ecotypes from Zn/Pb mine soils or non-metalliferous soil (Halimaa et al., 2014). We assume that elevation of *IREG2* expression was required to survive under excess Ni conditions. Whole genome sequence analysis of natural populations of the non-accumulator *Arabidopsis lyrata* revealed that a non-synonymous substitution in *IREG2* is strongly linked to adaptation to serpentine soils (Turner et al., 2010). *IREG2* might be a major target to be duplicated or modified for adaptation to Ni-rich soils in wild plants. For future study, it would be important to investigate the involvement of *IREG2* in intra- and inter-specific variations in Ni hyperaccumulation pattern and Ni tolerance using a

wide variety of species and accessions of *Brassicaceae* metal hyperaccumulators.

DATA AVAILABILITY STATEMENT

The raw data supporting the conclusions of this article will be made available by the authors, without undue reservation, to any qualified researcher.

AUTHOR CONTRIBUTIONS

SN designed the study and wrote the manuscript. SN, RT, SI, JY, and HN contributed to analyses. HN and NF assisted in the preparation of the manuscript. All authors contributed to data interpretation and approved the final version of the manuscript.

FUNDING

This work was supported, in part, by a grant from the Institute of Science and Engineering of Chuo University (NF and SN) and JSPS KAKENHI Grant Numbers JP16K18667, JP19K05756, and JP18KK0426 (SN).

ACKNOWLEDGMENTS

We thank the ABRC Stock Center for providing seeds of T-DNA insertion lines.

SUPPLEMENTARY MATERIAL

The Supplementary Material for this article can be found online at: https://www.frontiersin.org/articles/10.3389/fpls.2020.00610/full#supplementary-material

REFERENCES

Assunção, A. G., Bookum, W. M., Nelissen, H. J., Vooijs, R., Schat, H., and Ernst, W. H. (2003). Differential metal-specific tolerance and accumulation patterns among *Thlaspi caerulescens* populations originating from different soil types. *New Phytol.* 159, 411–419. doi: 10.1046/j.1469-8137.2003.00819.x

Brooks, R. R., Lee, J., Reeves, R. D., and Jaffré, T. (1977). Detection of nickeliferous rocks by analysis of herbarium specimens of indicator plants. *J. Geochem. Explorat.* 7, 49–57. doi: 10.1016/0375-6742(77)90074-7

Caille, N., Zhao, F. J., and McGrath, S. P. (2005). Comparison of root absorption, translocation and tolerance of arsenic in the hyperaccumulator *Pteris vittata* and the nonhyperaccumulator *Pteris tremula*. *New Phytol.* 165, 755–761. doi: 10.1111/j.1469-8137.2004.01239.x

Chaney, R. L., Angle, J. S., Broadhurst, C. L., Peters, C. A., Tappero, R. V., and Sparks, D. L. (2007). Improved understanding of hyperaccumulation yields commercial phytoextraction and phytomining technologies. *J. Environ. Qual.* 36, 1429–1443. doi: 10.2134/jeq2006.0514

Chao, D. Y., Silva, A., Baxter, I., Huang, Y. S., Nordborg, M., Danku, J., et al. (2012). Genome-wide association studies identify heavy metal ATPase3 as the primary determinant of natural variation in leaf cadmium in *Arabidopsis thaliana*. *PLoS Genet.* 8:e1002923. doi: 10.1371/journal.pgen.1002923

Curie, C., Cassin, G., Couch, D., Divol, F., Higuchi, K., Le Jean, M., et al. (2008). Metal movement within the plant: contribution of nicotianamine and yellow stripe 1-like transporters. *Ann. Bot.* 103, 1–11. doi: 10.1093/aob/mcn207

Freeman, J. L., Garcia, D., Kim, D., Hopf, A., and Salt, D. E. (2005). Constitutively elevated salicylic acid signals glutathione-mediated nickel tolerance in *Thlaspi* nickel hyperaccumulators. *Plant Physiol.* 137, 1082–1091. doi: 10.1104/pp.104.055293

Freeman, J. L., Persans, M. W., Nieman, K., Albrecht, C., Peer, W., Pickering, I. J., et al. (2004). Increased glutathione biosynthesis plays a role in nickel tolerance in *Thlaspi nickel hyperaccumulators*. *Plant Cell* 16, 2176–2191. doi: 10.1105/tpc.104.023036

Gendre, D., Czernic, P., Conéjéro, G., Pianelli, K., Briat, J. F., Lebrun, M., et al. (2007). TcYSL3, a member of the YSL gene family from the hyper-accumulator *Thlaspi caerulescens*, encodes a nicotianamine-Ni/Fe transporter. *Plant J.* 49, 1–15. doi: 10.1111/j.1365-313x.2006.02937.x

Halimaa, P., Lin, Y. F., Ahonen, V. H., Blande, D., Clemens, S., Gyenesei, A., et al. (2014). Gene expression differences between *Noccaea caerulescens* ecotypes help to identify candidate genes for metal phytoremediation. *Environ. Sci. Technol.* 48, 3344–3353. doi: 10.1021/es4042995

Hammond, J. P., Bowen, H. C., White, P. J., Mills, V., Pyke, K. A., Baker, A. J., et al. (2006). A comparison of the *Thlaspi caerulescens* and *Thlaspi arvense* shoot transcriptomes. *New Phytol.* 170, 239–260. doi: 10.1111/j.1469-8137.2006.01662.x

Hanikenne, M., and Nouet, C. (2011). Metal hyperaccumulation and hypertolerance: a model for plant evolutionary genomics. *Curr. Opin. Plant Biol.* 14, 252–259. doi: 10.1016/j.pbi.2011.04.003

Hanikenne, M., Talke, I. N., Haydon, M. J., Lanz, C., Nolte, A., Motte, P., et al. (2008). Evolution of metal hyperaccumulation required *cis*-regulatory changes and triplication of *HMA4*. *Nature* 453:391. doi: 10.1038/nature06877

Kramer, U., Smith, R. D., Wenzel, W. W., Raskin, I., and Salt, D. E. (1997). The role of metal transport and tolerance in nickel hyperaccumulation by *Thlaspi goesingense* halacsy. *Plant Physiol.* 115, 1641–1650. doi: 10.1104/pp.115.4.1641

Lasat, M. M., Baker, A. J., and Kochian, L. V. (1996). Physiological characterization of root Zn2+ absorption and translocation to shoots in Zn hyperaccumulator and nonaccumulator species of *Thlaspi*. *Plant Physiol.* 112, 1715–1722. doi: 10.1104/pp.112.4.1715

Lin, Y. F., Severing, E. I, te Lintel Hekkert, B., Schijlen, E., and Aarts, M. G. (2014). A comprehensive set of transcript sequences of the heavy metal hyperaccumulator *Noccaea caerulescens*. *Front. Plant Sci.* 5:261. doi: 10.3389/fpls.2014.00261

Lochlainn, S. Ó, Bowen, H. C., Fray, R. G., Hammond, J. P., King, G. J., White, P. J., et al. (2011). Tandem quadruplication of *HMA4* in the zinc (Zn) and cadmium (Cd) hyperaccumulator *Noccaea caerulescens*. *PLoS One* 6:e17814. doi: 10.1371/journal.pone.0017814

Mari, S., Gendre, D., Pianelli, K., Ouerdane, L., Lobinski, R., Briat, J. F., et al. (2006). Root-to-shoot long-distance circulation of nicotianamine and nicotianamine–nickel chelates in the metal hyperaccumulator *Thlaspi caerulescens*. *J. Exp. Bot.* 57, 4111–4122. doi: 10.1093/jxb/erl184

Marschner, H. (1995). *In Mineral Nutrition of Higher Plants*. London: Academic Press.

Merlot, S., Hannibal, L., Martins, S., Martinelli, L., Amir, H., Lebrun, M., et al. (2014). The metal transporter PgIREG1 from the hyperaccumulator *Psychotria gabriellae* is a candidate gene for nickel tolerance and accumulation. *J. Exp. Bot.* 65, 1551–1564. doi: 10.1093/jxb/eru025

Milner, M. J., Mitani-Ueno, N., Yamaji, N., Yokosho, K., Craft, E., Fei, Z., et al. (2014). Root and shoot transcriptome analysis of two ecotypes of *Noccaea caerulescens* uncovers the role of NcNramp1 in Cd hyperaccumulation. *Plant J.* 78, 398–410. doi: 10.1111/tpj.12480

Mizuno, N., Nosaka, S., Mizuno, T., Horie, K., and Obata, H. (2003). Distribution of Ni and Zn in the leaves of *Thlaspi japonicum* growing on ultramafic soil. *Soil Sci. Plant Nutr.* 49, 93–97. doi: 10.1080/00380768.2003.10409984

Mori, S., and Nishizawa, N. (1987). Methionine as a dominant precursor of phytosiderophores in Graminaceae plants. *Plant Cell Physiol.* 28, 1081–1092.

Morrissey, J., Baxter, I. R., Lee, J., Li, L., Lahner, B., Grotz, N., et al. (2009). The ferroportin metal efflux proteins function in iron and cobalt homeostasis in *Arabidopsis*. *Plant Cell* 21, 3326–3338. doi: 10.1105/tpc.109.069401

Na, G., and Salt, D. E. (2011). Differential regulation of serine acetyltransferase is involved in nickel hyperaccumulation in *Thlaspi goesingense*. *J. Biol. Chem.* 286, 40423–40432. doi: 10.1074/jbc.m111.247411

Nakagawa, T., Kurose, T., Hino, T., Tanaka, K., Kawamukai, M., Niwa, Y., et al. (2007). Development of series of gateway binary vectors, pGWBs, for realizing efficient construction of fusion genes for plant transformation. *J. Biosci. Bioeng.* 104, 34–41. doi: 10.1263/jbb.104.34

Nishida, S., Aisu, A., and Mizuno, T. (2012). Induction of *IRT1* by the nickel-induced iron-deficient response in *Arabidopsis*. *Plant Signal. Behav*. 7, 329–331. doi: 10.4161/psb.19263

Nishida, S., Kato, A., Tsuzuki, C., Yoshida, J., and Mizuno, T. (2015). Induction of nickel accumulation in response to zinc deficiency in *Arabidopsis thaliana*. *Int. J. Mol. Sci.* 16, 9420–9430. doi: 10.3390/ijms16059420

Nishida, S., Tsuzuki, C., Kato, A., Aisu, A., Yoshida, J., and Mizuno, T. (2011). AtIRT1, the primary iron uptake transporter in the root, mediates excess nickel accumulation in *Arabidopsis thaliana*. *Plant Cell Physiol*. 52, 1433–1442. doi: 10.1093/pcp/pcr089

Nozoye, T., Kim, S., Kakei, Y., Takahashi, M., Nakanishi, H., and Nishizawa, N. K. (2014). Enhanced levels of nicotianamine promote iron accumulation and tolerance to calcareous soil in soybean. *Biosci. Biotechnol. Biochem*. 78, 1677–1684. doi: 10.1080/09168451.2014.936350

Peer, W. A., Mahmoudian, M., Freeman, J. L., Lahner, B., Richards, E. L., Reeves, R. D., et al. (2006). Assessment of plants from the *Brassicaceae* family as genetic models for the study of nickel and zinc hyperaccumulation. *New Phytol*. 172, 248–260. doi: 10.1111/j.1469-8137.2006.01820.x

Peer, W. A., Mamoudian, M., Lahner, B., Reeves, R. D., Murphy, A. S., and Salt, D. E. (2003). Identifying model metal hyperaccumulating plants: germplasm analysis of 20 *Brassicaceae* accessions from a wide geographical area. *New Phytol*. 159, 421–430. doi: 10.1046/j.1469-8137.2003.00822.x

Persans, M. W., Yan, X., Patnoe, J. M. M., Krämer, U., and Salt, D. E. (1999). Molecular dissection of the role of histidine in nickel hyperaccumulation in *Thlaspi goesingense* (Hálácsy). *Plant Physiol.* 121, 1117–1126. doi: 10.1104/pp.121.4.1117

Reeves, R. D., Baker, A. J., Jaffré, T., Erskine, P. D., Echevarria, G., and van der Ent, A. (2018). A global database for plants that hyperaccumulate metal and metalloid trace elements. *New Phytol.* 218, 407–411. doi: 10.1111/nph.14907

Richau, K. H., Kozhevnikova, A. D., Seregin, I. V., Vooijs, R., Koevoets, P. L., Smith, J. A. C., et al. (2009). Chelation by histidine inhibits the vacuolar sequestration of nickel in roots of the hyperaccumulator *Thlaspi caerulescens*. New Phytol. 183, 106–116. doi: 10.1111/j.1469-8137.2009.02826.x

Salt, D. E., Smith, R. D., and Raskin, I. (1998). Phytoremediation. *Annu. Rev. Plant Biol*. 49, 643–668.

Schaaf, G., Honsbein, A., Meda, A. R., Kirchner, S., Wipf, D., and von Wirén, N. (2006). *AtIREG2* encodes a tonoplast transport protein involved in iron-dependent nickel detoxification in *Arabidopsis thaliana* roots. *J. Biol. Chem*. 281, 25532–25540. doi: 10.1074/jbc.m601062200

Suzuki, Y., Kawazu, T., and Koyama, H. (2004). RNA isolation from siliques, dry seeds, and other tissues of *Arabidopsis thaliana*. *Biotechniques* 37, 542–544. doi: 10.2144/04374bm03

Turner, T. L., Bourne, E. C., Von Wettberg, E. J., Hu, T. T., and Nuzhdin, S. V. (2010). Population resequencing reveals local adaptation of *Arabidopsis lyrata* to serpentine soils. *Nat. Genet*. 42:260. doi: 10.1038/ng.515

Ueno, D., Milner, M. J., Yamaji, N., Yokosho, K., Koyama, E., Clemencia Zambrano, M., et al. (2011). Elevated expression of *TcHMA3* plays a key role in the extreme Cd tolerance in a Cd-hyperaccumulating ecotype of *Thlaspi caerulescens*. *Plant J.* 66, 852–862. doi: 10.1111/j.1365-313x.2011.04548.x

Ueno, D., Yamaji, N., Kono, I., Huang, C. F., Ando, T., Yano, M., et al. (2010). Gene limiting cadmium accumulation in rice. *Proc. Natl. Acad. Sci.* 107, 16500–16505. doi: 10.1073/pnas.1005396107

Uraguchi, S., Weber, M., and Clemens, S. (2019). Elevated root nicotianamine concentrations are critical for Zn hyperaccumulation across diverse edaphic environments. *Plant Cell Environ*. 42, 2003–2014. doi: 10.1111/pce.13541

Vacchina, V., Mari, S., Czernic, P., Marquès, L., Pianelli, K., Schaumlöffel, D., et al. (2003). Speciation of nickel in a hyperaccumulating plant by high-performance liquid chromatography- inductively coupled plasma mass spectrometry and electrospray MS/MS assisted by cloning using yeast complementation. *Anal. Chem*. 75, 2740–2745. doi: 10.1021/ac020704m

van de Mortel, J. E., Villanueva, L. A., Schat, H., Kwekkeboom, J., Coughlan, S., Moerland, P. D., et al. (2006). Large expression differences in genes for iron and zinc homeostasis, stress response, and lignin biosynthesis distinguish roots of *Arabidopsis thaliana* and the related metal hyperaccumulator *Thlaspi caerulescens*. *Plant Physiol*. 142, 1127–1147. doi: 10.1104/pp.106.082073

Zhao, F. J., Hamon, R. E., Lombi, E., McLaughlin, M. J., and McGrath, S. P. (2002). Characteristics of cadmium uptake in two contrasting ecotypes of the hyperaccumulator *Thlaspi caerulescens*. *J. Exp. Bot*. 53, 535–543. doi: 10.1093/jexbot/53.368.535

Conflict of Interest: The authors declare that the research was conducted in the absence of any commercial or financial relationships that could be construed as a potential conflict of interest.

The handling Editor declared past co-authorship, with one of the authors, HN.

frontiers in Plant Science

ORIGINAL RESEARCH
published: 23 July 2020
doi: 10.3389/fpls.2020.01106

Deregulated High Affinity Copper Transport Alters Iron Homeostasis in *Arabidopsis*

Ana Perea-García[1], Amparo Andrés-Bordería[2†], Francisco Vera-Sirera[3], Miguel Angel Pérez-Amador[3], Sergi Puig[1] and Lola Peñarrubia[2]*

[1] Departamento de Biotecnología, Instituto de Agroquímica y Tecnología de Alimentos (IATA), Consejo Superior de Investigaciones Científicas (CSIC), Paterna, Valencia, Spain, [2] Departament de Bioquímica i Biologia Molecular and Estructura de Recerca Interdisciplinar en Biotecnologia i Biomedicina (ERI BIOTECMED), Universitat de València, Burjassot, Valencia, Spain, [3] Instituto de Biología Molecular y Celular de Plantas (IBMCP), Consejo Superior de Investigaciones Científicas (CSIC) —Universidad Politécnica de Valencia (UPV), Valencia, Spain

OPEN ACCESS

Edited by:
Louis Grillet, Academia Sinica, Taiwan

Reviewed by:
Takashi Hirayama, Okayama University, Japan
Jeeyon Jeong, Amherst College, United States
Ya-Fen Lin, National Taiwan University, Taiwan

***Correspondence:**
Lola Peñarrubia
penarrub@uv.es

†Present address:
Amparo Andrés-Bordería, Departamento de Fisiología, Facultad de Medicina, Universitat de València, Valencia, Spain

Specialty section:
This article was submitted to Plant Traffic and Transport, a section of the journal Frontiers in Plant Science

Received: *24 January 2020*
Accepted: *06 July 2020*
Published: *23 July 2020*

Citation:
Perea-García A, Andrés-Bordería A, Vera-Sirera F, Pérez-Amador MA, Puig S and Peñarrubia L (2020) Deregulated High Affinity Copper Transport Alters Iron Homeostasis in Arabidopsis. Front. Plant Sci. 11:1106. doi: 10.3389/fpls.2020.01106

The present work describes the effects on iron homeostasis when copper transport was deregulated in *Arabidopsis thaliana* by overexpressing high affinity copper transporters COPT1 and COPT3 (*COPT*^{OE}). A genome-wide analysis conducted on *COPT1*^{OE} plants, highlighted that iron homeostasis gene expression was affected under both copper deficiency and excess. Among the altered genes were those encoding the iron uptake machinery and their transcriptional regulators. Subsequently, *COPT*^{OE} seedlings contained less iron and were more sensitive than controls to iron deficiency. The deregulation of copper (I) uptake hindered the transcriptional activation of the subgroup Ib of basic helix-loop-helix (*bHLH-Ib*) factors under copper deficiency. Oppositely, copper excess inhibited the expression of the master regulator *FIT* but activated *bHLH-Ib* expression in *COPT*^{OE} plants, in both cases leading to the lack of an adequate iron uptake response. As copper increased in the media, iron (III) was accumulated in roots, and the ratio iron (III)/iron (II) was increased in *COPT*^{OE} plants. Thus, iron (III) overloading in *COPT*^{OE} roots inhibited local iron deficiency responses, aimed to metal uptake from soil, leading to a general lower iron content in the *COPT*^{OE} seedlings. These results emphasized the importance of appropriate spatiotemporal copper uptake for iron homeostasis under non-optimal copper supply. The understanding of the role of copper uptake in iron metabolism could be applied for increasing crops resistance to iron deficiency.

Keywords: *Arabidopsis thaliana*, copper uptake, high affinity copper importer 1, iron homeostasis, metal interactions, metal mobilization

INTRODUCTION

Copper (Cu) and iron (Fe) are transition metals with redox properties that form coordination complexes with organic molecules, acting as essential cofactors in numerous proteins, including components of the respiratory and photosynthetic electron transport chains (Puig et al., 2007; Nouet et al., 2011; Yruela, 2013). However, these redox properties also make Cu and Fe potentially

toxic since they facilitate the formation of reactive oxygen species (ROS). ROS produce damage at different levels, as they are able to react with proteins, DNA, and lipids in cell membranes, altering their function (Ravet and Pilon, 2013). Metal ion-dependent redox biology constitutes a fundamental theme of aerobic life. Nowadays, both multicopper oxidases (MCO), functioning as metallooxidases, and metalloreductases from the FERRIC REDUCTASE OXIDASE (FRO) family are necessary in redox cycling processes required for metal trafficking in eukaryotic cells (Kosman, 2018). Since evolved in an anaerobic environment, the proto-aerobe organisms developed metalloreductases to supply reduced metals Fe^{2+} and Cu^{+} to transporters. Changes in the bioavailability of both metals throughout the evolution of the atmosphere led to a decrease and increase in the Fe and Cu bioavailability, respectively, allowing their substitution as cofactors in different proteins to perform similar functions (Crichton and Pierre, 2001). For instance, in *Arabidopsis thaliana*, Cu/Zinc (Zn) superoxide dismutase (SOD) is replaced by its Fe counterpart when Cu is scarce (Yamasaki et al., 2007). Metalloprotein substitution contributes to the increase of Fe content under Cu deficiency and vice versa (Waters et al., 2012).

Higher plants have developed sophisticated mechanisms to efficiently acquire and use micronutrients such as Cu and Fe. Cu and specially Fe deficiencies cause losses in agriculture by decreasing the productivity and nutritional value of crops. The deficiency of Fe in agriculture is due to its low bioavailability, especially in alkaline soils (Marschner, 2012). From the two classically described pathways for Fe acquisition in plants, *Arabidopsis* uses strategy I that is based on the reduction of Fe^{3+} to Fe^{2+} by the reductase FRO2 present in the root plasma membrane (Robinson et al., 1999). The ZIP-type divalent cation transporter IRON-REGULATED TRANSPORTER 1 (IRT1) incorporates the Fe^{2+} into the root cell (Connolly et al., 2002; Varotto et al., 2002; Vert et al., 2002). In the chloroplast, Fe participates in the electron transport chain, chlorophyll biosynthesis, the assembly of Fe/S clusters, and the biosynthesis of heme groups, among other processes (Yruela, 2013). Mitochondria are also high Fe consumer organelles mainly for the electron transport chain and the assembly of Fe/S groups (Nouet et al., 2011). Therefore, due to the possibility of forming ROS, Fe is complexed by the ferritin protein (Reyt et al., 2015). The transcription factor FIT (bHLH29) (FER-like IRON DEFICIENCY INDUCED TRANSCRIPTION FACTOR) is a basic helix-loop-helix (bHLH) that binds to DNA in response of Fe deficiency (Colangelo and Guerinot, 2004). FIT interacts and forms heterodimers with the subgroup Ib of bHLH proteins (bHLH38, bHLH39, bHLH100 and bHLH101), which are required to properly respond to Fe deficiency (Wang et al., 2013). Among the genes activated by FIT are those encoding the reductase *FRO2* and the Fe and Cu transporters *IRT1* and *COPT2*, respectively (Colangelo and Guerinot, 2004). FIT activity is regulated at multiple levels by hormones, oxidative stress, and other signals, being considered as a hub modulating the *Arabidopsis* strategy I response to Fe deficiency (Kobayashi, 2019).

Other regulators of Fe uptake are the IRON MAN/FE-UPTAKE-INDUCING PEPTIDE (IMA/FEP), a group of conserved plant peptides induced under Fe deficiency in vascular tissues (Grillet et al., 2018; Hirayama et al., 2018). Moreover, several phytohormones are involved in modulating Fe deficiency responses in plants. Ethylene, auxin, gibberellin, and salicylic acid function as positive factors of the Fe-deficiency responses, whereas cytokinin, brassinosteroid, abscisic acid, and jasmonic acid act as negative factors of Fe uptake (Kobayashi, 2019). The balance between cellular proliferation and differentiation in the *Arabidopsis* root has been attributed to the transcription factor UPBEAT1 (UPB1), which regulates this balance through ROS control (Tsukagoshi et al., 2010). Among the upstream regulators is ILR3 (bHLH105), from the subgroup IVc of bHLH transcription factors, which is induced under Fe deficiency and inhibits the expression of genes such as *At-NEET*, *FER1*, and *FER3* (Tissot et al., 2019). ILR3 and bHLH115 interact with the E3 ubiquitin ligase BRUTUS (BTS), which ubiquitinates them for degradation (Selote et al., 2015). BTS is a protein that participate in Fe sensing, with highly conserved domains including 3 hemerythrin domains, and a protein-protein interaction domain denoted REALLY INTERESTING NEW GENE (RING) (Long et al., 2010; Kobayashi et al., 2013). BTS and its paralogs are negative regulators of Fe assimilatory responses (Hindt et al., 2017).

Cu is found in the form of Cu^{2+} in the soil, although under metal deficiency it is introduced in the root cells as Cu^{+} by high affinity Ctr transporters, denoted COPT (COPPER TRANSPORTERS) in plants (Puig, 2014; Peñarrubia et al., 2015). Previous to Cu^{+} uptake, reductases, from the FRO family participate in the reduction of Cu^{2+} (Bernal et al., 2012). The Ctr protein family is conserved in eukaryotes and mediates cellular Cu^{+} acquisition (Nevitt et al., 2012). The recently solved X-ray structure of a Ctr member has confirmed that each monomer contains three transmembrane segments that assemble as homotrimers or heterotrimers and that Cu^{+} is incorporated through a central pore (Ren et al., 2019). From the six genes identified in *Arabidopsis* that encode COPT transporters (Sancenón et al., 2003; Garcia-Molina et al., 2013), *COPT1* and *COPT3* are both induced by Cu deficiency and their encoded proteins are located into plasma membrane and at a compartment of the secretory pathway, respectively (Andrés-Colás et al., 2010; Andrés-Colás et al., 2018). The phenotypes of plants with altered levels of COPT1 and COPT3 correlate with their expression at the pollen grains and suggest a predominant role of COPT1, also expressed at the root tip, in the acquisition of Cu from the soil (Sancenón et al., 2004; Andrés-Colás et al., 2010; Andrés-Colás et al., 2018). Constitutive *COPT1* and *COPT3* overexpression ($COPT^{OE}$ plants) lead to increased Cu uptake, oxidative stress, and phenotypes related to altered circadian rhythms (Andrés-Colás et al., 2010; Rodrigo-Moreno et al., 2013; Perea-García et al., 2016; Sanz et al., 2019). Furthermore, the *Arabidopsis* COPT1 transporter has been overexpressed in *Oryza sativa* plants, leading to increased Fe content in polished grains (Andrés-Bordería et al., 2017). These results underscore the effects of Cu status on Fe traffic and mobilization. Moreover,

COPT2 is the *Arabidopsis* transporter with the highest expression along the root, and plants defective in *COPT2* are more resistant to double Cu and Fe deficiency (Perea-García et al., 2013). In fact, the *COPT2* promoter contains E-Box elements to which FIT binds (Colangelo and Guerinot, 2004). On the other hand, Cu deficiency involves the regulation of many metabolic processes to allocate the little Cu present to essential proteins. The Zn finger transcription factor SQUAMOSA-PROMOTER BINDING-LIKE PROTEIN 7 (SPL7) binds to GTAC consensus sequences present in the promoters of various genes that are expressed under Cu deficiency, such as *COPT2* (Yamasaki et al., 2009; Bernal et al., 2012). The presence of both cis regulatory elements justifies *COPT2* induction in the double deficiency of Cu and Fe (Perea-García et al., 2013).

The importance of the regulation of metal homeostasis, at both the cellular and the systemic levels, and its implications in agriculture and human health is evident. However, the molecular mechanisms underlying the interaction between both metals remain poorly understood (Gulec and Collins, 2014). As far as metal homeostasis networks for a specific metal are becoming well understood, the crosstalk between different metals is starting to emerge as a possibility to improve global metal nutritional levels for optimal organismal performing.

MATERIALS AND METHODS

Plant Growth Conditions and Treatments

Seeds of *A. thaliana*, ecotype *Columbia-0* (Col-0) and of the transgenic lines $COPT1^{OE}$ and $COPT3^{OE}$ were surface-sterilized and stratified for 2 days at 4°C and were germinated in ½ MS medium (Sigma) plates including 1% sucrose (Murashige and Skoog, 1962) (½ MS) or supplemented with 10 μM $CuSO_4$ (½ MS + 10 Cu) for the microarray analysis. Seedlings were grown as previously described (Andrés-Colás et al., 2010) for 7 days with a 12 h neutral photoperiod (65 μmol m^{-2} of cool-white fluorescent light) at 23°C/16°C temperature cycle.

In order to obtain ½ MS medium with the indicated concentrations of either Cu or Fe, the solution was prepared by adding macronutrients (Sigma) and micronutrients consisted in a mix of 50 μM H_3BO_3, 36.6 μM $MnSO_4$ H_2O, 15 μM $ZnSO_4$ $7H_2O$, 0.57 μM $NaMoO_4$ $2H_2O$, 0.25 mM KI, and 0.05 μM $CoCl_2$ $6H_2O$. Finally, 0.05% MES, 1% sucrose, and 0.8% phytoagar was added, and the pH was adjusted to 5.7–5.8 with diluted KOH. The Cu concentration in the Cu deficiency (0 μM $CuSO_4$) media including commercial phytoagar (Duchefa Biochemie) measured by ICP-MS is <0.008 μM Cu. To study the effects that the different Cu and Fe content have in plants, 50 μM Fe-citrate and 1 μM $CuSO_4$ $5H_2O$ were added to the medium for Cu and Fe sufficiency conditions. Moreover, seedlings were grown in Cu deficiency (0 μM $CuSO_4$) and Cu excess (10 μM $CuSO_4$). On the other hand, Fe-sufficient and slight or severe Fe deficiency medium was supplemented with 50, 10 and 0 μM Fe-citrate, respectively. Other metal concentrations and treatments were used for specific experiments as indicated in the Supplementary Figure Legends.

The chlorophyll content in seedlings and leaves was determined by the trichlorometric method (Parsons and Strickland, 1965). Root length was measured using the Image J 1.42q software (http://rsb.info.nih.gov./ij). Values represent the arithmetic mean ± standard deviation (SD) of three biological replicates (n = 3).

For the determination of ferroreductase activity, three seedlings of 7-day-old were collected and weighed. Next, a 1:1 mixture made with 300 μM bathophenantroline disulfonate (BPDS, Sigma) and 100 μM Fe III-EDTA was added to the seedlings and incubated at 30°C with stirring 225 rpm in the dark. After 30 min, the solution was collected and absorbance A_{535} was measured in a spectrophotometer (Grillet et al., 2014). Values represent the arithmetic mean ± standard deviation (SD) of three biological replicates (n = 3).

For root Fe^{3+} detection by Perl's staining, four to five seedlings of 11-day-old were vacuum infiltrated with equal volumes of 4% (v/v) HCl and 4% (w/v) K- ferrocyanide (Perl´s stain solution for 15 min) and incubated at room temperature for 30 min (Stacey et al., 2008). One representative photograph is shown in the figure. This method is based on the Fe^{3+} dependent conversion of ferrocyanide into insoluble crystals of Prussian blue under acidic conditions. Localization of Fe^{3+} was observed and analyzed with a (Olympus CX41) microscope equipped with (Leyca MC170HD) camera and (LAS V4.10) software.

Microarrays and Bioinformatics

Seven-day-old seedlings of the WT and the $COPT1^{OE}$ line were grown in the 12 h neutral photoperiod and three biological replicates were obtained for the (½ MS) treatment and four biological replicates were used as 10 μM $CuSO_4$, (½ MS + 10 Cu) samples. Total RNA was isolated using the RNeasy Plant Mini Kit (Qiagen) and aRNA was amplified using the MessageAmp™ II aRNA Amplification kit (Ambion). Long oligonucleotide microarrays were provided by Dr. David Galbraith (University of Arizona, http://www.ag.arizona.edu/microarray/). The hybridization and analysis were performed as described elsewhere (Bueso et al., 2007). The expression values (log_2) were obtained using the GenePix Pro 6.0 microarray-analysis software (Molecular Devices, Sunnyvale CA) and normalized with the GenePix Pro 6.0 and Acuity 4.0 software (Molecular Devices, Sunnyvale CA). Differential genes were identified with significance analysis of microarray (SAM) (Tusher et al., 2001) with false discovery rate (FDR) of <6% and 2-fold change ($log_2 \leq |1|$). Biological processes were identified with the Gene Ontology (GO) annotation (Ashburner et al., 2000), performed by the GeneCodis2.0 (http://genecodis.dacya.ucm.es/) (Carmona-Saez et al., 2007; Nogales-Cadenas et al., 2009) program (**Table 1**). The total differentially regulated genes are shown as Supplementary material (**Supplementary Tables SI** and **SII**). The microarray raw data were deposited in the NCBI's Gene Expression Omnibus (Edgar, 2002) and are accessible through GEO Series accession number GSE143857.

TABLE 1 | Differentially expressed iron- and tetrapyrrole-related genes in *COPT1*^{OE} vs. WT seedlings in low and high Cu.

Gene Name	ID Gen	Description	Value	
			MS	Cu
Fe homeostasis				
IRT1	AT4G19690	*Iron-regulated transporter 1*	**–1.74**	**–1.77**
FRO2	AT1G01580	*Ferric reduction oxidase 2*	—	**–1.30**
FRO3	AT1G23020	*Ferric reduction oxidase 3*	0.01	**1.24**
COPT2	AT3G46900	*Copper transporter 2*	**–0.92**	–0.05
CYP82C4	AT4G31940	*Cytochrome P450*	–	**–2.59**
FER1	AT5G01600	*Ferritin 1*	–0.15	**–2.17**
FER3	AT3G56090	*Ferritin 3*	–0,72	–0.71
At-NEET	AT5G51720	*Fe metabolism*	–0.51	**–2.30**
NAS4	AT1G56430	*Nicotianamine syntase 4*	**–1.51**	0.64
OPT3	AT4G16370	*Oligopeptide transporter 3*	**–1.14**	0.79
Fe regulators				
FIT/bHLH29	AT2G28160	*BHLH 29*	–	–0.39
bHLH039	AT3G56980	*Basic helix-loop-helix protein 39*	–0.15	**2.52**
bHLH101	AT5G04150	*Basic helix-loop-helix protein 101*	0.87	**2.15**
bHLH100	AT2G41240	*Basic helix-loop-helix protein 100*	0.22	**2,94**
bHLH115	AT1G51070	*Basic helix-loop-helix protein 115*	**–1.14**	–0.05
UPB1	AT2G47270	*Basic helix-loop-helix UPBEAT1*	**1.79**	–0.06
BTS	AT3G18290	*BRUTUS RING-ubiquitin ligase*	–0.26	**1.36**
FEP2/IMA2	AT1G47395	*Fe-Uptake-Inducing peptide2*	0.29	**3.32**
FEP3/IMA1	AT1G47400	*Fe-Uptake-Inducing peptide3*	0.42	**2.47**
Tetrapyrrole retrograde signaling				
CA1	AT3G01500		–0.32	**–1.06**
LHCB1.1	AT1G29920		0.34	**–0.97**
LHCB1.4	AT2G34430		–	**–1.10**
LHCB2.3	AT3G27690		–	**–1.80**
LHCB4.1	AT5G01530		–	**–1.30**
LHCB4.3	AT2G40100		–	**–1.34**
LHCB5	AT4G10340		**–1.12**	**–0.73**
Components				
HEMA1	AT1G58290	*glutamyl-tRNA reductase 1, chloroplast*	–2.13	**–1.46**
GUN4	AT3G59400	*genome uncoupled 4*	–1.00	**–1.36**
CHL27	AT3G56940	*Copper response defect 1*	–0.10	–0.76
SIG1	AT1G64860	*Chloroplast sigma factor 1*	–1.70	–1.16

Gene name, MIPS code, gene description, and the expression values (fold change) of differentially regulated genes with a log_2 ratio of ≥\|1\| in the COPT1^{OE} versus the WT were indicated under –Cu (MS) and + 10 μM Cu (Cu). In bold are the genes that passed the statistical analysis.

Gene Expression by Real-Time Quantitative PCR

Total *Arabidopsis* RNA was isolated using the RNeasy Plant Mini Kit (Qiagen), was quantified by UV spectrophotometry and its integrity was visually assessed on ethidium bromide-stained agarose gels. After treatment with Dnase I Amp Grade (Invitrogen), cDNA was generated by retro-transcriptase SSII (Invitrogen) as previously described (Andrés-Colás et al., 2006). Real-time quantitative PCR (RT-qPCR) was carried out with SYBR-Green qPCR Super-Mix-UDG with ROX (Invitrogen) with the specific primers detailed in **Table SVI** in a CFX96 Touch™ Real Time PCR Detection System (BioRad), with one cycle of 95°C for 2 min and 40 cycles consisting in 95°C for 30 s and 60°C for 30 s. Expression values were normalized to *UBQ10* and to the WT in deficiency conditions using the $2^{-\Delta\Delta Ct}$ method. Values represent the arithmetic mean ± standard deviation (SD) of three biological replicates (n = 3).

Oxygen Consumption Determination

To study O_2 consumption, 14–16 roots of 10-day-old seedlings, grown in different conditions, were used. The roots were cut with a scalpel and resuspended in 1.5 ml of ½ MS liquid medium, as it is described above but without sucrose. The roots were transferred to an airtight chamber and the measurement of O_2 consumption for a minimum of 5 min was performed using a Clark type electrode (Oxyview system). The rate of decrease of O_2, referenced to fresh weight (F.W.) of the roots (nmol O_2/ OD_{600} × F.W.) was taken as an index of respiratory capacity. Values represent the arithmetic mean ± standard deviation (SD) of three biological replicates (n = 3).

Metal and Hormone Determinations

Cu and Fe contents were determined by ICP-MS as described previously (Andrés-Colás et al., 2006; Carrió-Seguí et al., 2015) at the Servei Central de Suport a la Investigació Experimental (SCSIE) of the Universitat de València.

For the determination of the content of ABA, indol-3-acetic acid (IAA), and JA, 8-day-old seedlings were lyophilized, processed and analyzed by UHPLC (ultra-high-pressure liquid chromatography) Q-Exactive (ThermoFisher Scientific) as described previously (da Silva et al., 2017) in the plant hormone quantification service of the Institute of Molecular

and Cellular Plant Biology (IBMCP, Valencia). Values represent the arithmetic mean ± standard deviation (SD) of three biological replicates (n = 3).

Statistical Analysis

The statistical analysis of the relative gene expression was performed by the pair wise fixed reallocation randomization test (p-value <0.05) (Pfaffl, 2002). For the remaining parameters, the analysis was carried out using one or two-way ANOVA with the means compared by the Duncan test or a Kruskal–Wallis (p-value <0.05) test for a non-parametric measurements using the InfoStat software, version 2010 (http://www.infostat.com.ar) (Di Rienzo et al., 2011).

RESULTS

A Genome-Wide Expression Analysis Highlights That Iron Homeostasis Is Affected in *COPT1^{OE} Arabidopsis* Plants

To identify at a molecular level the global effects caused by the deregulation of Cu homeostasis in *Arabidopsis*, we performed a comparative transcriptomic analysis of 7-day-old wild-type (WT) and a previously generated COPT1 overexpressing (*COPT1^{OE}*) line (Andrés-Colás et al., 2010), grown under Cu deficiency (½ MS) and mild Cu excess (½ MS + 10 Cu) conditions. The induction of *COPT1* expression under Cu deficiency in the WT was corroborated by RT-qPCR, as well as its overexpression in *COPT1^{OE}* seedlings, both under deficiency and excess Cu conditions, in the samples that were used in the hybridizations of the DNA microarrays (data not shown). From the global analysis of gene expression, a total of 583 differentially expressed genes were identified with a $\log_2$ ratio of ≥|1| in the *COPT1^{OE}* versus WT (**Supplementary Figure S1** and **Tables SI** and **SII**). These were distributed in a total of 482 induced (ratio ≥1) and of 101 repressed genes (ratio ≥−1) in *COPT1^{OE}* seedlings for the two growth conditions tested (**Supplementary Figure S1** and **Supplementary Tables SI** and **SII**).

The number of genes induced was greater than that of genes repressed in the two conditions. On the other hand, the mild Cu excess condition showed the greatest number of genes with differential expression compared to Cu deficiency, with 393 genes (312 induced and 81 repressed) compared to 160 genes (142 induced and 18 repressed), respectively. The analysis of the gene ontology (GO) of differentially regulated genes between WT and *COPT1^{OE}* seedlings indicated that several the Biological Processes categories were overrepresented, including those linked to photosynthesis, photomorphogenesis, transport of metals such as Fe, Zn, manganese, cadmium, and phosphate, oxidative stress and responses to abscisic acid (ABA) and cold stress (**Supplementary Table SIII**). On the other hand, the Molecular Function of genes differentially regulated in *COPT1^{OE}* included the chlorophyll and tetrapyrrole binding (**Supplementary Table SIV**). GO analysis also revealed that the chloroplast was the subcellular compartment most affected by the changes observed in *COPT1^{OE}*, as 39% of the significantly enriched GO categories of Cellular Compartment are related to chloroplast (chloroplast, chloroplast envelope, thylakoid membrane, chloroplast membrane, stroma, photosystems I and II, and light-harvesting complex) (**Supplementary Table SV**). The Fe-related genes studied in this work, which expression was affected in *COPT1^{OE}* plants, are summarized in **Table 1**.

Fe Assimilation in the *COPT^{OE}* Seedlings

One of the most relevant result of the transcriptomic analysis in *COPT1^{OE}* is the altered expression of Fe-related genes (**Table 1**), such as *IRT1* and *FRO2*, involved in the strategy I of Fe uptake (**Table 1**). Expression of the Fe transporter *IRT1* was reduced in *COPT1^{OE}* seedling in both Cu deficiency (½ MS) or excess (½ MS + 10 Cu). In contrast, the genes encoding *FRO* reductases showed a different behavior; expression of *FRO2* was induced but that for *FRO3* was repressed in *COPT1^{OE}* seedlings only in Cu excess. In order to further assess the effects of Cu on their expression, seedlings were grown on hand-made ½ MS medium with three different $CuSO_4$ concentrations, including Cu deficiency (0 μM $CuSO_4$), sufficiency (1 μM $CuSO_4$), and mild Cu excess (10 μM $CuSO_4$). Furthermore, in addition to *COPT1^{OE}*, plants overexpressing the *COPT3* transporter (*COPT3^{OE}*) (Andrés-Colás et al., 2010) were also included to further assess the effect of deregulated Cu^+ entrance (**Figure 1**). *IRT1* expression slightly decreased in the WT seedlings as Cu increased in the medium, being significantly lower under Cu sufficiency and excess compared to deficiency conditions (**Figure 1A**). Similar to the global transcriptomic analysis, *IRT1* expression in *COPT^{OE}* (*COPT1^{OE}* and *COPT3^{OE}* lines) was lower than in WT under both Cu deficiency and excess. Since genes encoding reductases *FRO2* and *FRO3* displayed distinct regulation in *COPT1^{OE}* seedlings (**Table 1**), total ferroreductase activity was measured in the roots of 7-day-old *COPT^{OE}* seedlings (**Figure 1B**). No changes in ferroreductase activity were observed under Cu deficiency and sufficiency. However, a slightly lower ferroreductase activity was observed under Cu excess in the *COPT1^{OE}* plants compared to the WT (**Figure 1B**).

COPT1^{OE} and *COPT3^{OE}* seedlings were previously shown to incorporate more Cu, both under metal deficiency and excess in the growth medium (Andrés-Colás et al., 2010). Now, the Fe content was determined by ICP-MS in both shoots and roots from 7-day-old WT and *COPT^{OE}* seedlings grown under the different Cu conditions (**Figures 1C, D**). We observed that *COPT^{OE}* seedlings had slightly lower endogenous Fe concentration than the WT both in shoots and roots but only significant under Cu sufficiency and excess. This decrease was more evident in the roots of the *COPT3^{OE}* seedlings (**Figure 1D**), which is consistent with their exacerbated reduction in *IRT1* expression (**Figure 1A**).

To corroborate the expression changes of other Fe-related genes involved in Fe storage and metabolism in *COPT1^{OE}* seedlings, we further investigated the expression of genes included in these processes, such as *FER1*, *FER3*, and *At-NEET* (**Table 1** and **Figure 2**). Previous data have shown that the expression of *FER1* is higher among the four genes (*FER1*, *FER2*, *FER3* and *FER4*) that encode ferritins (Petit et al., 2001). *FER1* and *FER3* expression was down-regulated under Cu excess

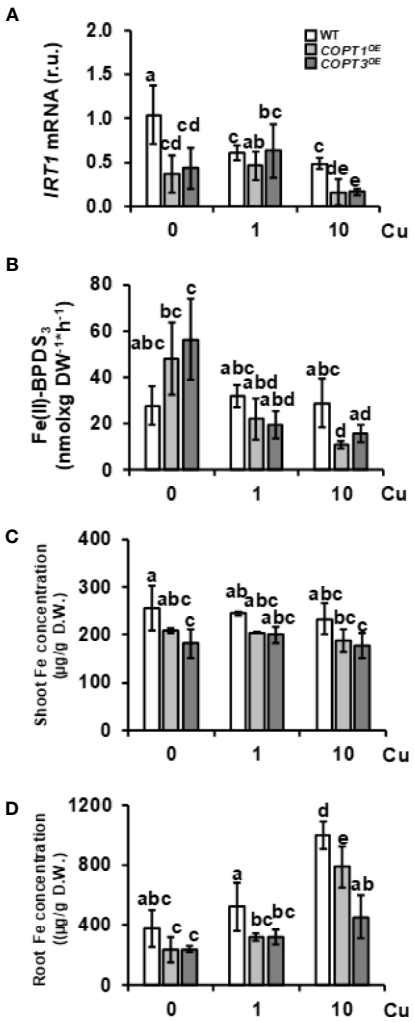

FIGURE 1 | Expression of strategy I components of Fe uptake in *COPT*^{OE} seedlings. **(A)** Relative expression of *IRT1* gene in 7-day-old WT (white bars), *COPT1*^{OE} (light grey bars), and *COPT3*^{OE} (dark grey bars) seedlings grown under Cu deficiency (0 µM $CuSO_4$), sufficiency (1 µM $CuSO_4$) or Cu excess (10 µM $CuSO_4$) was determined by RT-qPCR. Gene expression is represented as relative expression levels (r.u.) in relation to the WT under control conditions. *UBQ10* was used as housekeeping gene. Bars correspond to arithmetic means ($2^{-\Delta\Delta Ct}$) ± SD of biological replicates (n = 3). **(B)** Ferroreductase activity in 7-day-old WT and *COPT*^{OE} seedlings grown in the same conditions as in **(A)** measured at A_{535} nm. Bars correspond to arithmetic means ± SD of biological replicates (n = 3) **(C)** Shoot and **(D)** root Fe concentration in 7-day-old WT, *COPT1*^{OE} and *COPT3*^{OE} seedlings grown on $CuSO_4$ media specified in **(A)** and determined as µg/g of dry weight (D.W.). Bars correspond to arithmetic means ± SD of biological replicates (n = 3). Samples with a letter in common are not significantly different (*p*-value <0.05). D.W., dry weight.

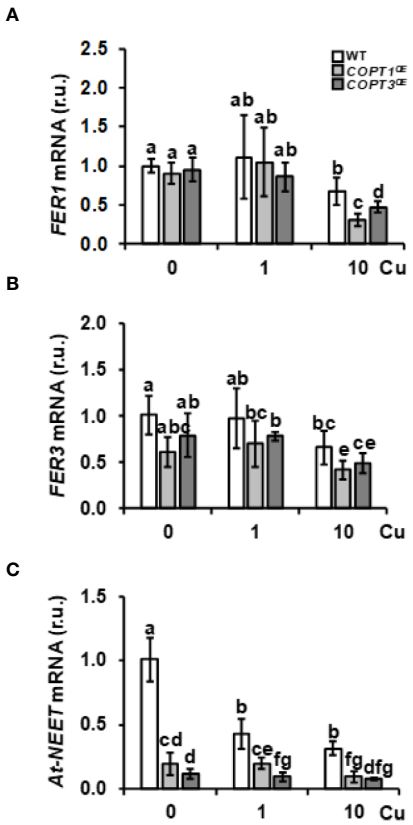

FIGURE 2 | Expression of Fe metabolism genes in *COPT*^{OE} seedlings. Relative expression of *FER1* **(A)**, *FER3* **(B)**, and *At-NEET* **(C)** genes in WT (white bars), *COPT1*^{OE} (light grey bars), and *COPT3*^{OE} (dark grey bars) seedlings grown under Cu deficiency (0 µM $CuSO_4$), sufficiency (1 µM $CuSO_4$) or Cu excess (10 µM $CuSO_4$) was determined by RT-qPCR. Gene expression is represented as relative expression levels (r.u.) in relation to the WT under control conditions. *UBQ10* was used as housekeeping gene. Bars correspond to arithmetic means ($2^{-\Delta\Delta Ct}$) ± SD of biological replicates (n = 3). Samples with a letter in common are not significantly different (*p*-value <0.05).

compared to Cu deficiency in WT and this decrease was more exacerbated in *COPT*^{OE} seedlings (**Table 1** and **Figures 2A, B**). This pattern is also in agreement with the lower Fe content in the *COPT*^{OE} under Cu excess (**Figure 1C**). *At-NEET* encodes a Fe/S protein involved, among other processes, in the Fe metabolism and ROS homeostasis (Nechushtai et al., 2012; Mittler et al., 2019). *At-NEET* expression was induced under Cu deficiency in the WT and reduced in the *COPT*^{OE} seedlings under all the Cu conditions studied (**Table 1** and **Figure 2C**). The expression of *FER1*, *FER3*, and *At-NEET* was also analyzed under different Cu and Fe contents in WT seedlings (**Supplementary Figure S2**). Whereas all of them were induced under Cu deficiency compared to control conditions, only *FER1* expression was repressed under Fe deficiency. *FER3* and *At-NEET* were not regulated by Fe levels (**Supplementary Figure S2**). Altogether, these results indicate that the deregulated Cu^+ entrance in *COPT*^{OE} prevents the induction of genes involved in Fe uptake, leading ultimately to a reduced endogenous Fe content, and suggesting that overexpression of *COPT* may alter the local response to Fe deficiency in roots.

Expression of Regulators of Fe Homeostasis in the *COPT*^{OE} Seedlings

Certain Fe deficiency responses are under the control of the Cu-responsive SPL7 transcription factor (Kastoori Ramamurthy

et al., 2018). To determine whether the inhibition of *IRT1* expression observed in *COPT*^{OE} could be a SPL7-mediated response, we checked the expression in *COPT*^{OE} seedlings of *SPL7* and *SPL7*-regulated markers of Cu deficiency responses, such as *COPT2* and *FSD1* (**Supplementary Figure S3**), the latter encoding FeSOD (Yamasaki et al., 2009). *SPL7* expression remained mostly unaffected in *COPT*^{OE}. Whereas *COPT2* expression was down-regulated in *COPT*^{OE} seedlings, *FSD1* expression was not affected under Cu deficiency (**Supplementary Figures S3B, C**). Furthermore, other SPL7 targets were not differentially expressed in the *COPT1*^{OE} seedlings under Cu deficiency (**Tables SI** and **SII**), indicating that the SPL7 factor was properly functioning in *COPT*^{OE} seedlings and it was not differentially affecting Cu deficiency responses in these plants. On the other hand, the expression of *CSD2*, encoding the chloroplastic Cu/Zn SOD *CSD2*, was reduced in *COPT*^{OE} seedlings under Cu sufficiency and excess (**Supplementary Figure S3D**).

To further address the role of Cu in the lack of Fe-deficiency response, we analyzed the expression of Fe-related bHLH transcription factors and other regulators (**Table 1** and **Figure 3**). A slight increase and a lower expression were observed for *FIT* under Cu deficiency and excess, respectively, in *COPT1*^{OE} seedlings compared to the WT (**Figure 3A**). Consistent with *FIT* inhibition under Cu excess, the expression of two of its targets, *IRT1* and *COPT2*, was slightly repressed in *COPT*^{OE} seedlings (**Figure 1A** and **Supplementary Figure S3B**), which suggests that high Cu in these plants represses the activity of this master Fe uptake regulator. The expression of the subgroup Ib of Fe-related bHLH (*bHLH38*, *bHLH39*, *bHLH100* and *bHLH101*) transcription factors was also analyzed (**Figures 3B, C**, **Supplementary Figures S4A, B**). We observed that, in the WT plants, expression of *bHLH-Ib* factors was in general greater as Cu increased in the growth medium. Remarkably, its expression was highly increased in *COPT1*^{OE} seedlings under Cu excess conditions (**Figure 3** and **Supplementary Figure S4**). Therefore,

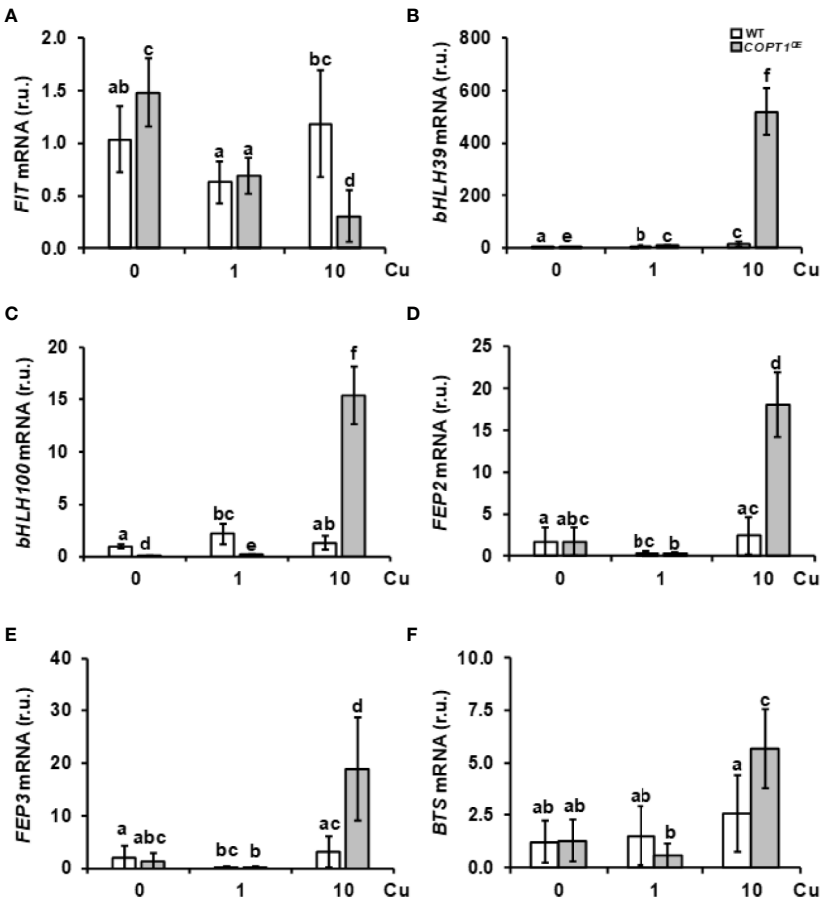

FIGURE 3 | Gene expression of Fe homeostasis regulators in *COPT1*^{OE} seedlings. The 7-day-old WT (white bars) and *COPT1*^{OE} plants (grey bars) seedlings grown under Cu deficiency (0 μM $CuSO_4$), sufficiency (1 μM $CuSO_4$) or Cu excess (10 μM $CuSO_4$). Expression of *FIT* **(A)**, *bHLH39* **(B)**, *bHLH100* **(C)**, *FEP2* **(D)**, *FEP3* **(E)**, and *BTS* **(F)** was determined by RT-qPCR. Gene expression is represented as relative expression levels (r.u.) in relation to the WT under control conditions. *UBQ10* was used as housekeeping gene. Bars correspond to arithmetic means ($2^{-\Delta\Delta Ct}$) ± SD of biological replicates (n = 3). Samples with a letter in common are not significantly different (*p*-value <0.05).

the opposite regulation in *COPT1*^{OE} seedlings under Cu excess was observed for *FIT* and the rest of regulatory *bHLH-Ib* factors. Whereas *FIT* expression was reduced under Cu excess in *COPT*^{OE} respect to the WT, *bHLH-Ib* expression was increased under Cu excess (**Figure 3** and **Supplementary Figure S4**).

Among the most induced Fe-related genes in the *COPT1*^{OE} line under Cu excess were the Fe peptide regulators *FEP2* and *FEP3* (**Table 1**). The expression of these responds to Fe deficiency in a FIT-independent manner (Hirayama et al., 2018). In agreement with low Fe levels in the *COPT1*^{OE} plants, *FEP2* and *FEP3* were clearly induced under Cu excess (**Figures 3D, E**). This result indicated that the FIT-independent signaling pathway for *FEP2* and *FEP3* induction was not affected by deregulated Cu uptake in *COPT1*^{OE} under Cu excess.

Taken together these results indicate that strategy I local responses to Fe deficiency cannot take place in *COPT*^{OE} seedlings under Cu excess despite the increased expression in *bHLH-Ib* transcription factors and *FEP* genes. This is probably due to the inhibition of *FIT* expression (**Figure 3A**), whereas the opposite occurs under Cu deficiency where, despite slightly enhanced *FIT* expression in the *COPT1*^{OE} seedlings, the low *bHLH-Ib* expression (**Figure 3** and **Supplementary Figure S4**) was precluding assimilatory Fe deficiency responses.

Regarding to upstream regulators of Fe homeostasis that were repressed in *COPT1*^{OE} (**Table 1**), we analyzed the expression of the subgroup IVc members of *bHLH* (*bHLH105/IRL3* and *bHLH115*) transcription factors. *IRL3* and *bHLH115* were repressed in *COPT3*^{OE} (**Supplementary Figures S4C, D**). On the other hand, BTS expression encoding an E3 ubiquitin ligase that participates in Fe sensing (Long et al., 2010; Kobayashi et al., 2013) was enhanced under Cu excess in WT plants and further increased in *COPT1*^{OE} (**Figure 3F**). This increased expression in BTS and the reduced Fe uptake response under Cu excess (**Figure 1**) was according to the BTS role as a negative regulator of Fe assimilatory responses (Hindt et al., 2017).

Plant hormones are involved in regulating the expression of Fe deficiency-responsive genes (Kobayashi, 2019). In order to check if hormone contents were significantly affected in *COPT1*^{OE} seedlings, abscisic acid (ABA), jasmonic acid (JA), and indol acetic acid (IAA) contents were determined (**Supplementary Figure S5**). Whereas the ABA levels were not significantly modified with respect to controls, JA and IAA levels decreased in *COPT1*^{OE} seedlings as Cu increased in the medium (**Supplementary Figure S5**).

Phenotype of *COPT*^{OE} Seedlings Under Fe Deficiency

Given the previous data, we studied the phenotype of *COPT*^{OE} seedlings under Fe deficiency (**Figure 4**). Thus, 7-day-old WT, *COPT1*^{OE}, and *COPT3*^{OE} seedlings were grown in media with Fe sufficiency (50 μM $FeSO_4$) and slight Fe deficiency (10 μM $FeSO_4$) (**Figure 4**). Whereas WT seedlings increased their root length under slight Fe deficiency conditions, *COPT*^{OE} presented a similar length of their roots in both media (**Figures 4A, B**). Root shortening in the *COPT*^{OE} with respect to WT under slight

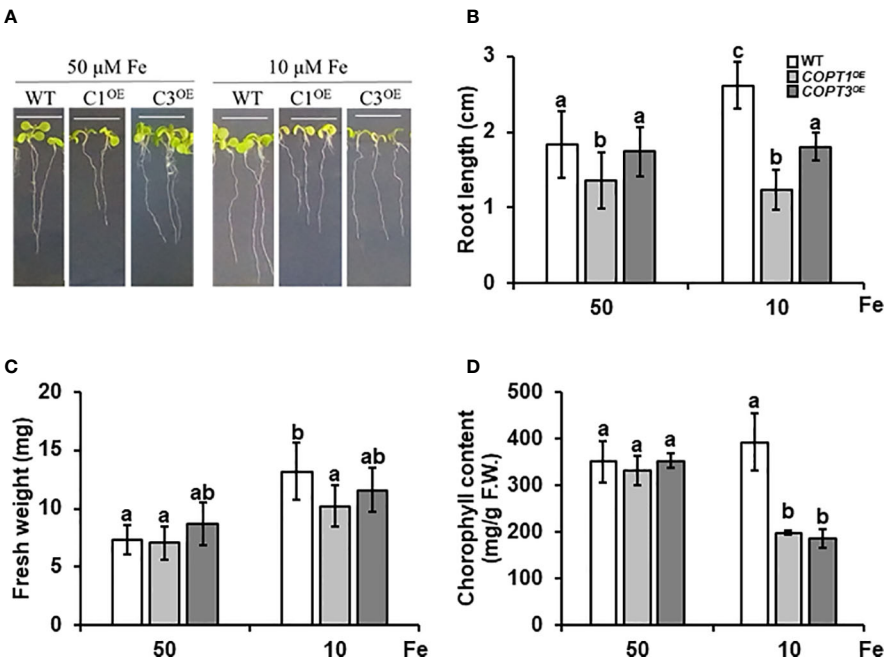

FIGURE 4 | Physiological characterization of *COPT*^{OE} seedlings under Fe deficiency. **(A)** Representative photographs of 7-day-old seedlings of WT, *COPT1*^{OE} and *COPT3*^{OE} under Fe sufficiency (50 μM $FeSO_4$) or slight Fe deficiency (10 μM $FeSO_4$). White scale bars represent 1 cm. **(B)** Root length of the of WT (white bars), *COPT1*^{OE} (light grey bars), and *COPT3*^{OE} (dark grey bars) under the same growth conditions as in **(A)**. **(C)** Fresh weight of 5 WT and *COPT1*^{OE} seedlings grown under the same conditions as in **(A)**. **(D)** Total chlorophyll content of WT and *COPT*^{OE} seedlings grown under the same conditions as in **(A)**. Bars correspond to arithmetic means ($2^{-\Delta\Delta Ct}$) ± SD of biological replicates (n = 3). Samples with a letter in common are not significantly different (*p*-value <0.05).

Fe deficiency was around 50%. No changes were observed in the seedlings fresh weight under sufficiency, while under slight Fe deficiency, the weight was reduced in *COPT1*^{OE} (**Figure 4C**). Moreover, the total chlorophyll content did not show significant changes in the WT, while *COPT*^{OE} seedlings displayed around 50% lower chlorophyll content in Fe deficiency (**Figure 4D**). Taken together, these data indicate that *COPT*^{OE} seedlings are more sensitive to slight Fe deficiency conditions than WT.

Then, we analyzed the expression of Fe homeostasis-related genes under Fe sufficiency and deficiency. *IRT1* expression increased under Fe deficiency in both WT and *COPT*^{OE} (**Supplementary Figure S6A**). On the other hand, an increase in *FIT* expression was observed under Fe deficiency in the WT plants, while in *COPT*^{OE} this increase was exacerbated (**Supplementary Figure S6B**). Furthermore, *FEP2* and *FEP3* expression was induced in WT plants under Fe deficiency but it was also highly increased in *COPT1*^{OE} (**Supplementary Figures S6C, D**). Taken together, these results indicated that *COPT*^{OE} seedlings properly responded to Fe deficiency under Cu sufficiency and that their defects in Fe homeostasis were restricted to Cu deficiency and excess conditions.

The expression of the Fe homeostasis regulators *FIT*, *bHLH38*, *bHLH100*, and *UPB1* was analyzed under different metal deficiency and excess conditions in the WT plants (**Supplementary Figure S7**). *FIT*, *bHLH38*, and *bHLH100* where induced under Fe deficiency whereas *UPB1* was repressed. Curiously, all of them but *FIT* were regulated in the same sense under Cu excess and Fe deficiency, either induced (*bHLH38* and *bHLH100*) or repressed (*UPB1*), suggesting that maybe there are certain similarities or common steps in signal transduction between the responses to Cu excess and Fe deficiency, leading to the induction of these transcriptional factors.

Expression of Genes Involved in Tetrapyrrole Biosynthesis in *COPT*^{OE} Seedlings

GO analysis of the global transcriptomic analysis revealed that the chloroplast was the subcellular compartment most affected in *COPT1*^{OE} (**Supplementary Table SV**). GO categories differentially enriched among genes differentially regulated in *COPT1*^{OE} seedlings were photosynthesis-associated nuclear genes (*PhANG*) and genes related to photomorphogenesis, and oxidative stress (**Table 1** and **Supplementary Tables SIII** and **SV**). Therefore, we decided to assess the alteration of the expression of genes in the tetrapyrrole biosynthesis pathway and the retrograde signaling components (**Table 1**). The *LHCB2.3* expression, a representant among the multiple *PhANG*, which are down-regulated in the *COPT1*^{OE} seedlings (**Table SII**), was confirmed to be repressed (**Figure 5A**). Moreover, the expression of *GUN4*, a regulator of the plastidic tetrapyrrole signaling (Davison et al., 2005), was also repressed in most conditions (**Figure 5B**). In addition, *CHL27/CDR1* (Bang et al., 2008) was also down-regulated in *COPT*^{OE} seedlings (**Figure 5C**), further confirming the involvement of tetrapyrrole signaling in Cu-dependent Fe deficiency responses. The regulation of a chloroplastic sigma factor *SIG1* involved in retrograde signaling (Macadlo et al., 2019) was also down-regulated under Cu deficiency in *COPT*^{OE} seedlings

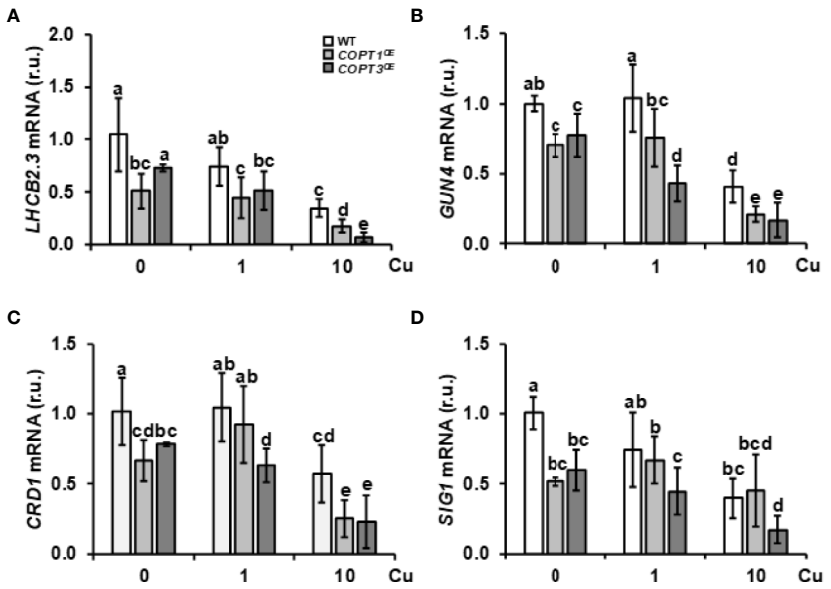

FIGURE 5 | Expression of genes related to tetrapyrrole biosynthesis and retrograde signaling in *COPT*^{OE}. Expression of the *LHCB2.3* **(A)**, *GUN4* **(B)**, *CDR1* **(C)**, and *SIG1A* **(D)** genes in WT (white bars), *COPT1*^{OE} (light grey bars), and *COPT3*^{OE} (dark grey bars) seedlings grown under Cu deficiency (0 μM $CuSO_4$), sufficiency (1 μM $CuSO_4$) or Cu excess (10 μM $CuSO_4$) was determined by RT-qPCR. Gene expression is represented as relative expression levels (r.u.) in relation to the WT under control conditions. *UBQ10* was used as housekeeping gene. Bars correspond to arithmetic means ($2^{-\Delta\Delta Ct}$) ± SD of biological replicates (n = 3). Samples with a letter in common are not significantly different (*p*-value <0.05).

(**Figure 5D**). Taken together, these results indicated that the tetrapyrrole signaling pathway was affected under both Cu deficiency and excess, probably as a consequence of the common Fe deficiency conditions faced by *COPT*^{OE} seedlings.

Root Respiration and Oxidative Stress in *COPT*^{OE} Seedlings

Since the respiratory electron transport chain is one of the most metal requiring processes, O_2 consumption was measured in 7-day-old roots of WT and *COPT1*^{OE} seedlings grown in deficiency (0 μM $CuSO_4$), sufficiency (1 μM $CuSO_4$) and excess $CuSO_4$ (10 μM $CuSO_4$) (**Figure 6A**). The results showed that O_2 consumption in WT seedlings did not exhibit significant changes between the three media, while *COPT1*^{OE} displayed lower O_2 consumption when the Cu conditions were not optimal, in both deficiency and in excess, with a decrease of 42 and 46% respectively, compared to WT (**Figure 6A**). In agreement with a defective functioning of the respiratory electron transport chain, expression of the *ALTERNATIVE OXIDASE 1D* (*AOX-1D*), aimed to restore electron flow in a non-phosphorylating bypass (Clifton et al., 2006; Selinski et al., 2018), was increased in *COPT1*^{OE} (**Figure 6B**). Moreover, other *AOX* genes, such as *AOX1A* (+2.46) and *AOX2* (+2.08), were also induced under Cu excess in *COPT*^{OE} (**Supplementary Table SI**). On the other hand, expression of the *LOW SULPHUR UPREGULATED1* (*LSU1*) has been shown to prevent chloroplastic ROS production by interacting with *FSD2* (Garcia-Molina et al., 2017). *LSU1* was also greatly induced under Cu excess (**Figure 6C**), as well as *LSU2* and *LSU3* (**Supplementary Table SI**). Inhibition of *FSD1* and *CSD2* expression in the *COPT*^{OE} plants (**Supplementary Figure S3**) suggested a defective antioxidant capacity by an increase in the radical superoxide ($O_2^{\cdot -}$) and a decrease in hydrogen peroxide (H_2O_2).

UPB1 spatially regulates ROS distribution in the root transition zone where the balance between $O_2^{\cdot -}$ and H_2O_2 controls the transition between root cell proliferation and differentiation (Tsukagoshi et al., 2010). *UPB1* expression was induced under Cu deficiency and sufficiency in *COPT1*^{OE} seedlings compared to WT (**Figure 6D**). Accordingly, two of its direct targets, *PER39* and *PER40*, were also up-regulated under Cu deficiency (**Supplementary Figures S8A, B**). Furthermore, *UBP1* expression under different metal stress conditions in the WT indicated that was repressed under Cu excess as well as when Fe is low (**Supplementary Figure S7D**). These responses indicated clearly different responses of Fe regulators to low and high Cu levels.

Since these results would lead to a further decrease in H_2O_2, seedlings were grown in Cu-deficient media in the presence of H_2O_2 and the reductants ascorbic acid (AsH) and 1,4-ditiothreitol (DTT) (**Supplementary Figure S9**). *COPT1*^{OE} seedlings showed shorter roots than controls under Cu

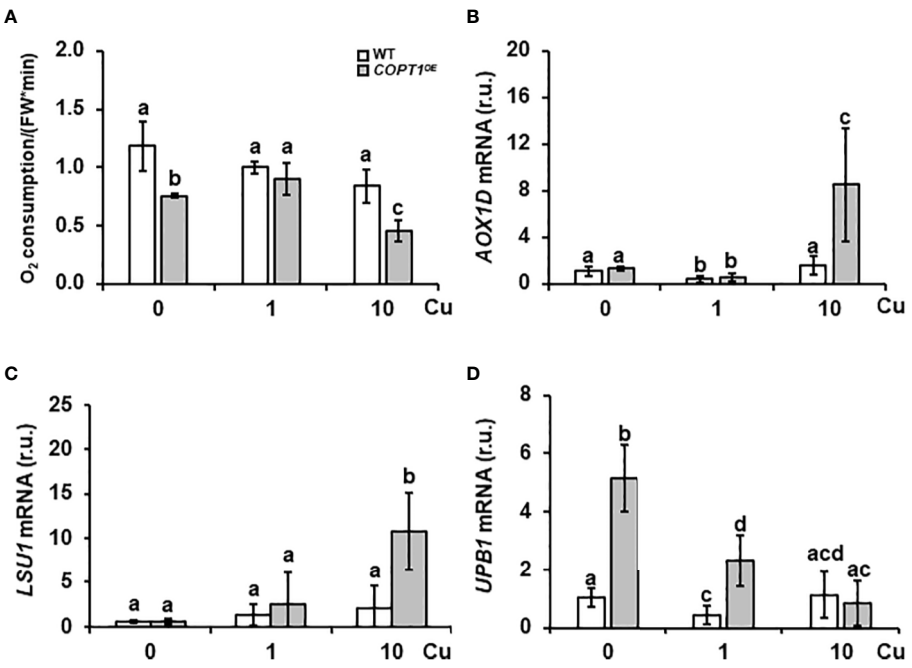

FIGURE 6 | Root O_2 consumption and expression of stress-related genes in *COPT1*^{OE}. **(A)** O_2 consumption in roots of 10-day-old WT and *COPT1*^{OE} seedlings cultivated with different $CuSO_4$ concentrations. The rate of O_2 decrease was referenced to roots F.W. (nmol O_2/OD600 * F.W). The values represented are the arithmetic mean ± SD of n = 3 biological replicates. Expression of the *AOX-1D* **(B)**, *LSU1* **(C)**, and *UPB1* **(D)** genes in WT (white bars) and *COPT1*^{OE} (grey bars) seedlings grown under Cu deficiency (0 μM $CuSO_4$), sufficiency (1 μM $CuSO_4$) or Cu excess (10 μM $CuSO_4$) was determined by RT-qPCR. Gene expression is represented as relative expression levels (r.u.) in relation to the WT under control conditions. *UBQ10* was used as housekeeping gene. Bars correspond to arithmetic means ($2^{-\Delta\Delta Ct}$) ± SD of biological replicates (n = 3). Samples with a letter in common are not significantly different (p-value <0.05).

deficiency. Whereas no clear effects were observed on root length for the H_2O_2 treatment, reductants such as AsH and DTT, improved the root growth of *COPT1*^{OE} compared to WT (**Supplementary Figure S9**) further pointing to increased oxidative stress in the overexpressing line under Cu deficiency.

Additionally, since the Fe content was lower in *COPT*^{OE}, a Fe excess treatment was also provided with no differential effect compared to controls (**Supplementary Figure S9**). In order to ascertain the Fe redox state in the roots, 7-day-old seedlings grown in the same media with different Cu content (0, 1, and 10 μM $CuSO_4$) were stained with the Perl´s blue to detect the presence of Fe^{3+}. The intensity of stained roots indicated that Fe^{3+} increased as Cu rise in the media from 0 to 10 μM Cu in all seedlings´ genotypes. Moreover, *COPT*^{OE} seedlings were more intensely stained than WT in all the conditions (**Figure 7**) and this result is reproducible in 11-day-old seedlings (**Supplementary Figure S10**), indicating that Cu^+ uptake through COPT is affecting the redox state of incorporated Fe leading to an increase in the Fe^{3+}/Fe^{2+} ratio in the *COPT*^{OE} roots since the lower total Fe concentration (**Figure 1D**).

These results suggested that the reduction in Fe content observed in *COPT*^{OE} could be due to the increased Fe^{3+}/Fe^{2+} ratio when Cu^+ entrance was enhanced and deregulated in *COPT*^{OE} seedlings. Thus, a model for the Cu excess effects on Fe homeostasis in *COPT*^{OE} seedlings has been proposed (**Figure 8**). The deregulated Cu^+ entrance in *COPT*^{OE} plants under high Cu activated the expression of the *bHLH-Ib* factors but not *FIT*. This effect redounded in Fe deficiency symptoms in *COPT*^{OE} probably as a consequence of the lack of Fe assimilatory response. Cu excess increased the Fe^{3+}/Fe^{2+} ratio in *COPT*^{OE} roots, probably leading to signaling pathways that could further inhibit Fe uptake.

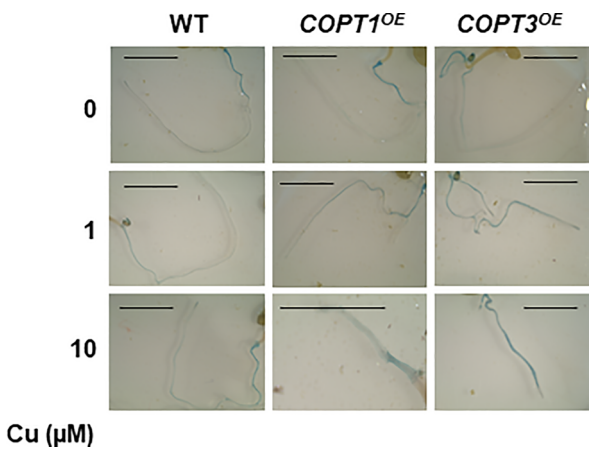

FIGURE 7 | Detection of Fe^{3+} in *COPT*^{OE} roots. Seven-day old roots of WT, *COPT1*^{OE} and *COPT3*^{OE} seedlings grown under Cu deficiency (0 μM $CuSO_4$), sufficiency (1 μM $CuSO_4$) or Cu excess (10 μM $CuSO_4$) were stained with Perl's blue to detect Fe^{3+}. Scale bars represent 1 cm.

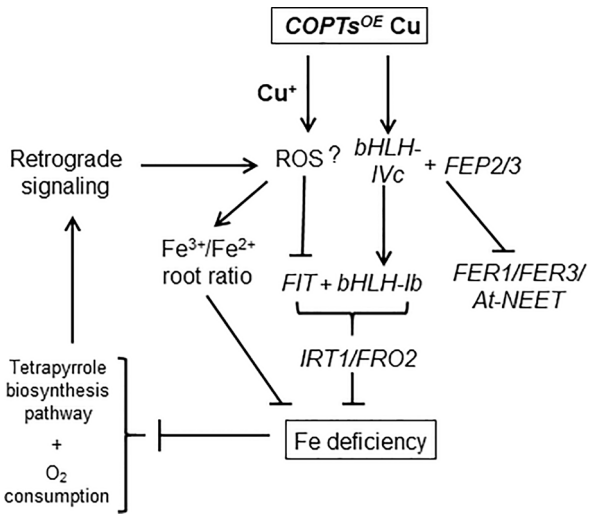

FIGURE 8 | Genetic model of the Cu effects on Fe homeostasis in *COPT*^{OE}. Deregulated Cu^+ entrance by constitutive COPT overexpression under high Cu increased the Fe^{3+}/Fe^{2+} ratio in roots. *COPT*^{OE} displayed Fe deficiency symptoms probably as a consequence of the lack of Fe assimilatory response (*IRT1/FRO2*), since under high Cu conditions *COPT*^{OE} plants activated the expression of the *bHLH-Ib* factors but not *FIT*. Cu excess increased ROS that could activate *FEP2/FEP3* expression, which up-regulate *bHLH-Ib* factors. *BTS* affected bHLH-IVc stability and expression of its target genes (*FER1*, *FER3* and *At-NEET*). Fe deficiency affected tetrapyrrole biosynthesis pathway and O_2 consumption that could further increase ROS production and inhibit Fe uptake through retrograde signaling.

DISCUSSION

In this report, we studied the effects of deregulated Cu^+ entrance in *COPT*^{OE} seedlings, which overexpress COPT Cu transporters (Andrés-Colás et al., 2010), on global gene expression when seedlings were grown in Cu concentrations within the physiological range that plants encounter in their natural environment. Our results indicate that Fe transport and homeostasis were altered in *COPT*^{OE}. Despite containing low Fe, *COPT*^{OE} was not able to orchestrate an optimal local Fe-uptake response at their roots under both Cu deficiency and excess (**Figure 1**). The causes for the Cu interference with the Fe-uptake response seem different in both conditions. Under Cu deficiency, *COPT*^{OE} induced *FIT*, but the expression of subgroup Ib of *bHLH* remained low. On the contrary, under Cu excess, *FIT* was repressed, despite high *FEP*s and *bHLH-Ib* expression (**Figure 3**). Based on the necessity of expressing both FIT and subgroup Ib of bHLH transcription factors for Fe-uptake responses (Yuan et al., 2008; Wang et al., 2013), *COPT*^{OE} seedlings were unable to properly respond to Fe deficiency under non-optimal Cu supply.

Fe and Cu homeostasis interact at different levels in plants (Puig et al., 2007; Bernal et al., 2012; Perea-García et al., 2013; Kastoori Ramamurthy et al., 2018). For instance, high Cu

concentrations in the media lower leaf Fe content (Waters et al., 2012; Waters and Armbrust, 2013). In our experimental conditions, a slight decrease in *IRT1* expression was observed in the WT seedlings under Cu excess, which was further exacerbated in $COPT^{OE}$. On the other hand, higher Cu content was observed under Fe deficiency in WT (Kastoori Ramamurthy et al., 2018). Among the reasons for increased Cu content under Fe deficiency are the increased uptake of both the unspecific Cu^{2+} entrance through ZIP transporters and the specific Cu^{+} entrance through *COPT2* (Colangelo and Guerinot, 2004; Perea-García et al., 2013). Nevertheless, the reason for Cu^{+} requirement under Fe deficiency remains unsolved.

Although recent data suggested that Fe deficiency responses are under the control of SPL7 (Kastoori Ramamurthy et al., 2018), Cu-dependent SPL7-mediated responses did not seem to be the cause of *IRT1* down-regulation in $COPT^{OE}$ since the expression of other SPL7 target genes was not significantly affected in these plants. On the other hand, different hormones are involved in modulating Fe deficiency responses in plants (Kobayashi, 2019). JA has been shown to inhibit the expression of *bHLH-Ib* and promote FIT degradation, resulting in reduced expression of the Fe uptake genes *IRT1* and *FRO2* and increased sensitivity to Fe deficiency (Cui et al., 2018). Since JA is a negative regulator of Fe deficiency responses and JA content was reduced in $COPT1^{OE}$, lower levels of JA could not justify the decrease in Fe uptake under our experimental conditions. However, auxins can enhance *FIT* and *FRO2* expression (Chen et al., 2010), and, in this sense, we cannot discard that IAA decreased levels in $COPT1^{OE}$ seedlings under Cu excess could at least partially account for the low *FIT* expression in $COPT1^{OE}$ plants.

The oxidative stress produced by metal deficiencies and excess could also account for the Fe and Cu crosstalk (Ravet and Pilon, 2013). Indeed, Cu phytotoxicity has been attributed to increased H_2O_2 production (Cuypers et al., 2010) and the deficiency of Cu affects the functioning of the respiratory and photosynthetic electron transport chains, which increases the production of the $O_2^{\cdot -}$ (Abdel-Ghany et al., 2005; Yamasaki et al., 2009). Therefore, the majority type of ROS could be different under conditions of metal deficiency or excess. Increased oxidative stress leading to lipid peroxidation has been previously reported to occur in $COPT^{OE}$ seedlings (Andrés-Colás et al., 2010). According to the slightly increased Cu content in $COPT^{OE}$ seedlings (Andrés-Colás et al., 2010), they should have increased *CSD2* levels under Cu excess, instead of the observed lower levels. This result suggests a difficulty of the $COPT^{OE}$ chloroplasts in detoxifying $O_2^{\cdot -}$ under Cu excess, since they cannot completely activate neither *FSD1* nor *CSD2* compared to the WT, maybe redounding in increased oxidative stress. The induction of several members of the LSU family (*LSU1*, *LSU2* and *LSU3*) under Cu excess in the $COPT^{OE}$ plants is in agreement with their induction under sulfur deficiency and by Fe deficiency and Cu excess (Garcia-Molina et al., 2017). LSU1 interacts with chloroplastic FSD2 and stimulates its enzymatic activity *in vivo* and *in vitro* conforming a hub in coordinating plant responses to a wide spectrum of abiotic stress conditions (Garcia-Molina et al., 2017). Moreover, $COPT1^{OE}$ seedlings showed higher Cu-induced K^{+} efflux and net Ca^{2+} influx at the root tip level compared to the WT (Rodrigo-Moreno et al., 2013), although no significant changes of the membrane potential were detected upon Cu addition (Sanz et al., 2019).

Although increased O_2 consumption has been also reported in sugar beet and cucumber roots (Lopez-Millan et al., 2000; Vigani et al., 2009), the ability to consume O_2 decreased in $COPT1^{OE}$ roots under both Cu deficiency and excess (**Figure 6A**). High Cu in $COPT1^{OE}$ triggers a response that includes the expression of genes related to mitochondrial stress (Arnholdt-Schmitt et al., 2006; Selinski et al., 2018), such as *AOX1A*, *AOX1D* and *AOX2*. Results shown here support the respiratory shield hypothesis, where the mitochondrial Fe proteins are necessary to maintain high O_2 consumption in the respiratory electron transport chain contributing to the microaerobic environment necessary to maintain a Fe^{2+} pool. The problem due to lack of respiratory shield could be aggravated in conditions of Fe deficiency and high and temporarily deregulated Cu^{+} entry. In this sense, the defect of Fe/S and heme proteins will lead to defective respiratory shield in strains with high metabolism (López-Torrejón et al., 2016; Wofford et al., 2019), aggravated in $COPT1^{OE}$ seedlings by deregulated Cu^{+} uptake. In any case, our observations support that optimal Cu supply is required for normal O_2 consumption in $COPT1^{OE}$ plants.

Cu deficiency affects Fe homeostasis specifically causing a defect in root-to-shoot translocation, which has been attributed to a decrease in Cu-dependent ferroxidase activity (Bernal et al., 2012; Waters and Armbrust, 2013). Assuming that a certain Fe^{3+}/Fe^{2+} and Cu^{2+}/Cu^{+} intracellular ratios are necessary for uptake/mobilization processes, Cu^{+} uptake could affect the Fe^{3+}/Fe^{2+} ratio at different levels. Firstly, due to its lower standard reduction potential, Cu^{+} could directly reduce Fe^{3+} to Fe^{2+}. However, this is not the case since increased Fe^{3+} was observed in $COPT^{OE}$ seedlings (**Figure 7**). Moreover, highly reactive, cytosolic free Cu^{+} is almost absent in the cytosol (Rae et al., 1999). Instead, increased oxidative stress provoked by deregulated Cu^{+} entrance (Rodrigo-Moreno et al., 2013) could influence intracellular general redox status, leading to Fe oxidation. On the other hand, Cu deficiency would facilitate Fe^{2+} incorporation through the enhanced expression of *FRO* metalloreductases and inhibit Cu-dependent ferroxidase activity (Bernal et al., 2012; Waters et al., 2012; Waters and Armbrust, 2013). Since the Fe^{3+}/Fe^{2+} ratio depends on the relative ferroxidase versus ferroreductase activities, an increased Fe^{3+}/Fe^{2+} ratio would be expected in the presence of excess Cu. The other way around, the Fe^{3+}/Fe^{2+} ratio should be decreased under Cu deficiency. Under our experimental conditions, we were not able to detect a significant change in ferroreductase activity and just a slight decrease is observed in $COPT^{OE}$ seedlings under Cu excess (**Figure 1B**), questioning this activity being the only cause of the Fe deficiency. Finally, Cu uptake increased Fe^{3+} in the roots, probably by means of the oxidative conditions created. As a consequence, decreased Fe mobilization in roots could lead to

Fe deficiency in leaves. In this sense, Cu excess and deregulated Cu^+ uptake in $COPT^{OE}$ seedlings increased the Fe^{3+}/Fe^{2+} ratio leading to Fe deficiency effects, being it at least one of the problems faced by Cu^+ toxicity (**Figure 8**). Accordingly, this suggestion could explain previous results where plants grown without Fe were more susceptible to Cu toxicity (Waters and Armbrust, 2013).

In order to address how Cu influenced the signaling pathways involved in the Fe deficiency response, the expression of *BTS* and several other genes encoding RING E3 ubiquitin ligases were induced in the $COPT1^{OE}$ seedlings. This result points to the putative Fe-sensing BTS (Selote et al., 2015), and maybe other RING E3 ubiquitin ligases, as candidates in upstream sensing of the lack of Fe mobilization in $COPT1^{OE}$ plants under mild Cu excess. On the other hand, our results indicated that tetrapyrrole signaling was affected under both Cu deficiency and excess, probably as a consequence of the common Fe deficiency conditions faced by $COPT^{OE}$ seedlings (**Supplementary Tables SIII** and **SIV**). Most of the genes involved in tetrapyrrole metabolism showed synchronized and light-dependent expression patterns (Matsumoto et al., 2004). Multiple *PhANG* were down-regulated in $COPT1^{OE}$ under both Cu deficiency and excess in addition to several regulators. Curiously, *CHL27/CRD1* (*COPPER RESPONSE DEFECT1*) was first characterized in a screening for Cu conditional phenotypes in *Chlamydomonas* where Cu scarcity in plastocyanin is counteracted by a heme-containing cytochrome (Moseley et al., 2000), although this substitution has not been shown to occur in *Arabidopsis*. Moreover, the GUN4 porphyrin-binding protein enhances Mg-chelatase activity (Davison et al., 2005) and its repression under Cu excess could play a role in the control of substrate flow into the heme or chlorophyll branch (Tanaka and Tanaka, 2007). On the other hand, nuclear-encoded sigma factor, such as SIG1, could be involved in the integration of light and circadian signals that regulate chloroplast transcription (Belbin et al., 2017). These results underscore the importance of tightly regulated Cu homeostasis at the spatial–temporal level, in order to orchestrate an optimal Fe distribution and to avoid oxidative damage to highly sensitive Fe-dependent processes, such as Fe/S cluster assembly and tetrapyrrole biosynthesis. It is tempting to speculate that Fe and other metals, which affect at the cellular redox state and either participate or interfere with sensitive processes, have to be subjected to differential diurnal variation in the expression patterns of their homeostatic components (Peñarrubia et al., 2015; Zhang and Krämer, 2018). In this sense, the induced expression of *UPB1* in $COPT^{OE}$ plants under Cu deficiency could emphasize the requirement of spatially appropriate Cu uptake at the root tip, where normally *COPT1* is expressed (Sancenón et al., 2003), to avoid oxidative interference along the root with Fe translocation to the aerial part (Tsukagoshi et al., 2010).

Taken together, these results indicated that high Cu renders increased Fe^{3+} in the root. Despite low Fe in the shoot, the presence of high Fe^{3+}/Fe^{2+} ratio in the root prevented local responses to Fe deficiency (**Figure 8**). The understanding of Cu influence on Fe mobilization and redistribution in the plant could help to ameliorate field treatments to maximize crop production under Fe deficiency through optimizing Cu homeostasis.

DATA AVAILABILITY STATEMENT

The datasets generated for this study can be found in the: The microarray raw data were deposited in the NCBI's Gene Expression Omnibus and are accessible through GEO Series accession number GSE143857.

AUTHOR CONTRIBUTIONS

LP and SP conceived the idea and wrote the manuscript. MP-A and FV-S performed the $COPT1^{OE}$ global analysis. AP-G and AA-B performed the physiological and molecular experiments in mutant plants. All authors contributed to the article and approved the submitted version.

FUNDING

This work was supported by grant BIO2017-87828-C2-1-P from the Spanish Ministry of Economy and Competitiveness, and by FEDER funds from the European Union.

ACKNOWLEDGMENTS

We acknowledge the SCSIE (Universitat de València) for the ICPMS service, and the Plant Hormone Quantification Service of the (IBMCP) (CSIC-UPV, Valencia) for hormone level quantification. This work was supported by grant BIO2017-87828-C2-1-P from the Spanish Ministry of Economy and Competitiveness, and by FEDER funds from the European Union.

SUPPLEMENTARY MATERIAL

The Supplementary Material for this article can be found online at: https://www.frontiersin.org/articles/10.3389/fpls.2020.01106/full#supplementary-material

REFERENCES

Abdel-Ghany, S. E., Burkhead, J. L., Gogolin, K. A., Andres-Colas, N., Bodecker, J. R., Puig, S., et al. (2005). AtCCS is a functional homolog of the yeast copper chaperone Ccs1/Lys7. *FEBS Lett.* 579, 2307–2312. doi: 10.1016/j.febslet.2005.03.025

Andrés-Bordería, A., Andrés, F., Garcia-Molina, A., Perea-García, A., Domingo, C., Puig, S., et al. (2017). Copper and ectopic expression of the Arabidopsis transport protein COPT1 alter iron homeostasis in rice (Oryza sativa L.). *Plant Mol. Biol.* 95, 17–32. doi: 10.1007/s11103-017-0622-8

Andrés-Colás, N., Sancenón, V., Rodríguez-Navarro, S., Mayo, S., Thiele, D. J., Ecker, J. R., et al. (2006). The Arabidopsis heavy metal P-type ATPase HMA5

interacts with metallochaperones and functions in copper detoxification of roots. *Plant J.* 45, 225–236. doi: 10.1111/j.1365-313X.2005.02601.x

Andrés-Colás, N., Perea-García, A., Puig, S., and Peñarrubia, L. (2010). Deregulated copper transport affects Arabidopsis development especially in the absence of environmental cycles. *Plant Physiol.* 153, 170–184. doi: 10.1104/pp.110.153676

Andrés-Colás, N., Carrió-Seguí, A., Abdel-Ghany, S. E., Pilon, M., and Peñarrubia, L. (2018). Expression of the intracellular COPT3-mediated Cu transport is temporally regulated by the TCP16 transcription factor. *Front. Plant Sci.* 9:910. doi: 10.3389/fpls.2018.00910

Arnholdt-Schmitt, B., Costa, J. H., and de Melo, D. F. (2006). AOX - a functional marker for efficient cell reprogramming under stress? *Trends Plant Sci.* 11, 281–287. doi: 10.1016/j.tplants.2006.05.001

Ashburner, M., Ball, C. A., Blake, J. A., Botstein, D., Butler, H., Cherry, J. M., et al. (2000). Gene Ontology: tool for the unification of biology. *Nat. Genet.* 25, 25–29. doi: 10.1038/75556

Bang, W. Y., Jeong, I. S., Kim, D. W., Im, C. H., Ji, C., Hwang, S. M., et al. (2008). Role of Arabidopsis CHL27 protein for photosynthesis, chloroplast development and gene expression profiling. *Plant Cell Physiol.* 49, 1350–1363. doi: 10.1093/pcp/pcn111

Belbin, F. E., Noordally, Z. B., Wetherill, S. J., Atkins, K. A., Franklin, K. A., and Dodd, A. N. (2017). Integration of light and circadian signals that regulate chloroplast transcription by a nuclear-encoded sigma factor. *New Phytol.* 213, 727–738. doi: 10.1111/nph.14176

Bernal, M., Casero, D., Singh, V., Wilson, G. T., Grande, A., Yang, H., et al. (2012). Transcriptome sequencing identifies SPL7-regulated copper acquisition genes FRO4/FRO5 and the copper dependence of iron homeostasis in Arabidopsis. *Plant Cell* 24, 738–761. doi: 10.1105/tpc.111.090431

Bueso, E., Alejandro, S., Carbonell, P., Perez-Amador, M. A., Fayos, J., Bellés, J. M., et al. (2007). The lithium tolerance of the Arabidopsis cat2 mutant reveals a cross-talk between oxidative stress and ethylene. *Plant J.* 52, 1052–1065. doi: 10.1111/j.1365-313X.2007.03305.x

Carmona-Saez, P., Chagoyen, M., Tirado, F., Carazo, J. M., and Pascual-Montano, A. (2007). GENECODIS: a web-based tool for finding significant concurrent annotations in gene lists. *Genome Biol.* 8, R3. doi: 10.1186/gb-2007-8-1-r3

Carrió-Seguí, A., Garcia-Molina, A., Sanz, A., and Peñarrubia, L. (2015). Defective copper transport in the copt5 mutant affects cadmium tolerance. *Plant Cell Physiol.* 56, 442–454. doi: 10.1093/pcp/pcu180

Chen, W. W., Yang, J. L., Qin, C., Jin, C. W., Mo, J. H., Ye, T., et al. (2010). Nitric oxide acts downstream of auxin to trigger root ferric-chelate reductase activity in response to iron deficiency in arabidopsis. *Plant Physiol.* 154, 810–819. doi: 10.1104/pp.110.161109

Clifton, R., Harvey Millar, A., and Whelan, J. (2006). Alternative oxidases in Arabidopsis: A comparative analysis of differential expression in the gene family provides new insights into function of non-phosphorylating bypasses. *Biochim. Biophys. Acta* 1757, 730–741. doi: 10.1016/j.bbabio.2006.03.009

Colangelo, E. P., and Guerinot, M. L. (2004). The essential basic helix-loop-helix protein FIT1 is required for the iron deficiency response. *Plant Cell* 16, 3400–3412. doi: 10.1105/tpc.104.024315

Connolly, E. L., Fett, J. P., and Guerinot, M. L. (2002). Expression of the IRT1 metal transporter is controlled by metals at the levels of transcript and protein accumulation. *Plant Cell* 14, 1347–1357. doi: 10.1105/tpc.001263

Crichton, R. R., and Pierre, J. L. (2001). Old iron, young copper: from Mars to Venus. *Biometals* 14, 99–112. doi: 10.1023/a:1016710810701

Cui, Y., Chen, C. L., Cui, M., Zhou, W. J., Wu, H. L., and Ling, H. (2018). Four IVa bHLH transcription factors are novel interactors of FIT and mediate JA inhibition of iron uptake in Arabidopsis. *Mol. Plant* 11, 1166–1183. doi: 10.1016/j.molp.2018.06.005

Cuypers, A., Karen, S., Jos, R., Kelly, O., Els, K., Tony, R., et al. (2010). The cellular redox state as a modulator in cadmium and copper responses in Arabidopsis thaliana seedlings. *J. Plant Physiol.* 168, 309–316. doi: 10.1016/j.jplph.2010.07.010

da Silva, E. M., Silva, G. F. F. E., Bidoia, D. B., da Silva Azevedo, ,. M., de Jesus, F. A., Pino, L. E., et al. (2017). microRNA159-targeted SlGAMYB transcription factors are required for fruit set in tomato. *Plant J.* 92, 95–109. doi: 10.1111/tpj.13637

Davison, P. A., Schubert, H. L., Reid, J. D., Iorg, C. D., Heroux, A., Hill, C. P., et al. (2005). Structural and biochemical characterization of Gun4 suggests a mechanism for its role in chlorophyll biosynthesis. *Biochemistry* 44, 7603–7612. doi: 10.1021/bi050240x

Di Rienzo, J. A., Casanoves, F., Balzarini, M. G., Gonzalez, L., Tablada, M., and Robledo, C. W. (2011). InfoStat.

Edgar, R. (2002). Gene Expression Omnibus: NCBI gene expression and hybridization array data repository. *Nucleic Acids Res.* 30, 207–210. doi: 10.1093/nar/30.1.207

Garcia-Molina, A., Andrés-Colás, N., Perea-García, A., Neumann, U., Dodani, S. C., Huijser, P., et al. (2013). The Arabidopsis COPT6 Transport Protein Functions In Copper Distribution Under Copper-Deficient Conditions. *Plant Cell Physiol.* 0, 1–13. doi: 10.1093/pcp/pct088

Garcia-Molina, A., Altmann, M., Alkofer, A., Epple, P. M., Dangl, J. L., and Falter-Braun, P. (2017). LSU network hubs integrate abiotic and biotic stress responses via interaction with the superoxide dismutase FSD2. *J. Exp. Bot.* 68, 1185–1197. doi: 10.1093/jxb/erw498

Grillet, L., Ouerdane, L., Flis, P., Hoang, M. T. T., Isaure, M. P., Lobinski, R., et al. (2014). Ascorbate efflux as a new strategy for iron reduction and transport in plants. *J. Biol. Chem.* 289, 2515–2525. doi: 10.1074/jbc.M113.514828

Grillet, L., Lan, P., Li, W., Mokkapati, G., and Schmidt, W. (2018). IRON MAN is a ubiquitous family of peptides that control iron transport in plants. *Nat. Plants.* 4, 953–963. doi: 10.1038/s41477-018-0266-y

Gulec, S., and Collins, J. F. (2014). Molecular mediators governing iron-copper interactions. *Annu. Rev. Nutr.* 34, 95–116. doi: 10.1146/annurev-nutr-071812-161215

Hindt, M. N., Akmakjian, G. Z., Pivarski, K. L., Punshon, T., Baxter, I., Salt, D. E., et al. (2017). BRUTUS and its paralogs, BTS LIKE1 and BTS LIKE2, encode important negative regulators of the iron deficiency response in Arabidopsis thaliana. *Metallomics* 9, 876–890. doi: 10.1039/c7mt00152e

Hirayama, T., Lei, G. J., Yamaji, N., Nakagawa, N., and Ma, J. F. (2018). The putative peptide gene FEP1 regulates iron deficiency response in Arabidopsis. *Plant Cell Physiol.* 59, 1739–1752. doi: 10.1093/pcp/pcy145

Kastoori Ramamurthy, R., Xiang, Q., Hsieh, E. J., Liu, K., Zhang, C., and Waters, B. M. (2018). New aspects of iron-copper crosstalk uncovered by transcriptomic characterization of Col-0 and the copper uptake mutant: Spl7 in Arabidopsis thaliana. *Metallomics* 10, 1824–1840. doi: 10.1039/c8mt00287h

Kobayashi, T., Nagasaka, S., Senoura, T., Itai, R. N., Nakanishi, H., and Nishizawa, N. K. (2013). Iron-binding haemerythrin RING ubiquitin ligases regulate plant iron responses and accumulation. *Nat. Commun.* 4, 2792–2804. doi: 10.1038/ncomms3792

Kobayashi, T. (2019). Understanding the complexity of iron sensing and signaling cascades in plants. *Plant Cell Physiol.* 60, 1440–1446. doi: 10.1093/pcp/pcz038

Kosman, D. J. (2018). The teleos of metallo-reduction and metallo-oxidation in eukaryotic iron and copper trafficking. *Metallomics* 10, 370–377. doi: 10.1039/c8mt00015h

Long, T. A., Tsukagoshi, H., Busch, W., Lahner, B., Salt, D. E., and Benfey, P. N. (2010). The bHLH transcription factor POPEYE regulates response to iron deficiency in arabidopsis roots. *Plant Cell* 22, 2219–2236. doi: 10.1105/tpc.110.074096

Lopez-Millan, A. F., Morales, F., Andaluz, S., Gogorcena, Y., Abadia, A., De Las Rivas, J., et al. (2000). Responses of sugar beet roots to iron deficiency. Changes in carbon assimilation and oxygen use? *Plant Physiol.* 124, 885–897. doi: 10.1104/pp.124.2.885

López-Torrejón, G., Jiménez-Vicente, E., Buesa, J. M., Hernandez, J. A., Verma, H. K., and Rubio, L. M. (2016). Expression of a functional oxygen-labile nitrogenase component in the mitochondrial matrix of aerobically grown yeast. *Nat. Commun.* 7, 1–6. doi: 10.1038/ncomms11426

Macadlo, L. A., Ibrahim, I. M., and Puthiyaveetil, S. (2019). Sigma factor 1 in chloroplast gene transcription and photosynthetic light acclimation. *J. Exp. Bot.* 71, 1029–1038. doi: 10.1093/jxb/erz464

Marschner, P. (2012). *Marschner's Mineral Nutrition of Higher Plants Third Edition* (Amsterdam: Elsevier).

Matsumoto, F., Obayashi, T., Sasaki-Sekimoto, Y., Ohta, H., Takamiya, K., and Tatsuru, , M. (2004). Gene expression profiling of the tetrapyrrole metabolic pathway in Arabidopsis with a mini-array system. *Plant Physiol.* 135, 2379–2391. doi: 10.1104/pp.104.042408

Mittler, R., Darash-Yahana, M., Sohn, Y. S., Bai, F., Song, L., Cabantchik, I. Z., et al. (2019). NEET Proteins: A new link between iron metabolism, reactive oxygen

species, and cancer. *Antioxid. Redox Signal.* 30, 1083–1095. doi: 10.1089/ars.2018.7502

Moseley, J., Quinn, J., Eriksson, M., and Merchant, S. (2000). The Crd1 gene encodes a putative di-iron enzyme required for photosystem I accumulation in copper deficiency and hypoxia in Chlamydomonas reinhardtii. *EMBO J.* 19, 2139–2151. doi: 10.1093/emboj/19.10.2139

Murashige, T., and Skoog, F. (1962). A Revised Medium for Rapid Growth and Bio Assays with Tobacco Tissue Cultures. *Physiol. Plant* 15, 473–497. doi: 10.1111/j.1399-3054.1962.tb08052.x

Nechushtai, R., Conlan, A. R., Harir, Y., Song, L., Yogev, O., Eisenberg-Domovich, Y., et al. (2012). Characterization of Arabidopsis NEET reveals an ancient role for NEET proteins in iron metabolism. *Plant Cell* 24, 2139–2154. doi: 10.1105/tpc.112.097634

Nevitt, T., Öhrvik, H., and Thiele, D. J. (2012). Charting the travels of copper in eukaryotes from yeast to mammals. *Biochim. Biophys. Acta* 1823, 1580–1593. doi: 10.1016/j.bbamcr.2012.02.011

Nogales-Cadenas, R., Carmona-Saez, P., Vazquez, M., Vicente, C., Yang, X., Tirado, F., et al. (2009). GeneCodis: Interpreting gene lists through enrichment analysis and integration of diverse biological information. *Nucleic Acids Res.* 37, 317–322. doi: 10.1093/nar/gkp416

Nouet, C., Motte, P., and Hanikenne, M. (2011). Chloroplastic and mitochondrial metal homeostasis. *Trends Plant Sci.* 16, 395–404. doi: 10.1016/j.tplants.2011.03.005

Parsons, T., and Strickland, J. (1965). Discussion of spectrophotometric determination of marine-plant pigments, with revised equations for ascertaining chlorophylls and carotenoids. *Deep Sea Res. Oceanogr. Abstr.* 12, 619. doi: 10.1016/0011-7471(65)90662-5

Peñarrubia, L., Romero, P., Carrió-seguí, A., Andrés-bordería, A., Moreno, J., and Sanz, A. (2015). Plant Traffic and Transport Temporal aspects of copper homeostasis and its crosstalk with hormones. *Front. Plant Sci.* 6, 255–273. doi: 10.3389/fpls.2015.00255

Perea-García, A., Garcia-Molina, A., Andrés-Colás, N., Vera-Sirera, F., Pérez-Amador, M. A., Puig, S., et al. (2013). Arabidopsis copper transport protein COPT2 participates in the cross talk between iron deficiency responses and low-phosphate signaling. *Plant Physiol.* 162, 180–194. doi: 10.1104/pp.112.212407

Perea-García, A., Andrés-Bordería, A., Mayo de Andrés, S., Sanz, A., Davis, A. M., Davis, S. J., et al. (2016). Modulation of copper deficiency responses by diurnal and circadian rhythms in Arabidopsis thaliana. *J. Exp. Bot.* 67, 391–403. doi: 10.1093/jxb/erv474

Petit, J. M., Briat, J. F., and Lobréaux, S. (2001). Structure and differential expression of the four members of the Arabidopsis thaliana ferritin gene family. *Biochem. J.* 359, 575–582. doi: 10.1042/0264-6021:3590575

Pfaffl, M. W. (2002). Relative expression software tool (REST(C)) for group-wise comparison and statistical analysis of relative expression results in real-time PCR. *Nucleic Acids Res.* 30:e36. doi: 10.1093/nar/30.9.e36

Puig, S., Andrés-Colás, N., García-Molina, A., and Peñarrubia, L. (2007). Copper and iron homeostasis in Arabidopsis: Responses to metal deficiencies, interactions and biotechnological applications. *Plant Cell Environ.* 30, 271–290. doi: 10.1111/j.1365-3040.2007.01642.x

Puig, S. (2014). Function and regulation of the plant COPT family of high-affinity copper transport proteins. *Adv. Bot.* 2014, 1–9. doi: 10.1155/2014/476917

Rae, T. D., Schmidt, P. J., Pufahl, R. A., Culotta, V. C., and O'Halloran, T. V. (1999). Undetectable intracellular free copper: The requirement of a copper chaperone for superoxide dismutase. *Sci. (80-.).* 284, 805–808. doi: 10.1126/science.284.5415.805

Ravet, K., and Pilon, M. (2013). Copper and iron homeostasis in plants: The challenges of oxidative stress. *Antioxid. Redox Signal.* 19, 919–932. doi: 10.1089/ars.2012.5084

Ren, F., Logeman, B. L., Zhang, X., Liu, Y., Thiele, D. J., and Yuan, P. (2019). X-ray structures of the high-affi nity copper transporter Ctr1. *Nat. Commun.* 10, 1386–1395. doi: 10.1038/s41467-019-09376-7

Reyt, G., Boudouf, S., Boucherez, J., Gaymard, F., and Briat, J. F. (2015). Iron- and ferritin-dependent reactive oxygen species distribution: Impact on arabidopsis root system architecture. *Mol. Plant* 8, 439–453. doi: 10.1016/j.molp.2014.11.014

Robinson, N. J., Procter, C. M., Connolly, E. L., and Guerinot, M. (1999). A ferric-chelate reductase for iron uptake from soils. *Nature* 397, 694–697. doi: 10.1038/17800

Rodrigo-Moreno, A., Andrés-Colás, N., Poschenrieder, C., Gunsé, B., Peñarrubia, L., and Shabala, S. (2013). Calcium- and potassium-permeable plasma membrane transporters are activated by copper in Arabidopsis root tips: Linking copper transport with cytosolic hydroxyl radical production. *Plant Cell Environ.* 36, 844–855. doi: 10.1111/pce.12020

Sancenón, V., Puig, S., Mira, H., Thiele, D. J., and Peñarrubia, L. (2003). Identification of a copper transporter family in Arabidopsis thaliana. *Plant Mol. Biol.* 51, 577–587. doi: 10.1023/A:1022345507112

Sancenón, V., Puig, S., Mateu-Andrés, I., Dorcey, E., Thiele, D. J., and Peñarrubia, L. (2004). The Arabidopsis Copper Transporter COPT1 Functions in Root Elongation and Pollen Development. *J. Biol. Chem.* 279, 15348–15355. doi: 10.1074/jbc.M313321200

Sanz, A., Pike, S., Khan, M. A., Carrió-Seguí, À., Mendoza-Cózatl, D. G., Peñarrubia, L., et al. (2019). Copper uptake mechanism of Arabidopsis thaliana high-affinity COPT transporters. *Protoplasma* 256, 161–170. doi: 10.1007/s00709-018-1286-1

Selinski, J., Scheibe, R., Day, D. A., and Whelan, J. (2018). Alternative Oxidase Is Positive for Plant Performance. *Trends Plant Sci.* 23, 588–597. doi: 10.1016/j.tplants.2018.03.012

Selote, D., Samira, R., Matthiadis, A., Gillikin, J. W., and Long, T. A. (2015). Iron-binding E3 ligase mediates iron response in plants by targeting basic helix-loop-helix transcription factors. *Plant Physiol.* 167, 273–286. doi: 10.1104/pp.114.250837

Stacey, M. G., Patel, A., McClain, W. E., Mathieu, M., Remley, M., Rogers, E. E., et al. (2008). The arabidopsis AtOPT3 protein functions in metal homeostasis and movement of iron to developing seeds. *Plant Physiol.* 146, 589–601. doi: 10.1104/pp.107.108183

Tanaka, R., and Tanaka, A. (2007). Tetrapyrrole biosynthesis in higher plants. *Annu. Rev. Plant Biol.* 58, 321–346. doi: 10.1146/annurev.arplant.57.032905.105448

Tissot, N., Robe, K., Gao, F., Grant-Grant, S., Boucherez, J., Bellegarde, F., et al. (2019). Transcriptional integration of the responses to iron availability in Arabidopsis by the bHLH factor ILR3. *New Phytol.* 223, 1433–1446. doi: 10.1111/nph.15753

Tsukagoshi, H., Busch, W., and Benfey, P. N. (2010). Transcriptional regulation of ROS controls transition from proliferation to differentiation in the root. *Cell* 143, 606–616. doi: 10.1016/j.cell.2010.10.020

Tusher, V., Tibshirani, R., and Chu, G. (2001). Significance analysis of microarrays applied to the ionizing radiation response. *Proc. Natl. Acad. Sci.* 98, 5116–5121. doi: 10.1073/pnas.091062498

Varotto, C., Maiwald, D., Pesaresi, P., Jahns, P., Salamini, F., and Leister, D. (2002). The metal ion transporter IRT1 is necessary for iron homeostasis and efficient photosynthesis in Arabidopsis thaliana. *Plant J.* 31, 589–599. doi: 10.1046/j.1365-313x.2002.01381.x

Vert, G., Grotz, N., Dédaldéchamp, F., Gaymard, F., Guerinot, L., Briat, J., et al. (2002). IRT1, an Arabidopsis transporter essential for iron uptake from the soil and for plant growth. *Plant Cell* 14, 1223–1233. doi: 10.1105/tpc.001388

Vigani, G., Maffi, D., and Zocchi, G. (2009). Iron availability affects the function of mitochondria in cucumber roots. *New Phytol.* 182, 127–136. doi: 10.1111/j.1469-8137.2008.02747.x

Wang, N., Cui, Y., Liu, Y., Fan, H., Du, J., Huang, Z., et al. (2013). Requirement and functional redundancy of Ib subgroup bHLH proteins for iron deficiency responses and uptake in arabidopsis thaliana. *Mol. Plant* 6, 503–513. doi: 10.1093/mp/sss089

Waters, B. M., and Armbrust, L. C. (2013). Optimal copper supply is required for normal plant iron deficiency responses. *Plant Signal. Behav.* 8, 1–5. doi: 10.4161/psb.26611

Waters, B. M., McInturf, S. A., and Stein, R. J. (2012). Rosette iron deficiency transcript and microRNA profiling reveals links between copper and iron homeostasis in Arabidopsis thaliana. *J. Exp. Bot.* 63, 5903–5918. doi: 10.1093/jxb/ers239

Wofford, J. D., Bolaji, N., Dziuba, N., Wayne Outten, F., and Lindahl, P. A. (2019). Evidence that a respiratory shield in Escherichia coli protects a low-molecular-mass FeII pool from O2-dependent oxidation. *J. Biol. Chem.* 294, 50–62. doi: 10.1074/jbc.RA118.005233

Yamasaki, H., Abdel-Ghany, S. E., Cohu, C. M., Kobayashi, Y., Shikanai, T., and Pilon, M. (2007). Regulation of copper homeostasis by micro-RNA in Arabidopsis. *J. Biol. Chem.* 282, 16369–16378. doi: 10.1074/jbc.M700138200

Yamasaki, H., Hayashi, M., Fukazawa, M., Kobayashi, Y., and Shikanai, T. (2009). SQUAMOSA promoter binding protein-like7 is a central regulator for copper homeostasis in Arabidopsis. *Plant Cell* 21, 347–361. doi: 10.1105/tpc.108.060137

Yruela, I. (2013). Transition metals in plant photosynthesis. *Metallomics* 5, 1090–1109. doi: 10.1039/c3mt00086a

Yuan, Y., Wu, H., Wang, N., Li, J., Zhao, W., Du, J., et al. (2008). FIT interacts with AtbHLH38 and AtbHLH39 in regulating iron uptake gene expression for iron homeostasis in Arabidopsis. *Cell Res.* 18, 385–397. doi: 10.1038/cr.2008.26

Zhang, H., and Krämer, U. (2018). Differential diel translation of transcripts with roles in the transfer and utilization of iron-sulfur clusters in arabidopsis. *Front. Plant Sci.* 871:1641. doi: 10.3389/fpls.2018.01641

Conflict of Interest: The authors declare that the research was conducted in the absence of any commercial or financial relationships that could be construed as a potential conflict of interest.

frontiers in Plant Science

MINI REVIEW
published: 07 August 2020
doi: 10.3389/fpls.2020.01102

How Does Rice Defend Against Excess Iron?: Physiological and Molecular Mechanisms

May Sann Aung * *and Hiroshi Masuda*

Department of Biological Production, Faculty of Bioresource Sciences, Akita Prefectural University, Akita, Japan

Iron (Fe) is an essential nutrient for all living organisms but can lead to cytotoxicity when present in excess. Fe toxicity often occurs in rice grown in submerged paddy fields with low pH, leading dramatical increases in ferrous ion concentration, disrupting cell homeostasis and impairing growth and yield. However, the underlying molecular mechanisms of Fe toxicity response and tolerance in plants are not well characterized yet. Microarray and genome-wide association analyses have shown that rice employs four defense systems to regulate Fe homeostasis under Fe excess. In defense 1, Fe excess tolerance is implemented by Fe exclusion as a result of suppression of genes involved in Fe uptake and translocation such as *OsIRT1*, *OsYSL2*, *OsTOM1*, *OsYSL15*, *OsNRAMP1*, *OsNAS1*, *OsNAS2*, *OsNAAT1*, *OsDMAS1*, and *OsIRO2*. The Fe-binding ubiquitin ligase, HRZ, is a key regulator that represses Fe uptake genes in response to Fe excess in rice. In defense 2, rice retains Fe in the root system rather than transporting it to shoots. In defense 3, rice compartmentalizes Fe in the shoot. In defense 2 and 3, the vacuolar Fe transporter *OsVIT2*, Fe storage protein ferritin, and the nicotinamine synthase *OsNAS3* mediate the isolation or detoxification of excess Fe. In defense 4, rice detoxifies the ROS produced within the plant body in response to excess Fe. Some *OsWRKY* transcription factors, *S-nitrosoglutathione-reductase* variants, p450-family proteins, and *OsNAC4*, *5*, and *6* are implicated in defense 4. These knowledge will facilitate the breeding of tolerant crops with increased productivity in low-pH, Fe-excess soils.

Keywords: iron excess, rice, OsNAS3, HRZ, OsVIT2, ROS, iron homeostasis, tolerant mechanism

OPEN ACCESS

Edited by:
Louis Grillet,
Academia Sinica, Taiwan

Reviewed by:
Karl Ravet,
Colorado State University, United States
Ping Lan,
Institute of Soil Science (CAS), China
Hannetz Roschzttardtz,
Pontificia Universidad Católica de chile, Chile

***Correspondence:**
May Sann Aung
mayaung@akita-pu.ac.jp

Specialty section:
This article was submitted to Plant Traffic and Transport, a section of the journal Frontiers in Plant Science

Received: *27 March 2020*
Accepted: *03 July 2020*
Published: *07 August 2020*

Citation:
Aung MS and Masuda H (2020) How Does Rice Defend Against Excess Iron?: Physiological and Molecular Mechanisms. Front. Plant Sci. 11:1102. doi: 10.3389/fpls.2020.01102

INTRODUCTION

Iron Acquisition by Rice

Iron (Fe) is a transition metal essential for the survival of virtually all living organisms. In plants, Fe participates in several important metabolic processes such as photosynthesis, chloroplast development, chlorophyll biosynthesis, electron transport, and redox reactions (Marschner, 1995). Graminaceous plants, including rice, acquire Fe from soil by chelation (strategy II) method (Römheld and Marschner, 1986). Rice synthesizes the Fe chelator 2′-deoxymugineic acid (DMA), a phytosiderophore of the mugineic acid (MA) family (Takagi, 1976), and secretes it into to the rhizosphere *via* the MA transporter (TOM1) (Nozoye et al., 2011). The secreted DMAs chelate

and solubilize insoluble Fe (III) in the rhizosphere to form Fe (III)-DMA complexes. These Fe complexes are taken up into root cells by yellow stripe 1 (YS1) and yellow stripe-like (YSL) transporters, *OsYSL15* (Curie et al., 2001; Inoue et al., 2009). Rice is typically grown in submerged paddy field conditions, where highly soluble ferrous ion (Fe^{2+}) is abundant. Under such conditions, unlike other gramineous plants, rice directly takes up ferrous ions *via* iron-regulated transporter 1 and 2 (*OsIRT1* and *OsIRT2*) (Ishimaru et al., 2006) together with phytosiderophores-based Fe uptake.

Iron Toxicity and its Damage to Rice Plants

The Fe^{2+} ions are abundant in paddy fields and absorption of them by rice roots causes severe Fe toxicity. The rhizosphere of acid sulfate soils with pH less than 5 contains the massive amount of Fe^{2+} about 10–2,000 mg kg^{-1} (da Silveira et al., 2007). The Fe^{2+} ions are highly soluble in water ($Ksp = [Fe^{2+}] [OH^-]^2 = 8 \times 10^{-16}$) compared to ferric ions (Fe^{3+}) ($Ksp = [Fe^{3+}] [OH^-]^3 = 1 \times 10^{-36}$) at 25°C (Stumm and Lee, 1961). Thus, Fe^{3+} ions merely dissolve in water (~1×10^{-9} mol L^{-1} at pH 5) while Fe^{2+} ions can dissolve proficiently (~800 mol L^{-1} at pH 5). Therefore, it states that all Fe^{2+} ions which exist in soil can be soluble in low pH (pH 5 or below). Among soil types, mainly acid sulfate soil, acid clay soil, and peat soil cause Fe toxicity (Becker and Asch, 2005). Acid soils occupy approximately 3,950 million hectares or 30% of the total landmass, representing more than 50% of potentially arable land (von Uexküll and Mutert, 1995). Thus, Fe toxicity is one of the major determinants of crop yield and quality, particularly in China, India, and Southeast Asia (NRCS, 2005; Mahender et al., 2019), west and central Africa (Gridley et al., 2006), and Brazil (Crestani et al., 2009).

Iron overload in plants causes tissue damage and disrupts cellular homeostasis. The sequential effects of Fe toxicity in rice plants are shown in **Figure 1**. Ferrous toxicity inhibits cell division and elongation of the primary roots and subsequently the growth of lateral roots (Li et al., 2015). High Fe absorption by the roots and its transport into the leaves by xylem *via* the transpiration stream lead to cellular Fe overload in plant tissues (Briat and Lobréaux, 1997).

Free Fe ions caused by Fe overload has a high affinity to bind with oxygen, leading to high oxygen tension and excess Fe accumulation in plant tissues. In plants, the Fe solubility varies in different cellular compartments and their pH is one of the

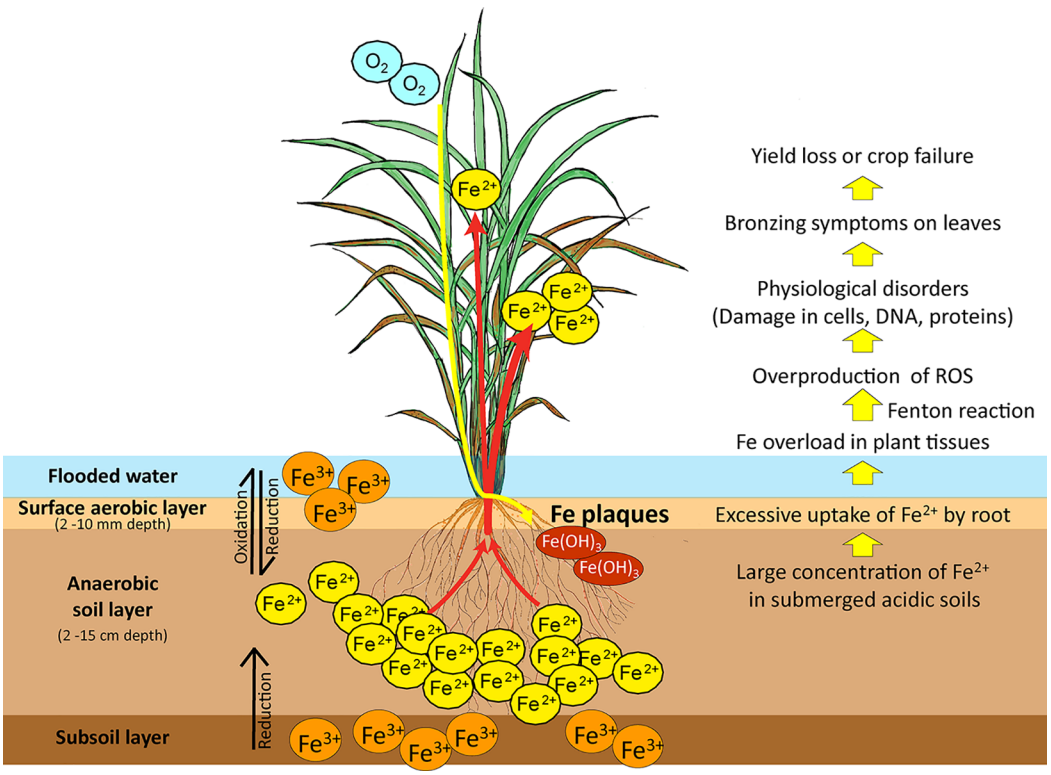

FIGURE 1 | Iron reduction in submerged low-pH soils and the effects of Fe toxicity on rice plants. In submerged soils with anaerobic and low pH conditions, ferric ion (Fe^{3+}) is reduced to the more soluble ferrous ion (Fe^{2+}). Excess ferrous ion is absorbed by the roots and transported by the xylem to the leaves, causing Fe overload in plant tissues. Excessive Fe accumulation in plant tissues causes overproduction of ROS by the Fenton reaction. These damage cellular structures, membranes, DNA, and proteins and impair physiological processes. Fe toxicity causes bronzing symptoms in leaves, followed by loss of rice yield or complete crop failure. Fe^{3+}, sparingly soluble ferric ion; Fe^{2+}, soluble ferrous ion; ROS, reactive oxygen species. Red arrows: Fe uptake and transport by rice; Yellow arrow: Rhizospheric oxidation of Fe^{2+} to Fe^{3+} by oxygen transport from shoot to root, leading to formation of Fe plaques on the root surface.

influential factors. For examples, in typical xylem sap at pH 5.5 (Ariga et al., 2014), the solubility of Fe^{3+} is ~3×10^{-10} mol L^{-1} and that of Fe^{2+} is ~80 mol L^{-1}; in the apoplast at pH 6 (Geilfus, 2017), the solubility of Fe^{3+} is ~1×10^{-12} mol L^{-1} and that of Fe^{2+} is ~8 mol L^{-1}; in the cytosol at pH 8 (Martinière et al., 2013), the solubility of Fe^{3+} is 1×10^{-18} mol L^{-1} and that of Fe^{2+} is ~8×10^{-4} mol L^{-1}. The Fe^{2+} ions can be oxidized to Fe^{3+} ions, and then those Fe^{3+} ions can readily be precipitated in most of the plant tissues where it becomes immobilized, less reactive, and thus less cellular toxicity. On the other hand, Fe^{2+} ions exist as a highly soluble and reactive form in the plant tissues with Fe overload and even numerous Fe^{2+} ions might exist as a free form in the cytosol if without any chelation or isolation, causing toxic reactions such as Fenton reaction. The Fenton reaction causes overproduction of reactive oxygen species (ROS), particularly the cytotoxic hydroxyl radical (•OH) (Becana et al., 1998; Thongbai and Goodman, 2000). Plant Fe toxicity disturbs photosystem II and elevates the cytochrome b6/f content of thylakoids, lowering the photosynthetic rate and accelerating oxygen production (Suh et al., 2002). Fe overload in chloroplasts results in oxidative damage caused by ROS (Balk and Schaedler, 2014). This leads to irreversible damage to cellular structures, membranes, DNA, and proteins (Briat et al., 1995; Stein et al., 2009a). Fe excess in cells impairs biological processes and leads to bronzing symptoms on leaves as a result of cell death. Leaf bronzing induced by Fe toxicity is closely associated with yield loss (Wu et al., 2014).

In this review, we summarize recent progress in the physiological and molecular mechanisms of Fe toxicity in rice, as well as its strategies to maintain Fe homeostasis.

PHYSIOLOGICAL AND MOLECULAR DEFENSE MECHANISMS AGAINST FE TOXICITY

Rice responds to Fe toxicity by means of four defense mechanisms (Defense 1, 2, 3 and 4). A model of the mechanisms of tolerance to excess Fe is shown in **Figure 2**.

Defense 1 (Fe Exclusion from Roots)

Under Fe excess condition, rice plants employ a defense mechanism of Fe exclusion, a root-based tolerant mechanism through inhibition of root Fe uptake. Rhizospheric oxidation of Fe^{2+} to Fe^{3+} by oxygen transport from shoots to roots leads to the formation of Fe plaques on the root surface due to Fe^{3+} precipitation, which acts as a barrier to the uptake of excess Fe^{2+} into root tissues (Becker and Asch, 2005). Tolerant genotype with Fe excluder may display the high formation of Fe plaque on the root surface (Mahender et al., 2019). Together with a larger diameter of the pith cavity of the shoots, the genotype with Fe excluder has high root oxidation power by an increase in aerenchyma volume and the number of lateral roots that favors the internal oxygen movement (Wu et al., 2014). Silicon supply mitigates the effect of Fe toxicity on rice by reducing Fe uptake (Ma and Takahashi, 1990). Also, its supply can strengthen the casparian bands in the root epidermis, which serves as a diffusion barrier and inhibits Fe flux into roots under excess Fe (Hinrichs et al., 2017; Becker et al., 2020). Therefore, rice genotypes with enhanced ability to exclude Fe such as high root oxidation power, large aerenchyma, several lateral roots, and strong casparian bands may be superior in Fe excess tolerance.

Microarray analyses have indicated that the expression of Fe uptake- and transport-related genes, such as *OsIRT1*, *OsIRT2*, *OsYSL2*, *OsYSL15*, and *OsNRAMP1*, is highly suppressed in roots in the presence of mild to high Fe excess levels (Aung et al., 2018b). high Fe excess level (Quinet et al., 2012), or very high Fe level (Finatto et al., 2015), suggesting that rice prevents Fe uptake and transport under Fe excess stress. Moreover, the expression of the genes involved in the biosynthesis of MAs, such as *OsNAS1*, *OsNAS2*, *OsNAAT1*, and *OsDMAS1*, is highly suppressed in roots, suggesting that plants restrain DMA release into the rhizosphere under excess Fe (Aung et al., 2018b). Therefore, rice utilizes defense 1 Fe exclusion to prevent Fe uptake by roots under Fe excess condition (**Figure 2**).

Role of HRZ in Fe Excess Tolerance (in Defense 1)

The HRZ, a Hemerythrin motif-containing Really Interesting New Gene- and Zinc-finger protein, is one of the key Fe homeostasis regulators. Kobayashi et al. (2013) identified two Fe-binding ubiquitin ligases, *OsHRZ1* and *OsHRZ2*, which negatively regulate Fe deficiency response in rice. *HRZ*-knockdown rice lines are hypersensitive to Fe toxicity, demonstrating severe growth defects and leaf bronzing since even under mild Fe excess conditions (Aung et al., 2018a). In addition, disruption of HRZ causes 5- to 10-fold hyperaccumulation of Fe in leaves, and the expression of Fe uptake- and transport-related genes including *OsIRT1*, *OsYSL2*, *OsYSL15*, *TOM1*, *OsNAS1*, *OsNAS2* and *OsIRO2* is severely elevated in roots of knockdown rice subjected to Fe excess stress (Aung et al., 2018a). Therefore, HRZ is an important protein to protect plant cells from Fe toxicity and maintain Fe homeostasis in plants under Fe excess by repressing the genes involved in Fe uptake and translocation (Aung et al., 2018a, **Figure 2**).

Interestingly, HRZ expression is highly induced in response to Fe deficiency (Kobayashi et al., 2013). However, several Fe-uptake genes are strongly induced in that condition. These results suggest that Fe uptake mechanism by plant should be strictly regulated, and thus *HRZ* is ready to regulate like a break to Fe uptake genes since under Fe deficiency condition. The hemerythrin domains of HRZs, likewise its homolog BRUTUS (BTS) in *Arabidopsis* (Selote et al., 2015; Hindt et al., 2017), are predominantly bound by Fe and zinc (Zn) (Kobayashi et al., 2013), and direct binding of the Fe to the key regulators including HRZ or BTS, may be responsible for intracellular Fe-sensing and signaling events (Kobayashi, 2019). Thus, it is conceivable that HRZ may play a major role as an Fe-binding sensor in the earliest response system to excess Fe.

In addition to defense 1 in roots, HRZs might have additional roles in other tissues or organs under Fe excess condition. Further studies are desirable to clarify HRZ-mediated regulations in other defenses.

Defense 2 (Fe Retention in Roots and Suppression of Fe Translocation to Shoots)

Rice can retain Fe in the root tissues and decrease Fe translocation from roots to shoots (Tadano, 1975) to avoid excessive Fe accumulation in leaves and maintain homeostasis (Becker and Asch, 2005; da Silveira et al., 2007). In the Fe-toxic field experiment, the tolerant genotype (EPAGRI 108) retains a higher Fe concentration in root symplast (7 mg g^{-1} dry weight) compared to the sensitive genotype (BR IRGA 409 with 1.93 mg g^{-1} dry weight) (Stein et al., 2014). Moreover, the tolerant genotype precipitates approximately 94% of the Fe in its root apoplast during Fe excess. Thus, tolerant genotypes likely to cope with an elevated intracellular and apoplastic Fe concentrations in roots. Hence, protecting aboveground parts from excessive Fe overload is crucial in determining plants' tolerance level.

In graminaceous plants, various metals absorbed by roots accumulate in the discrimination center (DC) in the basal part of the shoot, and the DC regulates mineral distribution to other plant parts (Mori, 1998). Protecting shoots, particularly the newest leaf, from Fe toxicity is important for the survival of rice plants, and the DC preferentially transports Fe to old leaves rather than new leaves (Aung et al., 2018b). Therefore, the DC may play an important role in Fe partitioning to aerial parts of plants and also act as a barrier to root-to-shoot transport of excessive Fe. Furthermore, Fe transport-related genes such as *OsIRT1*, *OsYSL2*, *OsTOM1*, *OsNRAMP1*, and *OsYSL15* are highly suppressed in the DC, as in roots under Fe excess, suggesting that these genes likely distribute less Fe to shoots, instead retaining Fe in roots and the DC (**Figure 2**).

Defense 3 (Fe Compartmentalization in Shoots)

When defense 1 and defense 2 systems are insufficient, plants may allow Fe transport from the roots through DC for the subsequent avoidance of Fe toxicity by Fe compartmentalization, disposal, or storage inside shoots. In fact, some tolerant genotypes accumulate more Fe in aerial shoots, thus maintaining healthy shoot growth (Onaga et al., 2013). Indonesian rice genotypes, such as Siam Saba, Mahsuri, Margasari, and Pokkali, reportedly exhibit shoot-based tolerance, as evidenced by a high shoot Fe concentration, reduced leaf bronzing, and a high grain yield (Nugraha et al., 2016).

Notably, the Fe concentration in roots increased nine-fold in the presence of 20-fold Fe excess treatment and then reached to constant at higher Fe treatments (Aung et al., 2018b). By contrast, the concentration in shoots increased in proportion to the level of Fe excess. Therefore, rice has a capacity to retain a limited amount of Fe in root tissues. At Fe levels greater than that can be coped with by defense 2, rice translocates excess Fe from roots to shoots. Interestingly, the higher the Fe excess levels, the more Fe was preferentially translocated to old leaves, which showed bronzing earlier than new leaves. The citrate efflux transporter, *OsFRDL1* is required for root-to-shoot Fe translocation and its expression in nodes is required for Fe distribution to rice grains (Yokosho et al., 2016). The expression of *OsFRDL1* and its homolog *OsFRDL2* is upregulated in roots and the DC at high Fe levels by microarray analyses (Aung et al., 2018b). Thus, *OsFRDL1* and *2* may be important in dividing Fe in DC under Fe excess, presumably for distributing Fe to old leaves than new leaves. To prevent Fe excess-mediated damage to new leaves, rice plants may have a mechanism to partition excess Fe to old leaves to prevent damage to the newest leaves.

Role of Ferritin and *OsVIT2* in Fe Excess Tolerance (in Defense 2 and 3)

The Fe^{2+} ions, once in the cells, can be associated into proteins or stored in cellular compartments such as ferritins and vacuoles. Ferritin is a ubiquitous Fe storage protein that stores up to 4,000 Fe atoms in a complex (Theil, 2003). Ferritin genes are transcriptionally induced in response to excess Fe in both monocot and dicot plants (Stein et al., 2009b; Briat et al., 2010). By microarray analyses, the rice ferritin genes, *OsFER1* and *OsFER2*, are strongly upregulated in roots and shoots by excess ferrous treatments (Quinet et al., 2012; Finatto et al., 2015; Aung et al., 2018b). Therefore, excess Fe is isolated into ferritin in a safe and bioavailable form by *OsFER1* and *OsFER2* in response to Fe overload as a part of defense mechanism (Briat and Lobréaux, 1997; Silveira et al., 2009).

Vacuoles are important cellular organelle for Fe isolation to prevent cellular toxicity. The vacuolar Fe transporters, *OsVIT1* and *OsVIT2*, are responsible for the sequestration of Fe into vacuoles *via* the tonoplast (Zhang et al., 2012). *OsVIT1* is less responsive to Fe abundance (Zhang et al., 2012) and its expression is suppressed in all tissues mainly in roots (Aung et al., 2018b). On the other hand, *OsVIT2* is highly responsive to Fe abundance (Zhang et al., 2012) and its expression is strongly upregulated in all tissues subjected to excess Fe (Quinet et al., 2012; Finatto et al., 2015; Aung et al., 2018b). Therefore, *OsVIT2* might be important for the sequestration of excess Fe into vacuoles in a non-toxic form.

In defense 2 and 3, plants allow internal Fe distribution or Fe sequestration in roots and shoots. To detoxify excess Fe in other compartments or tissues, plants transform excess Fe into non-toxic form by accumulation in ferritin and/or disposal of it in a vacuole *via OsVIT2*, or by exclusion from the symplast and efflux into the apoplast (**Figure 2**).

Role of *OsNAS3* in Fe Excess Tolerance (in Defense 2 and 3)

Nicotianamine (NA) is a major chelator of metal cations in higher plants. It is a chelate compound involved in Fe transport within the plant body. Among the three NA synthase genes in rice, *OsNAS1* and *OsNAS2* are involved in Fe deficiency response (Inoue et al., 2003). On the other hand, the expression of *OsNAS3* is strongly induced in response to Fe excess in various tissues including root, DC, stem, and old and newest leaves (Aung et al., 2018b). Also, the expression of the methionine cycle-related genes is not completely suppressed in Fe excess roots and other tissues. Thus, it is thought that methionine cycle works under excess Fe as well in producing NA along with *OsNAS3* (**Figure 2**).

Promoter-*GUS* (β-glucuronidase) analyses have revealed high-level *OsNAS3* expression in the vascular bundle, epidermis, and exodermis of the root, stem, and old leaf under Fe excess

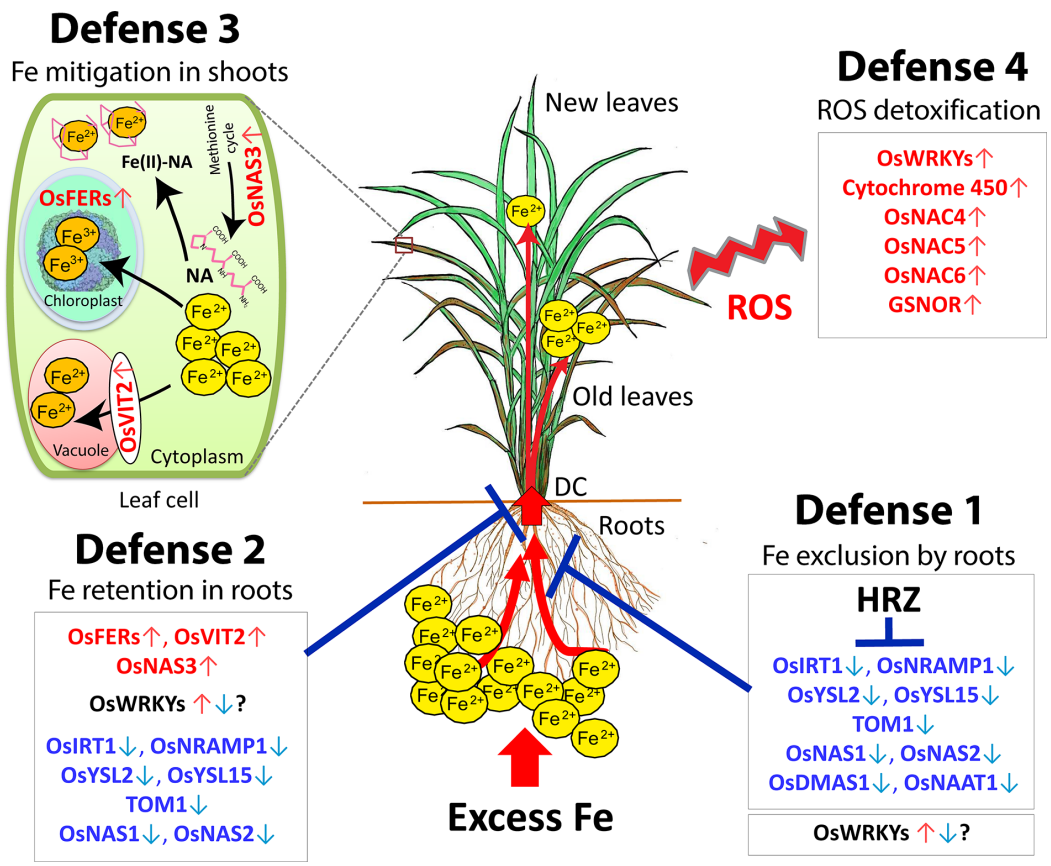

FIGURE 2 | Hypothetical model of the four defense mechanisms of rice against excess Fe. Defense 1: Fe excess tolerance by Fe exclusion in the roots. Defense 2: Fe-excess-tolerance by Fe retention in root and avoidance of Fe translocation to shoot. Defense 3: Fe excess tolerance by Fe compartmentalization in the shoot. Defense 4: Fe excess tolerance by ROS detoxification in the plant. DC, Discrimination center; NA, nicotinamine. Red letters, highly induced genes; Blue letters, highly suppressed genes. This figure is modified from the Supplemental figure of Aung et al., 2018b. The ferritin image was provided by Dr. David S. Goodsell (Scripps Research Institute, La Jolla, CA) and the RCSB PDB.

(Aung et al., 2019). Moreover, disruption of *OsNAS3* by T-DNA knockout increases sensitivity to excess Fe, reduces growth, causes severe leaf bronzing, and promote Fe accumulation in leaves. These findings provide the evidence that *OsNAS3* is crucial to mitigate excess Fe. NA synthesized by *OsNAS3* contributes to chelate excess Fe in roots and shoots, then it can be stored as a safe form since Fe chelated with NA does not cause the Fenton reaction. It may also protect the photosynthesis and water loss in leaves during Fe excess stress. NA involves in Fe-buffering to maintain Fe homeostasis under Fe excess (Pich et al., 2001) and plays a role in scavenging Fe and protecting the cells from oxidative damage (von Wirén et al., 1999). Therefore, it suggests NA synthesized by *OsNAS3* chelates excess Fe and contributes efficient Fe translocation and sequestration, exhibiting its important role in mitigation of excess Fe in defense mechanisms 2 and 3, and in Fe excess tolerance in rice.

Defense 4 (ROS Detoxification)

The fourth defense mechanism is Fe inclusion with tolerance to cellular Fe overload and damage in leaves, which is mediated by enzymatic detoxification in the symplast (Becker and Asch, 2005; Stein et al., 2009a), scavenging of ROS by antioxidants (e.g., ascorbic acid and reduced glutathione) (Fang et al., 2001; Gallie, 2013), and protection from ROS damage by the action of antioxidant enzymes (e.g., superoxide dismutase, peroxidase, and catalase) (Bode et al., 1995; Fang and Kao, 2000). Cultivation with various Fe excess intensities and microarray analyses revealed that the molecular defense mechanism of the defenses 1, 2, and 3 works since mild to moderate Fe excess conditions that do not seriously affect rice growth yet. However, the genes contribute to defense 4 work in molecular level in much severe Fe excess condition, which causes severe leaf bronzing and remarkably reduces the plant growth (Aung et al., 2018b).

Under severe Fe excess, plants induce the expression of genes associated with oxidative stress, oxygen and electron transfer, and those encoding cytochrome P450 family proteins (Quinet et al., 2012; Aung et al., 2018b), or transcription factors related to cell death and stress responses (*OsNAC4*, *OsNAC5*, and *OsNAC6*) (Finatto et al., 2015; Aung et al., 2018b). to alleviate the damage caused by excess Fe-induced ROS and other abiotic stresses caused by Fe excess.

Li et al. (2019) reported that *S-nitrosoglutathione-reductase* (GSNOR) promotes root tolerance to Fe toxicity by inhibiting Fe-dependent nitrosative and oxidative cytotoxicity in plants *via* the nitric oxide pathway. In *Arabidopsis*, knockout mutants display a root growth defect in the presence of high Fe (250 μM), demonstrating that GSNOR is important for root tolerance to Fe toxicity. Then, WRKY transcription factors are important superfamilies and key regulators of several processes associated with numerous abiotic and biotic stress tolerance in plants. Most WRKYs genes are critical in regulation of various contrasting stresses simultaneously, and also involved in ROS defense mechanism to various stresses including Fe excess stress (**Figure 2**).

Possible Working Model of Four Defenses

Given the roles of each Fe excess defense mechanism, the hypothesis is outlined in the model shown in **Figure 2**. Whenever the plant receives the Fe excess stress, defense 1 (Fe exclusion) works to inhibit root Fe absorption by the suppression of Fe uptake genes. This defense might protect well the plant in conditions of weak Fe toxicity. When Fe excess is more sever, defense 1 may no longer prevent the roots from excessive Fe uptake because some metal transporters also absorb Fe at the same time in the process of absorbing other essential metals such as Zn, copper (Cu) or manganese (Mn). In such a condition, defense 2 (Fe retention in roots and suppression of Fe translocation to shoots) works by accumulating Fe in a non-toxic form in safety compartments of roots that leads an increase in root Fe concentration, and also prevents the root-to-shoot Fe translocation by the suppression of the related genes. It is likely that defense 1 and 2 mechanisms constitutively drive since prior to the onset of visual damage in leaves and throughout the stress from low to severe Fe excess levels.

When defense 2 is insufficient to sequester excess Fe in root tissues, the excess Fe is translocated from root to shoot. In this case, defense 3 (Fe compartmentalization in shoots) begins to employ the functions of chelation, isolation and/or sequestration of excess Fe in a safe form in the shoot that leads an increase in shoot Fe concentration. Lastly, when free divalent Fe cannot be completely sequestered in safety form under severe Fe conditions, it becomes largely accumulated in the cytosol and causes Fenton reaction that generates ROS stress. In this condition, the corresponding genes in defense 4 (ROS detoxification) are induced to mitigate ROS stress in plants. Overall, these four defense mechanisms might work cooperatively and consecutively for Fe detoxification in rice depending on the degree of Fe excess progression.

FUTURE PROSPECTS FOR CROPS TOLERANT TO EXCESS FE

Gene Response and Regulatory Mechanism to the Fe Toxicity in Plants

There has been progress in our understanding of Fe excess defense and tolerance mechanisms in plants. Fe deficiency response and its regulation network in plants is well characterized and widely understood (Kobayashi et al., 2019). However, the Fe excess-signaling factor, transcription factors and regulatory genes conserved in the molecular mechanism of the Fe toxicity response are not well identified yet. Some genes involved in defense system may start to work after receiving a direct Fe excess signal mediated by ROS. Also, HRZ-mediated regulation to Fe-homeostasis-related genes is crucial in Fe excess as described above. But the other potent regulators and the genes participated in the Fe-excess responsive pathway are still largely unknown.

Viana et al. (2017) reported that the *cis*-regulatory elements involved in responses to abiotic stresses, such as light and salicylic acid pathway, participate in the molecular signaling involved in the response to Fe excess. However, promoter analyses of the functional *cis*-acting elements for the core Fe excess-responsive in rice still needs to be identified. Some bHLH transcription factors have important roles for Fe homeostasis in plants. OsIRO3 (OsbHLH063) acts as a negative regulator of the Fe deficiency response in rice (Zheng et al., 2010) and also involves in shoots-to-roots signal transmission which is important to prevent Fe toxicity in plants (Wang et al., 2020). Moreover, some WRKY transcription factors may also involve in Fe homeostasis in plants. Ricachenevsky et al. (2010) firstly reported the Fe-excess induced transcription factor, *OsWRKY80* in rice, which is also regulated by the dark-induced senescence- and drought- stress. In that study, *OsWRKY80* transcript level was increased up to threefold in roots and shoots after 9 days of Fe excess. Furthermore, microarray analyses have yielded 19 upregulated WRKYs in Fe-excess rice (Finatto et al., 2015). Then, *OsWRKY55-like*, *OsWRKY46*, *OsWRKY64*, and *OsWRKY113* are upregulated in an Fe-sensitive genotype, and *OsWRKY55-like* may be involved in the early stress response (Viana et al., 2017). Considering these results, some WRKY genes may also involve in defense mechanisms 1, 2 and 3 in addition to defense 4 (**Figure 2**). Therefore, transcription factors, such as some bHLHs and WRKYs, may involve in Fe excess response mechanism of the plants. Further comprehensive studies are required for the discovery of their specific roles in Fe excess. Therefore, exploration of Fe-excess responsive *cis*-acting elements, transcription factors, other potent regulators and candidate genes becomes a prerequisite for the deeper understanding of the mechanism of the excess Fe response and the development of rice varieties tolerant to Fe toxicity.

Developing Fe Excess Tolerant Rice *via* Molecular Breeding

Based on the tolerant rice lines selected by screening, the introduction of target genes into tolerant genotypes will increase further tolerance to Fe toxicity stress. As described above, the previous- and new-finding candidate genes encoding ferritin, VIT, NAS3, HRZ, GSNOR, and WRKYs may contribute to Fe excess tolerance in plants. In addition to these genes, there is a number of genes associated to the response to excess Fe; for example, overexpression of *Arabidopsis* Fe transporter, *AtNramp1*, leads to resistance to Fe toxicity (Curie et al., 2000). Use of these promising target genes and/or other candidate Fe homeostasis-

related genes in molecular-breeding approaches, such as marker-assisted breeding, transformation, or genome editing methods, will facilitate the development of genotypes that are well adapted to Fe toxicity and contribute to increasing rice productivity in hotspot sites of soils with excess Fe. In addition, Fe excess-responsive genes have potential for addressing the global issue of Fe biofortification in grains (Masuda et al., 2020).

CONCLUSION

Understanding of the molecular mechanisms of Fe excess tolerance in rice is essential for varietal development. There is a progress in discovery of candidate genes involved in the physiological and molecular response of rice to Fe overload, and their roles in Fe homeostasis, Fe detoxification, and Fe excess tolerance are becoming clear. These genes could be promising targets of genetic resources for the development of rice genotypes with increased Fe toxicity tolerance by breeding and to increase rice productivity in regions prone to Fe toxicity to meet the food demand for increasing population.

AUTHOR CONTRIBUTIONS

MSA and HM designed and wrote the manuscript. MSA led the writing of the manuscript. HM edited and improved the manuscript.

FUNDING

This publication was supported by a Grant-in-Aid for Young Scientists (B) (Grant No. 18K14367) from Japan Society for the Promotion of Sciences, JSPS KAKENHI (to MSA).

REFERENCES

Ariga, T., Hazama, K., Yanagisawa, S., and Yoneyama, T. (2014). Chemical forms of iron in xylem sap from graminaceous and non-graminaceous plants. *Soil Sci. Plant Nutr.* 60, 460–469. doi: 10.1080/00380768.2014.922406

Aung, M. S., Kobayashi, T., Masuda, H., and Nishizawa, N. K. (2018a). Rice HRZ ubiquitin ligases are crucial for response to excess iron. *Physiol. Plant* 163, 282–296. doi: 10.1111/ppl.12698

Aung, M. S., Masuda, H., Kobayashi, T., and Nishizawa, N. K. (2018b). Physiological and transcriptomic analysis of responses to different levels of iron excess stress in various rice tissues. *Soil Sci. Plant Nutr.* 64, 370–385. doi: 10.1080/00380768.2018.1443754

Aung, M. S., Masuda, H., Nozoye, T., Kobayashi, T., Jeon, J.-S., An, G., et al. (2019). Nicotianamine synthesis by *OsNAS3* is important for mitigating iron excess stress in rice. *Front. Plant Sci.* 10, 660. doi: 10.3389/fpls.2019.00660

Balk, J., and Schaedler, T. A. (2014). Iron cofactor assembly in plants. *Annu. Rev. Plant Biol.* 65, 125–153. doi: 10.1146/annurev-arplant-050213-035759

Becana, M., Moran, J. F., and Iturbe-Ormaetxe, I. (1998). Iron dependent oxygen free radical generation in plants subjected to environmental stress: toxicity and antioxidant protection. *Plant Soil* 201, 137–147. doi: 10.1023/A:1004375732137

Becker, M., and Asch, F. (2005). Iron toxicity in rice - conditions and management concepts. *J. Plant Nutr. Soil Sci.* 168, 558–573. doi: 10.1002/(ISSN)1522-2624

Becker, M., Ngo, N. S., and Schenk, M. K. A. (2020). Silicon reduces the iron uptake in rice and induces iron homeostasis related genes. *Sci. Rep.* 10, 5079. doi: 10.1038/s41598-020-61718-4

Bode, K., Döring, O., Lüthje, S., Neue, H. U., and Böttger, M. (1995). The role of active oxygen in iron tolerance of rice (*Oryza sativa* L.). *Protoplasma* 184, 249–255. doi: 10.1007/BF01276928

Briat, J. F., and Lobréaux, S. (1997). Iron transport and storage in plants. *Trends Plant Sci.* 2, 187–193. doi: 10.1016/S1360-1385(97)85225-9

Briat, J. F., Fobis-Loisy, I., Grignon, N., Lobréaux, S., Pascal, N., Savino, G., et al. (1995). Cellular and molecular aspects of iron metabolism in plants. *Biol. Cell.* 84, 69–81. doi: 10.1016/0248-4900(96)81320-7

Briat, J. F., Ravet, K., Arnaud, N., Duc, C., Boucherez, J., Touraine, B., et al. (2010). New insights into ferritin synthesis and function highlight a link between iron homeostasis and oxidative stress in plants. *Ann. Bot.* 105, 811–822. doi: 10.1093/aob/mcp128

Crestani, M., da Silva, J. A. G., da Souza, V. Q., Hartwig, I., Luche, H. S., de Sousa, R. O., et al. (2009). Irrigated rice genotype performance under excess iron stress in hydroponic culture. *Crop Breed. Appl. Biotechnol.* 9, 87–95. doi: 10.12702/1984-7033.v09n01a12

Curie, C., Alonso, J. M., Le Jean, M., Ecker, J. R., and Briat, J. F. (2000). Involvement of *NRAMP1* from *Arabidopsis thaliana* in iron transport. *Biochem. J.* 347, 749–755. doi: 10.1042/bj3470749

Curie, C., Panaviene, Z., Loulergue, C., Dellaporta, S. L., Briat, J. F., and Walker, E. L. (2001). Maize yellow stripe1 encodes a membrane protein directly involved in Fe (III) uptake. *Nature.* 409, 346–349. doi: 10.1038/35053080

da Silveira, V. C., de Oliveira, A. P., Sperotto, R. A., Espindola, L. S., Amaral, L., Dias, J. F., et al. (2007). Influence of iron on mineral status of two rice (*Oryza sativa* L.) cultivars. *Braz. J. Plant Physiol.* 19, 127–139. doi: 10.1590/S1677-04202007000200005

Fang, W. C., and Kao, C. H. (2000). Enhanced peroxidase activity in rice leaves in response to excess iron, copper and zinc. *Plant Sci.* 158, 71–76. doi: 10.1016/S0168-9452(00)00307-1

Fang, W. C., Wang, J. W., Lin, C. C., and Kao, C. H. (2001). Iron induction of lipid peroxidation and effects on antioxidative enzyme activities in rice leaves. *Plant Growth Regul.* 35, 75–80. doi: 10.1023/A:1013879019368

Finatto, T., Oliveira, A. C., Chaparro, C., Maia, L. C., Farias, D. R., Woyann, L. G., et al. (2015). Abiotic stress and genome dynamics: specific genes and transposable elements response to iron in rice. *Rice* 8, 13. doi: 10.1186/s12284-015-0045-6

Gallie, D. R. (2013). The role of l-ascorbic acid recycling in responding to environmental stress and in promoting plant growth. *J. Exp. Bot.* 64, 433–443. doi: 10.1093/jxb/ers330

Geilfus, C. M. (2017). The pH of the Apoplast: Dynamic Factor with Functional Impact Under Stress. *Mol. Plant.* 10, 1371–1386. doi: 10.1016/j.molp.2017.09.018

Gridley, H. E., Efisue, A., Tolou, B., and Bakayako, T. (2006). *Breeding for Tolerance to Iron Toxicity at WARDAl* (Cotonou, Benin: Africa Rice Center (WARDA)), 96–111.

Hindt, M. N., Akmakjian, G. Z., Pivarski, K. L., Punshon, T., Baxter, I., Salt, D. E., et al. (2017). BRUTUS and its paralogs, BTS LIKE1 and BTS LIKE2, encode important negative regulators of the iron deficiency response in Arabidopsis thaliana. *Metallomics* 9, 876–890. doi: 10.1039/c7mt00152e

Hinrichs, M., Fleck, A. T., Biedermann, E., Ngo, N. S., Schreiber, L., and Schenk, M. K. (2017). An ABC Transporter Is Involved in the Silicon-Induced Formation of Casparian Bands in the Exodermis of Rice. *Front. Plant Sci.* 8, 671. doi: 10.3389/fpls.2017.00671

Inoue, H., Higuchi, K., Takahashi, M., Nakanishi, H., Mori, S., and Nishizawa, N. K. (2003). Three rice nicotianamine synthase genes, *OsNAS1*, *OsNAS2*, and *OsNAS3* are expressed in cells involved in long-distance transport of iron and differentially regulated by iron. *Plant J.* 36, 366–381. doi: 10.1046/j.1365-313X.2003.01878.x

Inoue, H., Kobayashi, T., Nozoye, T., Takahashi, M., Kakei, Y., Suzuki, K., et al. (2009). Rice *OsYSL15* is an iron-regulated iron (III)-deoxymugineic acid transporter expressed in the roots and is essential for iron uptake in early growth of the seedlings. *J. Biol. Chem.* 284, 3470–3479. doi: 10.1074/jbc.M806042200

Ishimaru, Y., Suzuki, M., Tsukamoto, T., Suzuki, K., Nakazono, M., Kobayashi, T., et al. (2006). Rice plants take up iron as an Fe^{3+}- phytosiderophore and as Fe^{2+}. *Plant J.* 45, 335–346. doi: 10.1111/j.1365-313X.2005.02624.x

Kobayashi, T., Nagasaka, S., Senoura, T., Itai, R. N., Nakanishi, H., and Nishizawa, N. K. (2013). Iron-binding haemerythrin RING ubiquitin ligases regulate plant iron responses and accumulation. *Nat. Commun.* 4, 2792. doi: 10.1038/ncomms3792

Kobayashi, T. (2019). Understanding the Complexity of Iron Sensing and Signaling Cascades in Plants. *Plant and Cell Physiol.* 60, 1440–1446. doi: 10.1093/pcp/pcz038

Kobayashi, T., Nozoye, T., and Nishizawa, N. K. (2019). Iron transport and its regulation in plant. *Free Radic. Biol. Med.* 133, 11–20. doi: 10.1016/j.freeradbiomed.2018.10.439

Li, G., Song, H., Li, B., Kronzucker, H. J., and Shi, W. (2015). Auxin resistant1 and PIN-FORMED2 protect lateral root formation in *Arabidopsis* under iron stress. *Plant Physiol.* 169, 2608–2623. doi: 10.1104/pp.15.00904

Li, B., Sun, L., Huang, J., Gösch, C., Shi, W., Chory, J., et al. (2019). GSNOR provides plant tolerance to iron toxicity via preventing iron-dependent nitrosative and oxidative cytotoxicity. *Nat. Commun.* 10, 3896. doi: 10.1038/s41467-019-11892-5

Ma, J. F., and Takahashi, E. (1990). Effect of silicon on the growth and phosphorus uptake of rice. *Plant Soil* 126, 115–119. doi: 10.1007/BF00041376

Mahender, A., Swamy, B. P. M., Anandan, A., and Ali, J. (2019). Tolerance of iron-deficient and -toxic soil conditions in rice. *Plants* 8, 31. doi: 10.3390/plants8020031

Marschner, H. (1995). *Mineral nutrition of higher plants. 2nd edn* (London: Academic).

Martinière, A., Desbrosses, G., Sentenac, H., and Paris, N. (2013). Development and properties of genetically encoded pH sensors in plants. *Front. Plant Sci.* 4, 523. doi: 10.3389/fpls.2013.00523

Masuda, H., Aung, M. S., Kobayashi, T., and Nishizawa, N. K. (2020). "Iron Biofortification: The gateway to overcoming hidden hunger," in *The Future of Rice Demand: Quality Beyond Productivity*. Eds. A. C. de Oliveira, C. Pegoraro and V. E. Viana (Switzerland: Springer Nature), 149–177. doi: 10.1007/978-3-030-37510-2

Mori, S. (1998). "Iron transport in graminaceous plants," in *Iron Transport and Storage in Microorganisms, Plants and Animals. Vol. 35, Metal Ions in Biological Systems*. Eds. A. Sigel and H. Sigel (New York: Marcel Dekker), 215 – 237.

Nozoye, T., Nagasaka, S., Kobayashi, T., Takahashi, M., Sato, Y., Uozume, N., et al. (2011). Phytosiderophore efflux transporters are crucial for iron acquisition in graminaceous plants. *J. Biol. Chem.* 286, 5446–5454. doi: 10.1074/jbc.M110.180026

NRCS (2005). *Global soil regions map, National Resources Conservation Services (NRCS)* (Washington, DC: US Department of Agriculture (USDA), Soil Conservation Service). https://www.nrcs.usda.gov/wps/portal/nrcs/detail/soils/use/?cid=nrcs142p2_054013.

Nugraha, Y., Utami, D. W., Rosdianti, I. D. A., Ardie, S. W., Ghulammahdi, M., Suwarno, S., et al. (2016). Markers-traits association for iron toxicity tolerance in selected Indonesian rice varieties. *Biodivers.* 17, 753–763. doi: 10.13057/biodiv/d170251

Onaga, G., Edema, R., and Asea, G. (2013). Tolerance of rice germplasm to iron toxicity stress and the relationship between tolerance, Fe^{2+}, P and K content in the leaves and roots. *Arch. Agron. Soil Sci.* 59, 213–229. doi: 10.1080/03650340.2011.622751

Pich, A., Manteuffel, R., Hillmer, S., Scholz, G., and Schmidt, W. (2001). Fe homeostasis in plant cells: does nicotianamine play multiple roles in the regulation of cytoplasmic Fe concentration? *Planta* 213, 967–976. doi: 10.1007/s004250100573

Quinet, M., Vromman, D., Clippe, A., Bertin, P., Lequeux, H., Dufey, I., et al. (2012). Combined transcriptomic and physiological approaches reveal strong differences between short- and long-term response of rice (*Oryza sativa*) to iron toxicity. *Plant Cell Env.* 35, 1837–1859. doi: 10.1111/j.1365-3040.2012.02521.x

Römheld, V., and Marschner, H. (1986). Evidence for a specific uptake system for iron phytosiderophore in roots of grasses. *Plant Physiol.* 80, 175–180. doi: 10.1104/pp.80.1.175

Ricachenevsky, F. K., Sperotto, R. A., Menguer, P. K., and Fett, J. P. (2010). Identification of Fe-excess-induced genes in rice shoots reveals a WRKY transcription factor responsive to Fe, drought and senescence. *Mol. Biol. Rep.* 37, 3735–3745. doi: 10.1007/s11033-010-0027-0

Selote, D., Samira, R., Matthiadis, A., Gillikin, J. W., and Long, T. A. (2015). Iron-binding E3 ligase mediates iron response in plants by targeting basic helix-loop-helix transcription factors. *Plant Physiol.* 167, 273–286. doi: 10.1104/pp.114.250837

Silveira, V. C., Fadanelli, C., Sperotto, R. A., Stein, R. J., Basso, L. A., Vaz Junior, I. S., et al. (2009). Role of ferritin in the rice tolerance to iron overload. *Sci. Agric.* 66, 549–555. doi: 10.1590/S0103-90162009000400019

Stein, R. J., Duarte, G. L., Spohr, M. G., Lopes, S.II, and Fett, J. P. (2009a). Distinct physiological responses of two rice cultivars subjected to iron toxicity under field conditions. *Ann. Appl. Biol.* 154, 269–277. doi: 10.1111/j.17447348.2008.00293.x

Stein, R. J., Ricachenevsky, F. K., and Fett, J. P. (2009b). Differential regulation of the two rice ferritin genes (OsFER1 and OsFER2). *Plant Sci.* 177, 563–569. doi: 10.1016/j.plantsci.2009.08.001

Stein, R. J., Lopes, S.II, and Fett, J. P. (2014). Iron toxicity in field-cultivated rice: contrasting tolerance mechanisms in distinct cultivars. *Theor. Exp. Plant Physiol.* 26, 135–146. doi: 10.1007/s40626-014-0013-3

Stumm, W., and Lee, G. F. (1961). Oxygenation of ferrous iron. *Ind. Eng. Chem.* 53, 143–146. doi: 10.1021/ie50614a030

Suh, H. J., Kim, C. S., Lee, J. Y., and Jung, J. (2002). Photodynamic effect of iron excess on photosystem II function in pea plants. *Photochem. Photobiol.* 75, 513–518. doi: 10.1562/0031-8655(2002)075<0513:PEOIEO>2.0.CO;2

Tadano, T. (1975). Devices of rice roots to tolerant high iron concentrations in growth media. *Japan Agric. Res. Q.* 9, 34 –39.

Takagi, S. (1976). Naturally occurring iron-chelating compounds in oat- and rice root washing. I: activity measurement and preliminary characterization. *Soil Sci. Plant Nutr.* 22, 423–433. doi: 10.1080/00380768.1976.10433004

Theil, E. C. (2003). Ferritin: at the crossroads of iron and oxygen metabolism. *J. Nutr.* 133, 1549–1553. doi: 10.1093/jn/133.5.1549S

Thongbai, P., and Goodman, B. A. (2000). Free radical generation and post anoxic injury in an iron toxic soil. *J. Plant Physiol.* 23, 1887–1990. doi: 10.1080/01904160009382151

Viana, V. E., Marini, N., Finatto, T., Ezquer, I., Busanello, C., Dos Santos, R. S., et al. (2017). Iron excess in rice: From phenotypic changes to functional genomics of WRKY transcription factors. *Genet. Mol. Res.* 16 (3): gmr16039694. doi: 10.4238/gmr16039694

von Uexküll, H. R., and Mutert, E. (1995). "Global extent, development and economic impact of acid soils," in *Plant–Soil Interactions at Low pH: Principles and Management*. Eds. R. A. Date, N. J. Grundon, G. E. Raymet and M. E. Probert (Dordrecht, The Netherlands: Kluwer Academic Publishers), 5–19.

von Wirén, N., Klair, S., Bansal, S., Briat, J. F., Khodr, H., Shioiri, T., et al. (1999). Nicotianamine chelates both Fe-III and Fe-II. Implications for metal transport in plants. *Plant Physiol.* 119, 1107–1114. doi: 10.1104/pp.119.3.1107

Wang, F., Itai, R. N., Nozoye, T., Kobayashi, T., Nishizawa, N. K., and Nakanishi, N. (2020). The bHLH protein OsIRO3 is critical for plant survival and iron (Fe) homeostasis in rice (Oryza sativa L.) under Fe-deficient conditions. *Soil Sci. Plant Nutr.* doi: 10.1080/00380768.2020.1783966

Wu, L., Shhadi, M. Y., Gregorio, G., Matthus, E., Becker, M., and Frei, M. (2014). Genetic and physiological analysis of tolerance to acute iron toxicity in rice. *Rice* 7, 8. doi: 10.1186/s12284-014-0008-3

Yokosho, K., Yamaji, N., and Ma, J. F. (2016). *OsFRDL1* expressed in nodes is required for distribution of iron to grains in rice. *J. Exp. Bot.* 67, 5485–5494. doi: 10.1093/jxb/erw314

Zhang, Y., Xu, Y. H., Yi, H. Y., and Gong, J. M. (2012). Vacuolar membrane transporters *OsVIT1* and *OsVIT2* modulate iron translocation between flag leaves and seeds in rice. *Plant J.* 72, 400–410. doi: 10.1111/j.1365-313X.2012.05088.x

Zheng, L., Ying, Y., Wang, L., Wang, F., Whelan, J., and Shou, H. (2010). Identification of a novel iron regulated basic helix-loop-helix protein involved in Fe homeostasis in *Oryza sativa*. *BMC Plant Biol.* 10, 66. doi: 10.1186/1471-2229-10-166

Conflict of Interest: The authors declare that the research was conducted in the absence of any commercial or financial relationships that could be construed as a potential conflict of interest.

frontiers in Plant Science

CORRECTION
published: 20 November 2020
doi: 10.3389/fpls.2020.601527

Corrigendum: How Does Rice Defend Against Excess Iron?: Physiological and Molecular Mechanisms

May Sann Aung and Hiroshi Masuda*

Department of Biological Production, Faculty of Bioresource Sciences, Akita Prefectural University, Akita, Japan

Keywords: iron excess, rice, OsNAS3, HRZ, OsVIT2, ROS, iron homeostasis, tolerant mechanism

OPEN ACCESS

Approved by:
Frontiers Editorial Office, Frontiers Media SA, Switzerland

****Correspondence:***
May Sann Aung
mayaung@akita-pu.ac.jp

Specialty section:
This article was submitted to Plant Membrane Traffic and Transport, a section of the journal Frontiers in Plant Science

Received: *01 September 2020*
Accepted: *09 October 2020*
Published: *20 November 2020*

Citation:
Aung MS and Masuda H (2020) Corrigendum: How Does Rice Defend Against Excess Iron?: Physiological and Molecular Mechanisms. Front. Plant Sci. 11:601527. doi: 10.3389/fpls.2020.601527

A Corrigendum on

How Does Rice Defend Against Excess Iron?: Physiological and Molecular Mechanisms
by Aung, M. S., and Masuda, H. (2020). Front. Plant Sci. 11:1102. doi: 10.3389/fpls.2020.01102

In the original article, there was a mistake in **Figure 2** as published. **OsNAS↑ instead of OsNAS3↑ in Defense 3.** The corrected **Figure 2** appears below.

The authors apologize for this error and state that this does not change the scientific conclusions of the article in any way. The original article has been updated.

REFERENCES

Aung, M. S., Masuda, H., Kobayashi, T., Nishizawa, N. K. (2018b). Physiological and transcriptomic analysis of responses to different levels of iron excess stress in various rice tissues. *Soil Sci. Plant Nutr.* 64, 370–385. doi: 10.1080/00380768.2018.1443754

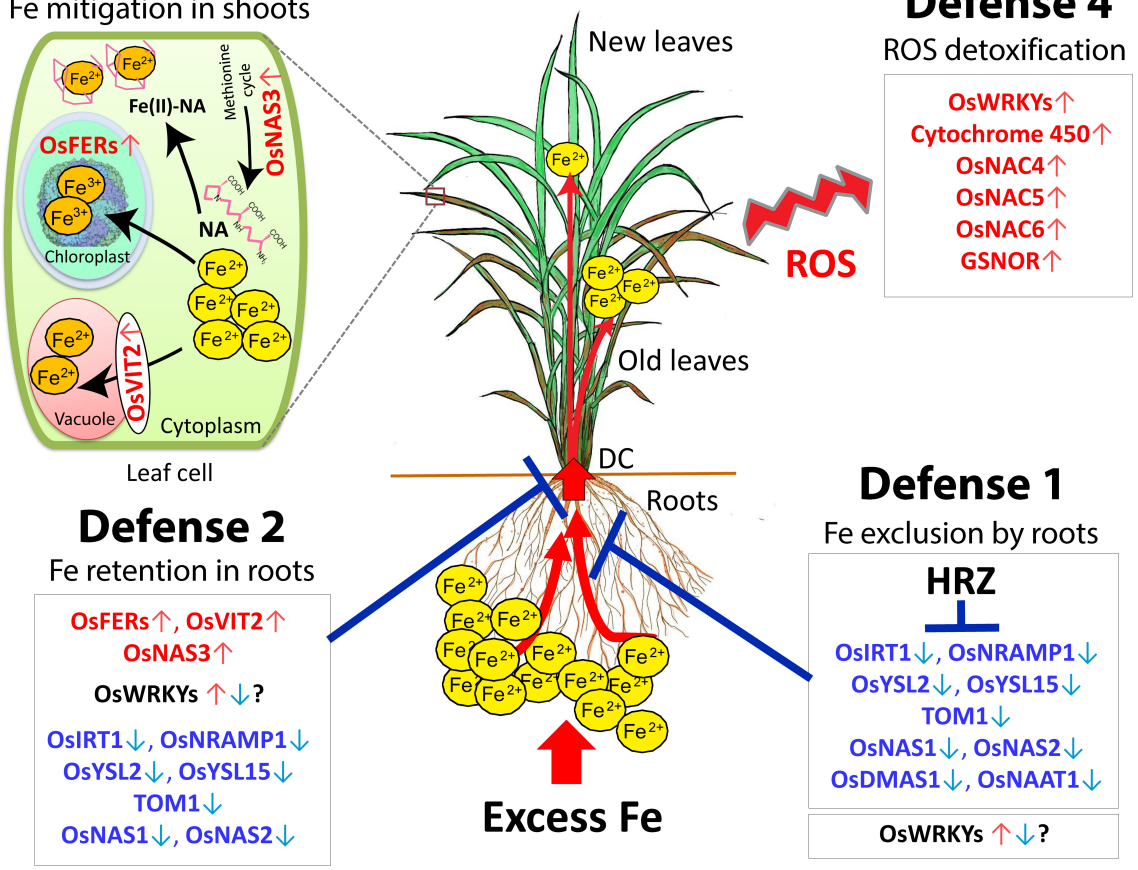

FIGURE 2 | Hypothetical model of the four defense mechanisms of rice against excess Fe. Defense 1: Fe excess tolerance by Fe exclusion in the roots. Defense 2: Fe-excess-tolerance by Fe retention in root and avoidance of Fe translocation to shoot. Defense 3: Fe excess tolerance by Fe compartmentalization in the shoot. Defense 4: Fe excess tolerance by ROS detoxification in the plant. DC, Discrimination center; NA, nicotinamine. Red letters, highly induced genes; Blue letters, highly suppressed genes. This figure is modified from the Supplemental figure of (Aung et al., 2018b). The ferritin image was provided by Dr. David S. Goodsell (Scripps Research Institute, La Jolla, CA) and the RCSB PDB.

Advantages of publishing in Frontiers

OPEN ACCESS
Articles are free to read for greatest visibility and readership

FAST PUBLICATION
Around 90 days from submission to decision

HIGH QUALITY PEER-REVIEW
Rigorous, collaborative, and constructive peer-review

TRANSPARENT PEER-REVIEW
Editors and reviewers acknowledged by name on published articles

Frontiers
Avenue du Tribunal-Fédéral 34
1005 Lausanne | Switzerland

Visit us: www.frontiersin.org
Contact us: frontiersin.org/about/contact

REPRODUCIBILITY OF RESEARCH
Support open data and methods to enhance research reproducibility

DIGITAL PUBLISHING
Articles designed for optimal readership across devices

FOLLOW US
@frontiersin

IMPACT METRICS
Advanced article metrics track visibility across digital media

EXTENSIVE PROMOTION
Marketing and promotion of impactful research

LOOP RESEARCH NETWORK
Our network increases your article's readership